Optimisation of

Permeable Reactive Barrier Systems

for the Remediation

of Contaminated Groundwater

A thesis
submitted in partial fulfilment
of the requirements for the Degree of
Doctor of Philosophy

at

Lincoln University

by

Brett D.M. Painter

Natural Resources Engineering
Lincoln University
April, 2005

Abstract of a thesis submitted in partial fulfilment of the
requirements for the Degree of Ph.D.

Optimisation of Permeable Reactive Barrier Systems for the Remediation of Contaminated Groundwater

by Brett D.M. Painter

Permeable reactive barriers (PRBs) are one of the leading technologies being developed in the search for alternatives to the pump-and-treat method for the remediation of contaminated groundwater. A new optimising design methodology is proposed to aid decision-makers in finding minimum cost PRB designs for remediation problems in the presence of input uncertainty. The unique aspects of the proposed methodology are considered to be:

- design enhancements to improve the hydraulic performance of PRB systems;
- elimination of a time-consuming simulation model by determination of approximating functions relating design variables and performance measures for fully penetrating PRB systems;
- a versatile, spreadsheet-based optimisation model that locates minimum cost PRB designs using Excel's standard non-linear solver; and
- the incorporation of realistic input variability and uncertainty into the optimisation process via sensitivity analysis, scenario analysis and factorial analysis.

The design methodology is developed in the context of the remediation of nitrate contamination due to current concerns with nitrate in New Zealand. Three-dimensional computer modelling identified significant variation in capture and residence time, caused by up-gradient funnels and/or a gate hydraulic conductivity that is significantly different from the surrounding aquifer. The unique design enhancements to control this variation are considered to be the customised down-gradient gate face and emplacement of funnels and side walls deeper than the gate. The use of velocity equalisation walls and manipulation of a PRB's hydraulic conductivity within certain bounds were also found to provide some control over variation in capture and residence time.

Accurate functional relationships between PRB design variables and PRB performance measures were shown to be achievable for fully penetrating systems. The chosen design variables were gate length, gate width, funnel width and the reactive material proportion. The chosen performance measures were edge residence, centreline residence and capture width.

A method for laboratory characterisation of reactive and non-reactive material combinations was shown to produce data points that could realistically be part of smooth polynomial interpolation functions. The use of smooth approximating functions to characterise PRB inputs and determine PRB performance enabled the creation of an efficient spreadsheet model that ran more quickly and accurately with Excel's standard non-linear solver than with the LGO global solver or Evolver genetic-algorithm based solver. The PRB optimisation model will run on a standard computer and only takes a couple of minutes per optimisation run.

Significant variation is expected in inputs to PRB design, particularly in aquifer and plume characteristics. Not all of this variation is quantifiable without significant expenditure. Stochastic models that include parameter variability have historically been difficult to apply to realistic remediation design due to their size and complexity. Scenario and factorial analysis are proposed as an efficient alternative for quantifying the effects of input variability on optimal PRB design. Scenario analysis is especially recommended when high quality input information is available and variation is not expected in many input parameters. Factorial analysis is recommended for most other situations as it separates out the effects of multiple input parameters at multiple levels without an excessive number of experimental runs.

Acknowledgements

This project has been an enriching experience due to the support and encouragement of a lot of people. Funding was provided by the New Zealand taxpayer through the Foundation for Research, Science and Technology under contracts LVL805 and LVLX0006. I would like to sincerely thank my Manager, Dr John Bright, and Chief Executive Officer, Dr Peter John, at Lincoln Ventures Ltd. for their belief in me and efforts in securing all necessary funding.

Thank you to all my supervisors for their guidance, ideas, challenges and expertise; to Dr Ross James and Dr Grant Read at the Management Science Department, University of Canterbury where this project began; and then to Dr Crile Doscher at Natural Resources Engineering, Lincoln University and Dr Mark Milke at Civil Engineering, University of Canterbury for the completion of the project.

Thank you to all my colleagues at Lincoln Ventures Ltd for their assistance and availability. Finally, thank you to my extended family and valued friends for their inspiration and motivation to make a positive difference wherever possible.

Table of Contents

List of Figures

List of Tables

Chapter One

Introduction and Literature Survey

1.1 Aim

Although permeable reactive barrier (PRB) systems are simple in concept, there is a great breadth of science and technology involved in reactive media selection for different contaminants and in the design, installation and monitoring of these emplacements in the subsurface. The aim of this thesis is to develop a practical methodology for the optimal design of PRB systems, with particular focus on the denitrification barrier as a case study. The methodology will be designed to enable decision-makers to explore PRB design options and the effects of input uncertainty with minimal processing time.

This objective will be achieved by:

- The design and testing of laboratory experiments for characterisation of reactive and non-reactive material combinations;

- Hydraulic simulation to investigate PRB design enhancements and develop functional relationships between PRB design variables and performance measures;

- PRB design optimisation using an Excel spreadsheet with the standard non-linear solver; and,

- Sensitivity, scenario and factorial analysis as practical methods for dealing with uncertainty and variability in input data.

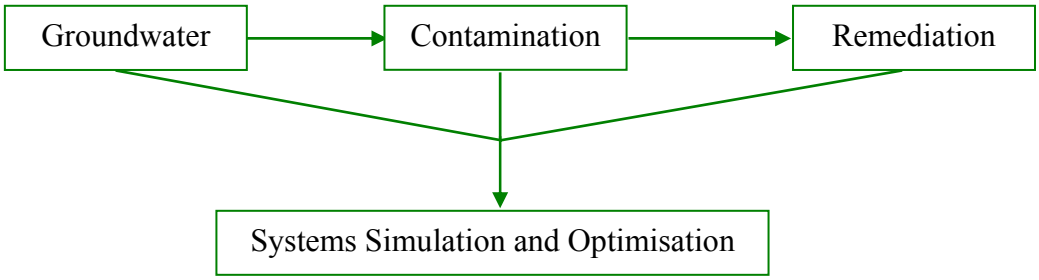

Fig. 1.1. Keywords of thesis.

1.2 Problem Definition

This research topic is defined by the key words as shown in Figure 1.1. *Groundwater* is water found beneath the surface of the ground. It is primarily water that has seeped down from the surface by migrating through the soil matrix and spaces in geologic formations. Groundwater is usually found in an *aquifer*. *Bear* [1979] defined aquifer as "a geological formation which is capable of storing and transmitting a significant quantity of water under ordinary field conditions." Groundwater in aquifers is important for irrigation, domestic and industrial uses. Unfortunately, groundwater has been seriously damaged by *contamination* (improper disposal or accidental release), and must be cleaned up before use. A *remediation* system attempts to control (and sometimes optimise) the cleanup processes for a particular groundwater contamination problem. The use of computers for *systems simulation and optimisation* has been shown to be a highly efficient and effective means of designing and controlling a remediation system.

Groundwater contamination problems are usually defined in terms of the type of contaminant, type of porous medium, and type of aquifer. Different contamination problems often require different remedial actions. *Gorelick et al.* [1993] described six general classes of groundwater remedial action, apart from physical containment, that are available for sites with contamination problems. They include:

- Plume stabilisation through hydraulic control to minimise spreading;
- Diversion of flow or redirection of contaminant plume to protect a well or other resource;
- Contaminant removal to clean up an aquifer;
- *In situ* biological treatment to reduce contaminant levels in the groundwater;

- Wellhead treatment to clean up groundwater withdrawn for a specific use; and,
- Monitoring of contaminant levels until need for one of the above remedial actions is confirmed, or until natural attenuation reduces contaminant levels.

The most commonly implemented active remediation technique is called *pump-and-treat.* Pump-and-treat entails pumping the contaminated water to the surface for above-ground (*ex situ*) treatment and then disposing of the treated water (e.g. to municipal wastewater treatment plants) or injecting it back into the aquifer via injection wells. Many researchers have worked at optimising this technique but the reliance on continuous energy inputs for many years without a guarantee of complete restoration has led them to look for cheaper and faster remediation systems.

Permeable Reactive Barriers (PRBs) are one of the leading alternative treatments proposed in this search. A PRB (see Figure 1.2) is a relatively low cost, low technology technique, which generally has a high public acceptance and is carried out *in situ*. A PRB is defined as:

> *"An emplacement of reactive materials in the subsurface designed to intercept a contaminant plume, provide a flow path through the reactive media, and transform the contaminant(s) into environmentally acceptable forms to attain remediation goals down-gradient of the barrier" (U.S. EPA, 1998).*

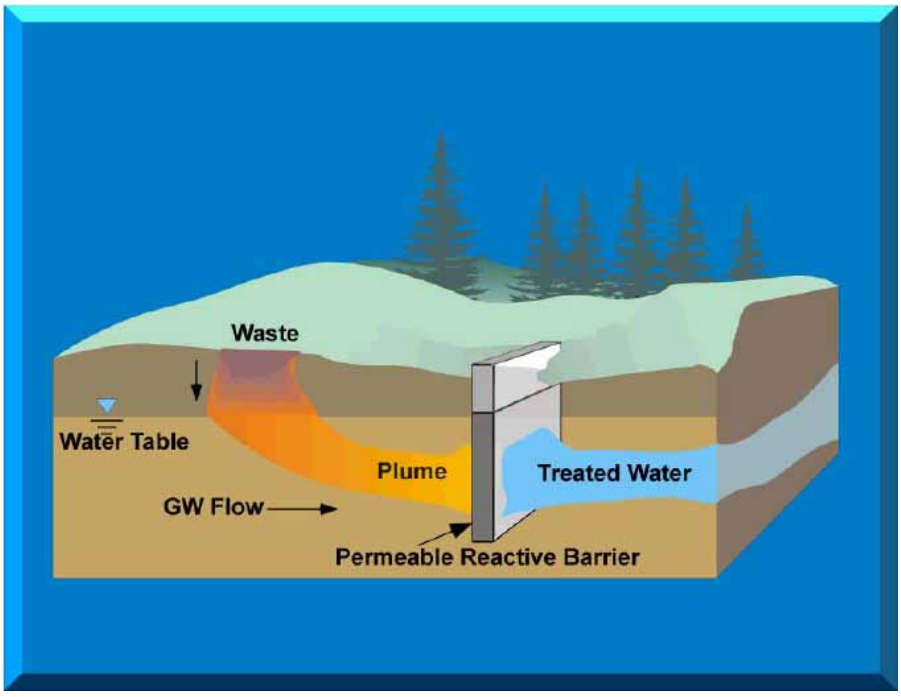

Fig. 1.2. Example PRB system (from U.S. EPA, 1998).

Figure 1.3 shows that the average total capital cost of the surveyed PRB systems was less than 15% of the average total capital cost of the surveyed pump-and-treat systems. *Quinton et al.* (1997) also demonstrated how a PRB system could be at least sixty percent cheaper than the equivalent pump-and-treat system.

Given the uncertainty and variability in natural environments, the primary challenge for the PRB technology is to design and construct appropriately so that the desired contaminants are captured and retained long enough to be remediated. A methodology to maximise the success of a PRB project is presented in Chapter 2.

EXHIBIT 6. CAPITAL COST COMPARISON OF P&T AND PRB SYSTEMS

Technology	Capital Cost Range[1]			Average Capital Cost[1] ($)	Number of Sites
	25th Percentile ($)	Median ($)	75th Percentile ($)		
P&T	1,700,000	2,000,000	5,900,000	4,900,000	32
PRBs	440,000	680,000	1,000,000	730,000	16

[1] All reported costs were adjusted for site locations and years when costs were incurred, as described in the text

Fig. 1.3. Comparison between cost of pump-and-treat and PRB technologies (from U.S. EPA, 2001)

Irrespective of the technology, remediation of contaminated groundwater is an expensive and/or lengthy process. The use of computer models to *simulate* and *optimise* remediation problems is necessary to help create the most efficient and effective design/operation solution possible. Simulation of a particular system is used to predict the system response to different design strategies. Optimisation is used to search for the "ideal" design strategy that will result in a desired outcome. Whether this strategy is the *global optimum* or just a *local optimum* depends on the shape of the function to be searched and the type of optimisation technique employed.

1.2.1 Systems Simulation

A *system* can be defined as a collection of interacting elements or components that act together to achieve a common goal. Systems can be studied by direct experimentation, by building prototypes, or by building mathematical/logical models. The purpose of systems study through *modelling* is to aid the analysis, understanding, design, operation, prediction, or control of systems without actually constructing and operating the real thing. The calibration of a model determines how closely it approximates the real system. The model's *assumptions* explain the differences between the model and the real system. Mathematical/logical models that are not easily amenable to conventional analytic or numeric solutions form a subset of models generally known as *simulation models*.

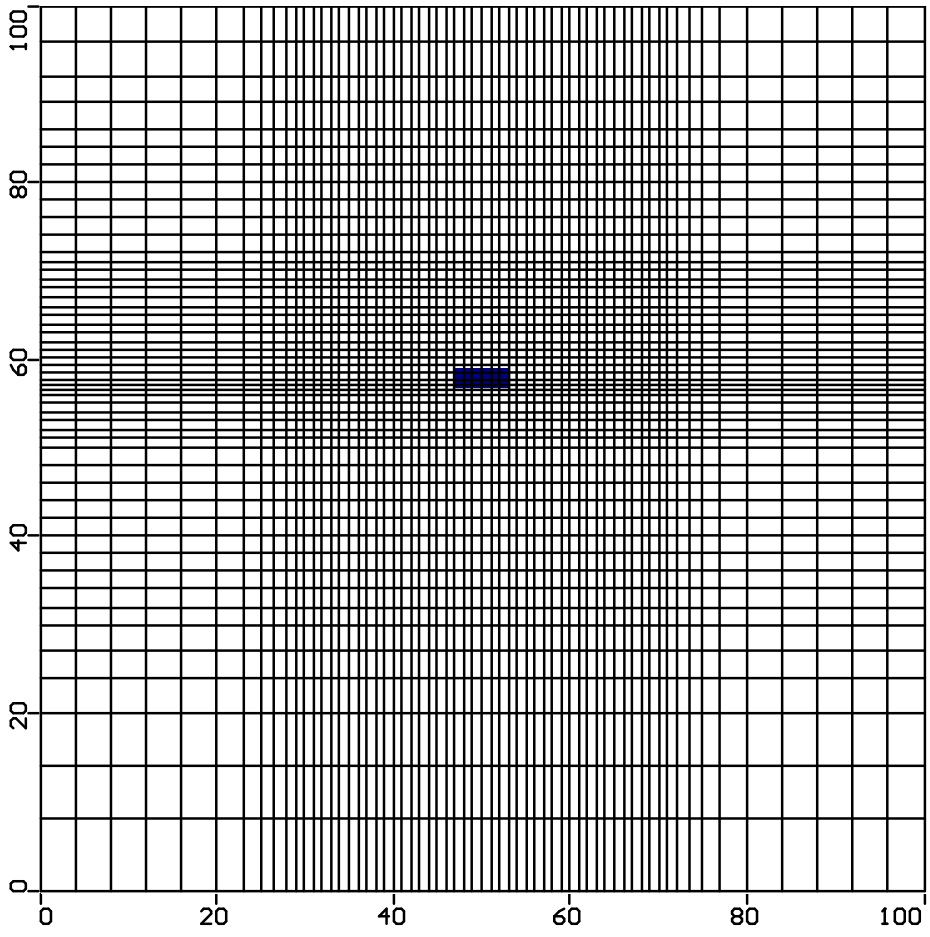

Fig. 1.4. Example discretised groundwater remediation system.

Simulation of a system is used to predict the system response to different input strategies. It can offer insights into the contamination process within an aquifer and the consequences of applying a particular remediation strategy. For example, the PRB system in Figure 1.2 can be

discretised into a numerical mesh, as shown in Figure 1.4. This particular mesh shows a permeable reactive barrier (in dark blue) and a grid spacing that decreases in the vicinity of the barrier. The groundwater flow and transport of contaminant in the system are then simulated numerically using computer software such as Visual MODFLOW (*Guiguer and Franz*, 1996).

Groundwater flow generally obeys *Darcy's law*, which states that the rate of flow, Q, is (1) proportional to the cross-sectional area A, (2) proportional to the difference in water level elevations in the inflow and exit levels of the filter (h_1-h_2), and (3) inversely proportional to the filter's length, L. The original form of Darcy's law is stated as

$$Q = KA(h_1-h_2)/L$$

where K is the *hydraulic conductivity*. Hydraulic conductivity is a measure of the capacity of a porous medium to transmit flow of a specific liquid. The lengths h_1 and h_2 are measured with respect to some common datum level. Variations to the horizontal and vertical hydraulic conductivity in an aquifer can have a significant effect on the flow patterns of contaminants in an aquifer. This effect is difficult and expensive to simulate, though, as a great number of measurements may be required.

The *pore velocity* (v) necessary to estimate residence time in a permeable reactive barrier (PRB) also requires estimation of the *effective porosity* (n) of the PRB. Effective porosity can be described as the "part of the total void space through which (most of the) flow is assumed to take place" (*Bear and Nitao*, 1999). Pore velocity can then be calculated as follows:

$$v = Q/An$$

The ideal geologic formation to simulate is both *homogeneous* and *isotropic*. An aquifer is said to be *homogeneous* if the hydraulic conductivity is uniform at all points within the aquifer. If the conductivity varies with location, the aquifer is *heterogeneous*. Likewise, an aquifer is said to be *isotropic* if the hydraulic conductivity is the same in all directions. If the conductivity varies with direction then the formation is *anisotropic*.

Once a contaminant comes into contact with groundwater, several contaminant-specific characteristics influence its capacity to be transported by flowing groundwater. These

characteristics include solubility, density, volatility, and toxicity. From the perspective of groundwater pollution, the most significant contaminant characteristic is *solubility*. The solubility of a solute is defined as the mass of the solute that will dissolve in a unit volume of solution under specified conditions and can be predicted using the *law of mass action*. Liquids with infinite solubilities in water are referred to as being *miscible* with water, while those with finite solubilities in water are referred to as being *immiscible* with water. When liquids that are immiscible with water fail to completely dissolve in groundwater, a stratified flow problem is produced with each liquid behaving as a separate phase. Multi-phase problems require the use of complicated numerical models for detailed analysis.

Contaminants dissolved in groundwater are transported by three processes: *advection*, *mechanical dispersion* and *molecular diffusion*. Advection is the movement of dissolved solute with flowing groundwater. Mechanical dispersion results from the convoluted paths that water and contaminant particles follow while flowing through porous and fractured media. Molecular diffusion is the process in which dissolved contaminants move from areas of high concentration to areas of low concentration in response to the presence of a concentration gradient. Mechanical dispersion and molecular diffusion are referred to collectively as *hydrodynamic dispersion*. All three processes operate simultaneously in flowing groundwater. In the process of being transported, many contaminants react with other compounds or ions in solution. Contaminants may also *adsorb* onto or *desorb* off the solid matrix. Chemical reactions, exchange, and adsorption/desorption processes can significantly slow the rate of contaminant transport. The amount of accuracy desired, and the characteristics of the contaminant(s) and system to be simulated will determine the complexity of the contaminant transport equations.

In simple systems, simulation may provide enough information by itself to enable a satisfactory decision to be made. However, if the *best* or *optimal* solution is desired then the simulation model can be coupled with an *optimisation* procedure. The simulation model is then used for scoping and screening alternative strategies prior to the application of the optimisation procedure, providing the transformation equation within the optimisation procedure, and conducting sensitivity analysis on the optimal solution produced by the optimisation procedure.

Simulation cannot predict future system behaviour exactly due to *uncertainty* in many system parameters. The greatest source of uncertainty in groundwater modelling is believed to be

hydraulic conductivity. Analyses of field data indicate that hydraulic conductivity can vary by an order of magnitude or more over the distance of a few metres (*Bakr*, 1976). Porosity is also known to vary, but its variation is not usually considered to be as significant. An important issue in simulation modelling is minimising parameter uncertainty while retaining computational feasibility.

1.2.2 Optimisation

Optimisation involves the determination of optimal values for a set of *decision variables* in a specific system. Optimality is defined with respect to a specified *objective function* and is subject to a set of *constraints*. For a single objective the objective function is the measure of effectiveness to be optimised, such as the minimisation of total costs associated with the design of a denitrification barrier for example. The decision variables for this example consist of the barrier construction materials, barrier dimensions and barrier placement. The associated constraints could include bounds on all variables and situation dependent constraints (e.g. physical, financial etc). Maximum contaminant concentrations down-gradient of the barrier could either be included as constraints or as penalty functions in the optimisation formulation. Penalty functions would enable different costs to be associated with different down-gradient contaminant concentrations.

Groundwater management problems are frequently *non-linear* because of the coupling that exists between the groundwater flow equation and the contaminant transport equation. They are coupled in three ways. First, they are coupled through the velocity vector components which appear in the transport equation but which are obtained through Darcy's law. Second, they are coupled through the hydrodynamic dispersion tensor, which is a function of the groundwater velocity. Third, they are coupled through the fluid source/sink term that serves to add or extract both water and contaminant to or from the aquifer.

When complete certainty of prediction using the groundwater flow and contaminant transport simulation model is assumed, a *deterministic* remediation design/control problem can be formulated. Unfortunately, complete certainty of prediction is not possible in the real world. Under certain circumstances a problem involving uncertainty can be converted to a deterministic problem with the substitution of *expected values* for random quantities, or the application of *chance constraints* (see Section 1.3.2). Otherwise, a *stochastic* remediation

design/control problem can be formulated where uncertainty is categorised and reliability is incorporated.

1.2.3 Nitrate Contamination and Denitrification

The contamination of aquifers by *nitrate* is becoming widespread, due to the increasing use of inorganic fertilisers and disposal of organic materials (farmyard manure, slurry and septic-system effluent) on or beneath the land surface. Vehicles and coal/oil burning devices add to the problem by emitting airborne nitrogen compounds, which are deposited on the land in wet and dry forms. Nitrogen not used by plants or returned to the atmosphere is converted to nitrate in the soil, which is soluble in water and can easily leach to the water table.

High nitrate levels can potentially harm humans through contaminated drinking water. For example, high nitrate levels in drinking water have been associated with "blue baby" syndrome – a potentially fatal condition characterised by a reduced ability of the blood to carry oxygen (see *Fan and Steinberg,* 1996). Studies on animals have also indicated that reduction of nitrate into nitrites in saliva may contribute to the formation of nitrosamines in the body, many of which are carcinogenic, mutagenic, or teratogenic (*U.S. EPA*, 1973; *NAS*, 1978). High nitrate levels also promote eutrophication (the enrichment of natural waters with inorganic material such that they support excessive growth of plants and algae) in surface-water flow systems. Another negative impact of environmental contamination (including nitrate) is that it is becoming an increasingly important aspect of trade negotiations between different countries.

Once nitrate enters the groundwater system, the only major removal process is *denitrification* whereby organic carbon helps biodegrade nitrate to nitrogen gas. Denitrification occurs in circumstances where there is high soil moisture content, low oxygen availability, a ready supply of carbon and a source of nitrate. It is hindered by high levels of ammonia, high flow rates, a low chemical oxygen demand/nitrogen (COD/N) ratio, and the presence of toxic substances in the groundwater system. A *permeable reactive barrier* containing organic carbon matter and situated in the path of a nitrate-contaminated plume has been shown to be effective for denitrification.

1.2.4 Permeable Reactive Barriers

Permeable reactive barriers are installed as a *horizontal layer* to prevent contaminants reaching the water table or as a *vertical wall* for treating existing contaminated plumes in horizontally flowing aquifers. *Cutoff walls* (the funnel) can be added to direct a wide plume through a narrow but highly conductive barrier. This combination is known as the *funnel-and-gate* or *trench-and-gate* system. Various PRB examples can be seen in Figure 1.5**.** Barriers can be installed as permanent, semi-permanent, or replaceable units depending on their cost effectiveness. Natural gradient transports contaminants through the strategically placed treatment media. PRBs offer several important advantages over other remediation technologies. The PRB system:

- Protects the quantity of the down-gradient groundwater resource because it involves no groundwater extraction;
- Provides reliability of continued protection of the down-gradient water quality because it involves minimal operation and maintenance and requires no mechanical equipment;
- Minimises the impact to natural groundwater flow patterns;
- Provides a physical barrier between potentially impacted waters and down-gradient water users;
- Is not subject to freezing or power outages;
- Requires virtually no above-ground structures to interfere with existing or future site uses; and,
- Significantly simplifies monitoring and regulatory compliance issues.

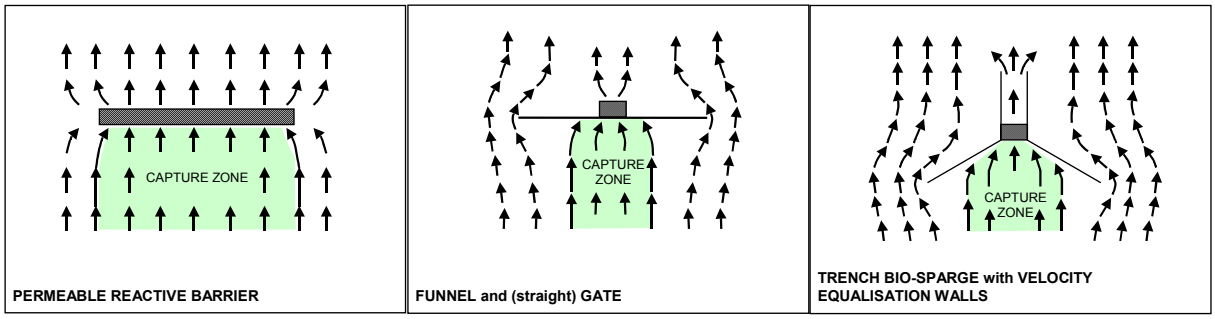

Fig. 1.5. Plan view of various PRB examples.

1.3 Literature Survey

In the last twenty years the field of simulation-optimisation groundwater management modelling has produced a continually increasing and improving body of literature. This is due to the fact that the remediation of contaminated groundwater is a hugely expensive task and so optimal management of the process is crucial to achieving results. Most of the research originates from the United States, where more than a billion dollars a year is spent on remediation projects via the U.S. Government's Superfund project. Superfund is the common name for the Comprehensive Environmental Response, Compensation and Liability Act (CERCLA) of 1980. This law was intended to clean up more than 1,000 hazardous waste sites across the United States and was to be funded mostly by a heavy tax on chemical and petroleum industries. However, only 12 percent of contaminated sites were cleaned up 12 years later, at a cost of US$11 billion. The average cost of a Superfund cleanup now exceeds US$25 million per site (*Davis*, 1995).

Most simulation-optimisation research has applied only to pump-and-treat systems. Pump-treat-inject is a more complex system to optimise. It was considered by *Ahlfeld et al.* [1988a] and *Dougherty and Marryott* [1991] but not fully examined until *Sun* [1995]. The decision variables are generally the well locations and the rate of pumping and/or injecting, and the objective is to minimise total cost or time required to achieve specific water quality standards. Although pump-and-treat systems are effective for containing contaminant plumes and removing contaminant mass, data from the past decade indicates that they are limited in their effectiveness for complete restoration (*Rorech and Morello*, 1995). In 1993 the (U.S.) National Research Council reported that pump-and-treat is neither a fast nor a cost-effective way to remediate contaminated groundwater, as the process requires continuous energy inputs for 10-200 years to achieve an acceptable level of restoration (*National Research Council*, 1993). As a result, these systems are being supplanted at many sites by "innovative technologies" including air sparging, reactive walls, pneumatic and hydraulic fracturing, bioremediation, vapour extraction and enhanced vapour extraction. Literature on the most promising of these technologies has emerged during the course of this project.

The earliest review of modelling methods (*Gorelick*, 1983) highlighted a number of important achievements. The application of finite difference and finite element methods to groundwater flow permitted complex, real world systems to be modelled. The use of linear and quadratic

programming allowed different management alternatives for these systems to be explored. *Gorelick and Voss* [1984] added to this literature with a simulation-optimisation methodology that included linear or non-linear objective functions subject to linear and non-linear simulation and water management constraints. The need to include non-linear constraints prompted the research of *Gorelick and Voss* [1984]. Non-linear constraints appear as a result of multiplying unknown concentrations and unknown velocity components from the advective and dispersive transport terms.

Groundwater quality management research since this time has proceeded in three main directions. Most deterministic simulation-optimisation research has been directed at reducing the computational burdens of the current state-of-the art simulation and optimisation formulations so they could be applied to field-scale problems. Stochastic simulation-optimisation research has attempted to understand and incorporate parameter uncertainty into the decision-making processes, so as to calculate more realistic remediation requirements. More recently Simulated Annealing (SA), Bayesian Decision Analysis, Tabu Search (TS), Genetic Algorithms (GAs) and Neural Networks (ANNs) have been introduced as alternative methods of finding the global optimum point without the computational burden created by classical optimisation algorithms. *Yoon and Shoemaker* [1999] compared eight different methods for groundwater bioremediation. They found that their chosen derivative-based method was the fastest on trial problems but an evolutionary algorithm displayed the most impressive combination of speed and accuracy.

1.3.1 Simulation-Optimisation Methods

1.3.1.1 Deterministic simulation-optimisation

Combined simulation-optimisation models have been a popular way to solve groundwater management problems. The mathematical model, expressing balance equations for water and contaminants, may be regarded as a constraint that must be satisfied at all times. Unfortunately, the only practical way to solve this model is by numerical simulation. Hence there is a need to combine the simulation of the groundwater system with the optimisation model. *Gorelick and Voss* [1984] were the first to publish research applying this approach to groundwater remediation. The optimising software MINOS (*Murtagh and Saunders*, 1987) was used, and has been in common usage since for non-linear problems. Other optimisation techniques such as the outer approximation (or relaxation) method (*Karatzas and Pinder*,

1993, 1996) and a combination of the cutting plane and primal methods (*Tucciarelli et al.*, 1998) have since been proposed for groundwater management problems. These methods were shown to be significantly faster than MINOS but were only presented with hypothetical problems.

A major hurdle between theory and application for simulation-optimisation models is the need to make the model as representative of the real system as possible while not making it so complex as to be unsolvable in a realistic time frame. Trade-offs explored in this area include the effects of modelling error (*Zhen and Uber* 1996), efficiency of model formulation and optimisation procedures, the modelling of groundwater flow in two rather than three dimensions, and the exclusion/inclusion of installation costs (*Sawyer*, 1992; *Sawyer et al.*, 1995; *Karatzas and Pinder*, 1993, 1996; *McKinney and Lin*, 1996b). Further research covered the choice of well locations from a pre-selected rather than continuous set (*Wang and Ahlfeld*, 1994), using time-invariant rather than time-variant pumping schedules (*Ahlfeld et al.*, 1988a; *Ahlfeld*, 1990; *Chang et al.*, 1992; *Culver and Shoemaker*, 1992), and optimisation in unconfined as well as confined aquifers (*Mansfield and Shoemaker*, 1999).

Application of deterministic optimisation to specific sites

Colarullo et al. [1984, 1985] formulated a dynamic model to design measures for hydraulically containing a contaminated plume travelling toward the city of Wichita in Kansas. The model contained a quadratic performance criterion based on the minimum total cost of pumping, subject to the physical and institutional constraints. The formulation worked well in theory but was too computationally inefficient to be applied to the field problem.

Atwood and Gorelick [1985] successfully applied a hydraulic-control formulation to a portion of the Rocky Mountain Arsenal site in Colorado. They kept their formulation simple by using a two-dimensional finite-difference simulation model, and assuming the location and rate for a single centrally located contaminant removal well.

Ahlfeld et al. [1988a, 1988b] applied sensitivity theory to their convective-dispersive transport equation, enabling them to solve field-scale problems with at least an order of magnitude less computational effort than when using perturbation methods. They used this approach to analyse alternate hypothetical remediation strategies at a Superfund site in Woburn, Massachusetts.

The most realistic use of simulation-optimisation models is often to analyse and compare different strategies rather than provide single solutions. *Ahlfeld et al.* [1995] reported on a site in coastal New Jersey where a finite-difference model was combined with optimisation to analyse remediation strategies. The constraints initially imposed by the decision-makers were shown to produce no feasible solution. The optimisation model was then used to analyse the trade-offs caused by the relaxation of constraints necessary to achieve a feasible operating strategy.

Xiang et al. [1996] presented an analysis of the remedial pumping design for a contaminated aquifer located in Ontario, Canada. The optimisation package NPSOL developed by *Gill et al.* [1986] was used to solve an optimisation problem complicated by multiple contaminants. Their results indicated that the specified cleanup levels control the performance of an optimisation algorithm based on gradient search, and that the objective function can be non-convex and non-smooth for some pumping schemes.

1.3.1.2 Stochastic simulation-optimisation

A mathematical model is only an approximate and simplified representation of a real world system. Many assumptions are usually made to create a solvable model. Because of the uncertainties inherent in groundwater parameters, deterministic optimisation models can be inadequate for effective remediation system design and operation. The amount of potential variation in uncertain parameters determines how the issue can be dealt with. If the potential variation to parameters will only result in small variations in constraints or the objective function then the substitution of the expected value for random quantities can be used to convert the stochastic problem to a deterministic one. If only the right-hand side of one (or more) of the inequality constraints is random, chance constraints can be efficiently applied. This approach can also convert stochastic problems into deterministic ones, given information on the cumulative distribution function (*Gorelick and Wagner*, 1987).

The uncertainty of groundwater parameters was first considered in a parametric linear programming groundwater problem using multi-objective decision-making (*Neuman*, 1973). The sensitivity of optimal well locations and pumping rates to the uncertainties in the correlated spatial variability of parameters such as transmissivity and storage coefficients was examined in simulation-optimisation models by *Aguando et al.* [1977] and *Gorelick* [1983, 1987]. *Gorelick* [1990] reviewed and compared progress on large-scale non-linear deterministic and stochastic formulations. He concluded that the ultimate formulations, from

the outset, should include all quantitative aspects of what we know and what we do not know in the simulation design process. The use of three-dimensional contaminant transport models rather than two-dimensional models and the use of stochastic rather than deterministic programming were strongly encouraged, despite the huge increase in complexity and size of such models. Gorelick also encouraged a further increase in model complexity to adequately deal with the case of decaying tracer migration represented in the contaminant transport equations.

Gorelick and Wagner [1987] presented the first published incorporation of parameter uncertainty into the decision-making process for optimal groundwater quality management. The objective was to optimise well site selection and pumping recharge rates to meet water quality standards at a particular reliability level. Their approach enabled modellers to estimate unknown aquifer parameters, quantify the uncertainty of the parameter estimates, simulate flow and transport responses, and automatically account for parameter uncertainty in the decision-making process through the simulation management problem. This procedure coupled three methods:

1) A finite element flow and transport simulation model combined with non-linear least squares multiple regression for simultaneous flow and transport parameter estimation.
2) First-order first and second moment analysis to transfer the information about the effects of parameter uncertainty to the management model.
3) Non-linear chance-constrained stochastic optimisation combined with flow and transport simulation for optimal decision making.

The methodology was demonstrated for steady state and transient aquifer reclamation design, and it was shown that remediation requirements could increase significantly due to variability in parameter estimates. Also stated was the need for intensive, repeated sensitivity simulations to gain enough information on the aquifer system to be confident of optimality despite the parameter uncertainty.

Wagner and Gorelick [1989] added to their previous research by explicitly incorporating the uncertainty due to spatial variability of hydraulic conductivity. More recently, *Freeze and Gorelick* [1999] and *Mylopoulous et al.* [1999] compared and contrasted stochastic optimisation and decision analysis as frameworks for the design of pump-and-treat systems. Both promoted combining the main advantages of the two methodologies; namely the determination of globally optimal solutions offered by stochastic optimization, and the

inclusion of all costs, benefits, as well as risks of failure due to uncertainties into a single objective function, as offered by decision analysis. Case studies were provided for illustrative purposes.

Hamed and Bedient [1999] presented a probabilistic modelling tool based on first- and second-order reliability methods (FORM and SORM) to account for parameter uncertainty in groundwater contaminant transport and remediation. The methodology was applied to analytical groundwater models to provide a simple screening tool for the assessment of contamination and pump-and-treat (or pump-to-contain) remediation.

Chance constraints

The use of chance constraints by *Gorelick and Wagner* [1987] followed the work of *Tung* [1986] in the related field of stochastic groundwater models for confined, homogeneous, and non-uniform aquifers. In this method certain constraints are not met exactly under all conditions, but instead are only met with a specified level of confidence. This is a useful technique for dealing with uncertainty in input parameters such as hydraulic conductivity and hydraulic gradient. *Ahlfeld and Mulligan* [2000] outlined an approach for characterising uncertainty in the value of hydraulic conductivity by representing it as a probability distribution.

Chance constrained models have the advantage that they are no larger than the corresponding deterministic models and thus are not too difficult to solve. However, they have the disadvantage that only the probability of violating a constraint is controlled, while the extent and consequences of a violation, when it does occur, are not taken into account. *Tiedeman and Gorelick* [1993] applied the approach of *Gorelick and Wagner* [1987] to a Superfund site near Lake Michigan. They found that the coefficient of variation in hydraulic gradient dictated whether the probabilistic constraints were obeyed. Their post-optimisation solute transport studies showed that increased reliability levels for hydraulic containment did not necessarily translate into faster plume cleanup times.

Morgan et al. [1993] introduced the mixed integer chance constrained programming solution method (MICCP) where uncertainty on both the left and right hand side coefficients was considered. Previous commonly used chance constrained techniques assumed that all the uncertainty was on the right-hand side of the optimisation. The method produced highly

reliable solutions to the groundwater management problem developed by *Gorelick* [1987] but at considerable computational cost.

Differential dynamic programming and feedback control

Andricevic and Kitanidis [1990] presented a stochastic dual control optimisation methodology for a pumping schedule to account for and reduce parameter uncertainty. This methodology had three components:

1) Differential dynamic programming for the solution of a deterministic problem.
2) Asymptotic approximation to a stochastic dual control problem so that parameter uncertainty is accounted for.
3) Parameter estimation or inverse modelling using the extended Kalman filter (EKF) which makes use of available measurements.

They compared this method to a deterministic feedback method created by eliminating parameter uncertainty from the problem formulation but updating the state estimate with a new measurement at the beginning of each time period. The results of Monte Carlo simulations showed that the dual control method performed better than the deterministic feedback method in terms of a lower average cost and standard deviation over all scenarios. *Andricevic and Kitanidis* [1990] concluded that the superior performance of the dual control solution was due to the fact that it takes advantage of the possibility to reduce the cost of operation by reducing the estimation error. The method was initially applied to a hypothetical one-dimensional bounded aquifer and was then extended to two-dimensional aquifer modelling by *Lee and Kitanidis* [1991]. The technique was further advanced by *Whiffen and Shoemaker* [1993], who added a non-linear weighted feedback law generated by the penalty function method coupled with differential dynamic programming. A significant advantage of this new method was that it allowed remediation planners to generate cost estimates with confidence measures, thus reducing the likelihood of cost overruns due to modelling errors.

Stochastic programming with recourse

Stochastic programming with recourse involves a two (or more) stage decision process. First a decision is made and implemented, then the reality of the situation unfolds. At a later stage recourse actions are taken, usually at some cost. The cost of a decision then consists of (1) a deterministic cost incurred “here and now” as the decision is put into effect, and (2) a stochastically distributed “wait and see” penalty or recourse cost, which is incurred after the

stochastic elements of nature are realised. In contrast with chance constraints, stochastic programming with recourse allows increasingly higher penalties to be incurred for increasingly larger violations of constraints. Recourse models are often much larger than the corresponding deterministic models, and require different solution techniques. However, due to advances in both stochastic optimisation methods and in computer technology, useful problems have been formulated and solved without excessive computer resources.

Wagner et al. [1992, 1994] published the first groundwater model to include the concept of recourse to account for costs due to unforeseen circumstances. They considered the approach and hypothetical problem analysed by *Gorelick* [1987] but removed his response matrix and added the concept of recourse. The recourse problem was solved using the extended finite generation algorithm (*Wagner*, 1988) and the sub-problems were solved directly using GAMS/MINOS (*Brooke et al.*, 1988). The model allowed considerable flexibility to the decision-maker in the representation of, and managerial response to, uncertainty. Solutions obtained to the hypothetical problem in general produced strategies involving less pumping than solutions obtained by a deterministic model. The stochastic solutions could be characterised as "wait-and-see" strategies, where initially a low cost plan is implemented with the intent of having money set aside to pay possible recourse costs.

Application of stochastic optimisation to specific sites

Model complexity and computer resource requirements have limited the potential of applying stochastic optimisation models to specific sites. *Gailey and Gorelick* [1993] published the first application to the Gloucester Landfill site, located near Ottawa, Canada. They used the groundwater quality management technique developed by *Gorelick and Wagner* [1987] to over-design the pumping rates so that possible design error is overcome. Analysis of the results indicated that design reliability could be increased from 50 to 90 percent by additional pumping. *Reichard* [1995] presented a new simulation/optimisation modelling approach that explicitly incorporated the uncertainty of surface water supplies. This model was applied to the Santa Clara-Callegus Basin in southern California. Model results indicated that control of seawater intrusion required significant reduction in water use, and that the current artificial recharge program was effective and would benefit from expansion.

1.3.1.3 Simulated annealing, Bayesian decision analysis and tabu search

Simulated annealing

Simulated annealing (SA) is a heuristic/probabilistic global optimisation method that has been applied to a wide range of problems. The basic algorithm uses a random search technique for locating candidate solutions, and a probabilistic criterion for accepting or rejecting those solutions that would not lead to improved configurations. The method derives its name from an analogy with the thermodynamic process of cooling solids. When a material is melted and allowed to cool slowly (anneal), a crystal lattice emerges that minimises the energy of the system. SA uses this analogy to search for "minimum energy" configurations of the decision variables, where energy is represented by the objective function value for a particular solution.

Compared with other optimisation techniques, its advantages include the capability of handling non-smooth objective functions and multiple remedial techniques, and the computational savings associated with not requiring functional gradients. On the other hand SA also has disadvantages; only a limited number of decision variables can be considered in the optimisation and computation time increases significantly as the maximum number of decision variables increase.

Simulated annealing was first presented by *Kirkpatrik et al.* [1983] for solving hard combinatorial optimisation problems. *Marryott* [1989] applied SA to a real-world remediation problem in a heterogenous, phreatic aquifer but encountered substantial computational requirements. *Dougherty and Marryott* [1991] and *Kuo et al.* [1992] used SA to generate optimal pumping schedules for a variety of simple hypothetical problems. *Marryott et al.* [1993] reported on the application of their previous work as post-mortem analysis on a pump-and-treat remediation system at a proposed Superfund site in central California. Their analysis found an improved design that had about 40 percent lower costs than the actual remediation design. To make the problem computationally feasible they reduced the Markov chain length which, in this case, reduced the number of simulations performed. This procedure reduced the likelihood of finding the global optimum solution so a balance was needed between the two conflicting requirements.

Marryott [1996] reported on the way in which SA was able to incorporate a number of different remedial technologies at the same time in the design process. New technologies could be added or subtracted at any time. This flexibility can lead to remedial design

strategies that are more consistent with field implementations where pumping is often combined with other technologies such as drains, slurry walls, low permeability caps or recharge of extracted water. These control technologies were included in hypothetical remedial design problems to illustrate the applicability of a simulated annealing formulation.

Rizzo and Dougherty [1996] extended the variable-length multiple-management-period approach of *Culver and Shoemaker* [1992] by replacing the deterministic optimiser with a modified simulated annealing algorithm. They used an importance function to bias well locations in areas of the domain where the information available suggested the most beneficial impact on the remediation of the contaminant plume. This method proved to be very efficient in providing good, though sub optimal, solutions to a field site at the Lawrence Livermore National Laboratory.

Bayesian decision analysis

Wijedasa and Kemblowski [1993] applied Bayesian statistical decision analysis as a global optimisation method to design a groundwater interception well for capturing a contaminated plume. The investigation was performed using two specific utility functions. These functions took into account the risk associated with not intercepting contaminated groundwater, the cost of pumping and treating the groundwater, and the cost of sampling and laboratory analysis. The optimal pumping rates obtained for the two utility functions were significantly different, and the commonly used quadratic form of the utility function seemed to give erroneous results. Although the technique was shown to work in theory, the choice of utility function was concluded to have a large impact on practical applications.

Tabu search

Tabu search (TS) is a global optimisation method based on the human memory process. The basic principle of TS is to maintain a list of recent transitions from solution to solution (not the solutions themselves). A tabu condition formed from the list of attributes of recently visited solutions is maintained and used to minimise repetition of computation and entrapment around local minima. *Zheng and Wang* [1999] presented an integrated tabu search/linear programming method for optimal pump-and-treat design. The deterministic form of TS was chosen although a probabilistic form also exists. The proposed benefits of this approach are adaptive learning (unlike GA and SA), the decomposition of a large problem into smaller sub problems, and the incorporation of a highly efficient forward-solution updating procedure. A two-dimensional example problem demonstrated these benefits.

1.3.1.4 Artificial neural networks and genetic algorithms

The Artificial Neural Network (ANN) approach was developed by analogy to the collective processing behaviour of neurons in the human brain (*Hopfield and Tank*, 1985). ANNs are designed to "learn" the complex relationships between parameters in the flow/transport model and the decision variables. Once this "knowledge base" is created, the ANN can replace the sequential calling of the flow/transport model during optimisation and link up with a search technique (such as a genetic algorithm) to find the optimal strategies. Although the ANN training, testing and verification processes can take considerable time and information, the research presented in this section shows that it has some advantages over conventional optimisation methods that sequentially call the flow/transport model. The ANN approach seems particularly suited to the more complicated problems, for example those that are discontinuous, highly non-linear and non-convex.

Genetic Algorithms (GAs) are random search techniques designed to mimic some of the most salient features of natural selection and natural genetics in order to find near-optimal solutions in a search space. They can be combined with conventional flow/transport numerical models, or an equivalent ANN as described above. As stated by *Goldberg* [1989], the structure of the GA differs from more traditional optimisation methods in four major ways:

1) the GA typically uses a coding of the decision variable set, not the decision variables themselves;
2) the GA searches from a population of decision variable sets, not a single decision variable set;
3) the GA uses the objective function itself, not derivative information; and
4) the GA uses probabilistic, not deterministic, search rules.

The second characteristic is especially important for multiple objective optimisation. Working with a population of decision variable sets makes it possible to optimise simultaneously for several solutions along the trade-off curve/surface.

Rogers [1992] provided one of the first published approaches to optimal groundwater remediation using artificial neural networks and a genetic algorithm in her Ph.D. thesis. This approach was further investigated in *Rogers and Dowla* [1994]. *Ranjithan et al.* [1993] presented a 2D ANN model incorporating the uncertainty due to the spatial variability of hydraulic conductivity. This was expanded to a 3D multi-phase model by *Rogers et al.*

[1995]. *Smalley et al.* [2000] proposed the relatively new "noisy" GA as a computationally efficient method for incorporating highly complex forms of uncertainty into remediation design.

Comparison of GA/ANN techniques with conventional optimisation techniques has been used to gauge research progress. *Ritzel et al.* [1994] applied a genetic algorithm to a multiple-objective groundwater contamination problem. They showed that the trade-off curve approximated the solution previously obtained by the mixed integer chance constrained programming solution method (MICCP) (*Morgan et al.,* 1993). *McKinney and Lin* [1994] compared a non-linear programming method to their GA in formulating and solving a pump-and-treat example problem, obtaining a similar solution with both methods. *Wang and Zheng* [1998] compared GA, simulated annealing (SA) and conventional non-linear techniques for three pump-and-treat example problems. They showed that the GA and SA methods produced nearly identical or lower cost solutions than conventional methods on all examples. The methods also provided more modelling options than conventional methods at the expense of increased computational effort. Hybrid methods combining conventional methods with GA or SA were considered worthy of future research. *Aly and Peralta* [1999a] compared an integer non-linear programming method to their GA in formulating and solving pump-and-treat example problems. The GA performed as well or better than mathematical programming (in terms of the objective's numerical value) for all tested problems when response functions were used for each.

Application of ANN/GA techniques to pump-and-treat problems has been presented by *Johnson and Rogers* [1995], *Wang and Zheng* [1997] and *Aly and Peralta* [1999b]. *Smalley et al.* [2000] applied a Noisy GA within a risk-based corrective action (RBCA) framework to an *in situ* bioremediation design case study.

McKinney and Lin [1996a] studied the performance of GAs when solving optimal aquifer remediation design problems. Their results indicated that GA models with decision variables encoded as short strings of binary digits (rather than real numbers), large population sizes (150~200), high multiple-point crossover probabilities (0.6~0.8), small mutation probabilities (0.01~0.1), and tournament selection, provide optimal performance for the example problems considered. They also identified three main difficulties with current models:

1) Premature convergence;

2) Difficulties in choosing the most appropriate parameters and approaches for the GA model as these are often problem specific;
3) Inability to perform local hill climbing as GAs search for the optimal solution by manipulating the high performance schemata in the population instead of focusing on individual strings. A potential solution to this problem involved a hybrid method suggested by *Holland* [1975]. This method combined an initial GA search followed by a gradient-based approach for the high performance regions of the solution space.

Reed et al. [2000] summarised recent development of theoretical relationships for population sizing and timescale analysis that increased the efficiency of GA methods. Application of the method to a monitoring design test case identified robust parameter values in significantly fewer runs than standard trial-and-error methods. *Erickson et al.* [2002] studied the sensitivity of a niched Pareto genetic algorithm to population size, tournament size and niche radius for a hypothetical pump-and-treat situation. This approach uses the concept of "fitness sharing" to maintain diversity within the Pareto optimal set (that is, the locally non-dominated set, which is drawn from the current population). The "shared fitness" of an individual is a function of the "distance" between individual solutions and the minimum desired "distance" between "niches". *Erickson et al.* [2002] found that the performance of this algorithm compared favourably to the performance of a single objective genetic algorithm and a random search method for three scenarios.

1.3.2 Denitrification

Nitrate (NO_3) is found in shallow groundwater as a result of soil leaching (see Appendix A). Nitrate accumulates in soils due to the activities of nitrogen fixing plants (legumes), decomposition of plant debris, animal waste and nitrogen based fertilisers. Nitrate as Nitrogen (NO_3-N) levels in groundwater can range naturally between 0.1 and 10 mg/l. Increased levels result mainly as a product of intensive agriculture and high fertiliser application rates. The issues associated with nitrate contamination internationally and in New Zealand have been well-documented (e.g. *Lincoln Environmental,* 1997).

The potential for the removal of nitrate from wastewater by bacterial reduction coupled with the oxidation of organic carbon matter has been recognised for several decades. Various solid, liquid and gaseous carbon sources have been evaluated over the years. These include sawdust, cellulose, whey, cracked corn, straw, marl, pelletized jute, kitchen wastewater,

ethanol, biogas, methanol, sucrose, and acetic acid (see *Boussaid et al.*, 1988; *Mateju et al*., 1992; *Vogan*, 1993; and *Wakatsuki et al.*, 1993).

Liquid carbon sources such as methanol and ethanol generally result in the highest rate of denitrification and are used routinely to remove nitrate from agricultural and municipal wastewater (e.g. *Grady and Lim*, 1980; *WPCF*, 1983). The techniques are not generally feasible in the farm-field environment, though, because of their relatively large capital costs and maintenance requirements. More recently, nitrate removal by hydrogen-coupled denitrification has also been proposed using flow-through, packed-bed bioreactors. Application to drinking water supplies (e.g. *Smith et al.*, 2005) and *in situ* groundwater remediation have been proposed (*Haugen et al.*, 2002).

The advantages of a simple bioreactor containing solid organic carbon for *in situ* denitrification are its low cost and ability to operate virtually maintenance-free for many years. The use of solid organic carbon for passive *in situ* denitrification was first presented by *Stewart et al.* [1979] for septic systems and by *Boussaid et al.* [1988] for nitrate-contaminated drinking water supplies. *Blowes et al.* [1994] later proposed the use of organic carbon for nitrate removal from agricultural drainage. Granular iron (*Gandhi et al.*, 2002) and sulphur granules combined with autotrophic sulphur-oxidizing bacteria (*Moon et al.*, 2004) have also been shown to effectively degrade nitrate contamination. Other proposed denitrification technologies include reverse osmosis, ion exchange and catalytic reduction (*Centi and Perathoner*, 2003). The Interstate Technology and Regulatory Council has produced a systematic approach to nitrate remediation (*ITRC*, 2002b).

Mathematical modelling and numerical simulation are very important considerations when optimising a process such as denitrification. *Baveye and Valocchi* [1989] presented an overview of mathematical models that describe the transport of biologically reacting solutes in saturated soils and aquifers. *Van der Hoek et al.* [1988] developed a mathematical model to describe the combined ion exchange/biological denitrification process for nitrate removal from groundwater. They showed that it is possible to optimise the procedure by introducing a buffer in the regeneration circuit after the ion exchange column. With this configuration, nitrate limitations that resulted in low denitrification reactor capacities can be avoided.

Kinzelbach et al. [1991] proposed a model specifically for the natural and enhanced denitrification processes in aquifers. It described the interactive transport of oxygen, nitrate,

organic substrates (e.g. organic carbon) and microbial mass in two spatial dimensions, including the possibility of diffusion-limited exchange between different phases in the aquifer. *Zysset et al.* [1994] presented a one-dimensional macroscopic model for the transport of dissolved substances in groundwater-biofilm systems. Their model was able to reproduce the transport of nitrate (acting as a dissolved electron acceptor) in two different laboratory column experiments (*von Gunten and Zorbrist*, 1992, 1993). A one-dimensional soil column simulation model was used by *Shouche et al.* [1993] to optimise the injection of acetate via a well into a nitrate-contaminated plume. The optimal injection strategy reduced microbial biomass accumulation around the well by an order of magnitude over the base case, thus extending the life of the well.

Commercial and free software packages are now available to model the flow and transport of reactive solutes in up to three dimensions. *Wang et al.* [2003] modified the FEMWATER model to simulate multiple reactive solute transport, and then successfully applied it to the simulation of a nitrate and chloride contaminated plume near Taupo in New Zealand. FEMWATER (*Lin et al*., 1996) contains a finite element numerical program developed for simulating three-dimensional water flow and single species solute transport. The FEMWATER model was chosen because it had the required level of complexity, except for the ability to model more than one reactive solute, and had freely available source code.

Determining the correct denitrification rate function is a very important part of denitrification wall design. Research into factors affecting denitrification rate has been undertaken from the perspectives of soil science, field and laboratory studies, and analysis of denitrification technologies in the field. An understanding of naturally occurring denitrification processes (e.g. *Korom*, 1992) is important when considering the performance potential of constructed denitrification barriers. Denitrification rate dependencies that may affect denitrification walls are described below. The detail of denitrification wall field trial research is presented in Section 1.3.3.4.

- The order of the denitrification reaction seems to be affected by nitrate and substrate concentrations. At high nitrate concentrations, the diffusion of nitrate becomes an important factor to the determination of order (*Phillips et al.*, 1978). For example, *Bowman and Focht* [1974] demonstrated first order kinetics at low concentration, which became zero order at higher concentrations. *Bowman and Focht* [1974] recognised that

the kinetics of denitrification must reflect both substrate (e.g. carbon) and nitrate availability. For example, multiple-Monod kinetics was found to be appropriate for biodegradation reaction processes that involve several solutes (*Kinzelbach et al.* 1991). *Pauwels et al.* [1998] presented first order nitrate degradation coefficients for field tracer tests. *Haugen et al.* [2002] presented first and second order nitrate degradation coefficients for laboratory experiments using a membrane module with hydrogen gas as the electron donor. *Korom et al.* [2005] presented apparent zero order denitrification rates for field tracer tests.

- If the nitrate concentration is sufficiently small, it may become the limiting part of the reaction. Dissimilatory nitrate reduction to ammonium may occur instead for denitrification in a nitrate limited environment (*Korom*, 1992). Denitrification rates using a reactive material containing sawdust as the energy source have been measured in a laboratory column study by *Vogan* [1993], and in field trials by *Robertson and Cherry* [1995], *Robertson et al.* [2000], *Schipper and Vojvodic-Vukovic* [1998, 2000, 2001], and *Fahrner* [2002].

- An environment without oxygen (anaerobic) is ideal for denitrification; the denitrification rate will decrease with increasing oxygen concentration as oxygen affects both the activity and synthesis of the denitrifying enzymes (*Knowles*, 1982). The oxygen concentration is affected mainly by the soil texture, moisture content, and temperature. *Tiedje* [1988] showed a dramatic drop in denitrification rate with a slight increase in oxygen concentration for a soil core experiment.

- The main effect of temperature on the denitrification process is on biological activity. At low temperatures, denitrification decreases markedly but is measurable between 0 and 5ºC (*N.A.S*, 1978). As temperature increases up to a maximum of 65^{o}C (*Nommik*, 1956), the rate of denitrification increases due principally to increasing biological activity but also to reducing oxygen solubility. The reducing oxygen solubility with increasing temperature also causes the denitrification reaction to produce increasing proportions of N_2 and decreasing proportions of N_2O. *Volokita et al.* [1996] reported a linear relationship between nitrate removal and temperature between 19 to 30°C for cotton-supported heterotrophic denitrification. This linear relationship was not observed after 30°C by *Della Rocca et al.* [2005] in subsequent experiments.

- The supply of organic carbon influences denitrification directly by supplying the necessary substrate for growth, and indirectly through the consumption of oxygen by other micro-organisms that deplete oxygen in the soil (*Rolston,* 1981). Dentrification is still more likely than dissimilatory nitrate reduction to ammonium when organic carbon supplies are limiting (*Korom*, 1992). The type of carbon source has a large effect on the denitrification rate. Carbon sources such as methanol, where the carbon is readily available, produce much greater denitrification rates than carbon sources like sawdust where the carbon must dissolve before it can provide an energy source for denitrifying bacteria. *Carmichael* [1994] found that the surface area of sawdust did not have a significant effect on the rate of denitrification.

- The system pH is not a serious limiting factor in the denitrification process. Denitrification has been shown to occur from pH 4 to pH 11 with maximum rate between pH 6 and 8 (*Firestone*, 1982). *Fahrner* [2002] showed significant nitrate reduction in a denitrification wall with pH of 6.0 and an even lower pH in the surrounding aquifer. However, pH was found to have a more marked effect on denitrification of high strength waste waters (2700 mg/l NO_3-N), where *Glass and Silverstein* [1998] found significant inhibition of denitrification when the pH was 6.5 or 7.0. The effect of pH on the nature of gaseous products by denitrification may also be important. In acidic material the predominant gases would be NO and NO_2, while in neutral or alkaline material N_2O and N_2 would be predominant (*Bollag et al.*, 1973).

- The presence of high concentrations of ammonium may reduce the rate of denitrification (*Steingruber et al.*, 2001). Plumes containing both ammonia and nitrate are documented in the literature (e.g. *Smith and Duff*, 1988; *Ptacek*, 1998).

- The presence of high concentrations of certain toxic substances may hinder the denitrification process (*Garrido*, 1998). It may be necessary to remediate these other substances before denitrification is worth considering.

Research has also been undertaken on the effect of total versus extractable soil carbon on denitrification rates (*Stanford et al.*, 1975), the comparison of different denitrification processes and carbon sources (*Mateju et al.*, 1992), and on denitrification rate measurement

techniques (e.g. *Smith and Duff*, 1988; *Bragan et al.,* 1997a, 1997b; *Well et al.*, 2003; *Smith et al.*, 2004).

1.3.3 Permeable Reactive Barriers

A permeable reactive barrier (PRB) is a passive *in situ* treatment zone of reactive material that degrades or immobilises contaminants as groundwater flows through it (see Section 1.2.4). Permeable barriers are installed as a horizontal layer to prevent contaminants reaching the water table or as a vertical wall for treating existing contaminated plumes in horizontally flowing aquifers. Cutoff walls (the funnel) can be added to direct a wide plume through a narrow but highly conductive barrier. Natural gradient transports contaminants through the strategically placed treatment media.

McMurty and Elton [1985] introduced the concept of combining cutoff walls and *in situ* reactors. Since this time most of the research has come from people at, or associated with, the University of Waterloo in Ontario, Canada. There have been many applications at research and commercial sites using PRBs to remediate a variety of contaminants. The rest of this section of literature survey will focus on the development of PRB technology and its application to the remediation of nitrate contaminated groundwater.

The potential of the *in situ* reactive wall as a viable alternative to pump-and-treat was presented by *Blowes and Ptacek* [1992], *Burris and Cherry* [1992] and *Gillham and Burris* [1992]. *Starr and Cherry* [1994] and *Christiansen and Hatfield* [1994] extended this technology to include cutoff walls. *Starr and Cherry* [1994] named it the funnel-and-gate system, and used two-dimensional computer simulation to illustrate the effects of cutoff wall and gate configuration on capture zone size and shape, and on the residence time for reaction of contaminants in the gate. *Vidic and Pohland* [1996] presented an early review of the technology and its potential. *Sedivy et al.* [1999] proposed that cut-off walls bent at right angles in an up-gradient direction could improve hydraulic capture efficiency for certain PRB designs. It also improved the homogeneity of the flow lines entering the gate.

Bowles et al. [1995] redesigned the funnel-and-gate technology for use in low hydraulic conductivity sediments such as glacial till. Modifications included the addition of an up-gradient high hydraulic conductivity trench and a down-gradient infiltration gallery. This technology was named the trench-and-gate system and a pilot scale version was installed at a

remediation site in Alberta, Canada. Results after a year of operation suggested improvements in the capture zone size over an equivalent funnel-and-gate system.

Wilson and MacKay [1995] proposed the use of passive interceptor wells as a PRB. Single or multiple rows of wells are installed across a contaminated plume. Interception of the plume is achieved by the cumulative effects of convergence of groundwater flow to open wells from the up-gradient direction and subsequent divergence of groundwater flow down-gradient from the wells. Reactants or nutrients, which induce or enhance degradation reactions, are introduced to the groundwater via the wells. This results in a decrease in contaminant concentration down-gradient of the interceptor wells. The main limitations of passive interceptor wells are the clogging of the aquifer around the injection wells and/or transport limitations of reactants to locations of contamination. *ITRC* [2000] presented an overview of this technology and *Hyndman et al.* [2000] showed that this technology could be applied in a cost-effective manner to a full-scale remediation project in Michigan.

Yang et al. [1995] investigated the feasibility of PRBs and offered some alternative designs. These included a dual-trench system, trickling filter system and a soil flushing system. The dual-trench system served a different purpose to the multiple reactor system of *Starr and Cherry* [1994] in that it utilised a portion of unexcavated soil between two small trenches. Trickling filters are a similar concept to the horizontal PRB and are widely used in facilities for biological wastewater treatment. The soil flushing system is an adaptation of the pump-treat-inject system. The systems were tested by computer simulation and field trials were expected to follow.

Christodoulatos et al. [1996] extended the funnel-and-gate technology by adding an air sparging system and a set of parallel-flow-field-equalisation-walls down-gradient of the reactor as an extension to the funnel. Air sparging involves pumping air into the saturated zone to help flush (bubble) the contaminants up into the unsaturated zone. An added benefit of air sparging is that it provides an oxygen source that helps stimulate the bioremediation of some contaminants (but not nitrate). The combination of the funnel-and-gate system with air sparging creates a technology that has the potential to remediate groundwater contaminated with solvents and other volatile organic compounds (VOCs). The equalisation walls were proposed as a way of mitigating velocity variations in the reactor that were observed during computer modelling of a funnel-and-gate system. Such velocity variations result in variable contaminant residence times that may inhibit the effectiveness of the reactor. As well as

reducing velocity variations, the walls were shown to increase residence times. Both these factors will increase the potential effectiveness of the reactor.

Jefferis et al. [1997] presented a case history where site geology and circumstances caused them to create a new version of the funnel-and-gate system (see Figure 1.6). *O'Brien et al.* [1997] successfully implemented a very similar system at an old mill site in California, U.S.A.

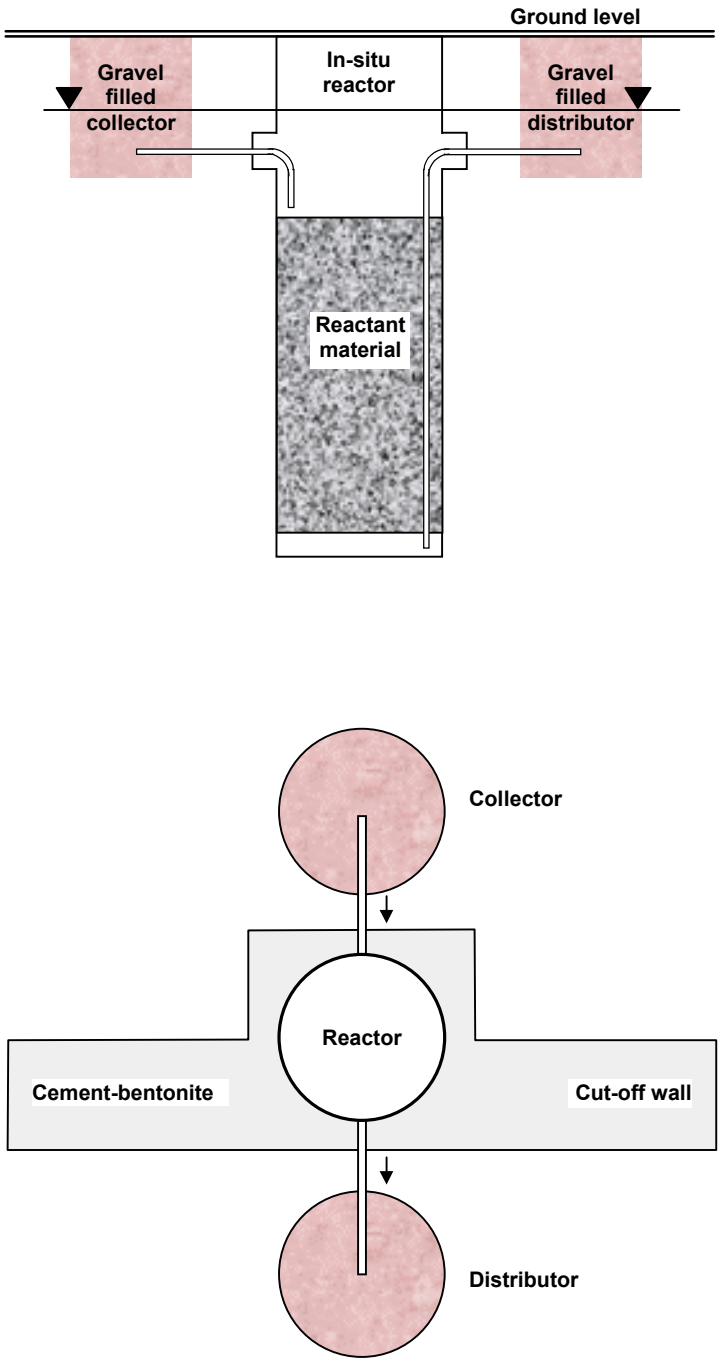

Fig. 1.6. The funnel-and-gate system of Jefferis et al. [1997].

The main design constraints in *Jefferis et al.* [1997] were the proximity of the contaminant source to a road, large seasonal variations in the water table, the risk of damage to nearby buildings if sheet piling was used, and the relatively low permeability and heterogeneity of the soil. A cement-bentonite cut-off wall containing the reactor was placed in the path of the contaminated plume. The flow to the reactor was piped from a highly permeable collector upstream of the wall. The remediated product was then piped downstream to a highly permeable distributor. Early results from this application were promising.

Day et al. [1999], *Meggyes and Simon* [2000] and *Benner et al.* [2001] detailed a variety of geotechnical techniques for the construction of PRBs. *Fiorenza et al.* [2000] tested combinations of several technologies for the remediation of chlorinated hydrocarbons. These technologies included:

- sequential *in situ* treatment using granulated iron and ORC^{TM} (oxygen-releasing compound);
- intrinsic remediation—use of natural attenuation to reduce environmental risk posed by groundwater contamination;
- sequential anaerobic–aerobic bioremediation; and
- *in situ* sequential treatment using granulated iron and oxygen sparging.

Based on the results of the study, the team designed and costed two hypothetical full-scale sequential permeable reactive barriers (SPRB). The SPRB designs and costs were compared to pump-and-treat systems designed to capture the same dimensions.

The choice of a funnel (impermeable barrier) that is cost effective and appropriate to the remediation site is an important aspect of optimising a PRB design. *Pearlman* [1999] conducted a global survey and comparison of impermeable barrier options, showing the potential for funnel emplacement in a wide variety of geological situations.

Simon et al. [2001] proposed increases in efficiency and long-term performance of PRBs by incorporating electrokinetic techniques to prevent barrier clogging and developing new reactive materials (natural zeolites, surface modified minerals). Their research found that an electric field applied upstream of the barrier may be able to reduce the amount of groundwater constituents that might impair the barrier function by coating or clogging through precipitates.

Czurda and Haus [2002] presented similar research which combined a reactive zone containing fly ash zeolites and down-gradient electrokinetic techniques.

1.3.3.1 PRB modelling considerations

The use of computer models can greatly assist in the search for optimal PRB designs. Three aspects of the system require modelling: the hydrogeologic (groundwater flow), geochemical (chemical reactions), and economic (construction and operational costs). These aspects can be modelled by a single combined model or by coupled independent models. The specific requirements and recommendations for permeable barrier simulation models include the following:

- 3D hydrogeologic models are ideal although 2D models can be more efficient where the site does not have significant vertical flow gradients and only fully penetrating PRBs are considered.

- The hydrogeologic model should be able to simulate large contrasts in hydraulic conductivity at the funnel walls. It should also be capable of incorporating grid blocks of variable size so that the area around the funnel and gate can be simulated more accurately than the surrounding areas.

- The hydrogeologic model should also be able to handle site complexities that may cause preferential flow pathways, groundwater sources, or groundwater sinks. These complexities include site heterogeneities, streams, drains, tunnels, and wells.

- The geochemical model needs to include both solute transport (including advection and dispersion) and the necessary chemical reactions. Contaminants such as heavy metals require a much more complex geochemical model than contaminants such as nitrate. This is because many simultaneous reactions occur in the attenuation of heavy metals whereas denitrification is assumed to involve only a single reaction.

- The economic model is generally the most straightforward as its job is to calculate the present value of the construction and operational costs for a particular PRB design. The model does need to be able to handle some complexities, though, such as piece-wise functions for construction techniques.

A large number of computer simulation codes are now available to solve theoretical and/or applied PRB problems. Choosing the right code for the problem is a matter of balancing the often-conflicting objectives of applicability, availability, price, ease of use, user support, and availability of source code if adjustments need to be made. A few of the more popular codes are discussed below.

1.3.3.2 Hydrogeological and geochemical modelling software in PRB design

Perhaps the most versatile and widely used groundwater modelling code has been **MODFLOW** (*McDonald and Harbaugh*, 1988). The latest version of this software is called **Visual MODFLOW** (*Guiguer and Franz*, 1996). The results from MODFLOW have been used in particle tracking codes such as **MODPATH** (*Pollock*, 1989) to calculate groundwater paths and tracking times. Additional simulation modules such as the **Horizontal Flow Barrier (HFB)** package (*Hsieh and Freckleton*, 1993) can link up with MODFLOW to perform additional tasks. The HFB package negates the need for MODFLOW users to represent a funnel by very thin cells with low hydraulic conductivity (K). It permits the user to assign the sides of certain cells as planes of low K, while still using a larger cell size at the funnel walls. Another useful module for funnel-and-gate design is the **Zone Budget** package (*Harbaugh*, 1990), which can be used to evaluate the volumetric flow through the cell for various design scenarios.

MODFLOW has already been used for PRB design at sites that include one in Sunnyvale, California (*PRC*, 1996); the Sommersworth Sanitary Landfill, New Hampshire; an industrial facility in Kansas; and GE Appliances, Wisconsin (*Gavaskar et al.*, 1998). MODFLOW has been used in conjunction with other modules, such as RWLK3D and MT3D. **RWLK3D** (*Naymik and Gantos*, 1995) is a 3D transport and particle-tracking code based on the Random Walk Approach to solute transport simulation. It has been used to simulate particle movement for the pilot-scale permeable cell installed at Moffett Federal Airfield (*Battelle*, 1996). **MT3D** (*Zheng*, 1990) is a 3D transport model for simulation of advection, dispersion and chemical reaction of contaminants in groundwater systems. It uses a mixed Eulerian-Lagrangian approach to the solution of the 3D advective-dispersive-reactive equation for a single contaminant.

A 2D, steady-state, groundwater flow model, **FLOWPATH** (*Waterloo Hydrogeologic, Inc.*, 1996), also has documented use at remediation sites (see *Gavaskar et al.*, 1998). These sites

include one in Belfast, Northern Ireland; Fairchild Air Force Base, Washington; and the DOE Kansas City site, Kansas.

FRAC3DVS (*Therrian and Sudicky*, 1995) is a 3D, finite-element model for simulating steady-state or transient, saturated or variably saturated groundwater flow and advective-dispersive solute transport in porous or discreetly fractured porous media. FRAC3DVS is a very powerful model and has already been used at sites containing porous or discreetly fractured porous media.

FEMWATER (*Lin et al*., 1996) contains a finite element numerical program developed for simulating three-dimensional saturated-unsaturated groundwater flow and single species solute transport. *Wang et al.* [2003] modified the FEMWATER model (renamed **FEMWATER-N**) to simulate multiple reactive solute transport, and then successfully applied it to the simulation of a nitrate and chloride contaminated plume near Taupo in New Zealand. This code shows great promise for the simulation of denitrification barriers. It is complex but efficient, containing a geochemical model of nitrate advection, dispersion and degradation.

1.3.3.3 PRB design considerations

Waller [1994] proposed a generalised design basis for PRB systems. A number of important simplifying assumptions hinder the applicability of this approach. The design basis only applies to fully penetrating PRB systems with no impermeable walls or funnels and the same hydraulic conductivity as the surrounding aquifer. The maximum expected contaminant concentration must be used to design the PRB flow-through distance as a plug flow reactor design is used. This design assumes there is no variation in concentration perpendicular to flow. The contaminant degradation process also assumes first order kinetics.

Starr and Cherry [1994] used a 2D, plan-view, steady-state flow simulation program, FLONET (*Guiguer et al.,* 1992). They investigated the effects of funnel-and-gate geometry (design) and reactive cell hydraulic conductivity (K_{gate}) on the size and shape of capture zone, the discharge groundwater flow volume through the gate, and the residence time in the reactive cell. Only fully penetrating barrier systems were simulated, as hanging systems require a 3D model. The following conclusions were made by these researchers based on simulation of several scenarios:

- The width of the capture zone produced by a funnel-and-gate system is proportional to the discharge through the gate. Increasing the width, length and hydraulic conductivity of the gate and the width of the funnel can increase this discharge. A unit increase in gate width increases the gate discharge significantly more than a unit increase in funnel width.

- The 180-degree (straight) funnel produces the largest capture zone for any single flow direction, but it does not produce the largest composite capture zone if flow directions fluctuate.

- Balance between maximising the size of the gate's capture zone and maximising the retention time of contaminated groundwater in the gate must be achieved. In general, capture zone size and retention time are inversely related. For example, discharge through the gate (of a given design) increases significantly as $K_{gate}/K_{aquifer}$ increases up to $K_{gate}/K_{aquifer}$ =10. However, reactive material with high hydraulic conductivity usually has large grain size and hence low surface area-to-mass ratios. This generally results in lower reaction rates and shorter residence time. To rectify this situation the residence time could easily be increased (without substantially affecting the capture zone) by making the gates longer in the direction of groundwater flow.

Hatfield et al. [1996] presented a new analytical non-equilibrium model for contaminant transport in saturated, non-homogeneous or mixed porous media. The model was used to determine critical hydraulic residence times achieving desired contaminant removals in funnel-and-gate systems. Residence time information was then used with the hydraulic design model of *Christiansen and Hatfield* [1994] and *Howard et al.* [1995] to size and dimension hypothetical funnel-and-gate systems.

Focht et al. [1997] linked the determination of barrier thickness via the barrier hydraulic residence time to the need for accurate determination of groundwater flow velocities. They presented the results of attempts to measure the groundwater flow velocity through two pilot-scale *in situ* treatment zones, comparing a bromide tracer test, calculations using water table measurements, a mathematical model, and a heat-pulse velocity meter. The results varied considerably between methods, with the velocity meters showing the greatest promise. Seasonal fluctuations were also shown to be an important consideration for the chosen sites.

Shikaze [1997] also produced a substantial modelling evaluation of the funnel-and-gate system. He used the FRAC3DVS code to examine 3D-groundwater flow in the vicinity of a partially penetrating (hanging) funnel-and-gate system for 16 different combinations of parameters. These parameters were the ratio of K_{gate} to $K_{aquifer}$, the ratio of single funnel wall to depth of funnel-and-gate, the ratio of total funnel wall width to the gate width, and the hydraulic gradient. In addition to replicating many of the conclusions of *Starr and Cherry* [1994], but for a 3D system, Shikaze also arrived at the following conclusions:

- Absolute discharge through the gate increases as the hydraulic gradient increases. However, there is minimal effect on relative discharge or on the size of the relative capture zone.

- Increasing the ratio of single funnel width to funnel-and-gate width decreases the absolute discharge, relative discharge, and capture zone size. This is because an increasing amount of flow is diverted under the funnel rather than through the gate.

Using a numerical model, *Smyth et al.* [1997] also identified the need to balance the length-of-funnel to width-of-gate ratio. If the ratio is too high, groundwater flow may submerge beneath or travel around the system, resulting in contaminants bypassing the reactant material. They concluded that the hydraulic efficiency of permeable walls, and by inference passive well systems, appeared to be more favourable than funnel-and-gate systems for intercepting contaminated groundwater plumes. This was particularly the case where only partial penetration of the aquifer could be achieved. However, they accepted that hydraulic performance was only one aspect of the PRB design decision.

Warner et al. [1998] presented the considerations that may be important in designing a monitoring program for a permeable reactive barrier system. In particular they stressed the need for system designs that minimised the potential occurrence of non-uniform flow in the barrier. A barrier with non-uniform flow would require a more complex sampling system and greater number of sampling points than a barrier with uniform flow. Precautions to minimise non-uniform flow within the barrier include a homogeneous mixture and careful trade-off between capture zone and the barrier hydraulic conductivity / aquifer hydraulic conductivity ratio (*Benner et al.,* 1997, 2001).

Gavaskar et al. [2000] presented a PRB design guidance document for chlorinated solvent remediation that focussed on advances in the technology since their previous document in 1997. Some of this information was also presented in *Gavaskar* [1999] and *Gupta and Fox* [1999].

Excavation using backhoes, continuous trenchers, augers, or caissons was found to achieve accurate gate installation. The increasing use of biodegradable slurry (instead of sheet piles or cross-bracing) to stabilise the excavation was found to increase the convenience and safety of installing the reactive media in the ground. However, these excavation methods have varying depth limitations (generally between 9 and 15m below ground surface). Innovative installation methods, such as jetting, hydraulic fracturing, vibrating beam, deep soil mixing, and the use of mandrels, had been tested at some sites and offer potentially lower-cost alternatives for installing reactive media at greater depths (e.g. *Savoie et al.*, 2004). The practice of installing zones of high conductivity (using pea gravel) at the up and down-gradient faces of the gate was tested and found to provide only marginal benefit in homogenising influent flow and contaminant concentrations.

The authors also found that the economics of a PRB application depend largely on the useful life (longevity) of the reactive media, especially when treating plumes that are expected to persist for several years or decades. In the absence of reliable longevity predictions (given the relatively short history of PRB applications), this document suggests that multiple longevity scenarios be evaluated to place long-term PRB application costs (and benefits) in the context of varying life expectancies of the reactive medium.

A wide range of PRB applications was analysed. The authors concluded that:

- To date, most of the PRBs have used granular iron medium and have been successfully applied to address chlorinated volatile organic compound (CVOC) contaminants. The tendency of CVOCs to persist in the environment for several years or decades makes them an obvious target for a passive technology.
- Metals amenable to precipitation (e.g. hexavalent chromium and uranium), under the reducing conditions created by the common iron medium, have been the next most common targets. One concern is that, unlike CVOCs, metals do not degrade but instead accumulate in the reactive medium. At some point in time, the reactive medium (containing the precipitated metals) may have to be removed and disposed of. With

CVOCs, even after the PRB performance has declined, it is possible that the reactive medium can just be left in the ground.

- Although many initial applications were pilot-scale PRBs, most recent applications have been full-scale, indicating that confidence in this technology has grown.
- At sites where target cleanup levels have not been achieved in the down-gradient aquifer, the reason has generally been the inability of the PRB to achieve the designed plume capture or residence time, rather than the inability of the reactive medium to replicate laboratory-measured reactivity (contaminant half-lives) in the field.
- PRBs have been applied at sites with groundwater velocities (in the aquifer) reported at 0.0001 to 0.9 m/day.
- Although most PRB applications used iron as the reactive medium during the initial use of this technology, the use of other innovative media has been investigated in recent years at some sites.
- More of the recent applications have been configured as continuous reactive barriers rather than funnel-and-gate systems. One reason for this is that the unit cost of iron medium has declined from US$650/ton to about US$300/ton, plus shipping and handling. Although, in theory, the same amount of iron should be required for a given mass of plume contaminants, the heterogeneous distribution of the contaminant concentrations in the plume makes the amount of iron required in a uniformly thick continuous reactive barrier somewhat inefficient. However, the lower cost of iron and other benefits make continuous reactive barriers more attractive. Benefits of continuous reactive barriers include easier design and construction, and a propensity to generate less complex flow patterns.

In defence of funnel-and-gate systems, *Ott* [2000] presented the following reasons for considering the use of funnels even when the reactive material is relatively inexpensive (e.g. sawdust):

- Continuous trenches require media to be spread across an entire plume, while funnel and gate systems localise media in the gate area. The overall wall system is usually larger for a funnel and gate, but the amount of reactive media used is usually less. Zero-valent iron, the most common reactive material, is significantly more expensive than impermeable barrier materials such as sheet piling.
- Media in a localised gate is easier to maintain than that spread across a large trench.
- Monitoring costs are lower as a smaller down-gradient effluent area is created.

- Influent contaminant concentrations can be homogenised by upstream mixing so that reactive materials are not wasted on areas of low contaminant concentration.

Benner et al. [2001] showed how thicker barriers (required for funnel-and-gate PRBs) will have a more significant dampening effect on flux heterogeneities in the surrounding aquifer than the equivalent thinner continuous PRB. The addition of a funnel may therefore be especially beneficial for large and/or complex plumes and heterogenous aquifers. *Benner et al.* [2001] also investigated the effect of the gate hydraulic conductivity/aquifer hydraulic conductivity ratio for heterogenous aquifers. They found that increasing this ratio from 1 to 10 significantly increased preferential flow in the gate and the residence time range within the gate. Preferential flow and clogging within a zero-valent iron PRB for nitrate degradation was also investigated by *Kamolpornwijit et al.* [2003].

Eykholt et al. [1999] and *Bilbrey and Shafer* [2001] investigated the effect of heterogeneous flow domains on PRB design. *Eykholt et al.* [1999] also investigated the effect of reaction mechanism uncertainty on system performance. The heterogeneous realisations produced significant variation in capture width and residence time that the chosen safety factors were not always conservative enough to counter. Accurate site characterisation, reaction mechanism characterisation and modelling of heterogeneity were concluded to be important aspects of PRB design. *Bilbrey and Shafer* [2001] also presented some evidence for including down-gradient pumping wells to control hydraulic gradient through the gate.

MacQuarrie et al. [2001] used numerical simulation to investigate alternative denitrification layer designs for removing septic system nitrate from shallow groundwater in Ontario, Canada. They concluded that the denitrification layer technology was promising enough to warrant further field trials, particularly to examine the effect of design parameters on dissolved organic carbon (DOC) leaching.

The PRB Wall Team of the Interstate Technology and Regulatory Cooperation Work Group has offered internet-based training on the design, installation, maintenance and monitoring of PRBs (e.g. *ITRC*, 2001, 2002 and 2005). These seminars and documents proved to be a very useful way of keeping updated with progress in PRB technology and at PRB remediation sites.

A number of patents covering various aspects of the PRB technology have been issued. These include *Robertson et al.* [1994], *Blowes and Ptacek* [1994 and 1996], and *Blowes et al.* [1996].

1.3.3.4 PRB applications

Denitrification barriers

The first published field trials using PRBs (without cutoff walls) for passive *in situ* denitrification of septic-system nitrate began in 1991. *Robertson and Cherry* [1995, 1997] and *Robertson et al.* [2000] presented the results of these trials. Concurrent with the field trials, laboratory column experiments were undertaken to demonstrate the reactivity of a variety of solid carbon materials in promoting passive denitrification in porous media barriers (*Vogan*, 1993). Both barrier configurations were used in the field trials; the horizontal barrier positioned below a conventional septic-system infiltration bed, and a vertical barrier intercepting a horizontally flowing plume.

During the first year of operation both barrier configurations achieved substantial remediation (60 to 100%) of input nitrate levels up to 125 mg/L nitrate as nitrogen (NO_3^--N). During the next six to seven years of operation both barrier configurations demonstrated consistency by successfully remediating 58 to 91% of input nitrate at the four trial sites. Nitrate consumption rates were temperature dependent and ranged from 0.7 to 32 mg N/L/day, but did not deteriorate over the monitoring period. Organic carbon consumption by denitrification processes was estimated at 2-3% with less than 3% organic carbon lost through other processes (for example, dissolved oxygen and sulphate reduction or dissolved organic carbon leaching). The potential side effects of this technology were also tested. Down-gradient iron and dissolved organic carbon levels both rose during the trials, although their potential threat was considered much less than high nitrate levels.

Blowes et al. [1994] described the denitrification of agricultural nitrate using bioreactors containing organic carbon material. The field reactors were partially buried in the bank of the Kintore Creek located in Ontario, Canada. The reactors were connected to a single reservoir that was filled with tile-drainage water from a cornfield (or creek water during dry periods). Almost complete denitrification was observed for a period of one year after a start-up period of two weeks.

In 1993 the same author was involved in the construction of a funnel-and-gate system to remediate phosphate and nitrate caused by a school septic system in Ontario, Canada (*Ott*, 2000). The gate contained a 0.6m thick PO_4^{3-} treatment zone (6% Fe/Ca oxides, 9% limestone, 85% aquifer materials) and a 1.2m thick NO_3^- treatment zone (wood chips). Acceptable degradation of both contaminants was recorded. *Ott* [2000] also reported on the use of a GeoSiphon cell containing zero-valent iron in South Carolina for the remediation of nitrate and chlorinated solvents. Phase I of the remediation plan began in 1997 and Phase III (full-scale) was to be initiated some time after 1999.

Schipper and Vojvodić-Vuković [1998, 1999a, 1999b, 2000, 2001, 2004] from Landcare Research presented their findings from field trials to study the effects of a denitrification barrier containing a mix of sawdust and aquifer material. The research site is a dairy farm near Cambridge in the North Island of New Zealand where effluent from a nearby dairy factory was applied from 1985 to 1993. Estimates of denitrification rates were close to that measured in a similar study by *Robertson and Cherry* [1995].

A 30-week pilot-scale study using sand coated with soybean oil was reported on by *Hunter* [2001]. The barrier was most efficient during the first 10 weeks of the study when almost all of the nitrate-N was removed. Efficiency declined with time so that by week 30 almost no nitrate was removed by the system. Nitrite levels in the effluent water remained low throughout the study.

Related PRB applications

Pilot and full-scale PRB systems have also been documented for other contaminants (e.g. *Morrison*, 1998; *Blowes et al.*, 1999a, 1999b, and 1999c; *McMahon, et al.*, 1999; *U.S. EPA*, 1999, 2002a and 2002b; *Blowes et al.*, 2000; *Simon and Meggyes*, 2000; *Vidic*, 2001; *Smith et al.,* 2001; *Benner et al.*, 2002; *Guerin et al.*, 2002; *McGovern et al.*, 2002; *Morrison et al.,* 2002; *Oh and Alvarez*, 2002; *Amos and Younger*, 2003, *U.S. EPA*, 2004a, *and ITRC*, 2005). These include chlorinated solvents (from the dry-cleaning industry), sulphate, iron, nickel, copper and zinc (from acid mine drainage), phosphate (from domestic septic-system effluent), perchlorate, petroleum hydrocarbons, chromium, uranium, technetium and RDX (a military explosive compound).

The potential for PRB applications in cold climates has been tested for remediation of petroleum hydrocarbons and heavy metals (*Snape et al.,* 2001; *Woinarski et al.*, 2003).

Small-scale field and laboratory studies have also indicated the potential for PRB systems in remediating arsenic, cadmium, mercury, manganese, molybdenum, lead, selenium, vanadium and ammonium (e.g. *Lee et al.*, 2002; *Ahn et al.*, 2003). Accelerated laboratory experiments (*Tünnermeier et al.*, 2001) and field case studies (*PEREBAR*, 2001) have been undertaken to test the longevity of PRBs. Discussion of this literature is beyond the scope of this survey.

1.3.3.5 Optimal design of PRB systems

Howard et al. [1995] presented a minimum cost approach that employed non-linear programming using a pattern search method. It was applied to the funnel-and-gate system described by *Christensen and Hatfield* [1994] but could be adapted for PRBs without the sheet-piling funnel. This research was later included in the Funnel-and-Gate Design Method (FGDM), a multi-component, steady-state, analytical method for funnel-and-gate design and cost optimisation (see *Hatfield*, 1997).

This approach is not considered widely applicable to minimum cost PRB design. It is most useful when the cost of the catalyst material is the most significant part of the design and a comparatively wide plume needs to be captured in an aquifer that is not very deep. The approach contains the following assumptions:

- Fully penetrating system;
- Identical up and down-gradient funnels;
- One dimensional flow in the gate;
- Constant pore velocity in the gate;
- Constant porosity and hydraulic conductivity throughout the aquifer;
- Only one type of reactive media in the gate;
- The hydraulic conductivity of the reactive media must be a function of the grain size;
- The degradation reaction must be a first-order process; and,
- The minimum cost funnel and gate dimensions must include one of the ten unique gate width / funnel width ratios input by the user.

The only way this analytical solution can be applied to a PRB design situation is if these conditions hold. It has yet to be examined how close the analytical solution would be to reality if these conditions did not hold. One reason these conditions cannot be guaranteed for a general PRB is that a fully penetrating system with two funnels would rarely be the cheapest design solution. No full-scale systems have been sighted.

Howard et al.'s [1995] design methodology is especially unlikely for remediating nitrate plumes where the degradation rate is unlikely to be first-order (proportional to nitrate concentration) as in other media/contaminant combinations (see Sections 1.3.2 and 2.4). Reactive materials (e.g. sawdust) used in denitrification PRBs are also cheap relative to impermeable wall costs and minimum cost systems are unlikely to include impermeable walls. The hydraulic conductivity of a denitrification gate depends not on grain size but on the type of soil, the type of reactive material (e.g. sawdust), their respective hydraulic conductivities, and their respective proportions in the final (homogeneous) mix. The amount of reactive material also affects the denitrification rate and the time between replenishments. All these new decision variables and interrelationships would need to be included in any relevant formulation.

The cost objective function would also be affected but is easily adaptable. A cost not considered by *Howard et al.* [1995] was the present cost of any replenishments of the reactive material. While properly designed denitrification systems using sawdust have been shown to have the potential to last for decades (e.g. *Robertson and Cherry*, 1997), systems using a more readily available carbon source such as methanol would require regular replenishments.

Manz and Quinn [1997] proposed a relatively simple funnel-and-gate design and cost minimisation analysis for implementation at an industrial site and a closed municipal landfill. No optimisation procedure was used; the alternative designs were evaluated instead with the objective of achieving site closure in the most cost-effective manner. Design evaluation involved extensive groundwater modelling to ensure all contaminated groundwater passed through the treatment gates and not around or beneath the funnel. The results from this modelling and the measured contaminant concentrations determined the width and thickness of the gates. A factor of safety was included in the gate thickness calculation to offset the uncertainty in input parameters such as the groundwater velocity through the gate.

This approach shows potential for cases when only a few simple designs are to be compared. However, if a system is complex to model or if many designs are possible, then the addition of an optimisation procedure would be useful. The approach is also limited by its ability to only accommodate contaminants with first-order decay rates. The factor of safety could possibly be used to cover any under-design that resulted from using a first-order decay rate. It

could also be used to account for differences between measured bench-scale decay rates and actual *in situ* rates.

Teutsch et al. [1997] presented a relatively complex cost-optimisation approach for the design of *in situ* reactive wall systems. Their modular numerical/analytical model was developed to simulate the hydrogeological and geochemical processes at a specific site. Model results were fed into an economic model which was used to find minimum cost designs and to conduct sensitivity analysis.

This approach empowers the decision-maker by presenting them with a variety of options rather than a single solution. It also enables non-modelled aspects of a particular problem (e.g. site geology, parameter uncertainty) to be more easily included in the decision making. However, this approach is time consuming, as many simulation runs need to be performed and analysed on a site-specific model in order to accurately cover a range of potential PRB designs. Other issues relating to the approach of *Teutsch et al.* [1997] are discussed in Sections 4.5 and 5.5.3.

GROWFLOW is promoted as an innovative and flexible simulation and optimisation program for permeable barrier systems. It was developed by a team at Applied Research Associates, Inc. (*Everhart*, 1997) for the U.S. Air Force. GROWFLOW is a fully 3D saturated-unsaturated code that can handle complex geometry. The program is based on the Lagrangian smooth particle hydrodynamics (SPH) concepts traditionally used in astrophysical simulations. SPH is a continuum dynamics solution methodology in which all hydrodynamic and history information is carried on particles (similar to particle tracking codes). GROWFLOW was included as a software option in a PRB design report for the U.S. Air Force (*U.S. Air Force*, 1997), but no applications or further information on the software have been found.

1.3.4 Summary

This literature survey has covered optimal design of pump-and-treat and pump-treat-inject systems, the denitrification process, the PRB technology, PRB modelling, denitrification (and related) barrier applications, and optimal design of PRB systems.

The inclusion of research into remediation technologies other than PRBs (particularly pump-and-treat) was considered worthwhile as the PRB technology is still relatively new and correspondingly there has been significantly less research undertaken than for a related technology such as pump-and-treat. Many of the authors reviewed suggested ways of applying their techniques to other remediation technologies, so crossover potential seems positive.

Simulated annealing, Bayesian decision analysis and tabu search are global optimisation techniques worthy of testing on non-linear problems such as PRB design when they are coded into usable solver routines. The LGO Solver tested in Section 6.4 includes similar search methods. Artificial neural networks and genetic algorithms have been successfully applied to hypothetical and real world pump-and-treat examples and their ability to replace sequential calls to a hydraulic simulation model with a learned "knowledge base" fits the aims of this study. The Evolver add-in to Excel will be tested in Section 6.4 for its applicability to the chosen optimal PRB design methodology.

Stochastic optimisation and direct search methods show considerable promise for pump-and-treat type systems but still are not used as often as deterministic, gradient-based optimisation for real world problems due to their higher computational requirements. The continued increase in computational power and the recent research trend of combining the best aspects of multiple optimisation methodologies shows promise for the future application of stochastic optimisation and direct search methods to the PRB technology as well as pump-and-treat. In the mean-time, a combination of sensitivity analysis, scenario analysis and factorial analysis is proposed in Chapter 7 to make deterministic optimisation more applicable to real-world applications. These techniques enable decision-makers to explore design options and the effects of input uncertainty with minimal processing time.

Research into the denitrification process shows that it is reasonably well understood, although the high spatial variability exhibited by soil denitrification and the number of factors affecting

the denitrification rate that are difficult to control are particularly important issues for denitrification wall design. A design methodology for optimising PRB systems with particular emphasis on denitrification barriers is presented in Chapter 2. Laboratory experiments to determine the hydraulic and contaminant degradation properties of some reactive material combinations for denitrification walls are presented in Chapter 3.

The PRB technology has developed into a cost-effective alternative to pump-and-treat with wide applicability to groundwater remediation problems. Low conductivity aquifers have proven a problematic issue for PRBs to deal with, although the trench-and-gate system and the bio-curtain/passive interceptor wells show promise in this areas. Deep contamination has also provided challenges, but deep hydrofracting methods and the use of biodegradable slurries have shown to be effective solutions, if somewhat expensive. Many design aspects do not seem to have been compared in terms of hydraulic performance, either by computer modelling or pilot-scale testing. Results from hydraulic performance analysis of PRB designs using Visual MODFLOW are presented in Chapter 4. Visual MODFLOW was chosen for its strength in hydraulic modelling and its wide applicability. FEMWATER-N shows potential for geochemical modelling in future applications involving denitrification walls.

A survey of literature regarding PRB design highlighted a number of issues still requiring resolution. Two important issues requiring further research are considered to be the hydraulic efficiency of partially penetrating funnel-and-gate systems and the development of functional relationships between PRB design parameters, thus removing hydraulic simulation from the design optimisation process. Computer modelling experiments to make progress on these issues are presented and discussed in Section 4.4 and Chapter 5 respectively.

A variety of optimal design approaches for PRB systems has previously been proposed. The **GROWFLOW** software was not available to be analysed. A new generalised design methodology is presented in Section 6.2, including aspects of *Teutsch et al.'s* [1997] approach. The methodology is applied to a hypothetical example situation in Section 6.4.2. The chosen model required a number of limiting assumptions to make it solvable. Relaxation of these assumptions is covered in Chapter 8.

The success of PRB field trials and full-scale installations to remediate nitrate and other contaminants provides significant evidence to support future applications of this technology. Cost reduction of PRB design through increased tailoring of designs requires accuracy in

construction techniques, site characterisation and reactive material characterisation. Field trials and pilot-scale installations will be required to test the practicality of the proposed methodology.

Chapter Two

Design Methodology for PRB Systems

2.1 Introduction

In situ technologies such as permeable reactive barriers are highly dependent on site-specific parameters. A multitude of competing reactions and varied kinetics are believed to take place in the reactive cell of a permeable barrier, so stoichiometry cannot be the basis for predicting contaminant degradation and quantifying reaction products. A successful design relies on good site characterisation by the site hydrogeologist or site engineer, accurate treatability testing and relevant computer modelling and optimisation.

The methodology presented in this chapter was inspired by the work of *Gavaskar et al.* [1998, 2000]. They proposed a practical methodology for remediating chlorinated solvents and a benefit-cost approach for evaluating the economic feasibility of various designs. In the following sections, this methodology is extended to include an optimisation procedure and post-optimal analysis with application to denitrification walls. The methodology can easily be applied to other contaminants or multiple contaminants. Figure 2.1 presents an overview of this methodology.

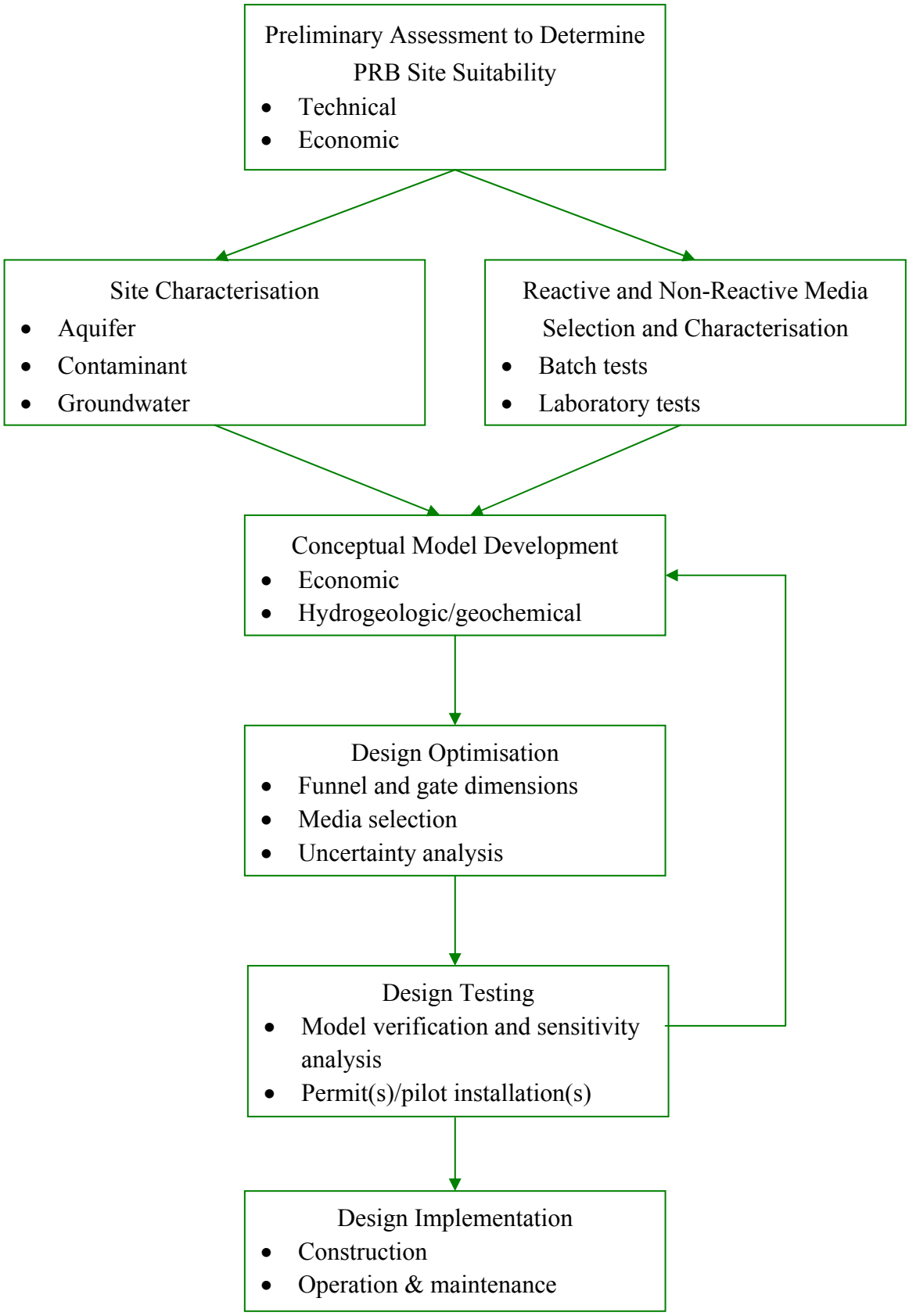

Fig. 2.1. PRB design methodology overview

2.2 Preliminary Assessment to Determine PRB Suitability

Typically, the first assessment that site managers must make is whether or not the site is suitable for a permeable barrier application. Although an unfavourable response to any of the following factors does not necessarily rule out a permeable barrier, such a response can make the application more difficult or costly. The necessary information required for a preliminary assessment includes:

- **Contaminant type.** Are the contaminants of a type reported in scientific and technical literature as amenable to remediation by a substance that can be stored in a reactive cell? Nitrate, for example, requires a form of solid organic carbon. Organic carbon from solid media such as sawdust and cellulose (from straw), and calcium carbonate have been shown to remediate nitrate at an economically feasible rate (see *Mateju et al*., 1992).

- **Plume size and distribution.** Is the plume very wide and/or very deep? The cost of the system naturally increases with the size of the plume. The depth of the plume is likely to be the more significant cost consideration because the cheapest construction methods (e.g. continuous trenching) only operate down to ~ 9m (*U.S.EPA,* 2001). With more innovative installation techniques (e.g. biopolymers) it is possible to install PRBs down to ~ 21m. To degrade nitrate at significant depths it may be more economically feasible to create a barrier out of injection wells. This system involves a more expensive carbon source such as methanol, but the remediation rate is much higher and the installation costs lower than a deep trench containing solid organic carbon. Deep nitrate plumes and denitrification do need to be considered though, as *Francis et al.* [1989] found that samples taken from depths down to 289m had denitrification potential.

- **Depth of aquitard.** How much deeper is the aquitard than the plume? This will determine whether partially penetrating PRBs are to be considered as well as fully penetrating barriers.

- **Competent aquitard.** Is the aquitard very thin or discontinuous? If so, there could be significant upward gradients across the aquitard. Also, if there are deeper aquifers that

could be affected by a breach of the aquitard during installation of a fully penetrating barrier, the system should be reassessed.

- **Geotechnical considerations.** Are there any geotechnical features at the site that may make installation more difficult? For example, the presence of consolidated sediments or large rocks may make some types of emplacement more difficult. Above-ground structures, such as buildings, that are in the vicinity of the installation may also impede the manoeuvrability of construction equipment.

- **Groundwater velocity.** Is the groundwater velocity reasonable? If it is too high, the reactive cell thickness required to obtain the design residence time may also be too high for economic feasibility. This situation is unlikely to occur when a relatively inexpensive carbon source such as sawdust is used unless the necessary excavation technique is expensive. However, problems can occur if the high velocity is caused by high hydraulic conductivity. When the aquifer hydraulic conductivity is high it may be difficult to create a reactive cell with hydraulic conductivity sufficiently great to attract the plume. If the groundwater velocity is too low, the contaminant may struggle to reach the reactive zone. *Bowles et al.* [1995] have suggested some design enhancements for this situation. In Chapter Four it will be shown that an up-gradient funnel increases the overall groundwater velocity and also the variation in velocity within a PRB system. This has a direct effect on the contaminant residence time and therefore the remediation potential.

2.3 Site Characterisation to Support PRB Design

If a preliminary assessment shows that the site is suitable, the next issue is whether or not the available site characterisation data are sufficient to locate and design the barrier. The required site information includes the following:

- **Aquifer characteristics.** The necessary aquifer characteristics include depth to groundwater, depth to aquitard, aquitard thickness and continuity, groundwater velocity, lateral and vertical gradients, site stratigraphy/heterogeneities, lateral and vertical hydraulic conductivities of the different layers, porosity, and dimensions and distribution

of the plume. This information is required for hydrogeologic modelling which assists in barrier design and location.

- **Contaminant characteristics.** The types of contaminant to be degraded (e.g. nitrate, chlorinated solvents) and their respective concentration distributions need to be known. This information will be used to select appropriate reactive media, conduct treatability tests, and design the flow-through thickness of the reactive barrier.

- **Groundwater characteristics.** Other information about the site groundwater is required to evaluate the long-term performance of the permeable barrier and select appropriate reactive media. For a denitrification barrier it is important to know the presence and concentrations of dissolved organic carbon, dissolved oxygen, ammonium (if close to the plume source), iron, manganese, and certain toxic substances. The presence of sufficient dissolved organic carbon may increase the denitrification rate if the reaction is carbon-limited. The presence of sufficient dissolved oxygen, ammonium or certain toxic substances may reduce the denitrification rate. Ferric iron and manganese may be reduced into their soluble forms as a result of the anaerobic environment. If this groundwater is extracted and aerated, the iron and manganese may precipitate, causing staining of laundry and sanitary ware. The New Zealand drinking water guidelines are currently 0.2 mg/L for iron and 0.05 mg/L for manganese (*N.Z. Ministry of Health*, 2000). Groundwater temperature and, to a lesser extent, pH are also important to measure as they may affect the denitrification rate if outside certain bounds.

2.4 Reactive and Non-Reactive Media Selection and Characterisation

Once the required site characterisation data have been obtained, the next step is to identify and screen potential reactive media and non-reactive media. Following identification of a short-list of potential media, column tests are conducted on reactive/non-reactive media combinations to determine their combined volume, porosity, hydraulic conductivity and degradation rate. It is recommended that column tests be performed with groundwater and aquifer material (if used) obtained from the site in order to generate design data that are as representative as possible. It is important to conduct the column tests over a realistic range of

temperatures where the remediation rate is temperature sensitive. This is the case for denitrification systems.

Even well-designed experiments may yield significantly different values from what will occur in the real system. Distributions are much more useful than point estimates of these values as they can be used in probabilistic models to design to a specific confidence level, typically around 90 percent (*Vidic*, 2001). Correction and safety factors can also be considered to account for differences between the laboratory and the field, and uncertainty in site-specific characteristics (e.g. *Gavaskar*, 1999).

The main considerations in identifying initial candidates are as follows:

- **Reactivity.** The candidate medium should be able to degrade the target contaminant(s) within an acceptable residence time. In most cases the higher the potential reaction rate, the better the media. A complicating factor when choosing media for remediating nitrate contamination is that the degradation rate may not be zero-order (constant) or first-order (proportional to nitrate concentration) as in other media/contaminant combinations. This is because of the potential influence of external factors such as dissolved organic carbon, dissolved oxygen, ammonium, certain toxic substances, temperature, and pH as discussed in the previous section. These factors may change continuously or seasonally, and may have different effects on different reactive media.

- **Hydraulic performance.** Selection of the particle size of the reactive medium should take into account the trade-off between reactivity and hydraulic conductivity. Generally, higher reactivity requires lower particle size (higher surface area to mass ratio), whereas higher hydraulic conductivity requires larger particle size. Non-reactive medium can be mixed with the reactive medium to increase or decrease PRB hydraulic conductivity.

- **Stability.** The candidate medium should be able to retain its reactivity and hydraulic conductivity over time. This consideration is governed by the potential for precipitate formation and depends on how well the candidate medium is able to address the inorganic components of the site groundwater.

- **Environmentally compatible by-products.** The by-products generated during degradation should not have any negative effect on the environment. The most important by-product to consider in denitrification is biodegradable dissolved organic carbon (BDOC) leachate, which has been shown to occur in denitrification barriers (see *Robertson and Cherry*, 1995) and carbon-filled PRBs for treating acid-mine drainage (see *Benner et al.*, 2000). *Huck* [1990] defined BDOC as the portion of dissolved organic carbon (DOC) that can be metabolised by heterotrophic micro-organisms. If the denitrification barrier contains substantially more DOC than is required to degrade the nitrate, then some may be flushed out of the trench by the incoming groundwater. Low levels of BDOC down-gradient from the PRB may be beneficial as it may help in degrading any remaining nitrate. High levels of BDOC affect the taste, odour, and colour of water. BDOC can also cause problems by inducing regrowth in drinking water distribution systems (see *Khan et al.,* 1998). To minimise risk, the rate of carbon conversion from the solid to liquid phase would need to be incorporated into the barrier design.

  Other potential by-products could occur as a result of incomplete denitrification. Reduction of nitrate to nitrogen gas involves reduction to nitrite, nitric oxide, nitrous oxide and finally nitrogen gas (see *Mateju et al.*, 1992). Nitrite in water may contribute to the formation of nitrosamines (known carcinogens); nitric oxide catalyses the decomposition of ozone; and nitrous oxide decomposes to nitric oxide if it reaches the stratosphere. There is no evidence to suggest that a denitrification barrier would release harmful levels of any of these substances, although *Spector* [1998] claimed that nitrous oxide was released during a laboratory denitrification experiment before being converted to nitrogen gas. As the vast majority of denitrification time is required to reduce nitrate to nitrite, it is extremely unlikely that nitrite, nitric oxide, or nitrous oxide could escape from a denitrification barrier before being reduced to nitrogen gas.

- **Availability and price.** The candidate medium should be easily available in large quantities at a reasonable price, although special site considerations may sometimes justify a higher price. Sawdust is an ideal candidate for denitrification barriers as it is readily available at about NZ$15.00 per cubic metre (*Perrys*, 1999).

2.5 Conceptual Model Development

While reactive media tests are being completed, the conceptual model can be set up. This model is site-specific, containing the necessary economic, hydrogeologic, and geochemical information for testing PRB designs.

2.5.1 Economic Model

The required economic information includes the capital and operational costs of the PRB system. There is likely to be strong scale dependence, particularly for capital costs. For example, there is often a minimum transportation cost for reactive media which declines with increasing volume. There are also very large mobilisation costs to bring excavation equipment or heavy sheet piling (for site dewatering or funnels) to a site. For this reason fixed and variable costs would normally be separated. Separate fixed cost inclusion is possible and beneficial with the chosen optimisation method. Functional relationships for the variable portion of costs can usually be developed for various construction techniques then normalised per unit area or volume in order to provide a flexible calculation basis. Within these relationships the technical limitations (e.g. maximum depth) of the individual construction techniques can be considered. The capital costs of a PRB system include the following:

- **Cost of the reactive medium.** The total cost of the reactive medium is found by multiplying its per-unit cost (price) by the amount required and adding any transport costs. The amount required depends primarily on the type and concentration of contaminants, regulatory treatment criteria, the site groundwater velocity, and the contaminant distribution in the aquifer.

- **Cost of the funnel (if required).** As with the reactive medium, the total cost is found by multiplying the per-unit cost (price) by the amount required and adding any transport costs.

- **Construction costs**. These costs depend on the construction technique, barrier dimensions, and geotechnical considerations (e.g. rocks or highly consolidated sediments).

- **Technology licensing costs.** Many of the reactive media and emplacement techniques are patented. The licensing costs of some emplacement techniques (e.g. sealed-joint piling) are built into the quoted price, but licensing costs for patented reactive media types are usually an extra cost.

- **Disposal and restoration costs.** There may be costs associated with disposal of spoils generated during barrier construction. The spoils may have to be disposed of as hazardous waste if the barrier is placed within the plume, incurring higher cost. The barrier may need to be excavated and filled in at the completion of the remediation project, and the site surface may need to be restored to its original grade and condition.

The operating and maintenance (O&M) plan is an important part of the conceptual model. Capital costs of a PRB system are likely to be higher than an equivalent pump-and-treat system but significantly lower O&M costs should make it more cost-effective overall (e.g. *ESTCP*, 1999). O&M costs include:

- **Compliance monitoring costs.** These are the annual costs associated with fulfilling regulatory requirements for monitoring breakthrough or bypassing of contaminants. A monitoring plan requires observation wells up-gradient, inside and down-gradient from the PRB. It may also include wells underneath and outside either edge of the PRB system. Monitoring costs that are proportional to gate width may influence the relative economic benefits of funnel-and-gate versus continuous (gate only) PRB systems. Highly heterogeneous aquifers will require carefully targeted monitoring.

- **Additional performance monitoring costs.** These are dependent on the objectives of the remediation project but are likely to be greatest when a relatively new construction technique or reactive medium is being used.

- **Periodic maintenance costs.** The reactive cell may have to be flushed or the reactive medium replaced if the hydraulic or chemical performance of the barrier falls below an acceptable level. Research suggests that appropriately designed barriers have the potential to last for many years without maintenance (e.g. *Robertson and Cherry*, 1997; *Robertson et al.*, 2000; *PEREBAR*, 2001; *Kamolpornwijit et al.*, 2003). It may therefore be some

time before enough PRBs have been replenished or completed to enable barrier longevity to be accurately estimated. Incorporating a longevity scenario distribution into the conceptual model provides a means for including this uncertainty in a probabilistic PRB design optimisation.

Any economic benefits from the permeable barrier application may be included if they differ from other considered applications. For example, if a permeable barrier system is being compared to a pump-and-treat system, the economic benefits of continued usage of the land should be considered. A pump-and-treat system involves above-ground structures that would inhibit economic land use, whereas a permeable barrier has no aboveground structures. Important intangible benefits, such as the risk reduction achieved with a more conservatively designed system, should also be considered.

The Remedial Action Cost Engineering and Requirements (RACER) System is an environmental costing program developed by the U.S. Air Force. Version 3.2 has been adapted especially for PRB applications and can estimate the costs for various phases of a PRB project. It has a cost database created mostly from the U.S. Army Corps of Engineers' Unit Price Book and supplemented by vendor and contractor quotes. The applicability of RACER to other countries will depend on the availability of contractors with the required technologies, and appropriate cost translations. More information on RACER can be found on the internet at http://talpart.earthtech.com/RACER.htm.

2.5.2 Hydrogeologic/Geochemical Model

Hydrogeologic modelling attempts to quantify the effect of a particular barrier design on the groundwater system. Geochemical modelling attempts to predict the concentrations of dissolved species in groundwater based on assumed chemical reactions. Very complex situations may require separate hydrogeologic and geochemical models that are coupled together, but usually the site and reactive material characterisation data can be included in the same model.

A two-dimensional computer model may be sufficient if the PRB can be assumed to be fully penetrating and groundwater flow horizontal. Otherwise a three-dimensional model as described in Chapter 4 will be required. The computer model has the following purposes:

- **Testing of functional relationships between the design variables.** Generic functional relationships can usually be used to estimate the expected capture zone and residence time for various designs. By testing these relationships on the conceptual model it can be determined whether they need to be expanded, constrained or replaced by more appropriate relationships.

- **Location of barrier.** Determine a suitable location for the permeable barrier with respect to the plume distribution, site hydrogeology, and site-specific features, such as property boundaries, underground utilities etc.

- **Monitoring plan.** Assist in planning appropriate monitoring well locations and monitoring frequencies.

- **Testing of optimal designs.** Optimal designs proposed in accordance with Section 2.6 require testing before proceeding to pilot and/or full-scale application. This is primarily to verify that the computer model behaves as expected given the chosen model assumptions.

2.6 Design Optimisation

The proposed design optimisation process couples a spreadsheet model and a non-linear solver. Data are input from the conceptual model. Significant variation is expected in inputs to PRB design, particularly in aquifer and plume characteristics. Uncertainty and variability are also expected in reactive material characteristics. Scenario analysis and factorial analysis (see Chapter 7) are proposed instead of point estimates to account for this uncertainty. The optimisation procedure manipulates the values of the design variables, as follows, with the aim of cost minimisation:

- **Reactive cell/gate dimensions.** Determine the optimal (or range of near-optimal) dimensions of the reactive cell(s). Determine whether an impermeable base is required and its dimensions.

- **Funnel dimensions.** Determine the optimal (or range of near-optimal) dimensions and angle(s) of the funnel(s) if required.

- **Media selection.** Aid in reactive media selection by identifying optimal media hydraulic conductivity (with respect to the aquifer hydraulic conductivity), and contaminant degradation rate.

2.7 Design Testing

Prior to full-scale implementation, it is strongly advised to test all designs identified by the optimisation procedure. The first stage of testing involves model verification to confirm the model performs as expected. This involves running the chosen designs through Visual MODFLOW (or similar computer software) to verify the accuracy of any functional approximations. The verification process may result in the conceptual model being adjusted and the optimisation redone. Once the suitability of a design (or designs) has been verified the necessary permitting procedures need to be followed. It also needs to be decided whether to run a pilot installation or proceed directly to a full-scale installation. Two of the most important reasons for running a pilot installation are for final comparison of multiple suitable designs and to determine how much the actual PRB performance differs from the expected performance based on the computer model. There are many possible sources of uncertainty in PRB design and full-scale installations that do not work as intended can be very costly to fix. The following factors could also make a field pilot installation desirable, although not necessary:

- **Complex site.** If the site is heterogenous and behaviour of the hydraulic flow system is not well understood, it may make sense to run a pilot test to reduce the risk of locating or installing a barrier improperly with respect to the flow system. The pilot barrier should be installed at the most likely location for the full-scale barrier to be emplaced.

- **New emplacement technique.** A pilot installation may be useful if a new emplacement technique is being used for the reactive cell or funnel walls.

- **Cost.** If the expected cost of a full-scale barrier system is very high, then it may be cost-efficient to install a pilot barrier as a means of testing the full-scale system.

2.8 Design Implementation

Design implementation involves installation of the full-scale PRB and monitoring devices. Monitoring must continue for as long as the plume is present. The performance of the permeable barrier can be monitored with the following objectives:

- **Remediation.** Evaluate adequate capture and treatment of the plume and ensure acceptable down-gradient water quality.

- **Design.** Evaluate how well the barrier meets its design objectives (e.g. residence time in the reactive cell).

- **Maintenance.** Evaluate the longevity of the barrier.

Monitoring may be conducted on a quarterly basis or as agreed with the regulators. It is important to attempt to quantify and understand the effect on the system of seasonal changes in external factors such as temperature, water table height and groundwater direction. If these factors differ significantly from the design factors, then the system may not work to its potential.

This chapter has outlined the proposed optimal PRB design methodology. All details will be covered in the following chapters.

Chapter Three

Laboratory Experiments with Reactive Media

3.1 Introduction

The required residence time for a contaminant to degrade in a PRB system is a function of the expected incoming contaminant concentration and the expected rate of contaminant degradation. When the required residence time is known, barrier flow-through length can be determined in conjunction with the expected groundwater pore velocity in the barrier. The relevant aspects of the system the decision-maker has control over are the length of up-gradient funnels, the physical dimensions of the barrier, and the type and volume of materials in the barrier.

Section 2.4 described a methodology for reactive and non-reactive material selection and characterisation. It recommends that column tests be conducted on reactive/non-reactive media combinations to determine their combined volume, effective porosity, hydraulic conductivity and degradation rate. Field tests are then required in order to determine how well the test results translate to the site in question.

In this chapter, a description is given of six combinations of sawdust and pea gravel injected with clean water and nitrate-contaminated water in separate laboratory column experiments to illustrate the first part of this methodology. Sawdust was the chosen reactive material due to its successful application in a permeable reactive denitrification barrier in New Zealand (*Schipper and Vojvodić-Vuković*, 1998, 1999a, 1999b, 2000, 2001, 2004). Pea gravel was chosen as the non-reactive material due to its high hydraulic conductivity and low cost.

3.2 Experimental Design

All necessary measurements were made with the help of a soil column apparatus, similar in design and operation to the wood chip soil column experiments of *Carmichael* [1994]. Six soil columns were made from PVC tubing, each 100 cm in length and 19 cm in diameter. The inside walls of all columns were coated with molten wax and clean sand to soften the interface between the column contents and the hard PVC wall. Each column had two piezometric head measurement points and was filled with a pre-determined homogeneous combination of sawdust and pea gravel (see Figure 3.1).

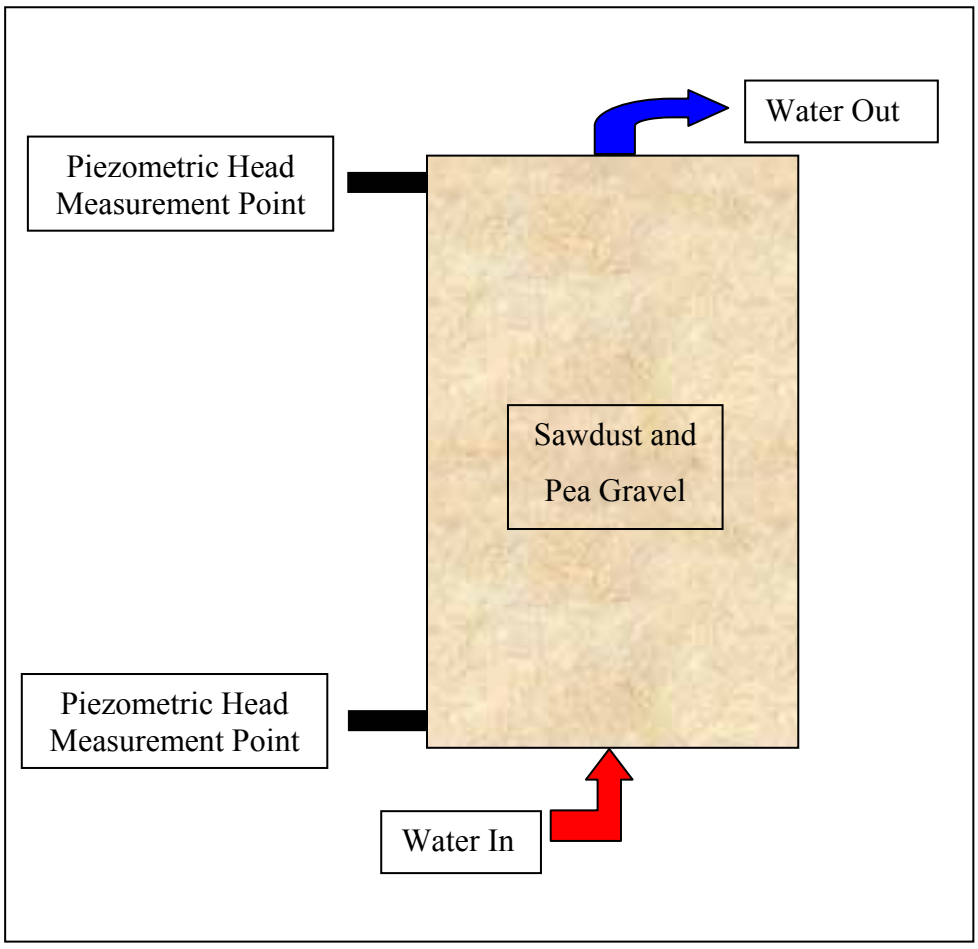

Fig. 3.1. Soil column design.

The base of each column contained an adjustable valve and stainless steel screen to prevent the drainage of any column material. For the hydraulic conductivity experiments, the base of the column was connected to a constant head tank with the adjustable valve used to control flow rate. A variable speed peristaltic pump was used to feed influent into the bottom of the columns for the denitrification rate experiments, as the required flow rate was much less than

for the hydraulic conductivity experiments. Flow rates are easier to control when influent is pushed up through columns rather than filled from the top. Low-oxygen water was used for the denitrification experiments as *Knowles* [1982] found that oxygen affects both the activity and synthesis of the denitrifying enzymes.

Sawdust:pea gravel volume ratios of 0, 0.2, 0.4, 0.6, 0.8 and 1.0 were chosen for the volumetric factor, hydraulic conductivity and drainable porosity experiments. Three replications of each experiment were undertaken to estimate the variability in carefully constructed soil columns. All combinations except 0% sawdust were also used for the denitrification rate experiments. The denitrification rate for pea gravel only was assumed to be zero but this would not be the case for other "non-reactive" materials that may in fact contain some form of carbon source. The 0% sawdust proportion was used as an anchor to interpolation functions applied to experimental results, enabling interpolated estimates between 0% and 20% sawdust.

Prior to conducting the column experiments, volumetric factors were calculated to determine the relationship between weight and volume for each sawdust:pea gravel ratio (Section 3.3.1). Three replicate columns were then constructed for each experiment and connected to the constant head tank. All columns were constructed dry to maximise control over the mixture. Influent flow rate was controlled separately for each column to produce a constant but significant head difference. Hydraulic conductivity was measured as in Section 3.3.2. The influent water was then switched off and drainable porosity measured as in Section 3.3.3, after which the columns were disconnected from the header tank and connected to the peristaltic pump. Each column was filled with a known concentration of nitrate and left stagnant for 7 days to allow bacterial acclimation and development of anaerobic conditions necessary for effective denitrification. The pump was then turned on and samples collected (influent and effluent) as in Section 3.3.4.

An additional procedure to minimise air entrapment that may hinder the development of anaerobic conditions is to fill the column with CO_2 gas prior to wetting the column, though this was not done for these experiments. Results presented in Section 3.4.4 show that nitrate concentration reduced in the columns despite this omission.

3.3 Methodology

3.3.1 Volumetric Factor Estimation

The mixing of materials such as pea gravel and sawdust will always result in a combined volume less than the sum of the individual volumes. This is because the finer sawdust particles will settle in the pore spaces between the larger pea gravel particles. The volumetric factor ($VF_{Mix(r)}$) for a particular sawdust proportion (r) is defined as the sum of the appropriate sawdust volume ($S_{Vol(r)}$) and pea gravel volume ($PG_{Vol(1-r)}$) divided by the combined volume ($SPG_{Vol(r)}$) as follows:

$$VF_{Mix(r)} = \frac{S_{Vol(r)} + PG_{Vol(1-r)}}{SPG_{Vol(r)}} \qquad \textbf{3.1}$$

The first step in determining volumetric factors is to estimate the air-dried bulk density of the sawdust and gravel. Bulk density is the ratio of the mass of dry solids to the bulk volume of sawdust or pea gravel. The bulk volume includes the volume of the solids and of the pore space. Four containers of different (known) volumes were filled twice with air-dried sawdust and twice with air-dried pea gravel. Average bulk density for each volume was taken as the average mass divided by container volume. A drying temperature of 105^{o}C is suggested in *Klute* [1986] for true bulk-density of mineral soils. This was not considered practical for the chosen experiments as they only required air-dried materials and this temperature would also be too hot for organic carbon materials.

The required masses of sawdust and pea gravel for the chosen sawdust proportions were then calculated from the bulk density ratio. Three replicates of each sawdust proportion were shaken (until they looked well-mixed) and then poured into a volumetric flask. The volumetric factor was then calculated from Equation 3.1 using the average combined volume ($SPG_{Vol(r)}$), plus $S_{Vol(r)}$ and $PG_{Vol(1-r)}$ back-calculated from the prescribed masses.

Similar experiments were then undertaken but this time with shaking plus gentle compaction by tapping the top of the mixture with the base of a glass volumetric flask. This was to approximate the effect of compaction caused by pouring layer upon layer of mixture into a column or PRB.

3.3.2 Hydraulic Conductivity Estimation

Hydraulic conductivity is the measure of a permeable medium's ability to transmit liquid, in this case water, and is expressed as the rate at which water can move through a unit thickness of the permeable medium when subject to unit gradient of piezometric head.

Hydraulic conductivity (*K*) can be calculated from the following rearrangement of Darcy's Law.

$$K = \frac{Q * l}{(h_1 - h_2) * A} \qquad \textbf{3.2}$$

where:
Q = the flow rate out the column (volume/time)
l = the distance between two piezometric head measurement points (distance)
h_1 = the piezometric head at the upper piezometric head measurement point (distance)
h_2 = the piezometric head at the lower piezometric head measurement point (distance)
A = the cross-sectional area of the column (area).

The volumetric factors and bulk densities estimated in Section 3.3.1 were combined with soil column measurements to calculate required sawdust and pea gravel masses for a 5cm column depth and the chosen sawdust proportions. Columns were filled by combining and shaking the prescribed sawdust and pea gravel weights, then pouring the mixture into a dry PVC column through a removable length of PVC tubing that was smaller in diameter than the column. The purpose of the removable tubing was to maintain constant pouring height above the mixture and keep the material from dislodging the wax/sand coating on the column sides while it was being poured.

The number of increments to fill the column just above the top piezometric head measurement point was noted as was the filled length of column. Three replicate column experiments per material mix were carried out. Hydraulic conductivity was then measured using the following methodology:

1. Turn tap on and fix any leaks.

2. Adjust column head until head difference has stabilised. Check stabilisation of head difference over 24-48 hours.
3. Note date, time, water temperature and air temperature on experimental reporting sheet. Note piezometric head levels. Remove output drainage tube from drain and start stopwatch as water flows into bucket. When bucket is nearly full (or 600 sec has elapsed), stop stopwatch and move drainage tube back to drain. Note sample time. Weigh water and calculate volume (1 litre water = 1 kg). Calculate flow rate = (water volume/sample time) and then hydraulic conductivity from Equation 3.2.
4. Repeat step 3 three times at approximately 24-hour intervals.

3.3.3 Drainable Porosity Estimation

Drainable porosity is defined as the drained pore volume divided by the utilised column volume. Drainable porosity was chosen as a cheaper and faster estimate of effective porosity than conventional tracer test methods. Subsequent laboratory experiments have shown a strong correlation ($r^2 = 0.91$, std. dev. of the residuals = 17.2) between drainable porosity and hydraulic conductivity measurements, which were similar to *in situ* hydraulic conductivity measurements of the same aquifer material as determined from field tracer tests (*Barkle et al.*, 2005).

Effective porosity has been defined as the "interconnected volume of void space per unit volume of porous medium" (*Bear and Nitao*, 1999). It is required to estimate average groundwater pore velocity in the barrier. This is combined with required residence time to determine barrier flow-through length. Drainable porosity was estimated at the completion of each hydraulic conductivity experiment as follows:

1. Turn water off at completion of hydraulic conductivity experiment and remove column cap. Fill column to saturation (when water level just covers column contents) and measure filled column length (Len_{Column}).
2. Drain column through valve in base into a bucket for 24 hours (all draining had ceased well before this time). Calculate drained volume of column ($Vol_{Drained}$) from water weight.
3. Calculate drainable porosity (Por_{Column}) from Equation 3.3 (where A is column cross-sectional area).

$$Por_{Column} = \frac{Vol_{Drained}}{Len_{Column} * A} \quad \textbf{3.3}$$

3.3.4 Denitrification Rate Estimation

Factors affecting the rate of denitrification were discussed in Section 1.3.2. Denitrification rates estimated from soil column experiments are expected to produce maximum rates under ideal conditions. Field experiments under a range of conditions are then required to produce a denitrification rate range estimate for each sawdust:pea gravel combination.

Single-point specific denitrification rates have been obtained from the measurement of NO_3 disappearance or production of N_2 and N_2O during laboratory incubation of disturbed or undisturbed sediment samples (*Yeomans et al*., 1992; *Smith et al*., 1996). Similar experiments have been carried out in field studies (*Trudell et al.*, 1986; *Istok et al.*, 1997; *Bragan et al.* 1997b; *Schroth et al*., 1998; *Schipper and Vojvodić-Vuković*, 2000). *Smith et al.* [1996] found that denitrification rates determined during laboratory incubation were substantially greater than *in situ* rates. Discrepancies between the two approaches were explained by *Well et al.* [2003] in terms of the reliability of laboratory experiments being limited by the difficulty to conserve biogeochemical properties of the samples and to simulate *in situ* conditions in the laboratory. Measurement of NO_3 disappearance was chosen for these experiments as it relates directly to PRB monitoring of contaminant concentrations up-gradient, down-gradient and inside PRB systems. Laboratory measurements of denitrification rates will be taken as maximum rates, with field measurements used for the final design.

Denitrification rate laboratory experiments required a small change to the soil column design used for the hydraulic conductivity experiments. The column inlet was re-connected via a peristaltic pump to a tank filled with a known concentration of potassium nitrate in a solution of low-oxygen water. A single tank-full was used for each experiment so input nitrate concentration remained constant. Peristaltic pumps enable the contaminated water to be pumped up through the soil columns at a very slow (known) rate, thus providing sufficient residence time for measurable denitrification. This is similar to the method used by *Carmichael* [1994].

Before starting the pump, the inlet valve was shut off and the soil column was manually filled from the top with the chosen nitrate concentration in solution. It was then left to sit for 7 days to allow bacterial acclimation and development of anaerobic conditions necessary for effective denitrification. The first influent and effluent samples taken after this time confirmed nitrate concentration reduction in the column.

The soil column inlet valve was then opened and the pump started. After approximately two pore volumes had passed through the soil column the denitrification rate measurements were started. Each measurement involved a sample from the tank to check initial NO_3-N concentration (N_{In}) and a sample from the soil column outlet pipe for final NO_3-N concentration (N_{Out}). Flow rate (Q) out the column was then calculated as in Section 3.3.2, column residence (Res_{Column}) was calculated from Equation 3.4, and denitrification rate ($DegU_{Mix(r)}$) for the chosen sawdust proportion (r) was calculated from Equation 3.5.

$$\mathrm{Re}\,s_{Column} = \frac{Len_{Column} * A * Por_{Column}}{Q} \qquad \textbf{3.4}$$

$$DegU_{Mix(r)} = \frac{N_{In} - N_{Out}}{\mathrm{Re}\,s_{Column}} \qquad \textbf{3.5}$$

3.4 Results

3.4.1 Volumetric Factor Results

The average bulk density for sawdust and pea gravel created from replicate experiments with four different volumes is presented in Table 3.1. Bulk density estimates for sawdust and gravel were found to remain relatively stable for all experiments. A mean bulk density of 0.175 g cm^{-3} was therefore chosen for sawdust and a bulk density of 1.66 g cm^{-3} was chosen for pea gravel.

Table 3.1 Bulk Density Experiments		
	Ave Bulk Density (g cm^{-3})	
Volume (cm^3)	Sawdust	Gravel
200	0.173	1.63
1000	0.165	1.64
3717	0.186	1.70
27200	0.176	1.67
Mean	0.175	1.66

A variety of sawdust:pea gravel combinations were then created with and without compaction to estimate the effect of compaction on the volumetric factor. Volumetric factors were calculated from Equation 3.1 and are presented in Figure 3.2.

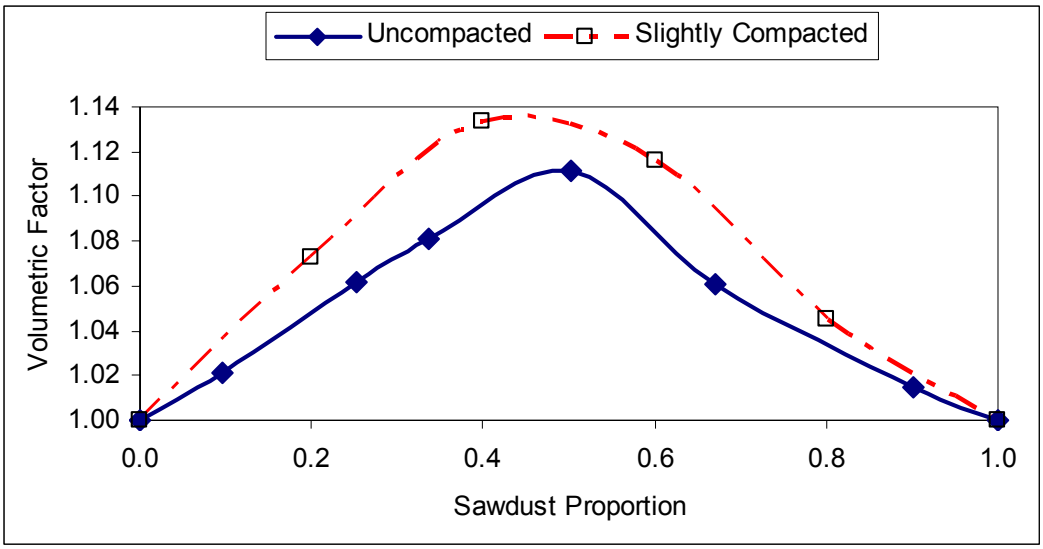

Fig. 3.2. Relationship between sawdust proportion and volumetric factor for uncompacted and slightly compacted experiments.

Figure 3.2 shows that sawdust proportion has a significant effect on volumetric factor and slight compaction increases volumetric factors by up to 4%. Compaction is expected to occur in PRB construction so the slightly compacted volumetric factors were chosen to calculate the required sawdust and gravel masses for each mixture increment in the column experiments. Further experiments have been conducted since this study to understand the effects of wet versus dry construction of denitrification walls. These experiments are presented in *Barkle et al.* (2005). Additional research regarding the amount and effects of compaction in different PRB construction techniques is recommended.

Volumetric factors were then combined with the chosen bulk densities for sawdust ($S_{BulkDen}$) and pea gravel ($PG_{BulkDen}$) to determine the masses of sawdust (S_{Mass}) and pea gravel (PG_{Mass}) that would combine to fill the soil column to a depth of 5cm. Filling each column with approximately twenty 5cm increments was time-consuming but considered necessary to maximise the homogeneity of the column. As the internal radius of each column was 9.5cm, the incremental sawdust and pea gravel masses were calculated as follows:

$$S_{Mass} = r * \pi * 9.5^2 * 5 * S_{BulkDen} * VF_{Mix(r)} \quad \textbf{3.6}$$

$$PG_{Mass} = (1 - r) * \pi * 9.5^2 * 5 * PG_{BulkDen} * VF_{Mix(r)} \quad \textbf{3.7}$$

The calculated weights from Equations 3.6 and 3.7 for the five sawdust proportion experiments plus a pea gravel-only experiment can be found in Table 3.2. Input to these equations included the chosen bulk densities of $S_{BulkDen}$ = 0.175 g cm^{-3} and $PG_{BulkDen}$ = 1.66 g cm^{-3}, and the appropriate volumetric factor shown in Figure 3.2. Three replicate columns were made for each experiment.

Table 3.2
Soil Column Increments

Sawdust Proportion	For 5cm depth	
	Sawdust (g)	Gravel (g)
0.0	0.0	2367.5
0.2	54.8	1979.1
0.4	115.7	1584.7
0.6	170.8	1073.1
0.8	213.3	508.2
1.0	255.2	0.0

3.4.2 Hydraulic Conductivity Results

Once the construction of all columns for each experiment was complete, the water was turned on and the adjustable valve in each column set so that a piezometric head difference of at least 20mm was achieved. Adjusting the flow-rate of one column affected the flow-rates of all other columns, so columns were left for an hour or so between adjustments and overnight after the final adjustment. Output flow-rate was then measured as described in Section 3.3.2 and hydraulic conductivity calculated from Equation 3.2. Air and water temperature were

also measured but only varied slightly within each experiment. Figure 3.3 presents the $\log_{10}$ of the averaged hydraulic conductivities for the five chosen sawdust proportion experiments and gravel-only experiment.

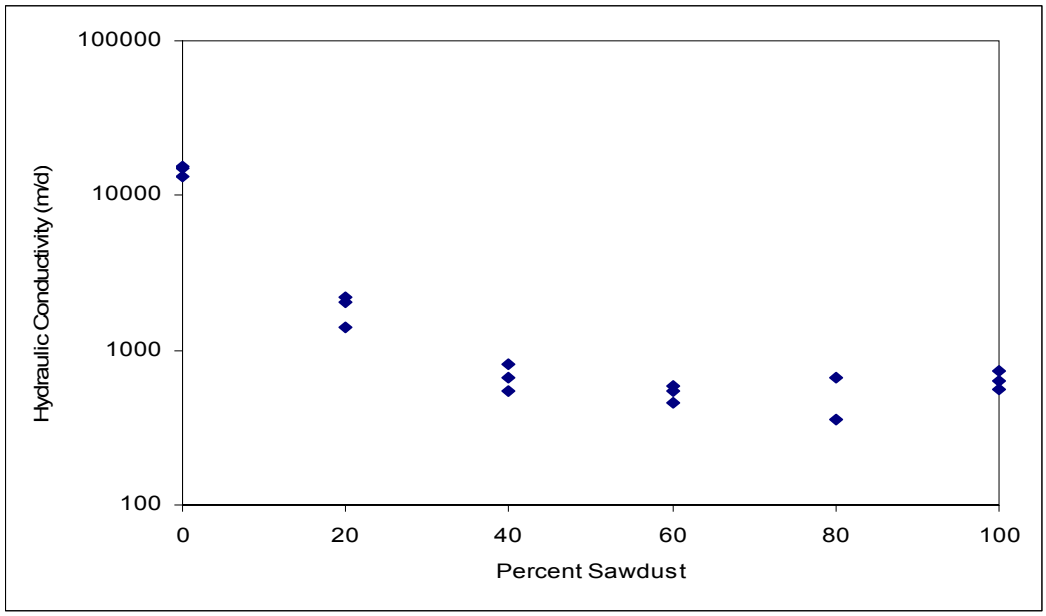

Fig. 3.3. Relationship between sawdust proportion and hydraulic conductivity for three replications of each sawdust proportion.

Figure 3.3 shows that hydraulic conductivity is highest when sawdust proportion is at its lowest and decreases significantly until the mixture is approximately 60%. The log of the hydraulic conductivity is used for this figure due to the magnitude of the difference between gravel-only experiments and sawdust/gravel combination experiments. The 60-100% sawdust proportion experiments in Figure 3.3 show variation between replications to be at least as great as variation between experiments. This result highlights the amount of variation in materials such as sawdust and pea gravel but also suggests that sawdust proportion does not have a significant effect on hydraulic conductivity when the mixture is at least 60% sawdust.

3.4.3 Drainable Porosity Results

On completion of each hydraulic conductivity experiment the columns were filled to saturation (as described in Section 3.3.3) and left to drain for approximately 24 hours. Drainable porosity was then calculated from Equation 3.3. Figure 3.4 shows that drainable porosity is lowest when the sawdust proportion is lowest and increases significantly with increasing sawdust proportion when the mixture is 40-100% sawdust. Variation between

replicates is most obvious for the gravel-only experiment, although variation is still only 14%. This is most likely due to the effect of pebble shape and size variation on pore space volume. In the combination experiments most sawdust particles were seen to sit in the space between gravel particles, thus lessening the effect of pebble shape and size variation.

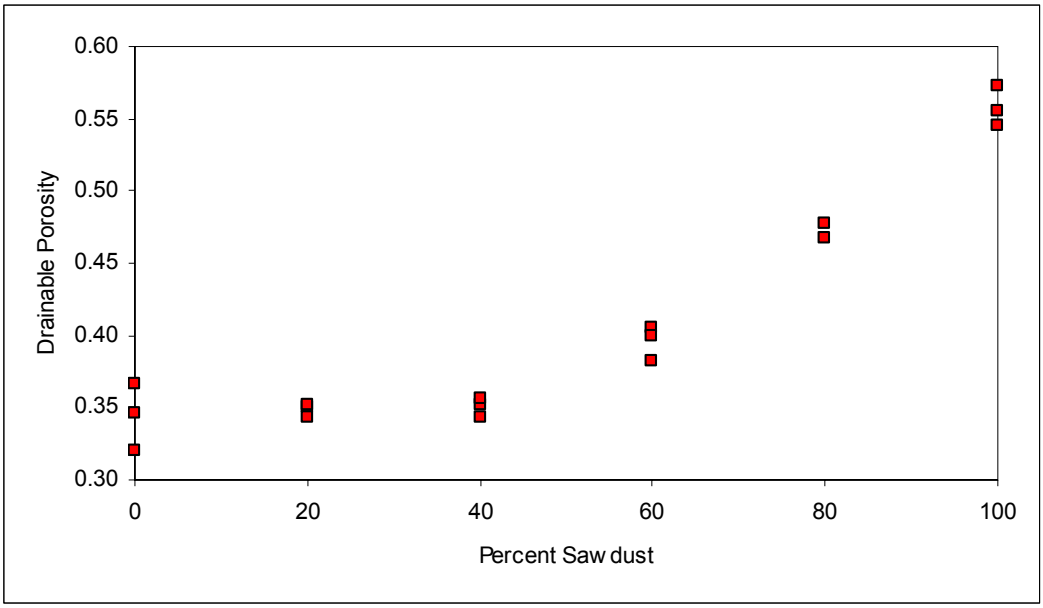

Fig. 3.4. Relationship between sawdust proportion and drainable porosity for three replications of each sawdust proportion.

3.4.4 Denitrification Rate Results

Denitrification rate experiments followed the methodology described in Section 3.3.4, with replicate experiments being run at the same time to minimise any effects caused by differences in significant variables such as water temperature, incoming contaminant concentration and oxygen concentration in the water.

Figure 3.5 presents the average denitrification rate for each experiment plotted against the sawdust proportion. It shows increasing denitrification rate with increasing sawdust proportion and variation of up to 30% between replicate experiments. This variation is not unexpected, as *Parkin* [1990] found that the spatial variability exhibited by soil denitrification is among the highest reported for soil processes, with coefficients of variation in the range of 100-500%. The rate of denitrification is highly dependent on the amount of nitrate, oxygen, and available carbon present. It is also dependent on the soil conditions, especially texture, temperature, pH, and ground cover. These dependencies are described in Section 1.3.2.

Methods for quantifying the effects of input uncertainty are presented in Chapter 7. Maximising degradation rate and minimising rate variation in the field are likely to be significant challenges for those designing and constructing PRB systems.

Denitrification rates have been measured in the field for pilot and full-scale PRBs. *Schipper and Vojvodić-Vuković* [1998] reported a maximum denitrification rate of 3.6 g N m^{-3} d^{-1} for a 30% sawdust:soil PRB. Figure 3.5 shows that a 30% sawdust:pea gravel laboratory column test could be expected to produce a denitrification rate of approximately 9 g N m^{-3} d^{-1}. *Robertson et al.* [2000] reported denitrification rates of 0.7 to 32 g N m^{-3} d^{-1} for four pilot-scale denitrification PRBs containing 15-100% wood mulch, sawdust and leaf compost.

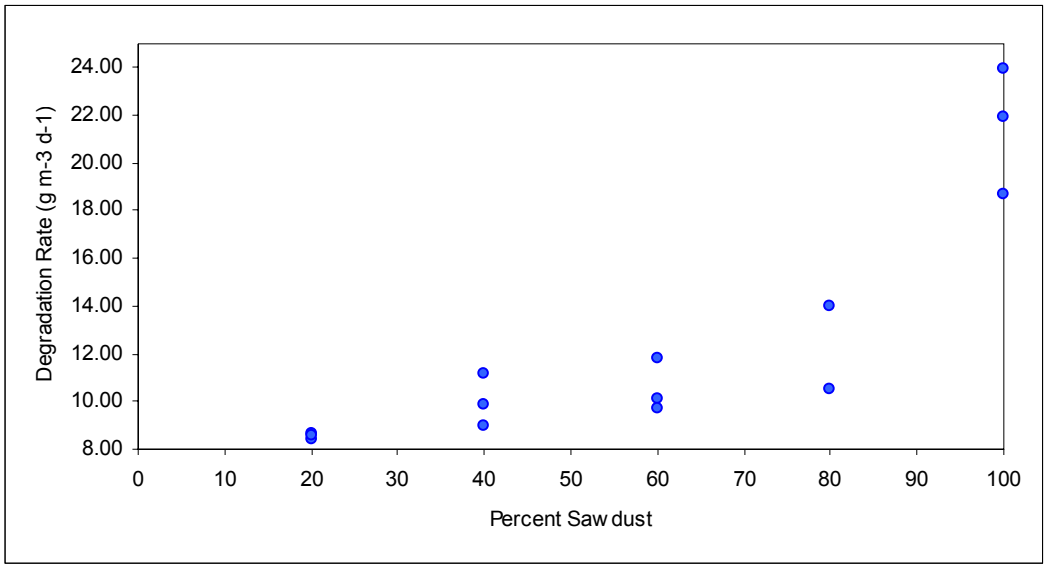

Fig. 3.5. Relationship between sawdust proportion and denitrification rate for three replications of each sawdust proportion.

3.5 Discussion

The experiments presented in Section 3.5 showed that measurable relationships are realistic under laboratory conditions between reactive/non-reactive material combinations and their volumetric factor, drainable porosity, hydraulic conductivity and degradation rate. The amount of each material required for a particular PRB can be calculated from the volumetric factors and individual material bulk densities. The expected groundwater pore velocity in a PRB can be calculated from drainable porosity, hydraulic conductivity and aquifer hydraulic gradient. The required residence time for a contaminant to degrade in a particular PRB system can then be calculated from the expected incoming contaminant concentration and the

expected rate of contaminant degradation. When the required residence time is known, barrier flow-through length can be determined in conjunction with the expected groundwater pore velocity in the barrier.

Sawdust proportion and slight compaction were both found to have an effect on the volumetric factor of a particular sawdust and pea gravel combination. Slight compaction increased volumetric factors by up to 4% and volumetric factors were greatest for approximately equal proportions of sawdust and pea gravel. Hydraulic conductivity was found to decrease with increasing sawdust proportion but levelled out when sawdust proportion was approximately 60%.

Drainable porosity was found to increase with increasing sawdust proportion, but no significant change was noted between 0% and 40% sawdust proportion. Denitrification rate was also found to increase with increasing sawdust proportion although variation between replicates of approximately 30% was measured for most experiments. Averaged values are presented in Table 3.3 as a laboratory characterisation of sawdust and pea gravel.

Table 3.3
Reactive/Non-Reactive Material Characterisation

Sawdust %		**0**	**20**	**40**	**60**	**80**	**100**
Volumetric Factor		1.00	1.07	1.13	1.12	1.04	1.00
Hydraulic Conductivity	$m\ d^{-1}$	14548.62	1881.74	669.49	529.22	510.38	640.32
Effective Porosity		0.34	0.35	0.35	0.40	0.47	0.56
Degradation Rate	$g\ m^{-3}\ d^{-1}$	0.00	8.54	10.01	10.55	12.26	21.52

The next step involves translation of laboratory results to particular field sites and estimation of their variability under site conditions. This is a very important aspect of PRB design. The optimal design methodology presented in Section 6.2 requires reactive/non-reactive material characterisation relevant to actual site conditions in the form of Table 3.3. The PRB design relationships to be presented in Section 6.3 assume that polynomial interpolation is appropriate between reactive material proportion and volumetric factor, hydraulic conductivity, drainable porosity and degradation rate. Before considering these issues, the hydraulic performance of a variety of PRB designs will be evaluated with the aim of understanding and then improving currently used designs. This will be the subject of Chapter 4.

Chapter Four

Hydraulic Performance Evaluation of PRB Design Enhancements

4.1 Introduction

Permeable reactive barrier (PRB) systems have two essential functions. The first is to capture the targeted contaminated groundwater and the second is to clean it up to the appropriate regulatory level. Once the preliminary assessment, site characterisation, reactive media selection and treatability testing processes have been completed (Sections 2.2.1 to 2.2.4), the computer models (economic, hydraulic and geochemical) can be set up. The purpose of the hydraulic model is to help design a PRB that will capture and degrade the plume in an efficient manner without negatively impacting the surrounding area.

Hydraulic performance analysis of standard PRB designs was used to confirm previously presented research that identified the potential for significant variation in residence time and capture zone (see discussion of *Benner et al.,* 2001; *Christodoulatos et al.,* 1996; and *Smyth et al.,* 1997 in Section 1.3.3). These variations can result in the need to oversize the system to ensure that down-gradient contaminant concentrations do not exceed imposed standards. A variety of new and existing PRB design enhancements for controlling residence time and capture variation were then tested. The most useful design enhancements were found to be customised down-gradient gate faces, velocity equalisation walls, deeper emplacement of the funnel than the gate, and careful manipulation of the hydraulic conductivity ratio between the gate and the aquifer. This research has been previously published (*Painter*, 2004).

Hydraulic performance analysis was also used to investigate conflicting conclusions between researchers regarding the effect of the hydraulic conductivity ratio (K_{prb}/K_{aq}) on hydraulic performance. *Starr and Cherry* [1994] used the two-dimensional software FLONET and defined hydraulic performance for fully penetrating PRB systems in terms of absolute and

relative discharge through the gate. Two primary conclusions were that the hydraulic performance of a PRB improved significantly with increasing gate width and hydraulic conductivity ratio (up to 10) but decreased with increasing funnel width. *Shikaze et al.* [1995], *Smyth, Shikaze and Cherry* [1997], and *Shikaze* [1997] used the three-dimensional FRAC3DVS software to analyse partially penetrating PRB systems. They used a capture zone size and shape estimated from particle streamlines as a measure of hydraulic performance. Modelling results showed that the hydraulic performance of partially penetrating PRB systems, like fully penetrating systems, improved appreciably only up to $K_{prb}/K_{aq} = 10$, and that hydraulic performance did not improve significantly in a moderately anisotropic aquifer ($K_{horizontal} = 2K_{vertical}$).

Teutsch et al. [1997] used MODFLOW to simulate the groundwater flow in two (horizontal) directions, assuming isotropic and homogeneous aquifer conditions. The advective transport was simulated using MODPATH. They state that they developed a special routine to automatically calculate capture width but do not elaborate. The primary conclusion from their numerical flow and advective transport simulations reads as follows:

> *"In general, the width of the capture zone of a funnel-and-gate^{TM} system is controlled by the effective hydraulic conductivity of the aquifer-gate combination, which can be approximated by the harmonic mean of $K_{aquifer}$ and K_{prb}. Therefore, $K_{prb} = 10\ K_{aquifer}$ has no significant effect on the width of the capture zone."*

They also state that this result seems to contradict the conclusions of *Star and Cherry* [1994]. *Teutsch et al.* [1997] proposed that the factor 10 ratio is only obtained if the model domain size is chosen too small and therefore the calculated width of the capture zone becomes affected by the model boundary conditions. This apparent contradiction obviously requires resolution.

The computer modelling experiments described in this chapter are proposed to address the issues of capture zone and residence time variation in isolation from the extra complexities presented by real life remediation design. The hydraulic performance of a PRB design is only one aspect of a remediation project. The most cost-effective design for a particular

application is also highly dependent on site-specific hydrogeologic, geochemical and economic information.

4.2 Modelling Approach

For this study, optimisation of the hydraulic performance of a PRB system is defined in terms of finding the balance between capture, residence time and barrier longevity that produces a minimum-cost acceptable design. This approach enables general hydraulic comparison between PRB designs as well as approximations to the functional relationships between PRB design decisions and hydraulic performance criteria (capture, residence time and longevity). This information can then be combined with site-specific hydrogeologic, geochemical and economic information in an optimisation formulation.

Visual MODFLOW (*Guiguer and Franz*, 1996) was chosen to simulate the groundwater flow and MODPATH (*Pollock*, 1989) was chosen to simulate the advective transport in three dimensions. This software combination enabled residence time and capture zone analysis via 3D particle tracking and volumetric flow analysis for mass balance estimation as well as identification of potentially detrimental flow regimes. The Horizontal Flow Barrier Module was another useful feature of MODFLOW, enabling the simulation of thin, impermeable walls without having to resort to extremely fine cell discretisation.

The chosen model domain was 100m wide by 100m long (in the direction of flow) by 10m deep, with the PRB system near the centre of the domain. The model described a homogeneous and isotropic aquifer with hydraulic gradient of 0.01 and effective porosity of 0.35. Grid discretisation was 4m x 4m x 1m at the boundaries, reducing to 0.25m x 0.25m x 0.25m in the vicinity of the PRB base. The "standard" partially penetrating PRB system chosen for analysis of the hydraulic performance criteria and comparison with enhanced systems contained 3m wide by 6m deep funnels (each side), 3m wide by 6m deep side walls and a 6m wide by 3m long by 6m deep gate. To create the equivalent fully penetrating system the bottom 4m of the grid was defined as inactive.

Figure 4.1 presents potential design components for a partially penetrating vertical PRB. The end-on view (Figure 4.1b) for the equivalent fully penetrating PRB would show the funnels

and gate keyed into the underlying aquitard. The gate contains an appropriate mixture of reactive and non-reactive material for capture and remediation of the desired contaminants. The funnel and side walls are constructed from impermeable materials such as sheet piling. Impermeable funnels are only proposed for the up-gradient face. *Christiansen and Hatfield* [1994] proposed the use of matching up and down-gradient funnels as part of an analytical 1D model but no evidence has been found to justify their extra cost.

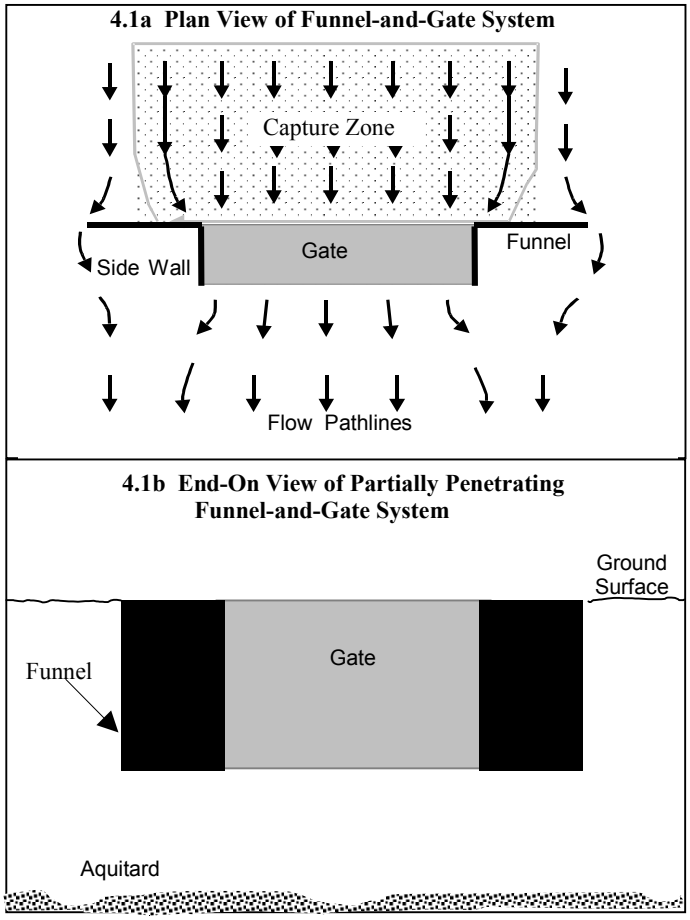

Fig. 4.1. Plan and end-on views of design components for a vertical PRB.

Three potential PRB design enhancements are presented in Figure 4.2 for controlling residence time and capture zone variation. All were initially modelled with three different hydraulic conductivity ratios (K_{prb}/K_{aq} = 0.1, 1 and 10) between the PRB and the surrounding aquifer. All gates were defined as homogeneous and isotropic. All funnels were set at 180^o to the gate as groundwater direction was assumed stable and *Starr and Cherry* [1994] found that 180^o funnels provide the greatest capture for any single flow direction.

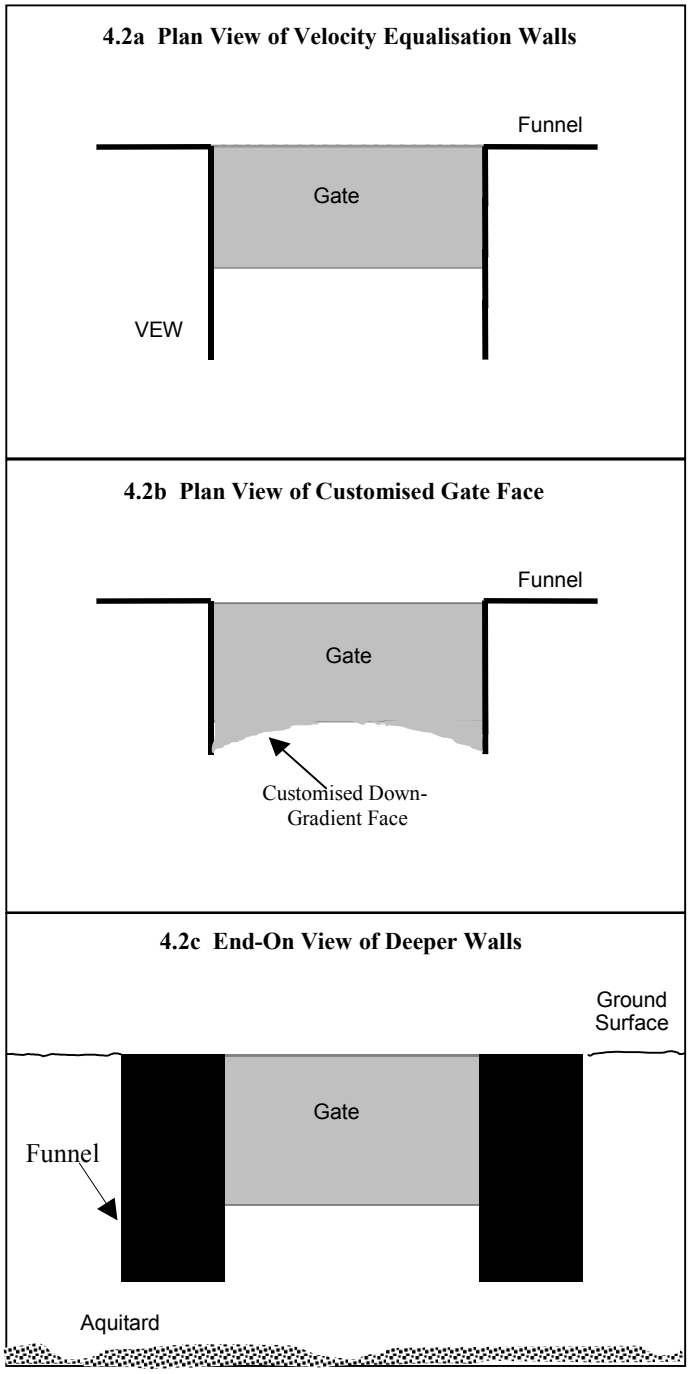

Fig. 4.2. Plan views of two potential design enhancements for controlling lateral variation in residence time and an end-on view of a potential design enhancement for controlling vertical variation in capture zone.

Figures 4.2a and 4.2b present a plan view of two design enhancements proposed to aid in controlling lateral variation in residence time for fully and partially penetrating PRB systems. In a homogeneous and isotropic aquifer and PRB system, significant lateral variation in residence time is primarily caused by the presence of a funnel and/or a gate hydraulic conductivity that is significantly different from the surrounding aquifer. *Christodoulatos et*

al. [1996] proposed the addition of velocity equalisation walls (VEWs) for the situation when the PRB design produced flow with a higher velocity near the side walls than down the centre of the gate. VEWs are extensions to the side walls for the purpose of increasing the time before flow can revert to natural patterns. This has the effect of decreasing the velocity of all flow in the gate, but particularly the higher velocity flow near the side walls.

The customised down-gradient gate face (Figure 4.2b) is a design enhancement that is believed to be new to the literature. It involves analysing the flow distribution for a standard PRB design and then extending the side walls and customising the shape of the down-gradient gate face to create the desired residence time distribution.

An end-on view of the third potential design enhancement is presented in Figure 4.2c. Emplacement of the impermeable funnel and side walls deeper than the gate is proposed to reduce vertical capture variation for particular PRB designs by funnelling flow through the gate that would have otherwise travelled under the PRB system. Deeper funnels combined with an impermeable base (instead of deeper side walls) have a similar effect. These design enhancements are also believed to be new to the literature.

Careful manipulation of the K_{prb}/K_{aq} ratio is proposed to provide adequate control of vertical variation in residence time for partially penetrating PRB systems. In a partially penetrating PRB, flow has the option of travelling under as well as around or through the PRB. Up to a point, increasing the K_{prb}/K_{aq} ratio will increase the PRB's capture zone and volumetric flow. But it will also increase residence time variation (vertically and laterally) and decrease overall residence time. By developing relationships between the K_{prb}/K_{aq} ratio and residence time for various PRB designs, an optimisation routine can be used to balance capture with residence time and produce the lowest cost design(s) for a particular scenario.

The volumetric flow measurements output by the MODFLOW Zone Budget Module were utilised as a general estimation of hydraulic performance and PRB longevity. The chosen approach involved dividing the gate of each PRB into six 1m wide zones. As the chosen PRBs and aquifer systems are symmetrical about the PRB centreline, these zones were grouped (totalling 2m wide each) as "Edge" (nearest the side walls), "Intermediate" and "Centre". A fourth zone was defined for the whole of the surrounding aquifer. Figure 4.3

shows a close-up of the PRB outline, grid discretisation and Zone Budget zones for a standard PRB.

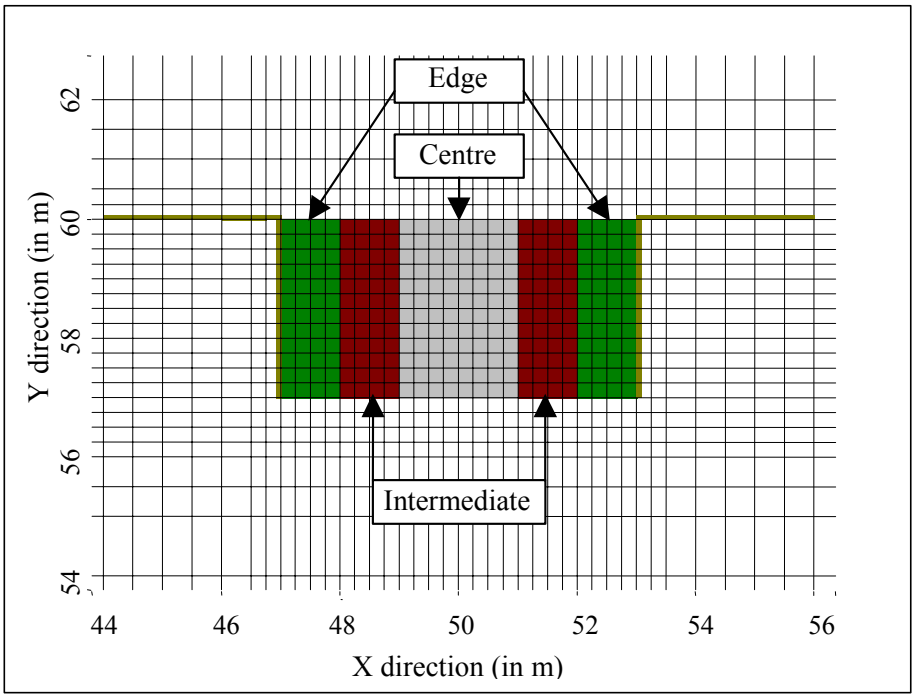

Fig. 4.3. Plan view of "standard" funnel-and-gate system: grid discretisation for modelling experiments and zone budget regions.

Three-dimensional particle tracking using MODPATH (*Pollock*, 1989) was chosen to provide detailed analysis of residence time and capture zone. Capture zone was calculated using the starting point of the most extreme particle captured from a line of 141 particles spaced 0.1m apart in the centre of each layer. Residence time was calculated by subtracting the entrance time from the exit time for captured particles. Particles were released at 1010 days and tracked for 1000 to 3000 days depending on the simulation. 1000 days was found to be sufficient time for the chosen model to reach steady-state using a time step discretisation of 75 and a time step multiplier of 1.2. Setting the time step multiplier greater than 1.0 meant that the earlier time steps involved fewer days than later time steps, thus increasing the accuracy of the initial conversion of the constant head boundaries into a hydraulic head at each cell.

Figure 4.4 presents particle-tracking output for a standard funnel-and-gate system with $K_{prb}/K_{aq} = 10$. Particles are released at the top of the figure and travel through or around the PRB near the base of the figure. Tick marks are placed every 50 days of particle travel for

visual comparisons and the three lines travelling across the figure are equipotential lines for estimation of regional gradients.

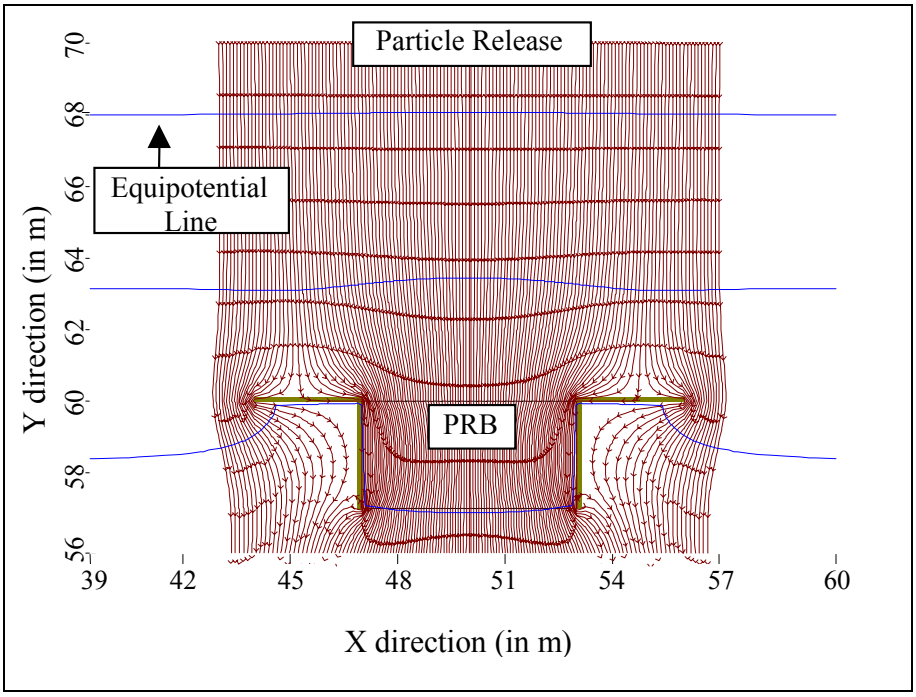

Fig. 4.4. Plan view of pathline output for the top fully-saturated layer of a partially penetrating standard funnel-and-gate system (K_{prb}/K_{aq}=10).

To enable accurate hydraulic comparison of different PRB designs, it is important to release the particles up-gradient from the portion of aquifer influenced by PRB emplacement (i.e. where the pathlines divert from their natural course). In this study, 10m up-gradient from the gate was found to be an acceptable distance for particle release.

4.3 Hydraulic Performance Criteria

4.3.1 Volumetric Flow

Volumetric flow for defined zones (groups of cells) in a Visual MODFLOW model is measured by the Zone Budget Module as the total volume of water per unit time passing between the zones. Volumetric flow through the three PRB zones defined in Figure 4.3 was used in particular to identify PRB designs with high lateral flow variation. As flowrate can affect the rates of change to gate permeability and reactivity over time, significant variation in flowrate across a PRB can lead to replenishment of the reactive material being required in some portions of the gate before others. When there is minimal flow variation within a zone, volumetric flow (Q) can be used to provide a quick estimation of average residence time from flow through length (l), effective porosity (n), and cross sectional area (A) as follows:

$$\textbf{Average Residence} = \frac{\mathbf{l * n * A}}{\mathbf{Q}} \qquad \textbf{4.1}$$

Hydraulic comparison with the natural state and with similarly sited alternative designs can be undertaken when the modelled flow through the defined zones with the PRB in place is divided by the flow through the same zones with no PRB in place. This dimensionless variable is defined as "relative flow". Different gate dimensions can only be included in comparisons if the effects of scale are understood. Figure 4.5 presents the relative flow output for the "edge", "intermediate" and "centre" zones of a standard partially penetrating funnel-and-gate system (as presented in Figures 4.1 and 4.3) with three K_{prb}/K_{aq} ratios (0.1, 1 and 10).

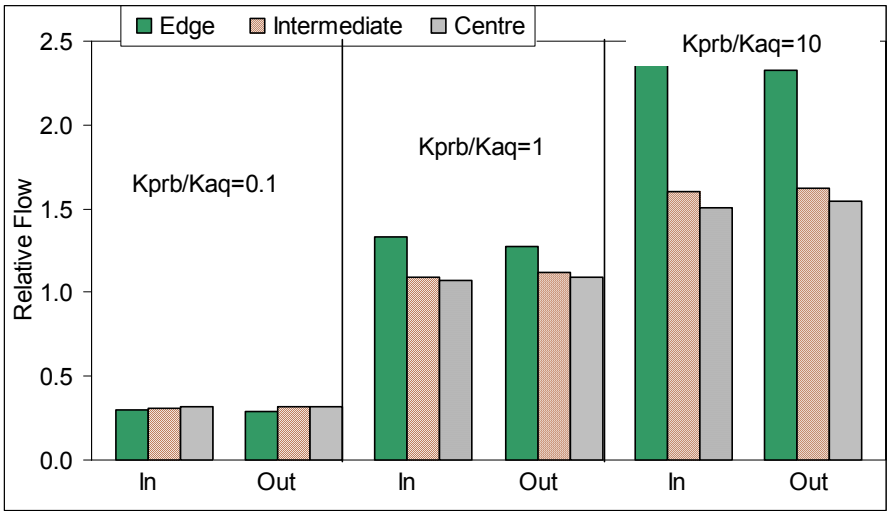

Fig. 4.5. Relative flow in and out of three zones for three partially penetrating standard funnel-and-gate systems (K_{prb}/K_{aq}= 0.1, 1 and 10).

Figure 4.5 shows that the K_{prb}/K_{aq} = 0.1 PRB produced flow approximately one third of that through the natural system. There is little variation between zones and between incoming and outgoing flow. The K_{prb}/K_{aq} = 1 PRB produced flow approximately one third greater than the natural system in the "edge" zone (due to the funnel) and less than 10% greater than the natural flow in the other zones. The slight reduction from incoming to outgoing flow in the edge zone and comparative increase in other zones suggests lateral inward movement for flow in the gate. The K_{prb}/K_{aq} = 10 PRB produced relative flows of approximately 2.4, 1.6 and 1.5 in the edge, intermediate and central zones respectively. The increase in flow is much more significant in the edge zone than the other zones. Slight lateral inward movement is again suggested for flow in the gate.

Figure 4.5 also indicates that the relationship between K_{prb}/K_{aq} ratio and volumetric flow is not linear for a particular PRB design. It can be shown that this relationship is best approximated by a sigmoid function (even for "gate only" systems) with flow tending toward minimum and maximum levels.

These results provide useful information about the longevity of the gate designs and their general relative hydraulic performance. In particular the significant difference between flow through the edge and other gate zones for the K_{prb}/K_{aq} = 10 system suggests that a homogeneous plume may cause the reactive material in the edge zone to decline at a greater rate than the rest of the gate. The extra flow may also result in the permeability and reactivity

of this zone changing over time at a greater rate than the rest of the gate, potentially altering the relative hydraulic performance balance between zones.

4.3.2 Residence Time

Particle residence time through a section of an unconfined, homogeneous aquifer in steady state can be calculated from the particle travel distance (d), aquifer effective porosity (n_{aq}), conductivity (K_{aq}) and hydraulic gradient ($grad_{aq}$) by the following equation:

$$\textbf{Natural Residence} = \frac{\mathbf{d} * \mathbf{n}_{aq}}{\mathbf{K}_{aq} * \mathbf{grad}_{aq}} \qquad \textbf{4.2}$$

Creation of a dimensionless variable, relative residence time, enabled PRB residence time comparison with the natural aquifer system as well as other similarly sized and sited PRB designs. Relative residence time (Equation 4.3) is calculated for each particle by dividing its simulated residence time by the "natural" residence time calculated by Equation 4.2 (with extra subscript $_{sim}$) for a particle travelling through the same part of the model without the PRB system in place. The simulated residence time is calculated from the particle time at the PRB up-gradient face (t_U) subtracted from the particle time at the PRB down-gradient face (t_D).

$$\textbf{Relative Residence} = \frac{\left(\mathbf{t}_D - \mathbf{t}_U\right) * \mathbf{K}_{aq\ sim} * \mathbf{grad}_{aq\ sim}}{\mathbf{length}_{PRB\ sim} * \mathbf{n}_{aq\ sim}} \qquad \textbf{4.3}$$

The place of PRB effective porosity in an optimal design formulation was examined via a series of computer modelling experiments. Table 4.1 and the laboratory experiments in Chapter 3 suggest that effective porosity should be considered independently from hydraulic conductivity for PRB modelling even though there is some correlation between the two.

Table 4.1
Unconsolidated Deposit Ranges

	Porosity	Hydraulic Conductivity (m/s)
Gravel	0.25 - 0.40	10^{-3} - 10^{0}
Sand	0.25 - 0.50	10^{-7} - 10^{-2}
Silt	0.35 - 0.50	10^{-9} - 10^{-5}
Clay	0.40 - 0.70	10^{-12} - 10^{-9}

(from *Freeze and Cherry*, 1979)

The stability of relative residence time to (actual porosity/simulated porosity) ratio was tested for a variety of PRB designs. Darcy's Law (Section 1.2.1) shows that residence (time/unit length) is proportional to porosity divided by the product of hydraulic conductivity and hydraulic gradient (see Equation 4.2). This means that a single effective (PRB porosity/aquifer porosity) combination should be able to be used to produce the relative residence for a particular PRB design, which would then be factored by the actual effective (PRB porosity/aquifer porosity) combination. The elimination of PRB effective porosity as a decision variable in the PRB design optimisation would greatly reduce the amount of modelling necessary to produce functional relationships between all decision variables. The design inputs for the chosen PRB systems are presented in Table 4.2 and the results in Figure 4.6.

Table 4.2

PRB Design Inputs for Porosity Experiments

PRB #	1	2	3
$Grad_{Aq}$	0.01	0.01	0.01
n_{Aq}	0.25	0.35	0.35
$Depth_{Aq}$ (m)	6	6	6
K_{PRB}/K_{Aq}	4	4	10
$Width_{PRB}$ (m)	6	6	9
$Length_{PRB}$ (m)	6	6	18
$Depth_{PRB}$ (m)	6	6	6
Funnel*2 (m)	6	6	18

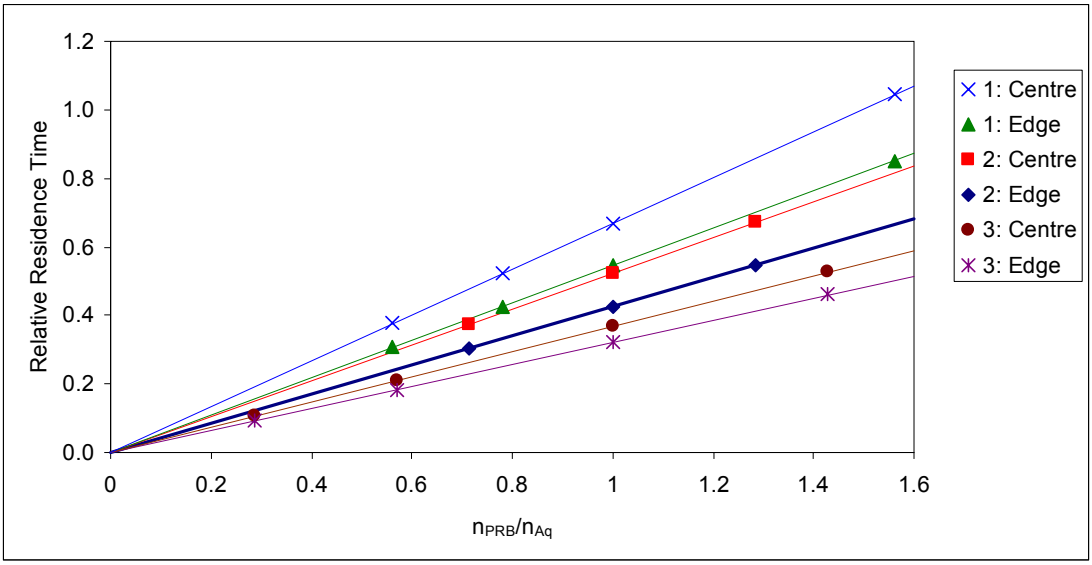

Fig 4.6. Effect of porosity ratio on relative residence time for a variety of designs.

The straight lines in Figure 4.6 suggest that the modelled relationship is true to the theoretical linear relationship. An effective porosity of 0.35 for PRB and aquifer was therefore chosen to produce the relative residence for all modelled PRB designs. The actual residence time in the optimisation formulation can be calculated from the appropriate simulated relative residence multiplied by the actual natural residence time and actual (PRB porosity/aquifer porosity) ratio as in Equation 4.4.

$$\mathbf{PRB\ \ Residence\ \ Time} = \frac{\mathbf{Relative\ Residence} * \mathbf{length}_{PRB} * \mathbf{n}_{aq}}{\mathbf{K}_{aq} * \mathbf{grad}_{aq}} * \frac{\mathbf{n}_{PRB}}{\mathbf{n}_{aq}}$$

$$= \frac{\mathbf{Relative\ Residence} * \mathbf{length}_{PRB} * \mathbf{n}_{PRB}}{\mathbf{K}_{aq} * \mathbf{grad}_{aq}} \qquad \mathbf{4.4}$$

Computer modelling experiments were then undertaken for a variety of partially and fully penetrating funnel-and-gate systems (K_{prb}/K_{aq} = 0.1, 1 and 10). Analysis of the experimental results showed that significant lateral variation in residence time can occur at any depth in fully and partially penetrating PRB systems, even if the PRB material is mixed homogeneously. Lateral variation in residence time is caused by extra flow funnelled through the gate as a result of the placement of an up-gradient funnel, or material in the gate that has a significantly different hydraulic conductivity from the surrounding aquifer. Significant vertical variation in residence time can also occur in partially penetrating PRB systems when the hydraulic conductivity of the gate is significantly different from the surrounding aquifer.

Pathline analysis in plan view of flow through the top fully saturated layer of a standard funnel-and-gate system (K_{prb}/K_{aq} = 10) was previously presented in Figure 4.4. A combination of the funnel length and high K_{prb}/K_{aq} ratio diverted extra flow through the gate, resulting in hydraulic capture approximately 1.5 times the gate width. This situation creates significant lateral variation in residence time for fully and partially penetrating PRB systems. The extent of the residence time variation is illustrated in Figure 4.7. Relative residence is graphed against the particle's lateral (x axis) entry point along the up-gradient gate face to show incoming flow distribution. Particle tracking can also be used to show how the lateral flow distribution changes throughout the flow-through distance of the gate, but this information is more easily attained from volumetric flow output for the purposes of estimating barrier longevity and time-dependent permeability changes.

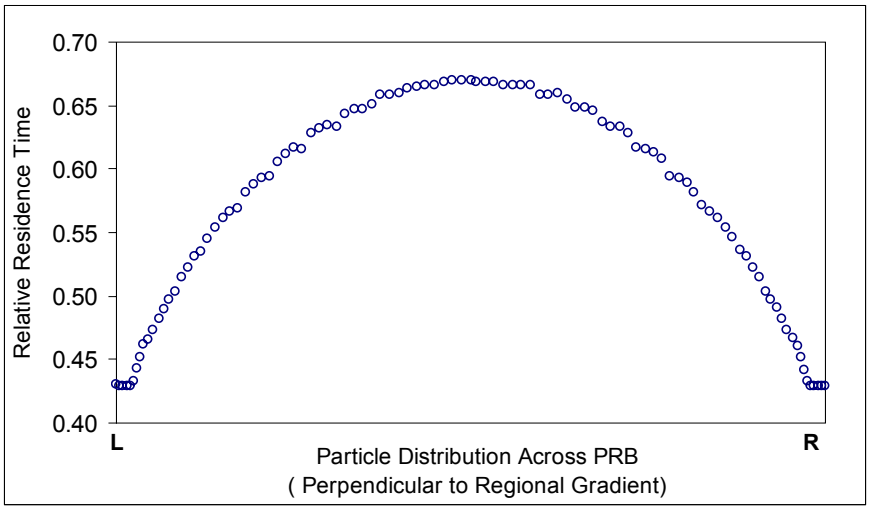

Fig. 4.7. Plan view of lateral variation in residence time for the top fully-saturated layer of a partially penetrating standard funnel-and-gate system (K_{prb}/K_{aq}=10).

The greatest density of particles in Figure 4.7 occurs adjacent to the side walls. This is the fastest travelling flow with a residence time approximately 43% of a particle travelling through the same part of the natural aquifer. Relative residence time increases from the edge to the centreline due to the reducing effect of the funnelled flow. Centreline relative residence time is approximately 67% of a particle travelling through the same part of the natural aquifer. If the plume requiring capture by this PRB was homogeneous, the required flow-through distance would be significantly greater near the side walls than the central portion of the gate.

Figures 4.8a and 4.8b illustrate a cause of vertical variation in residence time. Each figure shows a water table that descends from right to left and the side of a gate delineated by a shaded rectangle. The dark section at the base of Figure 4.8a contains inactive cells, creating a fully penetrating PRB. Flow travels through this PRB without any vertical deviation. Figure 4.8b presents the equivalent partially penetrating PRB design. As the gate is ten times more conductive than the aquifer, flow that would normally have travelled under the gate base is instead funnelled through its up-gradient face. This vertical funnelling works on the same principal as lateral funnelling, causing flow already travelling through the lower portion of the PRB to travel faster and on a different trajectory to flow travelling through the higher portions of the gate. The opposite effect occurs when the gate is less conductive than the surrounding aquifer.

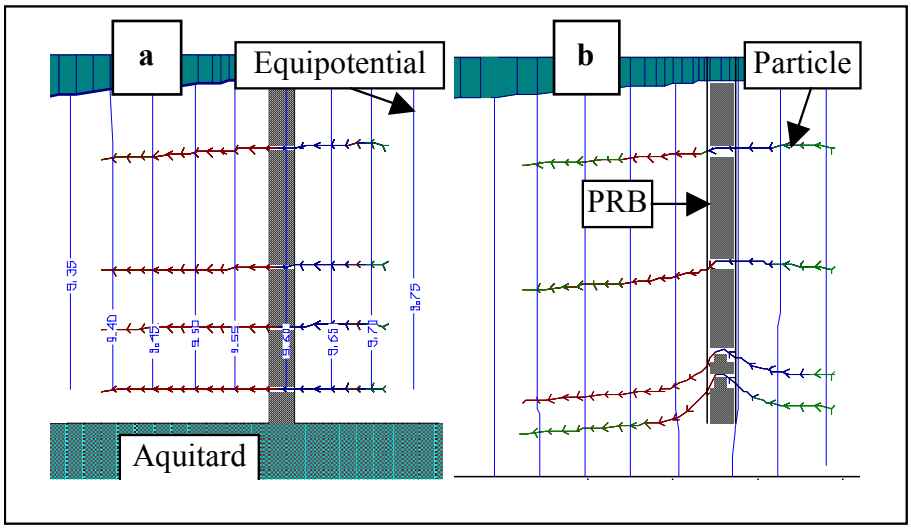

Fig. 4.8. Side view of flow travelling right to left through a) fully and b) partially penetrating PRB systems (shaded rectangles) when K_{prb}/K_{aq} = 10.

Table 4.3 presents relative flow and residence statistics for three partially penetrating standard PRBs with K_{prb}/K_{aq} ratios of 0.1, 1 and 10. Relative flow statistics are the average of the incoming and outgoing flow presented in Figure 4.5. Relative residence is presented for three particles at up to four release depths relative to the PRB base. The "edge" particle is the one travelling closest to the side wall. The "intermediate" particle is the one captured half way between the side wall and the centreline. The "centre" particle is the one travelling down the centreline.

Table 4.3
Relative Flow and Residence Comparison for
Three Standard (Partially Penetrating) PRB Designs

Design Name		Relative Flow	Relative Residence (4 release depths)			
			4.5m	2.5m	0.5m	-0.5m
K_{PRB}/K_{Aq}=0.1	Edge	0.30	3.49			
	Int	0.32	3.23			
	Centre	0.32	3.18			
K_{PRB}/K_{Aq}=1	Edge	1.31	0.72	0.76	0.01	
	Int	1.11	0.82	0.84	0.50	
	Centre	1.08	0.85	0.86	0.88	
K_{PRB}/K_{Aq}=10	Edge	2.35	0.43	0.42	0.31	
	Int	1.61	0.60	0.58	0.46	0.44
	Centre	1.53	0.65	0.62	0.49	0.48

All designs in Table 4.3 produce lateral and vertical variation in residence time. The K_{prb}/K_{aq} = 0.1 PRB produces very high residence times but captures no particles released in the lower half of the PRB (depth = 6m). Lateral variation in residence time for particles released 4.5m above the PRB base is approximately 10%.

The K_{prb}/K_{aq} = 1 PRB captures particles at all release depths above the PRB base. Lateral variation in residence time at 4.5m and 2.5m release depths are 18% and 13% respectively. This variation is entirely due to funnel effects as the PRB conductivity for this design matches the aquifer conductivity. Vertical variation in residence time is insignificant down the centreline and generally less than 5% for particles released at least 2.5m above the PRB base. The extra flow funnelled into the upper portions of the PRB causes flow entering just above the PRB base to descend out the base before reaching the down-gradient gate face. This results in dramatic decrease in residence time for most particles entering the PRB near its base.

The K_{prb}/K_{aq} = 10 PRB captures particles at all presented release depths, even below the PRB base. Capture width for particles released 0.5m below the PRB base is less than at other release depths and the residence time is approximately 35% less than the equivalent particle released at 4.5m. Lateral variation in residence time of 47% to 58% is presented for the three release depths above the PRB base. Vertical variation in residence time for these particles is 30% to 38%.

4.3.3 Capture Zone

Most PRB systems will have a local influence on the hydraulic gradient of the surrounding aquifer. It is important that particles used in hydraulic comparisons between PRB systems are released up-gradient from this portion of aquifer. Otherwise, the calculated capture widths will not have a common point of comparison (the natural capture width) with other PRB systems. Comparing the equipotential lines of the natural system with the system containing the PRB can identify the influenced portion of aquifer. For example, in Figure 4.4 the top equipotential line is horizontal while the other two lines deviate from the horizontal. All these lines were horizontal before incorporation of the PRB. The inward lateral deviation of the flow lines toward the gate centreline just up-gradient from the gate means that particle tracking or volumetric flow analysis that starts in this region will underestimate the capture

width relative to flow travelling through the natural system. A particle release distance of 10m up-gradient from the PRB was found to be satisfactory for all modelled PRB dimensions.

Relative capture at each release depth was calculated by dividing the distance between the y coordinate of the maximum (y_{max}) and minimum (y_{min}) particles captured by the gate width (W_G), which is the capture in the natural system.

$$\textbf{Relative Capture} = \frac{y_{max} - y_{min}}{W_G} \qquad \textbf{4.5}$$

For symmetrical PRB systems, modelling time can be saved by only releasing particles from the centreline of the gate (y_{centre}) to just past the maximum captured particle width (approximately 0.5*gate width + 0.8*funnel width for all modelled systems) and calculating the relative capture as follows:

$$\textbf{Relative Capture} = \frac{y_{centre} - y_{min}}{0.5 * W_G} \qquad \textbf{4.6}$$

When relative capture widths have been calculated at many depths, the PRB's relative capture zone (size and shape) can be approximated by interpolating between the relative capture width measurements. Figure 4.9 presents the capture zones for a standard partially penetrating funnel-and-gate system with three different hydraulic conductivity ratios (K_{prb}/K_{aq} = 0.1, 1 and 10).

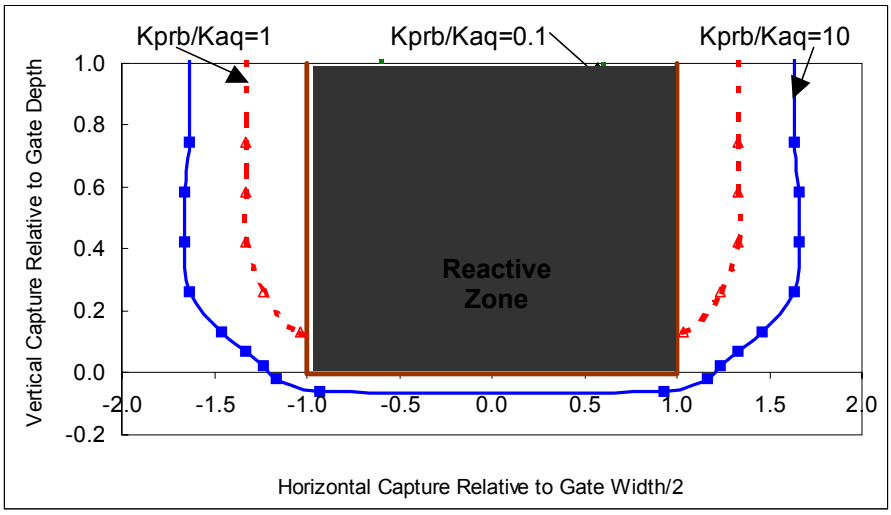

Fig. 4.9. End-on view of relative capture (= capture width/gate width) for three partially penetrating PRBs (K_{prb}/K_{aq} = 0.1, 1 & 10) compared to gate extent (–1 to +1) and funnel extent (–2 to +2).

In Figure 4.9 capture zone is shown to increase non-linearly with increasing K_{prb}/K_{aq} ratio, but the capture width in the lower portion of the K_{prb}/K_{aq} = 1 and K_{prb}/K_{aq} = 10 PRBs decreases with increasing depth. This result is consistent with conclusions reached by *Smyth et al.* [1997]. An increasing flow volume diverting under the funnel with increasing depth causes the vertical variation in capture width. There is essentially no vertical variation in capture width for the K_{prb}/K_{aq} = 0.1 PRB because there is no capture close to the base of the funnel. Full capture of a plume whose width and concentration does not decrease with increasing depth will always require this type of PRB to be deeper than the plume. This is considered inefficient, resulting in underutilised reactive material in sections of the reactive zone (gate).

The effect of hydraulic gradient on relative residence and capture was then examined in order to determine its role in the optimisation formulation. In theory, hydraulic gradient should have no effect on capture and a linear effect on residence. An example PRB with length=3m, width=6m, depth=6m, total funnel width=12m, effective porosity=0.35 and hydraulic conductivity=10m/day was modelled in partially and fully penetrating situations. The surrounding aquifer had effective porosity=0.35, hydraulic conductivity=10m/day, and hydraulic gradients of 0.0025, 0.005, 0.0075 and 0.01 m/m. Table 4.4 presents the relative residence (edge and centre) plus relative capture for particles released 10m up-gradient from the PRB and 4.5m above its base.

Table 4.4

Effect of Hydraulic Gradient on Relative Residence and Capture

(Particles released 4.5m above the base of 3x6x6m fully and partially penetrating PRBs with 12m funnels and K_{prb}/K_{aq} = 10)

Penetration	Relative to	Hydraulic Gradient (m/m)			
	Natural System	0.0025	0.005	0.0075	0.01
Full	Edge Residence	0.334	0.335	0.337	0.338
	Centre Residence	0.569	0.571	0.574	0.577
	Capture	2.067	2.067	2.067	2.067
Partial	Edge Residence	0.365	0.365	0.366	0.369
	Centre Residence	0.598	0.599	0.601	0.603
	Capture	2.100	2.100	2.100	2.100

Table 4.4 shows that hydraulic gradient has no effect on relative capture (for particles released 0.1m apart) and only a very small quasi-linear effect (approximately 1% increase for 4-fold increase in gradient) on relative residence for the example PRB. Hydraulic gradients greater than 0.01 m/m were not possible with the chosen grid layer depth of 1m and grid length of 100m and a coarser grid was considered detrimental to model accuracy. The partially penetrating PRB produced an edge residence approximately 10% greater than the equivalent fully penetrating system. Centre residence (~5%) and capture (~1.5%) were also slightly greater. These differences were due to the effect of vertical flow patterns described in Figure 4.8. The use of model results from fully penetrating systems would not be recommended for the equivalent partially penetrating system unless the K_{prb}/K_{aq} ratio was very close to 1.

The example was chosen for its significant effect on local flow regimes, providing the greatest potential for hydraulic gradient impacting on relative residence and capture. It was therefore concluded that a hydraulic gradient of 0.01 m/m would be used for determination of functional relationships between PRB design variables, with the actual hydraulic gradient of the aquifer under investigation to be used for determination of actual residence times. Extra care could be taken in post-optimisation simulation and pilot testing for aquifers with hydraulic gradient significantly greater than 0.01m/m. However, the variability in real aquifer

systems and the fact that slight underestimation of residence time is a useful safety factor would probably make investment into this aspect of PRB design unnecessary.

4.3.4 Hydraulic Performance Criteria Conclusions

The primary conclusion reached from this hydraulic performance analysis is that an understanding of residence time and capture zone variation is a crucial aspect of minimum cost PRB design. In most cases it is expected that this variation is more efficiently quantified by particle tracking than volumetric flow analysis. By using a very fine cell discretisation and high number of zones in the Zone Budget module volumetric flow analysis produced accurate output, even in variable flow situations. However, this method was found to be less computationally and analytically efficient than particle tracking.

Volumetric flow analysis was found to be particularly useful in the identification of flow regimes that may affect the permeability or reactivity of portions of the gate over time. The long term effects of flow variability within a gate are important hydraulic performance issues but are difficult to include in a PRB design optimisation, primarily because of a lack of field data due to the relative newness of the technology.

It is recommended that particles be released up-gradient from the portion of aquifer influenced by PRB emplacement and to a greater depth and width than the PRB dimensions. Calibration of modelled results with a specific site will require site characterisation of hydraulic conductivity, hydraulic gradient and porosity.

Hydraulic performance analysis can be used to compare a variety of PRB designs under specific objectives, for example maximisation of capture zone or minimisation of residence time variation. However, the primary objective of this modelling study was to identify design enhancements for controlling residence time and capture zone variation. These enhancements are considered necessary for maximising the potential of PRB systems for the remediation industry.

4.4 Design Enhancements for PRB Systems

4.4.1 Control of Lateral Variation in Residence Time

Customised down-gradient gate faces and velocity equalisation walls (see Figure 4.2) were analysed as potential PRB design enhancements for controlling lateral variation in residence time for fully and partially penetrating systems. No optimisation of these enhancements was attempted at this time. The fully penetrating funnel-and-gate system presented in Figure 4.3 (6 by 3 by 6m and 3m funnels) with K_{prb}/K_{aq} = 10 to maximise lateral variation in residence time was chosen as the standard PRB for comparative purposes. The customised down-gradient gate face design chosen for analysis is presented in Figure 4.10.

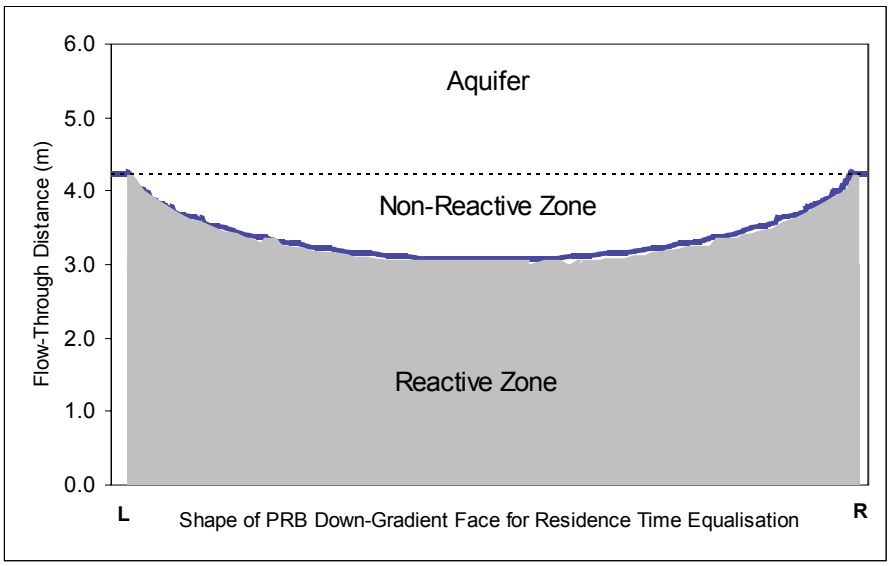

Fig. 4.10. Plan view of customised down-gradient gate face added to a fully penetrating funnel-and-gate system with K_{prb}/K_{aq} = 10 to equalise lateral variation in residence time.

The shape of the customised down-gradient gate face was created by first determining the required relative residence time distribution across the PRB based on plume, aquifer and PRB characteristics. It then found for each captured particle the flow-through distance where that residence time was met. The example gate face in Figure 4.10 achieves residence time equalisation for a plume with constant concentration across its width. The same approach can be applied to other scenarios, for example a plume with lower concentration at its edges than down its centreline. Figure 4.10 shows that the 3m side walls of the standard PRB were extended out to 4.25m and minimal extra flow-through length was added to the central two-

thirds of the gate width. This particular design increased gate reactive zone volume by approximately 13% and impermeable wall area by 20%. This compares to a 42% increase in reactive zone volume plus 20% increase in impermeable wall area if a traditional approach had been used, which would have set a constant 4.25m flow-through length based on the fastest moving flow at the edges.

The hydraulic conductivity of the gate non-reactive zone was set equal to the conductivity of the gate reactive zone. This was to stop flow travelling down the central portion of the gate from diverging toward the gate extensions near the side walls. In practice, if a high K_{prb}/K_{aq} ratio is desired then the non-reactive section of the gate will need to be excavated during PRB construction and replaced with appropriate material. This should not be necessary when the hydraulic conductivity of the gate and aquifer are similar provided excavating equipment can satisfactorily approximate the customised down-gradient face.

The velocity equalisation wall (VEW) design chosen for analysis involved extending the side walls of the standard PRB out by 3m, 6m and 9m but retaining the 3m gate flow-through length. Relative capture, flow and residence for the four enhanced designs are presented in Table 4.5 alongside those of the comparative standard PRB. The "Custom Gate" design improves the hydraulic performance of the standard "K_{prb}/K_{aq} = 10" design by increasing capture and eliminating lateral variation in residence time. Relative flow comparisons are not appropriate between these designs as they have different sized and shaped gates.

Comparison of VEW designs with the standard design shows that the VEW walls reduce lateral variation in residence time and increase overall residence time. However, this is at the expense of reduced capture and flow. 3m VEWs reduce the lateral variation in residence time from 58% in the standard design to 22%, but the increase from 3m VEWs to 9m VEWs only reduces lateral variation in residence time by a further 1.5%.

VEWs are likely to be most useful as a design enhancement when complete residence time equalisation is not required (e.g. the contaminant concentration decreases near the edge of the plume) and the extra reactive material required for a customised down-gradient face is expensive relative to impermeable wall costs. Customised down-gradient gate faces show potential as a design enhancement for controlling lateral variation in residence time provided

the gate extensions are cost-effective and able to be constructed to the required level of accuracy.

Table 4.5
Relative Capture, Flow and Residence Comparison for One Standard and Four Enhanced (Fully Penetrating) PRB Designs

Design Name	Relative Capture	Gate Zone	Relative Flow	Relative Residence
K_{prb}/K_{aq}=10	1.66	Edge	2.20	0.43
		Int	1.40	0.62
		Centre	1.31	0.67
Custom Gate	1.73	Edge	1.64	0.62
		Int	1.04	0.62
		Centre	0.97	0.62
3m VEWs	1.43	Edge	1.62	0.59
		Int	1.30	0.70
		Centre	1.26	0.72
6m VEWs	1.33	Edge	1.48	0.64
		Int	1.21	0.75
		Centre	1.18	0.78
9m VEWs	1.26	Edge	1.40	0.68
		Int	1.15	0.79
		Centre	1.13	0.82

4.4.2 Control of Vertical Variation in Capture Width

Deeper emplacement of all walls than the gate (Figure 4.2c) was analysed for its potential in controlling vertical variation in the capture width of partially penetrating PRB systems. Comparison of the residence statistics in Table 4.6 with the equivalent statistics for the standard "K_{prb}/K_{aq} = 10" design in Table 4.3 shows that the deeper emplacement of walls than the gate has minimal effect on residence time. Flow in the edge zone is increased by ~5%.

Figure 4.11 shows that the decrease in capture width associated with increasing depth in the standard partially penetrating PRB was not present in an enhanced design containing walls emplaced 2m deeper than the gate. The decrease in capture width for the standard PRB was

due to flow travelling under the wall rather than through the gate. The deeper walls increase the distance groundwater has to travel to dive underneath the PRB, thus diverting the desired flow through the gate. While the improvement in capture zone and flow from adding deeper walls is only ~5% in this case, the deeper walls prevent the need for the whole PRB depth to be increased if that extra flow had to be captured. Further investigation of this design enhancement is considered worthwhile.

Table 4.6
Relative Flow and Residence Statistics for
K_{prb}/K_{aq}=10 PRB Design Enhanced with 2m Deeper Walls

	Relative Flow	Relative Residence (4 release depths)			
		4.5m	2.5m	0.5m	-0.5m
Edge	2.46	0.42	0.40	0.34	
Int	1.65	0.59	0.57	0.45	0.44
Centre	1.55	0.64	0.61	0.48	0.47

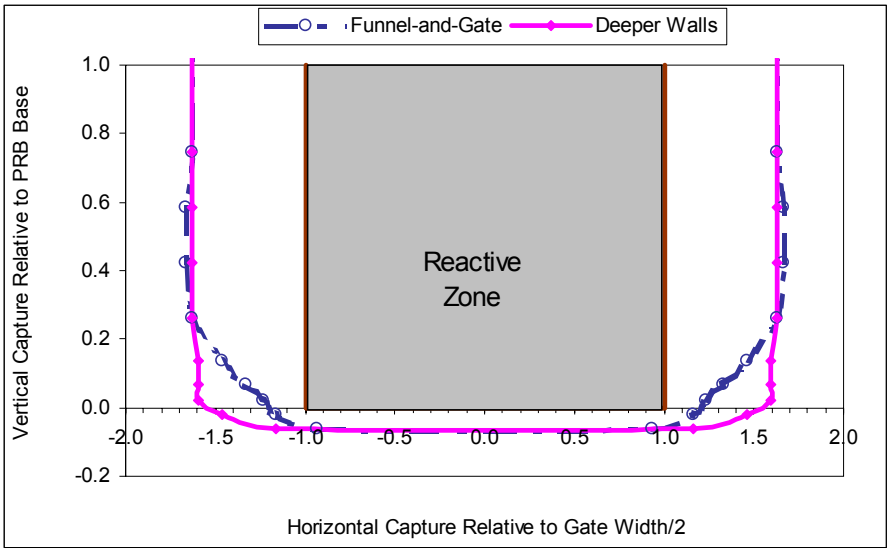

Fig. 4.11. End-on view of capture zone comparison for a partially penetrating funnel-and-gate system (K_{prb}/K_{aq} = 10) and an enhanced design containing 2m deeper walls.

4.4.3 Control of Vertical Variation in Residence Time

None of the aforementioned design enhancements were found to provide control over vertical variation in residence time for partially penetrating PRB systems. The primary cause of

vertical variation in residence time was found to be the K_{prb}/K_{aq} ratio, so more detailed analysis of an enhanced PRB system was undertaken.

The enhanced designs chosen for comparative purposes were partially penetrating PRBs with funnels, a customised down-gradient face, VEWs, deeper walls than the gate and four K_{prb}/K_{aq} ratios (see Table 4.7 and Figure 4.12). All gates were 6m wide by 6m deep, funnels were 3m wide by 8m deep on each side and side walls were 5m long by 8m deep on each side. The centreline flow-through lengths of the gates were set to achieve lateral equalisation of flow.

Table 4.7
Design Details for Four Enhanced PRB Systems

Design Name	Extra Wall Depth (m)	VEW Length (m)	Gate Length		Gate Volume (m^3)
			Edge (m)	Centre (m)	
K_{prb}/K_{aq}=1e	2.0	0.75	4.25	3.90	141.3
K_{prb}/K_{aq}=3e	2.0	0.75	4.25	3.65	133.0
K_{prb}/K_{aq}=5e	2.0	0.75	4.25	3.60	131.3
K_{prb}/K_{aq}=10e	2.0	0.75	4.25	3.50	128.0

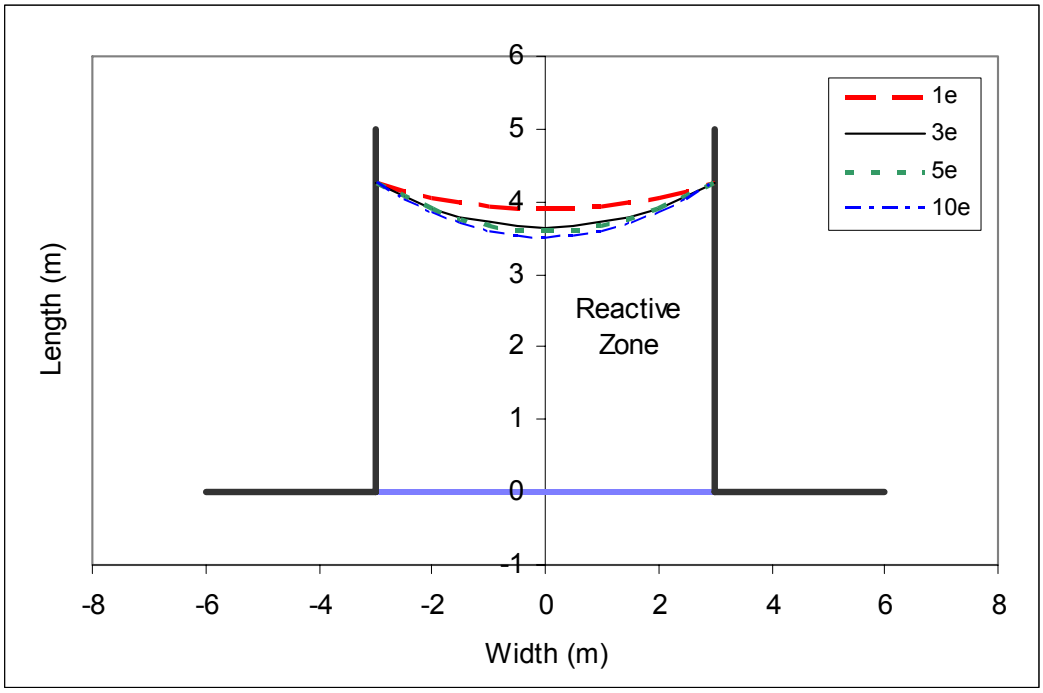

Fig. 4.12. Plan view of four partially penetrating enhanced PRB systems (K_{prb}/K_{aq} = 1, 3, 5 and 10) with unique customised down-gradient gate faces.

Manipulation of the hydraulic conductivity ratio is a complex issue. Up to a point, increasing the hydraulic conductivity will increase the PRB's capture zone and volumetric flow. Nevertheless, it will also increase residence time variation and decrease overall residence time. Control over the K_{prb}/K_{aq} ratio in the field is also difficult with the potential for significant variability in K_{aq} (and in K_{prb} if the gate construction techniques and materials are not carefully controlled).

Table 4.8 and Figure 4.13 present the relative flow, residence and capture for the four enhanced designs. The enhanced designs K_{prb}/K_{aq} = 1e and K_{prb}/K_{aq} = 10e can be compared with the equivalent standard designs K_{prb}/K_{aq} = 1 and K_{prb}/K_{aq} = 10 in Table 4.3 and Figure 4.9.

All of the enhanced designs eliminated lateral variation in residence time and vertical variation in capture width as expected. However, none managed to completely eliminate vertical variation in residence time. Variation is least in the K_{prb}/K_{aq} = 1e design and is just due to vertical flow effects close to the PRB base in the intermediate zone (with little or no flow captured in the edge zone). All flow released 0.5m above the base of the K_{prb}/K_{aq} = 3e design has ~18% less residence time than the flow travelling 4.5m above the PRB base. This residence time difference increases to >30% for flow near the side wall of the K_{prb}/K_{aq} = 10e design.

Remediation of a homogeneous plume requires PRB flow-through length to provide sufficient residence time for the whole plume. If the PRB base was approximately the same depth as the plume base, the K_{prb}/K_{aq} = 10e design would require >30% more flow-through distance than the K_{prb}/K_{aq} = 3e design. However, the extra capture width generated by the K_{prb}/K_{aq} = 10e design would result in it requiring ~8% less gate/funnel width than the K_{prb}/K_{aq} = 3e design. The minimum cost design is clearly dependent on the specific remediation problem to be solved and the relative cost of construction techniques and materials.

Table 4.8
Relative Flow and Residence Comparison for Four Enhanced (Partially Penetrating) PRB Designs

Design Name		Relative Flow	Relative Residence (4 release depths)			
			4.5m	2.5m	0.5m	-0.5m
K_{prb}/K_{aq}=1e	Edge	0.91	1.10	1.12		
	Int	0.84	1.10	1.11	1.00	
	Centre	0.83	1.10	1.11	1.11	
K_{prb}/K_{aq}=3e	Edge	1.41	0.78	0.76	0.68	
	Int	1.22	0.79	0.76	0.67	
	Centre	1.20	0.79	0.76	0.67	
K_{prb}/K_{aq}=5e	Edge	1.61	0.72	0.69	0.59	
	Int	1.36	0.73	0.69	0.58	0.57
	Centre	1.33	0.73	0.69	0.58	0.58
K_{prb}/K_{aq}=10e	Edge	1.81	0.67	0.63	0.51	
	Int	1.50	0.68	0.63	0.53	0.50
	Centre	1.46	0.68	0.63	0.55	0.50

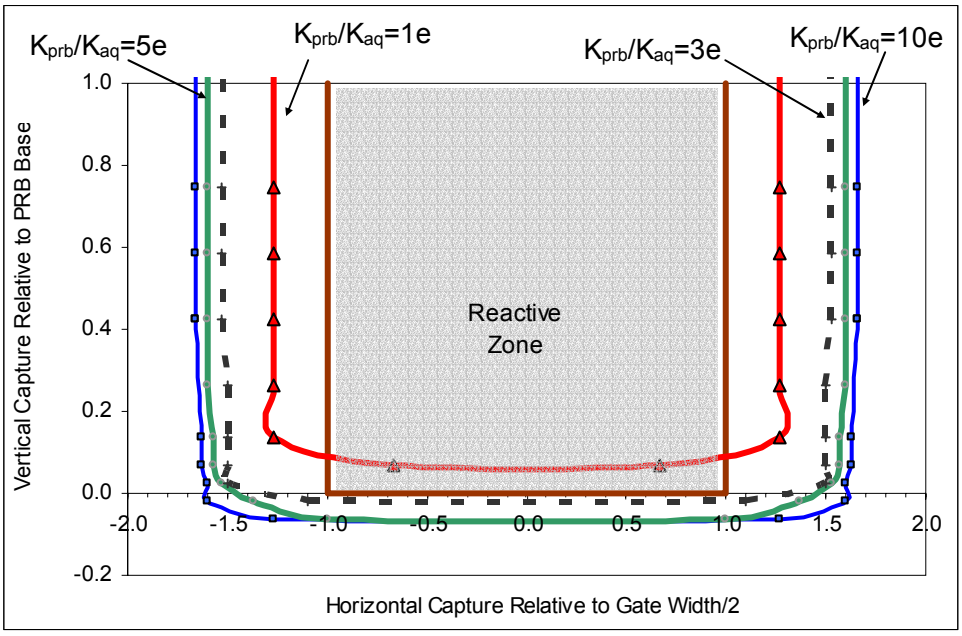

Fig. 4.13. End-on view of capture zone comparison for four partially penetrating enhanced PRBs (K_{prb}/K_{aq} = 1, 3, 5 and 10).

The most efficient way to minimise PRB design and construction costs is considered to be an optimisation formulation. In Chapter 5 the relationships between all design variables are analysed to determine what form this optimisation takes.

4.5 Effect of K_{prb}/K_{aq} Ratio on Capture Width

All PRB systems presented thus far have shown a significant difference in capture width between the K_{prb}/K_{aq} = 1 and K_{prb}/K_{aq} = 10 designs. This is consistent with the findings of *Starr and Cherry* [1994], *Shikaze* et al. [1995], *Smyth et al.* [1997], and *Shikaze* [1997], but not *Teutsch et al.* [1997]. A possible reason for this disagreement is considered to a flawed application of the harmonic mean by *Teutsch et al.* [1997]. Section 5.5.3 will also show that the low gate width/gate length ratios modelled by *Teutsch et al.* [1997] (where K_{prb}/K_{aq} = 1 and K_{prb}/K_{aq} = 10 do produce similar capture widths) may have led them to a generalised conclusion that is not accurate at larger gate width/gate length ratios.

Figure 4.14 presents a plan view of the only PRB system where it is expected that the harmonic mean of K_{prb} and K_{aq} would be sufficient to describe the overall head change.

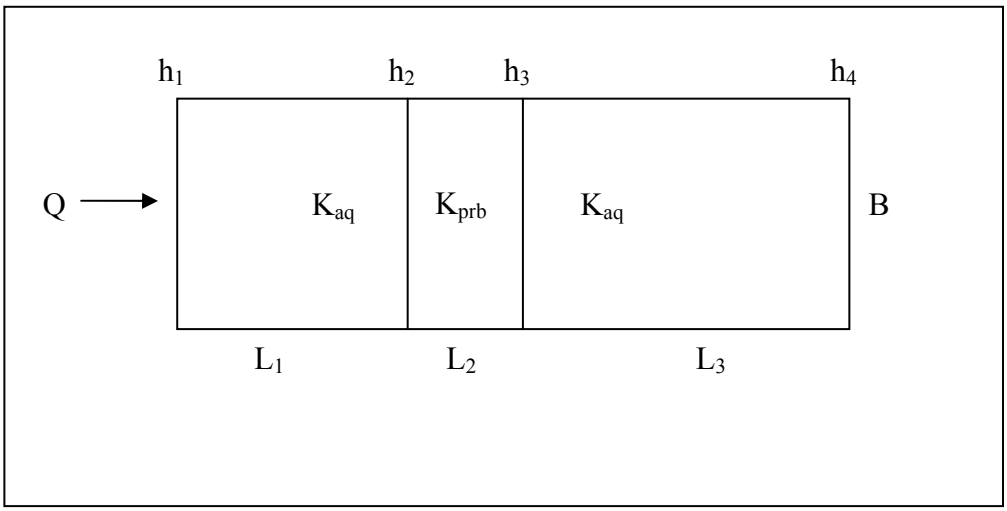

Fig. 4.14. Plan view of theoretical system where the harmonic mean would be appropriate to describe overall head changes.

The elements of the theoretical system in Figure 4.14 are the incoming flow (Q), the hydraulic conductivity of the aquifer (K_{aq}) and PRB (K_{prb}), the system width (B), the lengths of each section (L_1, L_2, and L_3) and the measured heads (h_1, h_2, h_3, and h_4). For Equation 4.7 to hold the top, bottom and side boundaries must be no-flow boundaries.

$$Q = \frac{B * K_{aq} * (h_1 - h_2)}{L_1} = \frac{B * K_{prb} * (h_2 - h_3)}{L_2} = \frac{B * K_{aq} * (h_3 - h_4)}{L_3} = \frac{B * K * (h_1 - h_4)}{L_1 + L_2 + L_3} \quad \textbf{4.7}$$

Head changes can be expressed in terms of the other parameters as in Equation 4.8:

$$(h_1 - h_2) = \frac{L_1 * Q}{B * K_{aq}}$$
$$(h_2 - h_3) = \frac{L_2 * Q}{B * K_{prb}}$$
$$(h_3 - h_4) = \frac{L_3 * Q}{B * K_{aq}} \quad \textbf{4.8}$$

and

$$(h_1 - h_4) = \frac{L_1 * Q}{B * K_{aq}} + \frac{L_2 * Q}{B * K_{prb}} + \frac{L_3 * Q}{B * K_{aq}}$$

The combined hydraulic conductivity (K) can then be calculated by rearranging and combining Equations 4.7 and 4.8, as in Equation 4.9:

$$\frac{Q}{B * (h_1 - h_4)} = \frac{K}{L_1 + L_2 + L_3} = \frac{1}{\left(\frac{L_1}{K_{aq}} + \frac{L_2}{K_{prb}} + \frac{L_3}{K_{aq}}\right)} \quad \textbf{4.9}$$

$$\therefore K = \frac{(L_1 + L_2 + L_3)}{\left(\frac{L_1}{K_{aq}} + \frac{L_2}{K_{prb}} + \frac{L_3}{K_{aq}}\right)}$$

The right-hand side of the hydraulic conductivity expression in Equation 4.9 is the definition of a harmonic mean. The problem with using this theoretical system to approximate 2-D (or 3-D) PRB systems is the necessary assumption of no-flow boundaries surrounding the system. The computer modelling presented in this chapter has shown that no-flow boundaries are not appropriate unless the K_{prb}/K_{aq} ratio is very close to 1. It will be shown in Section 5.5.3 that even for a fully penetrating PRB with $K_{prb}/K_{aq} = 10$ and no funnels, the gate length only needs to be a minimum of 0.33 times the gate width for the PRB to produce at least 24% more capture than the equivalent $K_{prb}/K_{aq} = 1$ PRB.

4.6 Summary

Hydraulic performance analysis of a variety of PRB systems was undertaken as the first step in formulating a PRB design optimisation. Three-dimensional computer modelling identified particle tracking as a useful way to estimate capture zone and residence time distributions. Volumetric flow analysis was found to be useful in the identification of flow regimes that may affect the permeability or reactivity of portions of the gate over time, but less efficient than particle tracking for analysing complex flow regimes. Capture zone measurements extended below the base of partially penetrating PRBs and were measured up-gradient from the portion of aquifer influenced by PRB emplacement. Residence time was measured laterally and vertically.

Variation in capture and residence time caused by up-gradient funnels and/or a gate hydraulic conductivity that is significantly different from the surrounding aquifer is believed to be negatively impacting on the cost-effectiveness of the PRB technology. The addition of velocity equalisation walls to a funnel-and-gate system was found to increase overall residence time while decreasing lateral variation in residence time. Customised down-gradient gate faces were found to enable maximum control over lateral variation in residence time. The emplacement of funnels and side walls deeper than the gate was found to minimise vertical variation in capture zone. Manipulation of a PRB's hydraulic conductivity within certain bounds was shown to be an effective means of minimising vertical variation in residence time while maximising hydraulic capture. Also suggested, but not analysed, was the replacement of deeper side walls with an impermeable base.

Ranking the hydraulic performance of these designs is dependent on the specific remediation problem to be solved and the relative installation and product costs. However, these experiments suggest that maximisation of the K_{prb}/K_{aq} ratio is unlikely to produce minimum cost PRB designs very often, especially for partially penetrating PRBs. The benefits of increased capture (to a point) with increasing K_{prb}/K_{aq} ratio are likely to be outweighed by the negative effects of reduced residence time, increased lateral and vertical variation in residence time, and increased gate maintenance costs associated with increased flow variation. Slightly higher K_{prb}/K_{aq} ratios are worth considering for fully penetrating PRBs, as vertical variation in residence time is not an issue.

Teutsch et al.'s [1997] use of the harmonic mean in their assertion that hydraulic capture of a fully penetrating funnel-and-gate system did not significantly increase with an increase in K_{prb}/K_{aq} from 1 to 10 was challenged. An explanation for the seemingly contradictory conclusions of *Teutsch et al.* [1997] and others (e.g. *Starr and Cherry* [1994], *Shikaze et al.* [1995], *Smyth, Shikaze and Cherry* [1997], and *Shikaze* [1997]) is discussed in Section 5.5.3.

The next challenge is to develop functional relationships between all design components so that PRB design can be optimised for cost minimisation. This is the subject of Chapter 5.

Chapter Five

Determination of Relationships between Design Variables and Performance Measures for Fully Penetrating PRBs

5.1 Introduction

In order to find the optimal PRB design for a particular remediation problem, the performance measures (outputs) of any desired set of PRB design variables (inputs) need to be determined. A computer simulation model of the desired PRB can be set up and run for each step of the optimisation process but this would be very time-consuming. Instead, it is proposed here that generalised functional relationships can be created between PRB inputs and outputs so that the performance of any PRB design within designated bounds can be estimated by application of a few equations.

Section 4.3.4 identified capture width and residence time as the most useful performance measures for this type of optimisation. Residence time is measured next to the side wall and down the centreline. This enables estimation of the appropriate down-gradient face for equalising residence time as presented in Appendix C. The specific design variables analysed are the gate width, gate length, funnel length and hydraulic conductivity ratio between the gate and aquifer. PRB depth is not varied at this point, thus eliminating the influence of the vertical flow component and reducing the complexity of the functions. The resulting functional relationships are therefore relevant only to fully penetrating PRB systems. Issues relating to the development of similar relationships for partially penetrating systems are discussed in Chapter 8.

Visual MODFLOW was used for all computer simulations using the modelling methodology outlined in Chapter 4. Dimensionless variables and ratios of model inputs and outputs were

created to enable generalisation and categorisation of model results. A four-stage functional approximation methodology was then applied to incorporate the desired design variable values one at a time. All simulation output and approximation functions for the first two stages are presented in Appendix B. Polynomial interpolation using the Lagrange Method (*Hamming*, 1962) was chosen for the third and fourth stages. A fully worked example details the application of this methodology and Visual MODFLOW comparisons are used to verify the approximating functions. Discussion is then presented on the limitations of the chosen simulation model dimensions and approximating functions. Evidence is also presented that supports (for a subset of PRB designs only) *Teutsch et al.'s* [1997] assertion that the K_{prb}/K_{aq} ratio does not have a significant effect on capture.

5.2 Methodology

The aim of the functional approximation approach is to fit a continuous set of functions to a discrete set of data points so that the edge residence, centreline residence and capture width of any combination (within defined bounds) of gate width, gate length, funnel width and hydraulic conductivity ratio can be approximated. PRBs with side walls set equal to the gate length (see Section 4.2) were chosen to examine the relationship between the design variables and performance measures.

Representation of the design variables and their modelled bounds are presented in Table 5.1. Please note that the PRB notation used in the previous chapters has now been divided up into gate (G) and funnel (F). For example, K_{prb}/K_{aq} is now notated as K_G/K_{Aq}. The 100m wide model grid restricted the L_G/W_G and $(W_F+W_G)/W_G$ ratios for large gate widths, but extra simulation and analysis with a larger model grid can be used to fill in the gaps if necessary. 800 Visual MODFLOW simulations were required to cover all chosen input combinations.

Table 5.1
Inputs to Functional Approximations

	Notation	Input Range
Gate Width (m)	W_G	3,6,9,18
Hydraulic Conductivity (Gate/Aquifer)	K_G/K_{Aq}	1,2,4,7,10
$\frac{\text{Gate Length}}{\text{Gate Width}}$	L_G/W_G	0.08 to 2.00 (W_G<=9) 0.08 to 1.00 (W_G<=18)
$\frac{\text{Funnel Width + Gate Width}}{\text{Gate Width}}$	$(W_F+W_G)/W_G$	1 to 10 (W_G<=6) 1 to 7 (W_G=9) 1 to 4.22 (W_G=18)

The four-stage process presented in Table 5.2 shows how the modelled design relationships (as presented in Table 5.1) are replaced one at a time by the desired design relationships (as calculated by the design variables). This process is run separately for each performance measure (PM): edge relative residence, centreline relative residence and relative capture.

Table 5.2
Functional Relationship Development for Three Performance Measures (PM)
{Edge Relative Residence, Centreline Relative Residence and Relative Capture}

Stage	Data Grouped by	Graph	Separate Graphs for	Approximation Method	Desired Relationship Incorporated
1	$(W_F+W_G)/W_G$	PM vs $(W_F+W_G)/W_G$	L_G/W_G K_G/K_{Aq} W_G	Best-Fit Curve. (Parameters a,b,c,d)	$(W_F+W_G)/W_G$
2	Parameters a,b,c,d	Parameter Value vs L_G/W_G	K_G/K_{Aq} W_G	Best-Fit Curve. (Parameters a_1-a_4, b_1-b_4,c_1-c_4,d_1-d_4)	L_G/W_G
3	W_G	PM for desired $(W_F+W_G)/W_G$ & L_G/W_G vs K_G/K_{Aq}	W_G	Lagrange Interpolation	K_G/K_{Aq}
4	All Together	PM for desired K_G/K_{Aq}, $(W_F+W_G)/W_G$ & L_G/W_G vs W_G		Lagrange Interpolation	W_G

All modelled output and the functional relationships developed for the first two stages can be found in Appendix B. Curve fitting for the first two stages was initially undertaken using regression analysis in the Excel and CurveExpert software packages. Best-fit curves for these stages were chosen based on the r^2 statistic (indicating the percentage of dependent variable variance explained by the independent variable).

The best stage one fit did not always result in an acceptable stage two fit so stage one parameters were manually adjusted with the aim of maximising total r^2 over both stages. The best-fit stage one curve types were reciprocal quadratics [$1/(a+bx+cx^2)$], quadratics [$a+bx+cx^2$] and 3rd degree polynomials [$a+bx+cx^2+dx^3$]. The best stage two curves were reciprocal quadratics, 3rd degree polynomials, rational functions [$(a+bx)/(1+cx+dx^2)$] and exponential associations [$a*(b-\exp^{-cx})$]. As this was strictly a curve fitting exercise, no further non-parametric investigations were made to determine curve suitability.

Polynomial interpolation using the Lagrange Method (*Hamming*, 1962) was chosen for the third and fourth stages as it produced close agreement with example data sets and left the Excel Solver free for the design optimisation. No pre-processing is required for this method; it is run in real time in the spreadsheet design model. The basic idea behind the Lagrange Method is first to find a polynomial that takes on the value 1 at a particular sample point and the value 0 at all the other sample points. Equation 5.2.1 (where the prime on the product means "excluding the k^{th} value") is such a polynomial of degree n; it is 1 when $x = x_k$ and 0 when $x = x_i$, $i \neq k$.

$$\mathbf{M_k(x)} = \frac{(x-x_1)(x-x_2)\ldots(x-x_{k-1})(x-x_{k+1})\ldots(x-x_{n+1})}{(x_k-x_1)(x_k-x_2)\ldots(x_k-x_{k-1})(x_k-x_{k+1})\ldots(x_k-x_{n+1})} \qquad \textbf{5.2.1}$$

$$= \frac{\prod_{i=1}^{n+1}{}'(x-x_i)}{\prod_{i=1}^{n+1}{}'(x_k-x_i)}$$

The polynomial $M_k(x)y_k$ takes on the value y_k at the sample point x_k and zero at all other sample points. It then follows that Equation 5.2.2 is a polynomial of degree n passing through the n+1 points (x_i,y_i).

$$y(x) = \sum_{k=1}^{n+1} M_k(x) y_k \qquad 5.2.2$$

Using stage three of the edge residence approximation as an example; *y(x)* is the edge relative residence of the desired K_G/K_{Aq} ratio *x*, $x_1 \ldots x_{n+1}$ and $y_1 \ldots y_{n+1}$ are the K_G/K_{Aq} ratios (1, 2, 4, 7 and 10) and their respective edge relative residence times, and $M_1 \ldots M_{n+1}$ are the multipliers that determine the proportion of each $y_1 \ldots y_{n+1}$ in the desired *y(x)*.

Figure 5.2a presents a 4th degree polynomial passing through 5 points. The points are the edge relative residence of the K_G/K_{Aq} ratios 1, 2, 4, 7 and 10. Creation of the polynomial enables estimation of edge relative residence for any K_G/K_{Aq} ratio between 1 and 10. The only problem with this polynomial is that it produces inaccurate interpolation between the K_G/K_{Aq} ratios of 7 and 10. The polynomial dips in preparation for a steep rise from K_G/K_{Aq} = 9.1, while actual relative residence is expected to tend asymptotically toward a minimum value (see *Starr and Cherry*, 1994). Dummy points at 99% and 98.5% of the modelled edge relative residence for K_G/K_{Aq} =10 were added for K_G/K_{Aq} ratios of 12 and 14 respectively (Figure 5.2b). This had the effect of smoothing out the polynomial approximation between the K_G/K_{Aq} ratios 7 and 10, thus providing closer agreement with theoretical values.

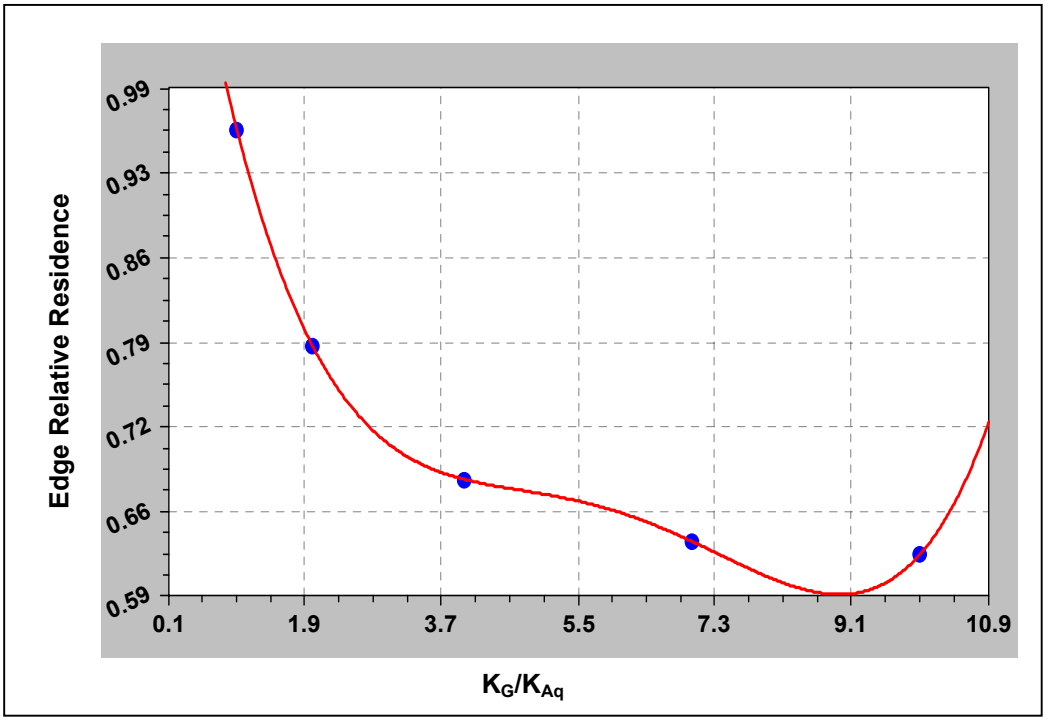

Fig. 5.2a. Polynomial interpolation example using the Lagrange Method and 5 points (no dummy points).

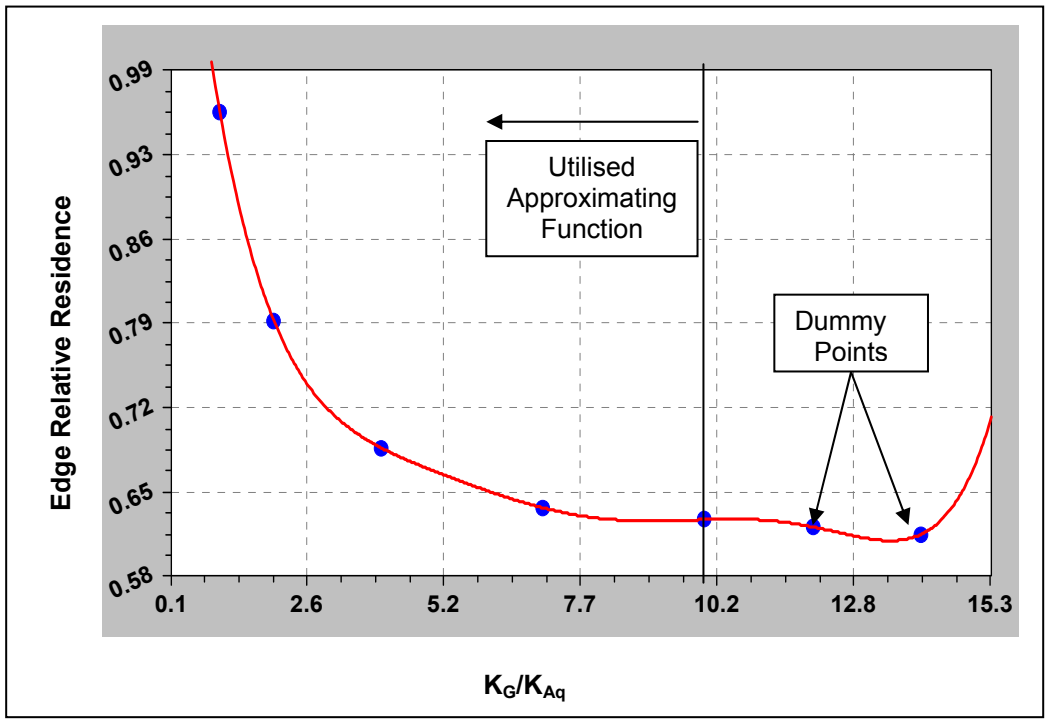

Fig. 5.2b. Polynomial interpolation example using the Lagrange Method with 5 points plus 2 dummy points.

The outcome of this polynomial approximation example was the edge relative residence of the desired gate length, funnel width and K_G/K_{Aq} ratio for gate widths of 3, 6, 9 and 18m. The final stage involved another polynomial interpolation using the same Lagrange Method to determine the edge relative residence for the desired gate width. Dummy points at 100% of the calculated edge relative residence for a gate width of 18m were added for gate widths of 21 and 24m, providing closer agreement with theoretical values between gate widths of 9 and 18m.

Dummy points for centreline residence were the same as edge residence. Dummy points for stage three of the relative capture approximations were at 101% and 101.5% of the modelled relative capture for K_G/K_{Aq} =10 (compared to 99% and 98.5% for relative residence). Relative capture functions increased asymptotically to a maximum while relative residence functions decreased asymptotically to a minimum. Dummy points for stage four of the relative capture approximations were the same as edge residence. A fully worked example of an edge residence functional approximation is detailed in the following section.

5.3 An Example Edge Residence Functional Approximation

The aim of this functional approximation example is to fit continuous functions to the discrete set of edge relative residence outputs provided by the Visual MODFLOW experiments. This enables the edge residence of any combination of gate width, gate length, funnel width and hydraulic conductivity ratio to be approximated. The chosen example estimates the edge relative residence for W_G = 15, L_G = 1.6, W_F = 25 and K_G/K_{Aq} = 7.2. The Visual MODFLOW simulations for each input variable combination defined in Table 5.1 produced the edge relative residence outputs presented in Appendix Tables B1-B4. The input data points for K_G/K_{Aq} = 1 and W_G = 6 (from Appendix Table B2) are presented in Table 5.3.

Table 5.3
K_G/K_{Aq}=1, W_G=6. Edge Relative Residence Input Data

	L_G/W_G						
$(W_F+W_G)/W_G$	0.08	0.17	0.33	0.67	1.00	1.33	2.00
1	0.96	0.96	0.96	0.96	0.96	0.95	0.95
2	0.42	0.50	0.61	0.73	0.79	0.82	0.85
3	0.30	0.36	0.45	0.56	0.64	0.69	0.75
4	0.24	0.29	0.37	0.46	0.54	0.59	0.67
5	0.20	0.25	0.31	0.40	0.47	0.52	0.59
7	0.16	0.20	0.25	0.32	0.38	0.42	0.49
10	0.13	0.15	0.19	0.25	0.29	0.33	0.39

5.3.1 Stage One

Stage one involved finding a suitable approximating function for each K_G/K_{Aq}, W_G, and L_G/W_G combination (one for each column in Table 5.3). These functions allow the incorporation of the desired $(W_F+W_G)/W_G$ ratio by interpolating between the modelled functions. Appendix Tables B5 to B8 show that reciprocal quadratics $[1/(a+bx+cx^2)]$ were found to provide a consistently accurate fit with an r^2 range of 0.9945 to 1.0000 (4 d.p.). The appropriate approximating parameters (from Appendix Table B5) and the resulting edge relative residence approximations are presented in Table 5.4.

Table 5.4

K_G/K_{Aq}=1, W_G=6. Stage One Reciprocal Quadratic Approximation

$$RelRes_{Edge} = \frac{1}{a + b*\left(\frac{W_F + W_G}{W_G}\right) + c*\left(\frac{W_F + W_G}{W_G}\right)^2}$$

	L_G/W_G						
$(W_F+W_G)/W_G$	0.08	0.17	0.33	0.67	1.00	1.33	2.00
1	0.96	0.96	0.96	0.97	0.97	0.96	0.96
2	0.44	0.51	0.61	0.71	0.77	0.80	0.84
3	0.29	0.36	0.45	0.57	0.64	0.69	0.75
4	0.23	0.28	0.37	0.47	0.55	0.60	0.67
5	0.19	0.24	0.31	0.40	0.48	0.53	0.60
7	0.16	0.19	0.24	0.32	0.38	0.42	0.50
10	0.14	0.16	0.19	0.24	0.29	0.32	0.38
Parameter a	-0.3435	0.0537	0.4104	0.6559	0.7786	0.8475	0.9107
Parameter b	1.4572	1.0321	0.6492	0.3836	0.2542	0.1926	0.1315
Parameter c	-0.0699	-0.0415	-0.0175	-0.0041	0.0018	0.0033	0.0038
r^2	0.9994	0.9995	0.9999	0.9992	0.9993	0.9990	0.9993

Taking L_G/W_G = 0.08 (column 1) as an example, edge relative residence is approximated for each $(W_F+W_G)/W_G$ ratio by Equation 5.3.1 as follows:

$$RelRes_{Edge} = \frac{1}{\left(-0.3435 + 1.4572*\left(\frac{W_F + W_G}{W_G}\right) - 0.0699*\left(\frac{W_F + W_G}{W_G}\right)^2\right)} \qquad 5.3.1$$

Thus $RelRes_{Edge}$ = 0.96 for $(W_F+W_G)/W_G$ = 1, $RelRes_{Edge}$ = 0.44 for $(W_F+W_G)/W_G$ = 2 etc. Figure 5.3a presents the example input data and approximating functions in graphical form. All functions appear to be continuous and smooth, providing justification for the functional approximation approach.

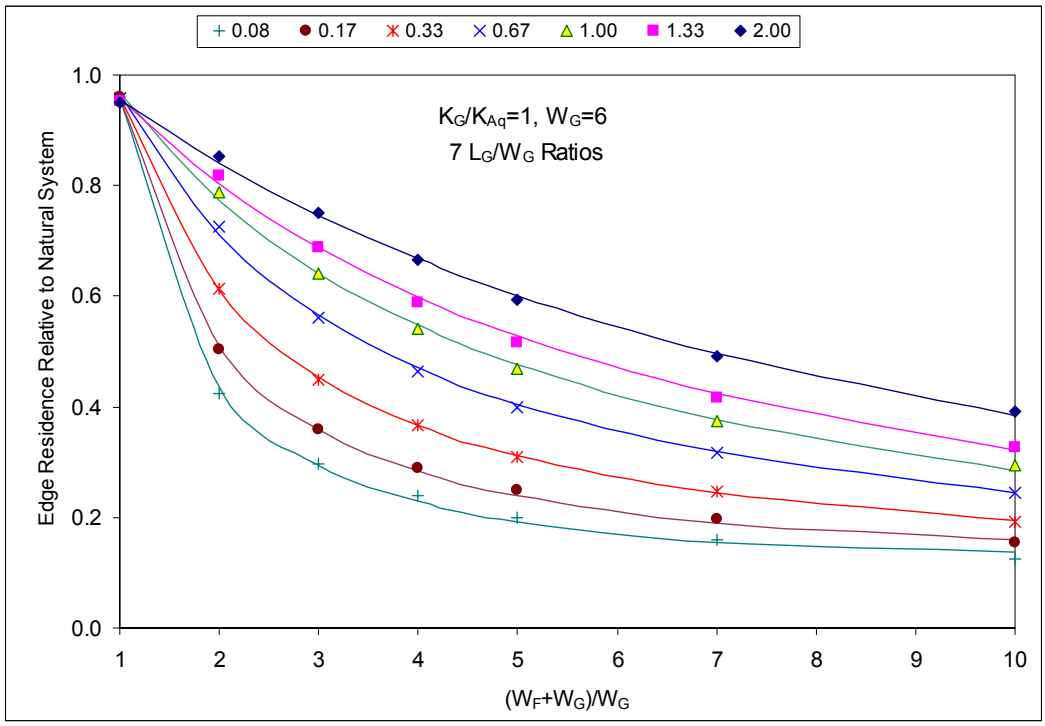

Fig. 5.3a. Fully penetrating PRB with $K_G/K_{Aq} = 1$ and $W_G = 6$m. Effect of $(W_F+W_G)/W_G$ on edge relative residence for seven L_G/W_G ratios between 0.08 and 2.00. Points are from computer modelling and lines from reciprocal quadratic function approximations.

5.3.2 Stage Two

The second stage of the process involved curve fitting on the seven points generated for each of the three stage-one reciprocal quadratic parameters (a, b and c). These interpolation functions produce the appropriate parameters a-c for the desired L_G/W_G ratio. Tables B9 to B12 show that rational functions were chosen for parameters a and c while reciprocal quadratics were chosen for parameter b. The overall r^2 range for stage two was 0.9927 to 1.0000 (4 d.p.). Table 5.5 presents the stage two interpolation parameters (from the first column of Table B10) for the example input data and Table 5.6 presents the resulting edge relative residence.

Table 5.5
K_G/K_{Aq}=1, W_G=6. Stage Two Interpolation Parameters

	Interpolation Parameters 1	2	3	4	r^2	Interpolating Function
a	-1.1670	7.6907	7.4753	-0.0943	0.9998	$a = \frac{a_1 + a_2 * \left(\frac{L_G}{W_G}\right)}{1 + a_3 * \left(\frac{L_G}{W_G}\right) + a_4 * \left(\frac{L_G}{W_G}\right)^2}$
b	0.4278	3.1956	0.2459		0.9999	$b = \frac{1}{b_1 + b_2 * \left(\frac{L_G}{W_G}\right) + b_3 * \left(\frac{L_G}{W_G}\right)^2}$
c	-0.1279	0.1495	7.6595	6.7944	0.9997	$c = \frac{c_1 + c_2 * \left(\frac{L_G}{W_G}\right)}{1 + c_3 * \left(\frac{L_G}{W_G}\right) + c_4 * \left(\frac{L_G}{W_G}\right)^2}$

Table 5.6
K_G/K_{Aq}=1, W_G=6. Stage Two Parameter Output

	L_G/W_G						
Parameters	0.08	0.17	0.33	0.67	1.00	1.33	2.00
a	-0.3243	0.0512	0.4012	0.6665	0.7784	0.8415	0.9127
b	1.4371	1.0339	0.6577	0.3749	0.2584	0.1951	0.1282
c	-0.0685	-0.0418	-0.0181	-0.0031	0.0014	0.0031	0.0039

Table 5.5 shows that parameters *a, b* and *c* are approximated for the chosen L_G/W_G ratios as follows:

$$a = \frac{-1.1670 + 7.6907 * \left(\frac{L_G}{W_G}\right)}{1 + 7.4753 * \left(\frac{L_G}{W_G}\right) - 0.0943 * \left(\frac{L_G}{W_G}\right)^2} \qquad \textbf{5.3.2}$$

$$b = \frac{1}{0.4278 + 3.1956 * \left(\frac{L_G}{W_G}\right) + 0.2459 * \left(\frac{L_G}{W_G}\right)^2} \qquad 5.3.3$$

$$c = \frac{-0.1279 + 0.1495 * \left(\frac{L_G}{W_G}\right)}{1 + 7.6595 * \left(\frac{L_G}{W_G}\right) + 6.7944 * \left(\frac{L_G}{W_G}\right)^2} \qquad 5.3.4$$

Thus for $L_G/W_G = 0.0833$ (column 1 of Table 5.6): a = -0.3243, b = 1.4371 and c = -0.0685, which compare well with the equivalent input parameter values in the first column of Table 5.4. Figures 5.3b and 5.3c present the stage two interpolation functions in graphical form. All functions appear to be continuous and smooth.

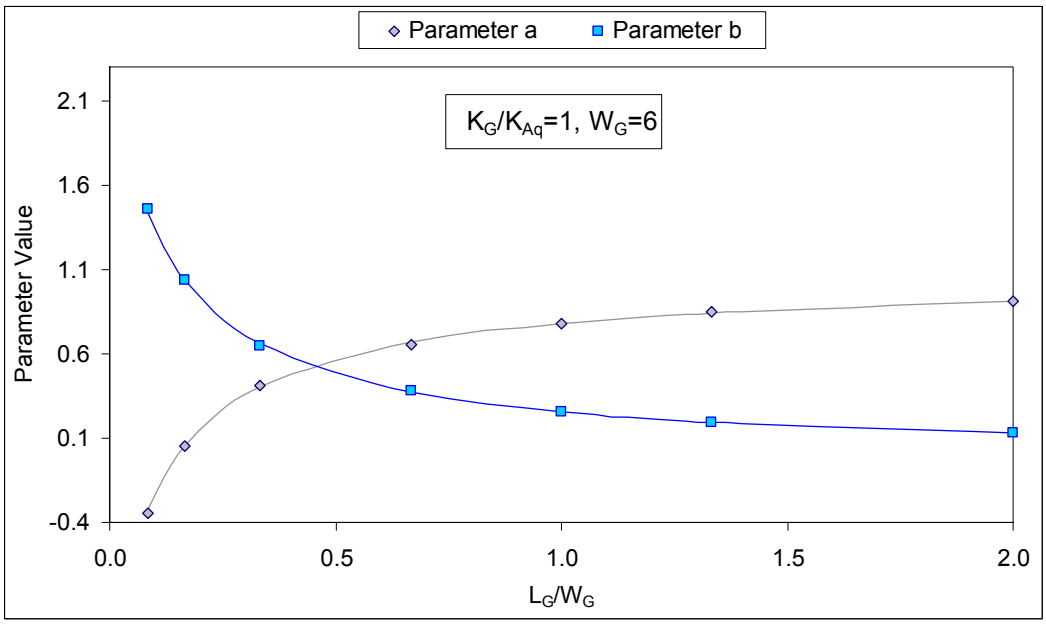

Fig. 5.3b. Fully penetrating PRB with K_G/K_{Aq} = 1 and W_G = 6m. Effect of L_G/W_G ratio on parameters 'a' and 'b' from edge relative residence approximation. Points are from stage one approximations and lines from rational function and reciprocal quadratic function interpolations respectively.

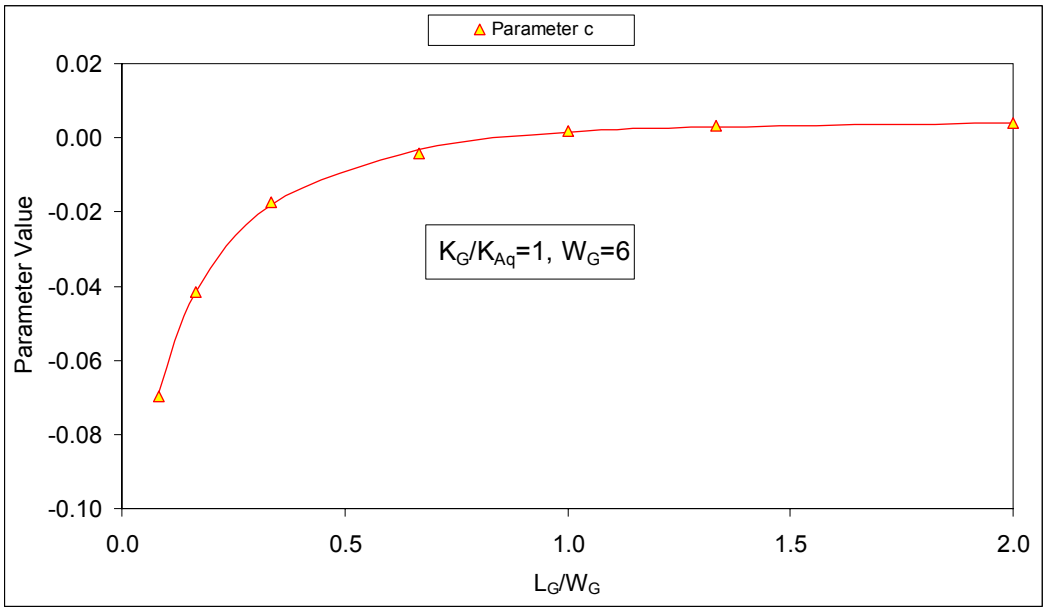

Fig. 5.3c. Fully penetrating PRB with K_G/K_{Aq} = 1 and W_G = 6m. Effect of L_G/W_G ratio on parameter 'c' from edge relative residence approximation for PRB. Points are from stage one approximations and the line from a rational function interpolation.

Next, the edge relative residence for specific input combinations of W_G and K_G/K_{Aq} need to be calculated. Edge relative residence is therefore notated as $RelRes_{Edge(w,k)}$ where *w=1..4* and *k=1..5* index the W_G and K_G/K_{Aq} inputs defined in Table 5.1. For the chosen example, incorporation of the desired L_G/W_G ratio (1.6/15 = 0.11) into Equations 5.3.2 to 5.3.4 produces a = -0.1930, b = 1.2962 and c = -0.0591. For the input combination of W_G = 6 (i.e. *w*=2) and K_G/K_{Aq} = 1 (i.e. *k*=1), the stage one reciprocal quadratic approximation from Table 5.4 can then be applied with the desired values of L_G = 1.6, W_G = 15 and W_F = 25. This produces an estimate of edge relative residence as follows:

$$RelRes_{Edge(2,1)} = \frac{1}{\left(-0.1930 + 1.2962 * 2.67 - 0.0591 * 2.67^2\right)} = 0.352 \qquad 5.3.5$$

as $(W_F+W_G)/W_G = (25+15)/15 = 2.67$.

To check the accuracy of the functional approximation so far, the equivalent Visual MODFLOW model was created and run. This model combined the example input values of W_G = 6 and K_G/K_{Aq} = 1 with the desired ratios of L_G/W_G = 0.11 and $(W_F+W_G)/W_G$ = 2.67.

Substituting $W_G = 6$ into these two ratios produces $W_F = 10$ and $L_G = 0.67$. Edge relative residence time for this model was 0.358, only 1.7% greater than the amount estimated by Equation 5.3.5.

The edge relative residence interpolation parameters for the input $W_G = 6$ and input K_G/K_{Aq} ratios 1, 2, 4, 7 and 10 (k = 1..5) can be found in Appendix Table B10. Application of Equations 5.3.2 - 5.3.5 to the example data yields the edge relative residence output in Table 5.7.

Table 5.7
W_G = 6. Stage Two Edge Relative Residence Output

	k				
	1	2	3	4	5
$RelRes_{Edge(2,k)}$	0.352	0.310	0.284	0.278	0.267

5.3.3 Stage Three

The purpose of the third stage is to interpolate between the input K_G/K_{Aq} ratios to produce the edge relative residence for the desired K_G/K_{Aq} ratio and each W_G input. This leaves only one more interpolation to incorporate the desired W_G value. The Lagrange Method is utilised to fit w polynomial interpolation curves to the $RelRes_{Edge(w,k)}$ generated by Equation 5.3.5 for all five K_G/K_{Aq} input ratios plus two dummy ratios (notated as Kin_k where k=*1..7*). Each polynomial has degree *w-1* as in Figure 5.2b. The first step involves estimating $RelRes_{Edge(w,k)}$ as outlined in Section 5.2 for the dummy ratios $Kin_6 = 12$ and $Kin_7 = 14$. For the $w = 2$ input, these values can be calculated from $RelRes_{Edge(2,5)}$ in Table 5.7 as follows:

$$RelRes_{Edge(2,6)} = RelRes_{Edge(2,5)} * 0.99 = 0.264 \qquad 5.3.6$$

$$RelRes_{Edge(2,7)} = RelRes_{Edge(2,5)} * 0.985 = 0.263 \qquad 5.3.7$$

Edge relative residence from Table 5.7 and Equations 5.3.6 and 5.3.7 can then be graphed against the input K_G/K_{Aq} ratios as in Figure 5.3d. This process is repeated for all other W_G inputs.

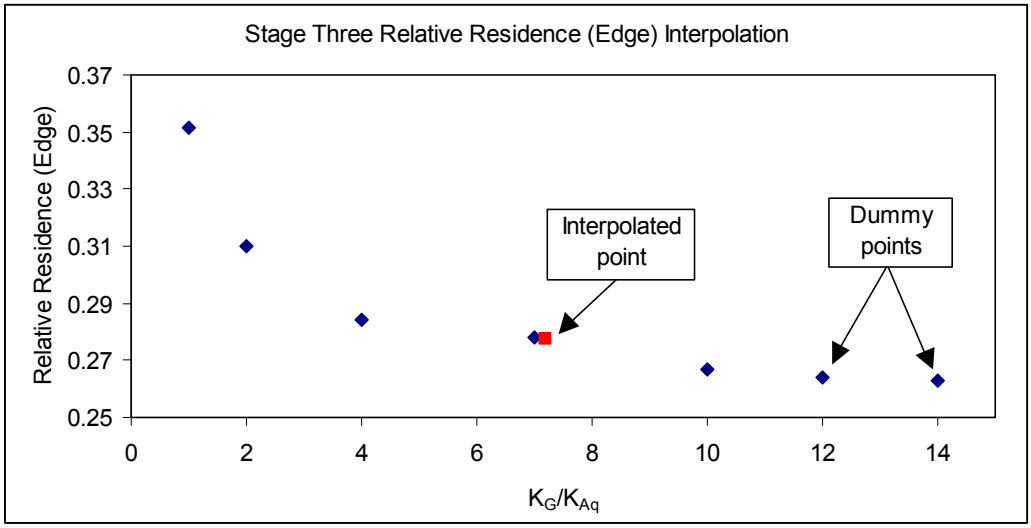

Fig. 5.3d. Fully penetrating PRB for input parameter W_G = 6m. Stage three Lagrange interpolation for K_G/K_{Aq} = 7.2, L_G = 1.6 and W_F = 25.

The interpolated point in Figure 5.3d is calculated as the sum of all relative residence values multiplied by the multiplying factors determined by the interpolation polynomial. These multipliers (M) are calculated using Equation 5.3.8 at each point *k* for the desired K_G/K_{Aq} (where the prime on the product means "excluding the k^{th} value").

$$\mathbf{M_k(K_G/K_{Aq})} = \frac{\prod_{i=1}^{7}{}'(\mathbf{K_G/K_{Aq} - Kin_i})}{\prod_{i=1}^{7}{}'(\mathbf{Kin_k - Kin_i})} \qquad \text{(for } k\text{=1..7)} \qquad \mathbf{5.3.8}$$

For example, when K_G/K_{Aq} = 7.2 and Kin_k = 1 (i.e. *k*=1), Equation 5.3.8 can be calculated as follows:

$$\mathbf{M_1(7.2)} = \frac{(7.2-2)*(7.2-4)*(7.2-7)*(7.2-10)*(7.2-12)*(7.2-14)}{(1-2)*(1-4)*(1-7)*(1-10)*(1-12)*(1-14)} \qquad \mathbf{5.3.9}$$

$$= \mathbf{-0.013}$$

Application of Equation 5.3.9 to Kin_k for *k*=1..7 produces the multipliers (M) in Table 5.8. The largest multiplier is for the input K_G/K_{Aq} ratio of 7 (*k* = 4), as it is very close to the desired ratio of 7.2. All other multipliers have very small magnitude, with their absolute

value decreasing outward from $M_4(7.2)$. The multipliers for k = 3 and 5, 2 and 6, and 1 and 7 also balance each other out with opposite signs. This means that the interpolated value will be very close to the edge relative residence of the input K_G/K_{Aq} ratio of 7.

Table 5.8
W_G = 6 (w=2). Stage Three Edge Relative Residence and Multipliers

	k						
	1	2	3	4	5	6	7
$RelRes_{Edge(2,k)}$	0.352	0.310	0.284	0.278	0.267	0.264	0.263
$M_k(7.2)$	-0.013	0.038	-0.068	0.998	0.065	-0.022	0.003

Once all multipliers have been calculated, the interpolated edge relative residence times $RelRes_{Edge(w)}$ for the desired L_G, W_F and K_G/K_{Aq} can be estimated for each w from Equation 5.3.10 as follows:

$$\mathbf{RelRes_{Edge(w)} = \sum_{k=1}^{7} M_k (K_G / K_{Aq}) * RelRes_{Edge(w,k)}} \qquad \mathbf{5.3.10}$$

For the chosen example, the edge relative residence for the input W_G = 6 (i.e. w = 2) and the desired L_G = 1.6, W_F = 25 and K_G/K_{Aq} =7.2 can be estimated from the data in Table 5.8 by Equation 5.3.11 as follows:

$$\begin{aligned} \mathbf{RelRes_{Edge(2)}} &= \mathbf{(-0.013 * 0.352) + (0.038 * 0.310) + (-0.068 * 0.284)} \\ &\quad \mathbf{+ (0.998 * 0.278) + (0.065 * 0.267) + (-0.022 * 0.264) + (0.003 * 0.263)} \qquad \mathbf{5.3.11} \\ &= \mathbf{0.277} \end{aligned}$$

This is the interpolated point in Figure 5.3d. The estimated result was then checked against the appropriate Visual MODFLOW model. This model combined the example input value of W_G = 6 with the desired input value of K_G/K_{Aq} = 7.2 and ratios of L_G/W_G = 0.11 and $(W_F+W_G)/W_G$ = 2.67. Only the K_G/K_{Aq} ratio has changed from the model used to check the stage two example results, W_F and L_G remained at 10.0 and 0.67 respectively. Edge relative residence time for this model was 0.273, only 1.5% less than the amount estimated by Equation 5.3.11. The same process (Equations 5.3.6 to 5.3.8 and 5.3.10) was used to generate

edge relative residence estimates for W_G = 3, 9 and 18. All estimates are presented in Table 5.9.

Table 5.9
W_G = 6. Stage Three Edge Relative Residence Output

	w			
	1	2	3	4
$RelRes_{Edge(w)}$	0.342	0.277	0.242	0.214

5.3.4 Stage Four

The final stage utilises the Lagrange Method to interpolate between the $RelRes_{Edge(w)}$ points (w = 1..7) so that the edge relative residence for the desired W_G = 15 can be estimated. W_G input values are renamed $WGin_w$ to avoid confusion with the desired W_G value. Dummy points $WGin_5$ = 21 and $WGin_6$ = 24 set equal to $RelRes_{Edge(4)}$ in Table 5.9 are added to stabilise the interpolating functions (see Section 5.2).

$$\mathbf{RelRes_{Edge(6)} = RelRes_{Edge(5)} = RelRes_{Edge(4)} = 0.214} \qquad \mathbf{5.3.12}$$

Edge relative residence from Table 5.9 and Equation 5.3.12 can then be graphed against the input $WGin_w$ ratios as in Figure 5.3e.

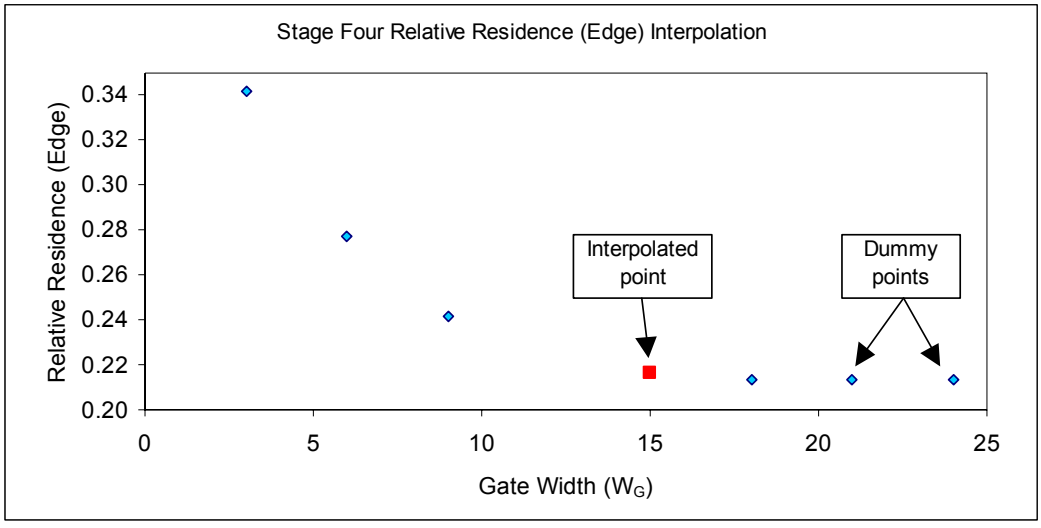

Fig. 5.3e. Fully penetrating PRB with W_G = 15, K_G/K_{Aq} = 7.2, L_G = 1.6 and W_F = 25. Stage four Lagrange interpolation to determine edge relative residence time.

The interpolated point in Figure 5.3e is calculated as the sum of all relative residence values multiplied by their appropriate multipliers. The multipliers $M_w(W_G)$ are calculated using Equation 5.3.13 at each point w for the desired W_G (where the prime on the product means "excluding the w^{th} value").

$$\mathbf{M_w(W_G)} = \frac{\prod_{i=1}^{6}{}' (\mathbf{W_G - WGin_i})}{\prod_{i=1}^{6}{}' (\mathbf{WGin_w - WGin_i})} \qquad \text{(for } w = 1..6\text{)} \qquad \mathbf{5.3.13}$$

For example, when $W_G = 15$ and $WGin_w = 6$ (i.e. $w = 2$), Equation 5.3.13 can be calculated as follows:

$$\mathbf{M_2(15)} = \frac{(15-3)*(15-9)*(15-18)*(15-21)*(15-24)}{(6-3)*(6-9)*(6-18)*(6-21)*(6-24)} \qquad \mathbf{5.3.14}$$

$$= \mathbf{-0.400}$$

Application of Equation 5.3.14 to $WGin_w$ for $w = 1..6$ produces the multipliers in Table 5.10. As the interpolated point in Figure 5.3e is not close to any of the modelled points, the magnitude of the multipliers show that most of the modelled points will have a significant effect on the magnitude of the interpolated point.

Table 5.10
Stage Four Edge Relative Residence and Multipliers

	w					
	1	2	3	4	5	6
$RelRes_{Edge(w)}$	0.342	0.277	0.242	0.214	0.214	0.214
$M_w(15)$	0.086	-0.400	0.600	1.200	-0.600	0.114

Once all multipliers have been calculated, the edge relative residence $RelRes_{Edge}$ for the desired W_G, L_G, W_F and K_G/K_{Aq} can be estimated from Equation 5.3.15 as follows:

$$\mathbf{RelRes_{Edge}} = \sum_{w=1}^{6} \mathbf{M_w(W_G) * RelRes_{Edge(w)}} \qquad \mathbf{5.3.15}$$

For the chosen example the edge relative residence for the desired W_G = 15, L_G = 1.6, W_F = 25 and K_G/K_{Aq} =7.2 can be estimated from the data in Table 5.10 as follows:

$$\begin{aligned}\mathbf{RelRes(15)} &= \mathbf{(0.086 * 0.342) + (-0.400 * 0.277) + (0.600 * 0.242)} \\ &\quad \mathbf{+ (1.200 * 0.214) + (-0.600 * 0.214) + (0.114 * 0.214)} \\ &= \mathbf{0.217}\end{aligned} \qquad \mathbf{5.3.16}$$

This is the interpolated point in Figure 5.3e. The estimated result was then checked against the appropriate Visual MODFLOW model. This model was created with all the desired input values (W_G = 15, L_G = 1.6, W_F = 25 and K_G/K_{Aq} =7.2). Edge relative residence time for this model was 0.2196, only 1.2% greater than the amount estimated by Equation 5.3.16. For this example, the accuracy of the functional approximations has been verified at each stage by the equivalent Visual MODFLOW model. Wider verification issues will be considered in the following section.

5.4 Verification of Functional Relationships

Verification of the chosen functional relationship development methodology involves checking the accuracy and correctness of the approximations. This was achieved for each stage in Section 5.3 by comparing the edge relative residence estimated by the functional approximation with the output from the equivalent Visual MODFLOW model. In general it is expected that verification only needs to occur after the final functional approximation stage and further verification on previous stages is only required when the accuracy of the functional approximation is not considered acceptable.

For example, centreline relative residence and relative capture were also estimated for the PRB example in Section 5.3. The final interpolations are presented in Figures 5.4a and 5.4b respectively. The functional relationship methodology generated values of 0.740 for centreline relative residence and 1.857 for relative capture. The appropriate Visual

MODFLOW model yielded centreline relative residence of 0.745 and relative capture of 1.850. All modelled and estimated values are within 1% of each other, which is considered acceptable. No further verification is required for this particular example.

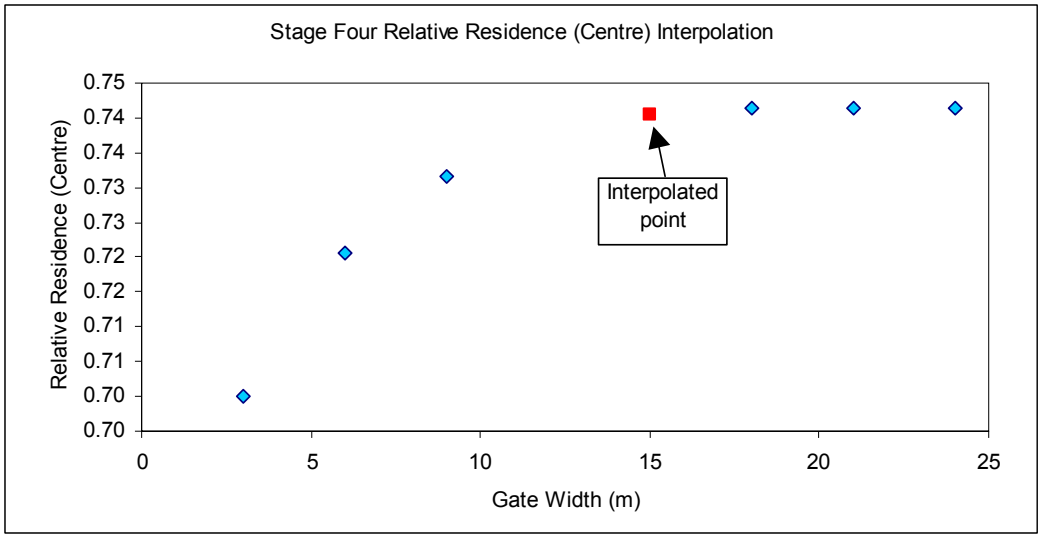

Fig. 5.4a. Fully penetrating PRB with W_G = 15, K_G/K_{Aq} = 7.2, L_G = 1.6 and W_F = 25. Stage four Lagrange interpolation to determine centreline relative residence time.

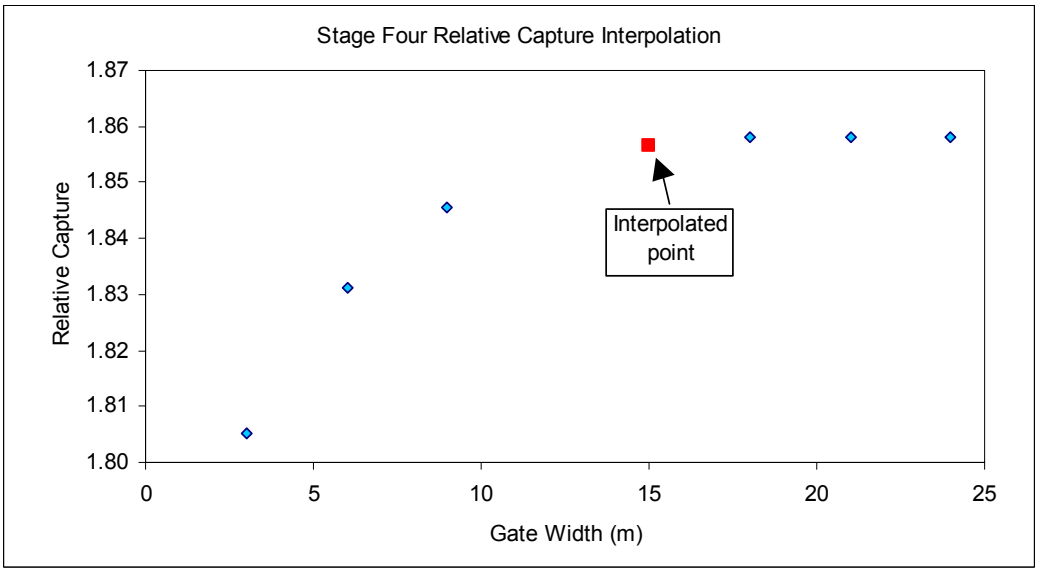

Fig. 5.4b. Fully penetrating PRB with W_G = 15, K_G/K_{Aq} = 7.2, L_G = 1.6 and W_F = 25. Stage four Lagrange interpolation to determine relative capture.

5.5 Discussion

Section 5.3 used a fully penetrating example to detail the estimation of edge relative residence by functional approximation. All relevant approximating functions and parameters can be found in Tables B1 to B12 of Appendix B. The same process was used to estimate centreline relative residence and relative capture. All relevant approximating functions and parameters can be found in Tables B13 to B24 and Tables B25 to B36 respectively.

For partially penetrating systems, functional relationships could be determined in a similar manner to produce capture and residence time at a specified number of depths. This would require a considerable amount of computer modelling and analysis. An alternative approach considered worthy of further research (for partially penetrating situations) is to initially assume a fully penetrating system with aquifer depth equal to plume depth. In the post-optimisation computer modelling phase with site specific data, any design changes due to the partial PRB penetration could be determined. Optimal PRB design in partially penetrating situations will be further discussed in Chapter 8.

5.5.1 Effect of Grid Restrictions

The 100m wide model grid restricted the ability to model large L_G/W_G and $(W_F+W_G)/W_G$ ratios for large gate widths, but it was determined that these modelling restrictions are unlikely to hinder the accuracy of the functional approximations. For example, Figure 5.5a compares edge relative residence with $(W_F+W_G)/W_G$ for PRBs with $K_G/K_{Aq} = 10$ and $L_G/W_G = 1.0$, the most extreme input combination with data for all gate widths.

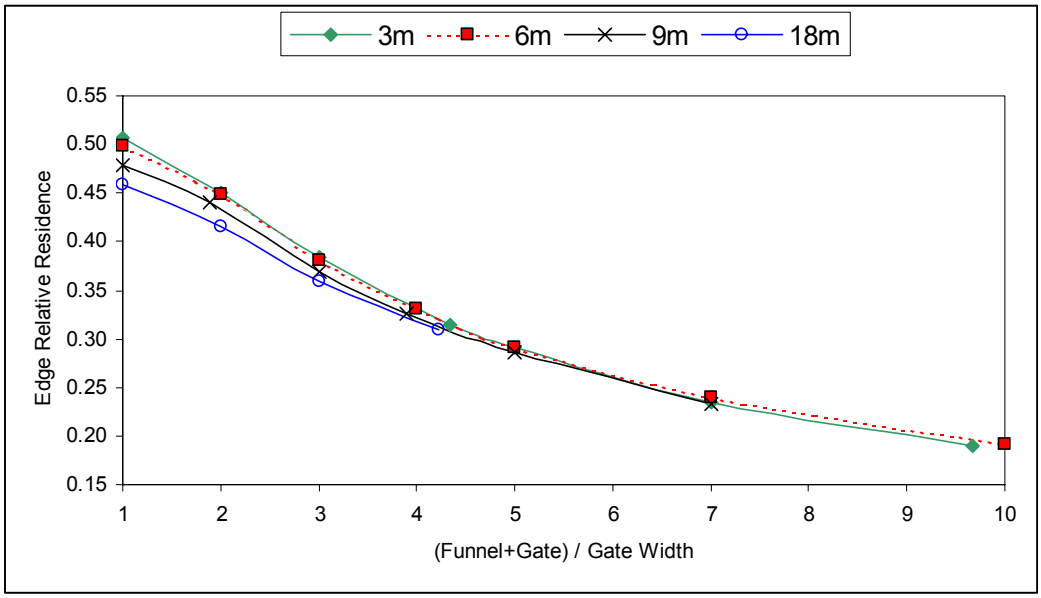

Fig. 5.5a. Fully penetrating PRB with $K_G/K_{Aq} = 10$ and $L_G/W_G = 1$. Effect of $(W_F+W_G)/W_G$ on edge relative residence for gate widths of 3, 6, 9 and 18m.

Increasing the gate width from 3m to 18m when no funnel is present ($(W_F+W_G)/W_G = 1$) causes an 11% decrease in edge relative residence (see the top left corner of Figure 5.5a). As $(W_F+W_G)/W_G$ increases, the effect of increasing gate width diminishes until it is insignificant for $(W_F+W_G)/W_G$ ratios greater than 4. This means that functional relationships developed for $W_G = 6$ should be accurate approximations for larger gate widths where data have not been collected.

5.5.2 Choice of Functions

The choice of functions for the first two approximating stages was determined by maximising total r^2 over both stages. Polynomial functions (including quadratic, inverse quadratic and rational functions) were chosen for all approximations, except for stage two of the relative capture approximation where two exponential association functions were used. Polynomial interpolation using the Lagrange Method (*Hamming*, 1962) was chosen for the third and fourth stages as it produced close agreement with example data sets and left the Excel Solver free for the design optimisation.

The computer modelling presented in Chapter 4 and similar research by *Starr and Cherry* [1994] and *Smyth et al.* [1997] showed the presence of maximum and minimum bounds on relative residence and capture. Sigmoidal-type relationships would therefore be expected for

a wide enough modelled range, however the chosen range did not confirm this expectation. Extrapolation of the proposed functional relationships is not recommended without further computer modelling.

5.5.3 PRB Designs where Capture Width is not affected by the K_G/K_{Aq} Ratio

In Section 4.5 the (seemingly) conflicting conclusions of *Teutsch et al.* [1997] and others, with regard to the effect of the K_G/K_{Aq} ratio on relative capture were discussed. During development of the functional relationships, a subset of PRBs where relative capture was not significantly affected by increasing K_G/K_{Aq} from 1 to 10 was found. This may help to explain the conclusions of *Teutsch et al.* [1997].

Figure 5.5b presents an example of the third degree polynomial fit on relative capture for PRBs with $K_G/K_{Aq} = 1$, $W_G = 6$m and seven L_G/W_G ratios between 0.08 and 2.00. Figure 5.5c presents the third degree polynomial fit for the same PRBs with $K_G/K_{Aq} = 10$.

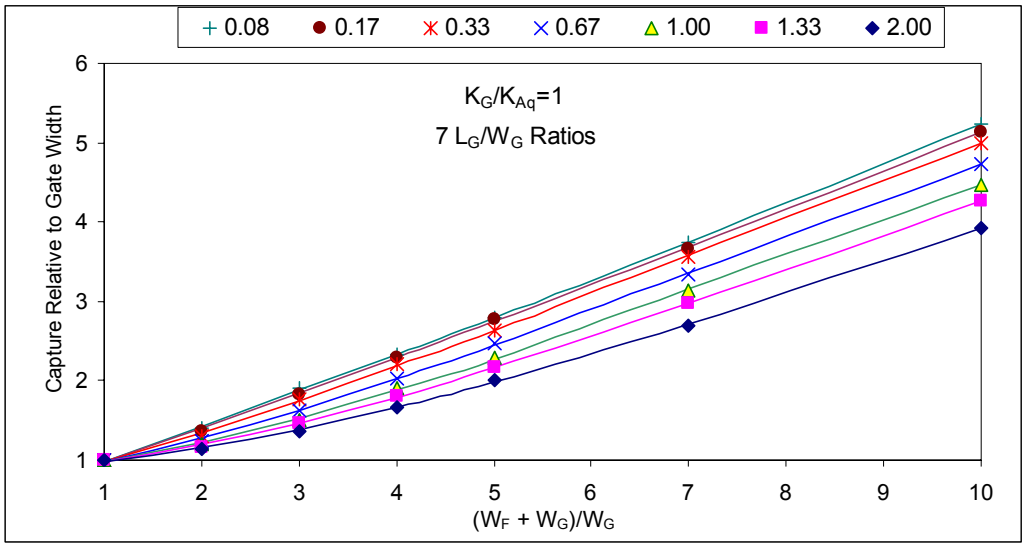

Fig. 5.5b. Fully penetrating PRB with $K_G/K_{Aq} = 1$ and $W_G = 6$m. Effect of $(W_F+W_G)/W_G$ on relative capture for seven L_G/W_G ratios between 0.08 and 2.00. Points are from computer modelling and lines from third degree polynomial approximations.

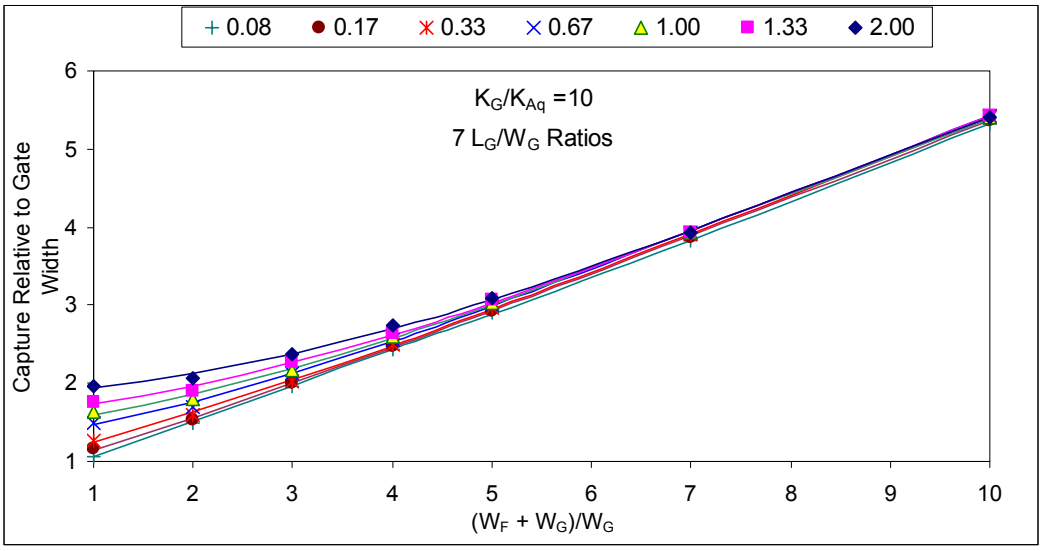

Fig. 5.5c. Fully penetrating PRB with K_G/K_{Aq} = 10 and W_G = 6m. Effect of $(W_F+W_G)/W_G$ on relative capture for seven L_G/W_G ratios between 0.08 and 2.00. Points are from computer modelling and lines from third degree polynomial approximations.

A comparison of Figures 5.5b and 5.5c shows relative capture to be significantly different for K_G/K_{Aq} ratios of 1 and 10, except where L_G/W_G = 0.08 and 0.17. For these PRBs the $(W_F+W_G)/W_G$ ratio provides the dominant effect on relative capture as the gate length is not sufficient for the K_G/K_{Aq} ratio to be important. As discussed in Section 4.5, *Teutsch et al.* [1997] stated that the K_G/K_{Aq} ratio does not have a significant effect on capture. This conclusion does appear to be accurate for the L_G/W_G ratios of 0.025 to 0.1 they chose in combination with a variety of funnel lengths. Figures 5.5b and 5.5c show however that their conclusion is not likely to be generalisable to L_G/W_G ratios larger than 0.33.

5.6 Summary

Functional relationships between PRB design variables and PRB performance measures have been developed for fully penetrating systems. Chosen design variables were gate length, gate width, funnel width and the reactive material proportion represented by the K_G/K_{Aq} ratio. Chosen performance measures were edge residence, centreline residence and capture width. Parameter tables, approximating functions and interpolating functions have been produced for inclusion in an optimisation formulation. Suggestions were presented for the use of these functions in partially penetrating situations.

A series of Visual MODFLOW simulations were first run to cover a wide range of PRB design variable combinations. Simulation results for each performance measure were categorised according to the dimensioned design variable W_G (representing gate width), the dimensionless design variable ratios L_G/W_G and $(W_F+W_G)/W_G$, and the dimensionless ratio K_G/K_{Aq} (determined by the design variable RM_{prop}). The use of dimensionless ratios enabled the generalisation of simulation results to other similarly proportioned PRB designs.

A four-stage process was presented in which the desired design variable values were incorporated one at a time into the generalised relationships. An edge relative residence example detailed this process. Verification was provided by comparing estimated values with the appropriate Visual MODFLOW model for each stage. Centreline relative residence and relative capture were also estimated and verified for the example system. Extrapolation of the chosen functions is not recommended without verification by a Visual MODFLOW simulation. However, as discussed in Section 5.5.1, it may be possible to use a W_G = 6m PRB to produce performance estimates for larger PRBs, as size seems to have minimal effect on performance above a $(W_F+W_G)/W_G$ ratio of approximately 5.

Evidence was presented to support the conclusion of *Teutsch et al.* [1997], where they stated that the K_G/K_{Aq} ratio did not have a significant effect on capture. All their modelled PRBs had $L_G/W_G < 0.33$, where it was found that the $(W_F+W_G)/W_G$ ratio dominates relative capture as the gate length is not sufficient for the K_G/K_{Aq} ratio to take effect. However, Tables B25 to B28 and Figures 5.5b and 5.5c show that the conclusion of *Teutsch et al.* [1997] can not be generalised to L_G/W_G ratios larger than 0.33.

Inclusion of the functional approximations presented in this chapter in an optimisation formulation will enable efficient analysis of the hydraulic performance of any design within the model constraints. The development of this formulation is presented in Chapter 6.

Chapter Six

Optimal Design Development and Application

6.1 Introduction

In Section 1.3.8, four minimum-cost designs were analysed and discounted as general methods for optimal PRB design. The aim of this chapter is to develop and test an optimal design methodology that can be used to find the minimum cost design (or designs) for fully penetrating remediation situations. The methodology includes simplified economic, hydraulic and geochemical aspects of the remediation situation and needs to be followed up with site-specific computer modelling and pilot-scale testing before full-scale construction begins.

Reactive material characteristics are provided by the laboratory experiments described in Chapter 3. The customised down-gradient gate face described in Chapter 4 and Appendix C is included to equalise residence time laterally. Plume capture and residence time performance measures are determined by the functional relationships presented in Chapter 5 for fully penetrating PRBs. Partially penetrating situations can be covered if appropriate functional relationships are developed (see Chapter 8).

The proposed optimisation model presents all input data in an Excel spreadsheet and locates minimum-cost designs using Excel's standard non-linear solver routine. A performance comparison with other potential solvers is described in Section 6.4.1. The use of carefully chosen multiple starting points proved highly likely to produce globally optimal solutions to all design examples analysed.

A hypothetical example provides a practical application of the methodology. Further applications for sensitivity and uncertainty analysis will be covered in Chapter 7.

6.2 A New Optimal Design Methodology

A new optimal design methodology is proposed for PRB systems. This methodology is similar to a generalised form of *Teutsch, Tolksdorff and Schad* [1997], as discussed in Section 1.3.8, with the addition of an optimisation procedure. The approach of *Howard, Hatfield and Christensen* [1995] was not considered, as it requires a fully penetrating PRB system with up-gradient and down-gradient funnels. These requirements are expected to add unnecessary cost for most PRB design situations. The approach of *Manz and Quinn* [1997] was also not considered as it was expected to be too simplistic. It did not incorporate an optimisation procedure and it was limited to contaminants with first-order decay rates.

The remainder of this chapter describes the new optimal design methodology and then applies it to two example situations. The proposed methodology combines the hydrogeological, geochemical, and economical aspects of a fully penetrating PRB system. Extension of this methodology to partially penetrating situations will be discussed in Chapter 8 along with relaxation of all other assumptions. The following assumptions are proposed for the chosen methodology:

1. Remediation of the whole plume down to the contaminant regulatory level.
2. Fully penetrating PRB systems.
3. Only one contaminant requiring remediation.
4. Only one reactive and one non-reactive material in the methodology at a time. (The optimal designs for different combinations of reactive and non-reactive materials can be compared post-optimisation.)
5. Gate and aquifer are homogeneous, isotropic and characterisation is not time-dependent over modelled area and time frame.
6. PRB system is centred on centre of plume and groundwater flow direction does not change with time.
7. Funnels are installed at right angles to the side walls.
8. Side wall length equals the gate length at its edge.
9. Contaminant concentration does not change over space (within plume) or time and natural attenuation is negligible.
10. All input parameters remain constant during PRB operating period.
11. All utilised functional relationships are continuous and differentiable.

6.2.1 PRB Design Definitions with Bounds Determined by Computer Modelling Experiments

Table 6.2.1
Design Variables

Name	Description	Units	Lower Bound	Upper Bound
L_G	Gate length at its edge – y direction	m	0.75	18.00
$Prop_{RM}$	Reactive material proportion in gate	-	0.01	1.00
W_F	Total funnel width in two equal sections – x direction	m	0.00	60.00
W_G	Gate width – x direction	m	3.00	18.00

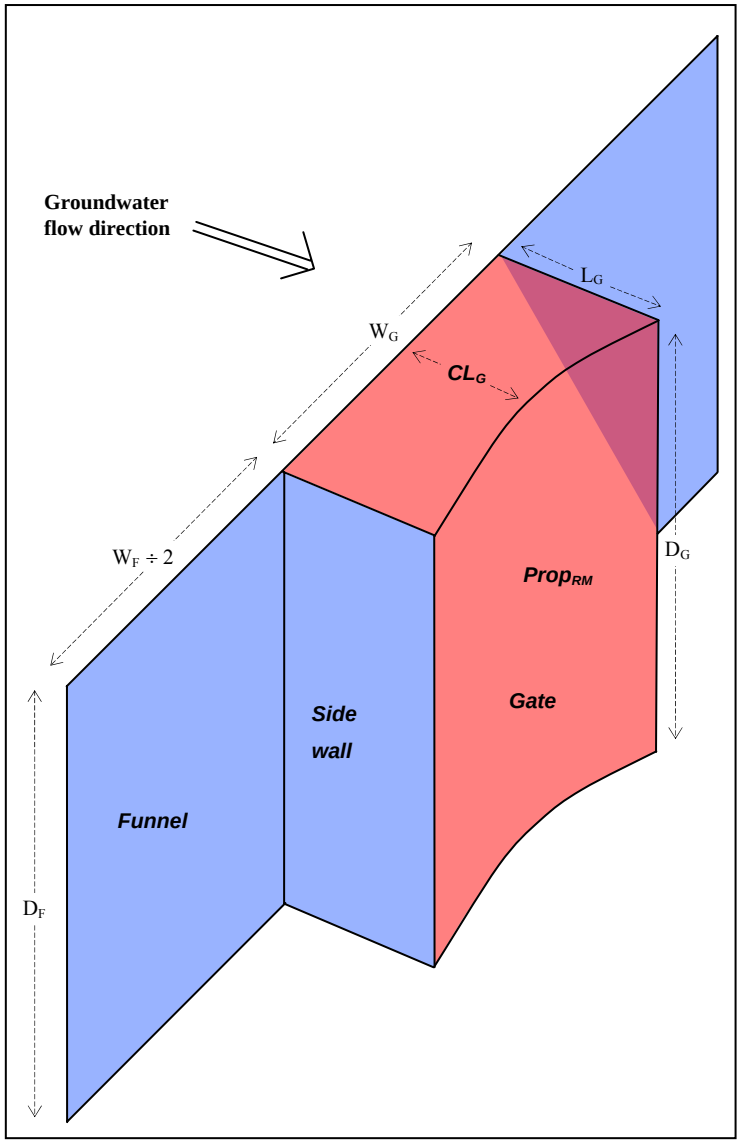

Fig. 6.1. Three dimensional view of PRB design.

Figure 6.1 presents a three-dimensional view of the chosen subset of PRB designs. All design variables are described in Table 6.2.1. Funnel and gate depths are not design variables as the PRB is fully penetrating.

Table 6.2.2
User Inputs

Name	Description	Units
$Avail_{Sub}$	Available proportion of substrate (reactive portion of the reactive material) after initial losses	-
$BulkDen_{Sub}$	Bulk density of substrate	$g\ m^{-3}$
D_{Aq}	Depth from ground surface to first confining layer of aquifer	m
D_{Pl}	Plume depth – z direction	m
D_{Water}	Depth from ground surface to historic high water mark	m
$Grad_{Aq}$	Hydraulic gradient of aquifer	$m\ m^{-1}$
$Initial_{Cont}$	Initial contaminant concentration	$g\ m^{-3}$
K_{Aq}	Saturated hydraulic conductivity of aquifer	$m\ d^{-1}$
$K_{Mix(r)}$	Hydraulic conductivity of each reactive material input proportion *r*	-
L_{TP}	Number of days in a time period (for interest rate calculations)	d
$Limit_{Cont}$	Regulatory concentration limit for contaminant immediately down-gradient from PRB	$g\ m^{-3}$
$Lost_{Sub}$	Regular proportion of substrate lost, e.g. via flushing	d^{-1}
Min_{Sub}	Minimum substrate for contaminant degradation	$g\ m^{-3}$
$Moles_{Cont}$	Moles of contaminant from stoichiometric equation	-
$Moles_{Sub}$	Moles of substrate from stoichiometric equation	-
$Por_{Mix(r)}$	Porosity for each reactive material input proportion *r*	-
R	Real discount rate per time period, incorporating combined effects of inflation, productivity and risk (see *U.S. EPA*, 1993)	%
$DegU_{Mix(r)}$	Contaminant degradation rate upper bound for each reactive material input proportion *r*	$g\ m^{-3}\ d^{-1}$
RM_{Sub}	Proportion of substrate in reactive material	-
TotalTime	Expected length of time PRB needs to operate for	d
$VF_{Mix(r)}$	Volumetric factor for each reactive material input proportion *r*	-
W_{Pl}	Plume width – x direction	m
$Weight_{Cont}$	Molecular weight of contaminant	g
$Weight_{Sub}$	Molecular weight of substrate	g

The following tables contain descriptions of all other parameters, variables and inputs to the proposed design methodology. These are required for the design relationships and calculations in Section 6.3.

Table 6.2.3
Design Dependent Parameters
(Directly dependent on design variables)

Name	Description	Units
CL_G	Gate length at its centre – y direction	m
D_F	Total funnel depth – z direction	m
D_G	Gate depth – z direction	m
L_{SW}	Side wall length – y direction	m
V_{NRM}	Volume of non-reactive material in gate	m^3
V_{RM}	Volume of reactive material in gate	m^3

Table 6.2.4
Fixed Input Parameters from Functional Relationships

Name	Description
$a_{1(w,k)}$ to $d_{4(w,k)}$	Relative residence and capture fixed input parameters for *k=1..5* and *w=1..4*
Kin_k	*k=1..7* K_G/K_{Aq} ratio inputs (1, 2, 4, 7 and 10) and dummy inputs (12 and 14)
$RMin_r$	*r=1..10* reactive material ratio inputs (0, 0.2, 0.4, 0.6, 0.8 and 1.0) and dummy inputs (-0.1, -0.05, 1.05 and 1.1)
$WGin_w$	*w=1..6* gate width inputs (3, 6, 9 and 18) and dummy inputs (21 and 24)

Table 6.2.5
Derived Parameter Descriptions
(Used in PRB design calculations)

Name	Description	Units
Capture	Width of plume captured at a defined distance up-gradient from PRB (up-gradient from the portion of aquifer influenced by PRB emplacement)	m
Deg_G	Actual contaminant degradation rate in the gate	g m^{-3} d^{-1}
$DegU_G$	Upper bound on contaminant degradation rate in the gate	g m^{-3} d^{-1}
DF	Accumulated discount factor to transform future costs to the present day	-
$Final_{Cont}$	Average down-gradient contaminant concentration of plume to be compared with regulatory limit	g m^{-3}
$Init_{Sub}$	Initial substrate in the solid phase	g
$M_k(K_G/K_{Aq})$	Multipliers calculated by the Lagrange Method in the stage 3 interpolations (relative residence and capture) for each Kin_k input *k* and the required K_G/K_{Aq} ratio	-

Table 6.2.5 continued…

Name	Description	Units
$M_r(Prop_{RM})$	Multipliers calculated by the Lagrange Method for each $RMin_r$ input *r* and the required $Prop_{RM}$ ratio	-
$M_w(W_G)$	Multipliers calculated by the Lagrange Method in the stage 4 interpolations (relative residence and capture) for each $WGin_w$ input *w* and the required W_G ratio	-
Num_{Repl}	Number of replenishments	-
Por_G	Effective porosity of gate for chosen mixture	-
PV_{Repl}	Present value of replenishments	$
$PVCost_{Con}$	Present value of fixed replenishment costs	$
RelCapt	Actual plume width captured divided by gate width (the "natural" capture)	-
$RelRes_{Centre}$	Residence time for a particle travelling down the centreline of the gate relative to residence time of same particle through same part of natural aquifer	-
$RelRes_{Edge}$	Residence time for a particle travelling next to a side wall of the gate relative to residence time of same particle through same part of natural aquifer	-
Res_{Centre}	Actual residence time for a particle travelling down the gate centreline	d
Res_{Edge}	Actual residence time for a particle travelling next to a side wall of the gate	d
Sub_{Rate}	Rate of consumption of available substrate by degradation	$g\ m^{-3}\ d^{-1}$
$Time_{Repl}$	Time between replenishments	d
$TotCost_{Mon}$	Total monitoring costs	$
V_{GRZ}	Volume of gate reactive zone	m^3
V_{GRNZ}	Volume of gate non-reactive zone	m^3
VF_G	Volumetric factor for gate contents	-

Table 6.2.6
Cost Inputs

Name	Description	Units
$Cost_{Con}$	Total (present) fixed construction costs including mobilisation and transportation costs	$
$Cost_{DAq}$	Total present cost of disposing aquifer material (after initial construction)	$ m^{-3}
$Cost_{DG}$	Total present cost of disposing gate mixture (after each replenishment)	$ m^{-3}
$Cost_{F}$	Total present cost of funnel material (e.g. sheet piling)	$ m^{-2}
$Cost_{Mon}$	Total present cost of monitoring, proportional to gate width and time	$ L_{TP}^{-1} m^{-1}
$Cost_{NRM}$	Total present cost of non-reactive material (e.g. pea gravel)	$ m^{-3}
$Cost_{Pre}$	Total pre-construction costs including preliminary site assessment, site characterisation, laboratory tests, PRB modelling and optimisation	$
$Cost_{RM}$	Total present cost of reactive material (e.g. sawdust)	$ m^{-3}
$Cost_{SW}$	Total present cost of side walls (e.g. sheet piling)	$ m^{-2}

6.2.2 Objective Function

The objective is to minimise the following:
Cost of Funnel + Cost of Side Walls + Cost of Reactive Material + Cost of Non-Reactive Material + Cost of Future Replenishments + Pre-Construction Costs + Fixed Construction Costs + Fixed Construction Costs for Future Replenishments + Monitoring Costs + Disposal Costs for Aquifer and Gate Materials.

The objective function can therefore be written as follows:

$$\mathbf{MINIMISE\ (W_F * D_F * Cost_F) + (2 * L_{SW} * D_F * Cost_{SW}) + VF_G * V_{GRZ} * (Prop_{RM} * Cost_{RM} + Prop_{NRM} * (1 - Cost_{RM})) + V_{GNRZ} * Cost_{NRM} + VF_G * V_{GRZ} * PV_{Repl} + Cost_{Pre} + Cost_{Con} + PVCost_{Con} + Cost_{Mon} + (L_G * W_G * D_G) * (Cost_{DAq} + Cost_{DG} * Num_{Repl})}$$

The partial derivatives of the objective function with respect to each decision variable are as follows. These equations represent the shape of the objective function when only the chosen decision variable is allowed to vary.

$\partial(\text{Cost})/\ \partial(W_F) = D_F * \text{Cost}_F$

$\partial(\text{Cost})/\ \partial(L_G) = W_G * D_G * (\text{Cost}_{DAq} + \text{Cost}_{DG} * \text{Num}_{Repl})$

$\partial(\text{Cost})/\ \partial(W_G) = L_G * D_G * (\text{Cost}_{DAq} + \text{Cost}_{DG} * \text{Num}_{Repl})$

$\partial(\text{Cost})/\ \partial(\ \text{Prop}_{RM}) = VF_G * V_{GRZ} * \text{Cost}_{RM}$

6.2.3 Constraints

Constraints on design (decision) variables or combinations of design variables and other inputs restrict the values that design variables can take. Any combination of design variables that satisfies every constraint is called a *feasible solution* and the set of all feasible solutions forms the *feasible region*. The optimisation solving routine will search for the minimum cost solution in the feasible region.

Some constraints deal with realistic limits on design variables (see Table 6.2.1). For example, no PRB design variable can be negative. All gate dimensions also must be non-zero otherwise no gate exists. There may be site characteristics such as physical obstacles that restrict PRB dimensions. There may also be political or legal restrictions on PRB dimensions. The limits of the functional relationships between design variables and PRB performance measures will also limit the design variables (see Chapter 5).

Other constraints restrict combinations of design variables or design variables and other inputs due to limitations of the functional relationships or model assumptions. For example, this model assumes the whole plume is to be captured and remediated. Therefore, capture width must be at least as great as the plume width and down-gradient contaminant concentration must be no more than the regulatory limit. The required constraints to satisfy all model assumptions are:

- Upper and lower bounds on decision variables.
- Upper bound (=regulatory limit) and lower bound (=0) on final contaminant concentration.
- Lower bound (=plume width) on capture width.
- Upper and lower bounds on L_G/W_G, K_G/K_{Aq} and $(W_F+W_G)/W_G$ as extrapolation of functional relationships developed by computer modelling is not advised (see Chapter 5).

6.3 PRB Design Relationships and Calculations

The natural environment can be very complex with many of the model's input parameters likely to vary significantly over time and space. PRB design relationships will be stated in terms of specific relationships for the chosen subset of PRBs defined in Section 6.2. The issues of input parameter uncertainty and variation will be covered in Chapter 7.

In Chapter 5 and Appendix C, methods were presented for estimating relative residence, relative capture, customised down-gradient gate shape and gate volume. The general form of these equations will be presented in the following sections along with other equations to describe changes in contaminant concentration and reactive material over time. The equations are used in a spreadsheet-based optimisation methodology with the objective function presented in Section 6.2.2.

The purpose of the laboratory experiments in Chapter 3 and functional relationship development in Chapter 5 is to remove the hydraulic and geochemical simulations from the optimisation methodology. This creates a much more efficient optimisation process. The following equations describe the resulting analytical model that calculates plume capture, down-gradient contaminant concentrations and the constrained input relationships presented in Section 6.2.3 for the current set of design variables. For a given contamination problem, the task of the user is to find an initial feasible solution (where all constraints are satisfied) by adjusting the design variables. The solution calculated by the analytical model is analysed by the solving routine, which produces successive sets of design variables until a minimum cost solution is found.

Equations 6.3.1 to 6.3.19 describe the calculation of relative residence and capture. These were previously presented in Chapter 5. Equation 6.3.20 calculates capture width as described in Section 4.3.3. Equations 6.3.21 to 6.3.28 apply the Lagrange Method presented in Chapter 5 to the results of the reactive material laboratory experiments presented in Chapter 3. Equations 6.3.29 to 6.3.32 use the method described in Appendix C for calculating reactive and non-reactive zone volumes, and therefore the initial volume of reactive and non-reactive materials. Calculations can then be carried out for the length of time before the gate contents require replenishment (Equations 6.3.33 to 6.3.35), the number of required replenishments given the expected PRB operating time (Equation 6.3.36) and the present cost of all replenishments (Equations 6.3.37 and 6.3.38). The down-gradient average contaminant concentration is then calculated from the input up-gradient concentration minus the product of the calculated degradation rate and residence time (Equation 6.3.39). Total monitoring costs are calculated by Equations 6.3.40 and 6.3.41 and the total PRB cost is calculated by the objective function in Section 6.2.2.

6.3.1 Edge Relative Residence Time

Relative residence time was defined in Section 4.3.2 and its relationship with the design variables presented in Chapter 5. It is dependent on the PRB and aquifer characteristics.

From the stage two interpolation described in Section 5.3.2, first calculate parameters $a_{w,k}$, $b_{w,k}$ and $c_{w,k}$ for all $WGin_w$ and Kin_k as in Equations 6.3.1 to 6.3.3. Input parameters $a_{1(w,k)}$ to $c_{4(w,k)}$ are in Tables B9 to B12.

$$\mathbf{a_{w,k}} = \frac{\mathbf{a_{1(w,k)}} + \mathbf{a_{2(w,k)}} * \frac{\mathbf{L_G}}{\mathbf{W_G}}}{\mathbf{1} + \mathbf{a_{3(w,k)}} * \frac{\mathbf{L_G}}{\mathbf{W_G}} + \mathbf{a_{4(w,k)}} * \left(\frac{\mathbf{L_G}}{\mathbf{W_G}}\right)^2} \qquad \textbf{6.3.1}$$

$$\mathbf{b_{w,k}} = \frac{\mathbf{1}}{\mathbf{b_{1(w,k)}} + \mathbf{b_{2(w,k)}} * \frac{\mathbf{L_G}}{\mathbf{W_G}} + \mathbf{b_{3(w,k)}} * \left(\frac{\mathbf{L_G}}{\mathbf{W_G}}\right)^2} \qquad \textbf{6.3.2}$$

$$c_{w,k} = \frac{c_{1(w,k)} + c_{2(w,k)} * \frac{L_G}{W_G}}{1 + c_{3(w,k)} * \frac{L_G}{W_G} + c_{4(w,k)} * \left(\frac{L_G}{W_G}\right)^2} \qquad \textbf{6.3.3}$$

Next estimate each edge relative residence $RelRes_{Edge(w,k)}$ as follows:

$$RelRes_{Edge(w,k)} = \frac{1}{a_{w,k} + b_{w,k} * \frac{W_F + W_G}{W_G} + c_{w,k} * \left(\frac{W_F + W_G}{W_G}\right)^2} \qquad \textbf{6.3.4}$$

For the stage three polynomial interpolation, multipliers $M_k(K_G/K_{Aq})$ are first calculated at each point k for the desired K_G/K_{Aq} (where the prime on the product means "excluding the k^{th} value").

$$M_k(K_G/K_{Aq}) = \frac{\prod_{i=1}^{7}{}' (K_G/K_{Aq} - Kin_i)}{\prod_{i=1}^{7}{}' (Kin_k - Kin_i)} \qquad \text{(for k=1..7)} \qquad \textbf{6.3.5}$$

w edge relative residence times $RelRes_{Edge(w)}$ for the desired L_G, W_F and K_G/K_{Aq} can then be estimated as follows:

$$Y_w(K_G/K_{Aq}) = \sum_{k=1}^{7} M_k(K_G/K_{Aq}) * y_{w,k} \qquad \textbf{6.3.6}$$

For the final stage, $M_w(W_G)$ are first calculated at each point *w* for the desired W_G (where the prime on the product means "excluding the w^{th} value").

$$M_w(W_G) = \frac{\prod_{i=1}^{6}{}' (W_G - WGin_i)}{\prod_{i=1}^{6}{}' (WGin_w - WGin_i)} \qquad \text{(for w=1..6)} \qquad \textbf{6.3.7}$$

The edge relative residence *RelRes(W_G)* for the desired W_G, L_G, W_F and K_G/K_{Aq} can then be estimated as follows:

$$\mathbf{RelRes_{Edge}} = \sum_{w=1}^{6} \mathbf{M_w(W_G) * Y_w(K_G / K_{Aq})} \qquad \mathbf{6.3.8}$$

Finally, actual edge residence (in days) can be estimated from Equation 6.3.9 as follows:

$$\mathbf{Res_{Edge}} = \frac{\mathbf{RelRes_{Edge} * L_G * Por_G}}{\mathbf{Grad_{Aq} * K_{Aq}}} \qquad \mathbf{6.3.9}$$

6.3.2 Centreline Relative Residence Time

Centreline relative residence time is calculated using the same methodology as described for edge relative residence in Section 6.3.1. A gate length equal to the edge gate length is used initially. The centreline gate length required to equalise residence time is then calculated in Equation C1. Parameters $a_{w,k}$, $b_{w,k}$ and $c_{w,k}$ are first calculated for all $WGin_w$ and Kin_k as in Equations 6.3.10 to 6.3.12. Input parameters $a_{1(w,k)}$ to $c_{4(w,k)}$ are in Tables B21 to B24.

$$\mathbf{a_{w,k} = a_{1(w,k)} + a_{2(w,k)} * \frac{L_G}{W_G} + a_{3(w,k)} * \left(\frac{L_G}{W_G}\right)^2 + a_{4(w,k)} * \left(\frac{L_G}{W_G}\right)^3} \qquad \mathbf{6.3.10}$$

$$\mathbf{b_{w,k} = b_{1(w,k)} + b_{2(w,k)} * \frac{L_G}{W_G} + b_{3(w,k)} * \left(\frac{L_G}{W_G}\right)^2 + b_{4(w,k)} * \left(\frac{L_G}{W_G}\right)^3} \qquad \mathbf{6.3.11}$$

$$\mathbf{c_{w,k} = c_{1(w,k)} + c_{2(w,k)} * \frac{L_G}{W_G} + c_{3(w,k)} * \left(\frac{L_G}{W_G}\right)^2 + c_{4(w,k)} * \left(\frac{L_G}{W_G}\right)^3} \qquad \mathbf{6.3.12}$$

Equations 6.3.4 to 6.3.7 are then applied (as the multipliers (M) are only dependent on K_G/K_{Aq} and W_G, so are the same as for edge residence) and centreline relative residence can be estimated as follows:

$$\mathbf{RelRes_{Centre}} = \sum_{w=1}^{6} \mathbf{M_w(W_G) * Y_w(K_G / K_{Aq})} \qquad \mathbf{6.3.13}$$

Finally, actual centreline residence (in days) can be estimated as follows (see Equation 4.4):

$$\mathbf{Res_{Centre}} = \frac{\mathbf{RelRes_{Centre} * L_G * Por_G}}{\mathbf{Grad_{Aq} * K_{Aq}}} \qquad \mathbf{6.3.14}$$

6.3.3 Relative Capture

Relative capture was defined in Section 4.3.3 and its relationship with the design variables presented in Chapter 5. Like relative residence it is dependent on the PRB and aquifer characteristics. Parameters $a_{w,k}$, $b_{w,k}$, $c_{w,k}$ and $d_{w,k}$ are first calculated for all $WGin_w$ and Kin_k as in Equations 6.3.15 to 6.3.18. Input parameters $a_{1(w,k)}$ to $d_{4(w,k)}$ are in Tables B33 to B36.

$$\mathbf{a_{w,k} = a_{1(w,k)} * \left(a_{2(w,k)} - e^{-a_{3(w,k)} * \frac{L_G}{W_G}} \right)} \qquad \mathbf{6.3.15}$$

$$\mathbf{b_{w,k} = b_{1(w,k)} * \left(b_{2(w,k)} - e^{-b_{3(w,k)} * \frac{L_G}{W_G}} \right)} \qquad \mathbf{6.3.16}$$

$$\mathbf{c_{w,k} = c_{1(w,k)} + c_{2(w,k)} * \frac{L_G}{W_G} + c_{3(w,k)} * \left(\frac{L_G}{W_G} \right)^2 + c_{4(w,k)} * \left(\frac{L_G}{W_G} \right)^3} \qquad \mathbf{6.3.17}$$

$$\mathbf{d_{w,k} = d_{1(w,k)} + d_{2(w,k)} * \frac{L_G}{W_G} + d_{3(w,k)} * \left(\frac{L_G}{W_G} \right)^2 + d_{4(w,k)} * \left(\frac{L_G}{W_G} \right)^3} \qquad \mathbf{6.3.18}$$

Equations 6.3.4 to 6.3.7 are then applied and relative capture *RelCap* for the desired W_G, L_G, W_F and K_G/K_{Aq} can be estimated as follows:

$$\mathbf{RelCap} = \sum_{w=1}^{6} \mathbf{M_w(W_G) * Y_w(K_G / K_{Aq})} \qquad \mathbf{6.3.19}$$

Finally, actual capture (in metres) can be estimated from Equation 6.3.20 as follows:

$$\mathbf{Capture} \quad = \quad \mathbf{RelCap} * \mathbf{W_G} \qquad \mathbf{6.3.20}$$

6.3.4 Hydraulic Conductivity Ratio (Gate/Aquifer)

Hydraulic conductivity was introduced in Section 1.2.1 and a method to determine its relationship with reactive mixtures in the laboratory was presented in Section 3.5.2. The laboratory experiments produce the K_G/K_{Aq} ratio $K_{Mix(r)}$ for the chosen reactive material ratio inputs $RMin_r$ = (0, 0.2, 0.4, 0.6, 0.8 and 1.0) with r=3..8. Dummy inputs (see Section 5.2) are then added as $RMin_r$ = (-0.1, -0.05, 1.05 and 1.1) for r=1, 2, 9 and 10. Dummy inputs less than zero are required as the lowest $RMin_r$ is zero. $K_{Mix(r)}$ is calculated for the dummy inputs as follows:

$$\mathbf{K_{Mix(1)} = K_{Mix(2)} = 0.99 * K_{Mix(3)}} \qquad \mathbf{6.3.21}$$

$$\mathbf{K_{Mix(9)} = K_{Mix(10)} = 1.01 * K_{Mix(8)}} \qquad \mathbf{6.3.22}$$

Multipliers $M_r(Prop_{RM})$ are first calculated at each point r for the desired $Prop_{RM}$ (where the prime on the product means "excluding the r^{th} value").

$$\mathbf{M_r(Prop_{RM})} \quad = \quad \frac{\prod_{i=1}^{10}{}' (\mathbf{Prop_{RM} - RMin_i})}{\prod_{i=1}^{10}{}' (\mathbf{RMin_r - RMin_i})} \qquad \text{(for r=1..10)} \qquad \mathbf{6.3.23}$$

The desired K_G/K_{Aq} can then be estimated as follows:

$$\mathbf{K_G / K_{Aq}} \quad = \quad \sum_{r=1}^{10} \mathbf{M_r(Prop_{RM}) * K_{Mix(r)}} \qquad \mathbf{6.3.24}$$

6.3.5 Gate (Effective) Porosity

As with hydraulic conductivity, effective porosity was introduced in Section 1.2.1 and a method to determine its relationship with reactive mixtures in the laboratory was presented in Section 3.5.1. Porosity estimation follows the methodology presented in Section 6.3.4, requiring the multipliers (M) calculated in Equation 6.3.23 and the input porosities $Por_{Mix(r)}$ for the chosen and dummy reactive material ratio inputs $RMin_r$.

$$\mathbf{Por_G} = \sum_{r=1}^{10} \mathbf{M_r (Prop_{RM}) * Por_{Mix(r)}} \qquad \mathbf{6.3.25}$$

6.3.6 Contaminant Degradation Rate

The degradation rate is the rate at which contaminants flowing through a PRB system are transformed by chemical and/or biological means to less harmful by-products. The rate at which this happens in the natural environment is called natural attenuation. These rates are usually estimated from laboratory and field experiments. A method to determine the relationship between reactive/non-reactive material mixtures and their combined volume in the laboratory was presented in Section 3.5.3.

Contaminant degradation rates in the gate are primarily affected by incoming contaminant concentrations, available substrate, groundwater velocity, and other considerations such as seasonal changes in temperature or pH (see Section 2.2.4 and Chapter 3). Other processes that affect contaminant concentrations (e.g. dispersion) can also be factored into the degradation rate. For contaminants such as nitrate, the rate is usually first-order (linear) at low concentrations but tails off asymptotically to some zero-order (constant) maximum at high concentrations. The expected (maximum) degradation rate range directly affects the flow-through-length dimensions of the PRB and indirectly affects the time between replenishment of the gate contents.

Degradation rate (upper bound) estimation follows the methodology presented in Section 6.3.4, requiring the multipliers (M) calculated in Equation 6.3.23 and the input porosities $DegU_{Mix(r)}$ for the chosen and dummy reactive material ratio inputs $RMin_r$.

$$\mathbf{DegU_G} = \sum_{r=1}^{10} \mathbf{M_r(Prop_{RM}) * DegU_{Mix(r)}} \qquad \mathbf{6.3.26}$$

The main limiting factors for the actual degradation rate Deg_G are assumed to be the reactive material potential and the incoming contaminant concentration. Either can limit the actual degradation rate as follows:

$$\mathbf{Deg_G = MIN}\left(\mathbf{DegU_{Rate}}, \frac{\mathbf{Initial_{Cont}}}{\mathbf{L_G * Rel Res_{Edge} * \frac{Por_G}{Grad_{Aq} * K_{Aq}}}} \right) \qquad \mathbf{6.3.27}$$

6.3.7 Reactive Zone Volumetric Factor

When two materials are combined to create a reactive mixture, the combined volume is rarely the sum of the individual volumes. This is due to the smaller particles occupying some of the void space between the larger particles. A method to determine the relationship between reactive mixtures and their combined volume in the laboratory was presented in Section 3.5.4. Volumetric factor estimation follows the methodology presented in Section 6.3.4, requiring the multipliers (M) calculated in Equation 6.3.23 and the input porosities $Por_{Mix(r)}$ for the chosen and dummy reactive material ratio inputs $RMin_{r.}$

$$\mathbf{VF_G} = \sum_{r=1}^{10} \mathbf{M_r(Prop_{RM}) * VF_{Mix(r)}} \qquad \mathbf{6.3.28}$$

6.3.8 Reactive Zone/Material Volume

Section 4.4.1 presented customised down-gradient gate faces as a design enhancement for PRB systems. Figure 4.13 defined the reactive and non-reactive zones for these systems. Appendix C describes a methodology for approximating the down-gradient gate face by a simple quadratic. A generalisation of Equation C.4 to include PRB systems where the reactive material only starts at the historical (maximum) water table depth D_{Water} produces:

$$V_{GRZ} = W_G * (D_G - D_{Water}) * \left(CL_G + \frac{(L_G - CL_G)}{3} \right) \quad \textbf{6.3.29}$$

The required volume of reactive material can then be calculated from:

$$V_{RM} = Prop_{RM} * VF_G * V_{GRZ} \quad \textbf{6.3.30}$$

6.3.9 Non-Reactive Zone/Material Volume

The purpose of the non-reactive zone presented in Figure 4.13 is to maintain the flow patterns of the reactive zone without the costly reactive material. This is achieved by a cheaper non-reactive material combination with a similar hydraulic conductivity and effective porosity to the reactive zone. The non-reactive zone volume is then just the original gate volume minus the reactive zone volume as follows (provided this difference is non-negative):

$$V_{GNRZ} = MAX(0, W_G * (D_G - D_{Water}) * L_G - V_{GRZ}) \quad \textbf{6.3.31}$$

The required volume of non-reactive material can then be calculated from:

$$V_{NRM} = (1 - Prop_{RM}) * VF_G * V_{GRZ} + V_{GNRZ} \quad \textbf{6.3.32}$$

6.3.10 Initial Substrate in the Solid Phase

The relationship between the physical volume of reactive material and the amount of substrate available for contaminant degradation is not fully understood. Often the substrate needs to be transformed to another (e.g. liquid) phase before it is available for contaminant degradation. If the substrate does not transform fast enough to the required phase it may limit the degradation reaction. These issues need to be examined in laboratory and field experiments.

For the purposes of this optimisation it is assumed that initial (solid phase) substrate has been determined as a linear combination of gate reactive zone volume, reactive material proportion in gate, solid substrate proportion in reactive material, substrate bulk density and available proportion of substrate after initial losses as follows:

$$\mathbf{Init_{Sub} = V_{GRZ} * Prop_{RM} * RM_{Sub} * BulkDen_{Sub} * Avail_{Sub}} \qquad \mathbf{6.3.33}$$

6.3.11 Average Consumption Rate of Substrate

Solid phase substrate will decline over time as a result of a variety of processes. This decline can usually be measured during laboratory/field degradation experiments from a sample of gate material extracted at known time intervals. The average rate of substrate consumption due to degradation is assumed to be directly proportional to the actual degradation rate as follows:

$$\mathbf{Sub_{Rate} = Deg_G * \frac{Moles_{Sub}}{Moles_{Con}} * \frac{Weight_{Sub}}{Weight_{Con}}} \qquad \mathbf{6.3.34}$$

It will be important to determine site-specific conditions that may significantly affect the rate of substrate decline. It will also be important to estimate the minimum amount of solid substrate that does not provide a limitation to the degradation rate. This will have implications on the time between replenishments.

6.3.12 Replenishment Calculations

The time at which the gate contents require replenishing can be defined as the time at which the level of solid substrate reduces the degradation rate beyond an acceptable level. Laboratory and field experiments have been used to estimate replenishment time for a variety of reactive materials (e.g. *Carmichael*, 1994; *Robertson et al.*, 2000). In practice, this knowledge would usually be combined with analysis of core samples from the gate in conjunction with water samples from up and down-gradient observation wells to determine the replenishment time.

As some losses are assumed to be proportional to the mass of substrate remaining, the time between replenishments $Time_{Repl}$ is calculated iteratively with a daily time step from the initial substrate $Init_{Sub}$, gate reactive zone volume V_{GRZ}, minimum level of substrate required for degradation Min_{Sub}, average consumption rate of substrate Sub_{Rate} and daily substrate losses $Lost_{Sub}$.

$$\begin{aligned}
&\mathbf{Sub = Init_{Sub}} \\
&\mathbf{Time_{Repl} = 0} \\
&\mathbf{Do\ while\ Sub > (V_{GRZ} * Min_{Sub})} \\
&\quad \mathbf{Time_{Repl} = Time_{Repl} + 1} \\
&\quad \mathbf{Sub = Sub - \left(Sub_{Rate} * V_{GRZ}\right) - (Sub * Lost_{Sub})} \\
&\mathbf{Loop}
\end{aligned} \qquad \textbf{6.3.35}$$

Alternative processes, such as barrier clogging due to build-up of secondary precipitates, could also cause a PRB to require replenishment before the minimum level of substrate required for degradation has been reached. Further equations to estimate length of time between replenishments for each process could be included in the PRB design model, with the minimum process time chosen for inclusion in Equation 6.3.36.

The total number of replenishments required Num_{Repl} is then calculated from the total expected operating time of the PRB and the length of time between replenishments.

$$\mathbf{Num_{Repl} = int\left(\frac{TotalTime}{Time_{Repl}}\right)} \qquad \textbf{6.3.36}$$

The net present value of all replenishments requires a Unitary Net Present Value (UNPV) to transform future costs to the present day. This factor is calculated from the discount rate R, time between replenishments $Time_{Repl}$, the number of replenishments Num_{Repl} and the length of a time period L_{TP} (in days). A real discount rate of 2.9% combining the effects of inflation, productivity and risk was recommended by the 1993 update to the U.S. EPA Office of Management and Budget (OMB) circular (*U.S. EPA*, 1993). R is usually an annual amount which would make L_{TP} = 365.25. Current discount rates for the U.S. can be found on the internet at http://www.frbdiscountwindow.org. This calculation is only appropriate where large market fluctuations (for example, due to resource scarcity and demand) are not anticipated.

$$\mathbf{UNPV = 0}$$

$$\mathbf{For\ t = 1\ to\ Num_{Repl}}$$

$$\mathbf{UNPV = UNPV + \frac{1}{(1+R)^{\left(\frac{t*Time_{Repl}}{L_{TP}}\right)}}} \qquad \mathbf{6.3.37}$$

$$\mathbf{Next\ t}$$

The net present value of fixed construction costs can then be calculated as can the net present value of all replenishments from the reactive material cost, non-reactive material cost, reactive material proportion in the gate and Unitary Net Present Value, as follows:

$$\mathbf{PVCost_{Con} = Cost_{Con} * UNPV}$$
$$\mathbf{PV_{Repl} = Cost_{RM} * Prop_{RM} + Cost_{NRM} * (1 - Prop_{RM}) * UNPV} \qquad \mathbf{6.3.38}$$

6.3.13 Down-Gradient Average Contaminant Concentration

The average contaminant concentration at the down-gradient gate face of a PRB is a function of the up-gradient concentration, average degradation rate and residence time as follows:

$$\mathbf{Final_{Cont} = MAX\left(0, Initial_{Cont} - Deg_G * Res_{Edge}\right)} \qquad \mathbf{6.3.39}$$

A feasible solution to this methodology requires that the average final contaminant concentration $Final_{Cont}$ does not exceed the defined regulatory limit $Limit_{Cont}$. Section 8.2.1 presents a penalty function approach that could be used when a hard constraint is not desired for $\mathrm{Final_{Cont}}$.

6.3.14 Total Monitoring Costs

The present value of all monitoring costs requires a new Unitary Net Present Value (UNPV2) to transform future costs to the present day. This factor is calculated from the discount rate R, expected operational time horizon for PRB $TotalTime$, and the length of a time period L_{TP} (in days).

$$\begin{aligned} &\mathbf{UNPV2 = 0} \\ &\mathbf{For\ t = 1\ to\ \frac{TotalTime}{L_{TP}}} \\ &\quad \mathbf{UNPV2 = UNPV2 + \frac{1}{(1+R)^t}} \\ &\mathbf{Next\ t} \end{aligned} \qquad \mathbf{6.3.40}$$

The present value of all monitoring costs can then be calculated from the monitoring cost (annual cost proportional to gate width), gate width and discount factor, as follows:

$$\mathbf{Monitor_{Cost} = Cost_{Mon} * W_G * UNPV2} \qquad \mathbf{6.3.41}$$

6.4 Application of Optimal Design Methodology

6.4.1 Choice of Solver

The non-linear relationships presented in Section 6.3 produce a non-linear objective function. Section 1.3.1 identified three potential solution techniques for this type of function:

- Non-linear methods such as the generalised reduced gradient (GRG),
- Global search methods such as simulated annealing, bayesian decision analysis and tabu search, and
- Artifical neural network (ANN) and genetic algorithm (GA) combinations.

Solver add-ins to Excel were located and compared for all three methods; Excel's standard GRG2 solver, a trial version of the LGO global solver V5.0 from Frontline Systems Ltd. (www.solver.com), and a trial version of the Evolver genetic algorithm-based solver from Palisade Corporation (www.palisade.com).

For minimum cost optimization, the reduced gradient method searches a solution space by iteratively finding the direction of steepest descent and moves as far as possible in that direction until the objective function stops decreasing or the solution becomes infeasible. It then searches for a new direction and continues until the objective function does not decrease in any feasible direction. Without knowing the shape of the objective function there is no

guarantee, therefore, that the reduced gradient method will find the global minimum cost. The best insurance against missing out on the global minimum is to start the search from many different points spanning the feasible region, hoping that the global optimum will be one of the minimum cost solutions found.

The LGO global solver uses a combination of global (*continuous branch and bound* and *adaptive random search*) and local (including a version of the *reduced gradient method*) search methods with a global multi-start search option. Even with the multi-start option it was found that the starting point often affected the final LGO solution. Communication with Frontline Systems Ltd. confirmed the LGO solver does not guarantee finding the global optimum and is affected by the choice of starting point.

The Evolver solver uses GA technology to create environments where possible solutions continuously crossbreed, mutate, and compete with one another, until they "evolve" into an optimal solution. As a result, Evolver can find optimal solutions to virtually any type of problem, from the simple to the most complex.

A hypothetical PRB design problem was constructed and tested with each solver using the same six starting points. The reactive material proportion (which determines degradation rate and gate/aquifer hydraulic conductivity ratio) and the funnel width were chosen to determine the starting points as both were found to have a significant effect on solver results. The starting points presented in Table 6.4.1 were chosen as they spanned the extent of the feasible region. All other decision variables were then manually adjusted to create each feasible starting point (i.e. one that satisfies all bounds and constraints). All solvers were run on the same Pentium III personal computer. The Evolver solver took a comparatively long time to converge to a solution (> 15 minutes) compared to the GRG2 solver (~ 10 seconds) and the LGO solver (1-2 minutes) so it was abandoned for this application. A variety of solver options and convergence criteria were tried without success to improve the performance of the Evolver solver. Computational efficiency is important because the uncertainty analysis presented in Chapter 7 requires the optimisation model to be run many times. The minimum cost solutions for the GRG2 and LGO solvers at each starting point are presented in Table 6.4.1.

Table 6.4.1
Comparison of GRG2 and LGO Solvers on Hypothetical PRB Design

Starting Point		Minimum PRB Cost	
Reactive Material Proportion	Funnel Width (m)	GRG2	LGO
0.25	0	$485,221	$403,443
0.75	0	$546,817	$403,443
0.95	0	$472,067	$403,443
0.25	10	$468,666	$485,221
0.75	10	$403,443	$403,443
0.95	10	$403,443	$403,443

Table 6.4.1 shows that both solvers reached the same overall minimum cost solution (with cost $403,443) but the LGO solver reached this solution from more starting points than the GRG2 solver. Sixteen further experiments were then undertaken using the same starting points and solvers as the previous experiment. The overall minimum cost solution for each solver found from the 6 starting points is presented in Table 6.4.2. It can also be shown that the LGO solver was again more consistent but slower than the GRG2 solver for these experiments. More importantly though, Table 6.4.2 shows that on experiments 1, 5, 8 and 15 the LGO solver failed to find a solution as cheap as the GRG2 solver. Experiments 3, 6, 9 and 13 also show slight cost differences between the solvers, but the designs were effectively the same.

Table 6.4.2
Comparison of GRG2 and LGO Solvers
on 16 Hypothetical PRB Experiments

Experiment	Overall Minimum Cost		Optimal Solver
	GRG2	LGO	Choice
1	$199,824	$222,264	GRG2
2	$180,692	$180,692	GRG2 & LGO
3	$229,929	$229,977	GRG2 & LGO
4	$332,758	$332,758	GRG2 & LGO
5	$175,706	$199,082	GRG2
6	$253,620	$253,520	GRG2 & LGO
7	$135,801	$135,801	GRG2 & LGO
8	$549,413	$586,324	GRG2
9	$297,625	$297,629	GRG2 & LGO
10	$289,638	$289,638	GRG2 & LGO
11	$262,029	$262,029	GRG2 & LGO
12	$180,353	$180,353	GRG2 & LGO
13	$319,590	$319,584	GRG2 & LGO
14	$220,700	$220,700	GRG2 & LGO
15	$463,720	$470,389	GRG2
16	$109,293	$109,293	GRG2 & LGO

The higher design costs for the LGO solver in experiments 1, 5, 8 and 15 shown in Table 6.4.2 are due to higher reactive material proportion and higher funnel width than the design found by the GRG2 solver. In experiments 1, 8 and 15 the overall minimum cost design produced by the LGO solver was actually higher than one of the feasible starting points. In further experiments, the GRG2 solver was also found to produce lower minimum cost solutions when the minimum cost design was close to a sudden change in design cost caused by an extra PRB replenishment (replacement of the reactive material). This was a surprising result, as the global search methods contained in the LGO solver were expected to perform better than the reduced gradient approach in the vicinity of sudden changes in the objective function.

The superior performance of the GRG2 solver over the LGO and Evolver solvers suggests that the chosen feasible region is not highly non-linear (except for sudden changes caused by an extra PRB replenishment). With the performance advantage of the GRG2 solver combined with its speed and free inclusion with the Excel software, there is a strong case for concluding it to be the most practical option for the chosen PRB design methodology. Only the GRG2 solver will be used for the remaining analysis.

6.4.2 Optimal Design Example

The proposed design methodology is described by way of a hypothetical example situation involving a homogeneous nitrate plume with maximum concentration of 100 g/m^3 NO_3-N that extends the full depth of the aquifer. Following the methodology outlined in Chapter 2, the first step involves preliminary assessment to determine PRB suitability. Laboratory and field experiments found that a reactive zone containing sawdust and pea gravel was able to degrade the nitrate down to the regulatory limit of 10 g/m^3 NO_3-N (e.g. *Blowes et al.*, 1994). Standard construction techniques can be used, as the aquifer is only 6m deep. It is recommended to key the gate, side walls and any funnels 0.5m into the underlying aquitard. The reactive zone is only to be emplaced from the depth of the historical high water table mark and will be capped with native aquifer material.

The second stage of the methodology involves reactive/non-reactive material characterisation and site characterisation. Characterisation of reactive/non-reactive material combinations was introduced in Section 2.4 and fully described in Chapter 3. Column tests are proposed for sawdust and pea gravel in combinations ranging from 0-100% sawdust proportion. Data are required on the hydraulic conductivity, porosity, degradation rate upper bound and volumetric factor. Polynomial interpolation using the Lagrange Method (*Hamming*, 1962) as described in Sections 6.3.4 to 6.3.7 is then undertaken so that the characteristics of any reactive material proportion can be estimated. The 0% reactive material proportion is primarily an anchor for the polynomial, but can also be the natural attenuation remediation option if there are species present in the groundwater that attenuate the contaminant over time.

Output from the chosen hypothetical laboratory column experiments is presented in Table 6.4.3. These data were used as the inputs to Equations 6.3.21 to 6.3.28 in the optimal design spreadsheet. Table 6.4.3 shows that an increase in sawdust proportion produces a decrease in

hydraulic conductivity, and increases in porosity and degradation rate. The volumetric factor is approximately normally distributed (see Figure 3.2) with its maximum value between 40 and 50%.

Table 6.4.3
Reactive/Non-Reactive Material Characterisation

$Prop_{RM}$		**0.00**	**0.20**	**0.40**	**0.60**	**0.80**	**1.00**
$K_{Mix(1)}$	$m\ d^{-1}$	24.00	20.00	16.00	8.00	6.00	3.50
$Por_{Mix(1)}$		0.35	0.35	0.36	0.38	0.46	0.55
$DegU_{Mix(1)}$	$g\ m^{-3}\ d^{-1}$	0.02	3.00	4.50	5.50	6.00	6.00
$VF_{Mix(1)}$		1.000	1.073	1.133	1.116	1.045	1.000

User input relating to the aquifer, plume and reactive material is presented in Table 6.4.4. Most of this information is obtained from the hypothetical site characterisation as described in Section 2.3. Constraint bounds for this example are presented in Table 6.4.5. Plume capture width must be at least as great as the plume width entered in Table 6.4.4. Down-gradient contaminant concentration must be non-negative and less than the regulatory limit entered in Table 6.4.4. All decision variables and modelled ratios are constrained to be between the bounds modelled in Chapter 5.

The third stage of the optimal design methodology requires the creation of economic and hydrogeologic/geochemical models. All relevant costs from the hypothetical example were obtained from a local contractor (*Perrys*, 1999) and are presented in Table 6.4.6. Fixed construction costs were not included at this time. The hydrogeologic model involved Tables B9 to B12, B21 to B24 and B33 to B36 as input to Equations 6.3.1 to 6.3.20. All inputs for the geochemical model were presented in Tables 6.4.3 and 6.4.4. The model was then created by application of Equations 6.3.26, 6.3.27 and Equations 6.3.33 to 6.3.39.

Table 6.4.4
Site Characterisation and other User Inputs

Name	Amount	Units
$Avail_{Sub}$	0.50	
$BulkDen_{Sub}$	1500000.00	g m^{-3}
D_{Aq}	6.00	m
D_{Pl}	6.00	m
D_{Water}	0.50	m
$Grad_{Aq}$	0.013	m m^{-1}
$Initial_{Cont}$	100.00	g m^{-3}
K_{Aq}	3.50	m d^{-1}
L_{TP}	365.25	d
$Limit_{Cont}$	10.00	g m^{-3}
$Lost_{Sub}$	0.001	d^{-1}
Min_{Sub}	100.00	g m^{-3}
$Moles_{Cont}$	0.80	
$Moles_{Sub}$	1.00	
Por_{Aq}	0.30	
R	0.029	
RM_{Sub}	0.50	
TotalTime	10000.00	d
W_{Pl}	10.00	m
$Weight_{Cont}$	14	g
$Weight_{Sub}$	12	g

Table 6.4.5
Constraint Bounds

	Lower	Upper	Units
Capture	10.00		m
$Final_{Cont}$	0.00	10.00	g m^{-3}
K_G/K_{Aq}	1.00	10.00	
L_G	0.75	18.00	m
L_G/W_G	0.00	2.00	
RM_{Prop}	0.01	1.00	
W_F	0.00	60.00	m
$(W_F+W_G)/W_G$	0.00	10.00	
W_G	3.00	18.00	m

Table 6.4.6
Costs (all inclusive)

Name	Amount	Units
$Cost_{DAq}$	5.00	\$ m^{-3}
$Cost_{DG}$	25.00	\$ m^{-3}
$Cost_F$	150.00	\$ m^{-2}
$Cost_{Mon}$	0.00	\$ L_{TP}^{-1} m^{-1}
$Cost_{NRM}$	20.00	\$ m^{-3}
$Cost_{Pre}$	1000.00	\$
$Cost_{RM}$	40.00	\$ m^{-3}
$Cost_{SW}$	150.00	\$ m^{-2}

The final step before solving the model is to choose an initial solution. Normally a feasible solution is chosen in case the shape of the infeasible region inhibits the solver. However, the solver was also found to operate from some initial infeasible solutions, especially solutions that just required an increase in gate length to reach feasibility. Initial feasible solutions were found by setting W_F and RM_{Prop} to pre-defined levels, and manually adjusting W_G and L_G (see Section 6.4.1). For example, it can be shown that by setting $W_F = 0$ and $RM_{Prop} = 0.25$, a

variety of W_G and L_G combinations satisfy all the constraints in Table 6.4.3. Figure 6.2 shows that one such combination is W_G = 10.0 and L_G = 6.0, with a cost of $64,528. This starting point produces the solution shown in Figure 6.3, with W_F = 0.0, W_G = 9.98, L_G = 1.28, RM_{Prop} = 1.00 and a cost of $14,039.

	A	B	C	D	E	F
1	**Permeable Reactive Barrier Design**					
3		Lower		Amount		Upper
4	**Design Variables**					
5	Total funnel width in two equal sections (m)	0.00	<=	**0.00**	<=	60
6	Gate width (m)	3.00	<=	**10.00**	<=	18
7	Gate length at edge (m)	0.75	<=	**6.00**	<=	18
8	Reactive material proportion in gate (-)	0.01	<=	**0.25**	<=	1
10	**Constraints**					
11	Hydraulic conductivity ratio (PRB / Aquifer)	1.00	<=	5.50	<=	10.00
12	Gate length/gate width	0.00	<=	0.60	<=	2.00
13	(Funnel width +gate width)/gate width	0.00	<=	1.00	<=	10.00
14	Capture (m)	10.00	<=	13.40		
15	Ave final concentration (g/m^3)	0.00	<=	2.97	<=	10.00
17	**Design Dependent Parameters**					
18	Funnel depth (m)			6.50		
19	Side wall length (m)			6.00		
20	Gate depth (m)			6.00		
21	Gate length at centre (m)			4.72		
22	Reactive material volume (m^3)			77.323		
23	Non-reactive material volume (m^3)			278.734		
25	**Objective: MIN PRB Cost =**	**$64,528.08**				Formula

Fig. 6.2. Screen shot of initial feasible solution for hypothetical example.

Figure 6.3 shows that the solution satisfies all constraints. Application of the six starting points proposed in Section 6.4.1 produced the same minimum cost solution every time. It is highly likely, therefore, that the global minimum for the chosen solution space has been found.

	A	B	C	D	E	F
1	**Permeable Reactive Barrier Design**					
2						
3		Lower		Amount		Upper
4	**Design Variables**					
5	Total funnel width in two equal sections (m)	0.00	<=	**0.00**	<=	60
6	Gate width (m)	3.00	<=	**9.98**	<=	18
7	Gate length at edge (m)	0.75	<=	**1.28**	<=	18
8	Reactive material proportion in gate (-)	0.01	<=	**1.00**	<=	1
9						
10	**Constraints**					
11	Hydraulic conductivity ratio (PRB / Aquifer)	1.00	<=	1.00	<=	10.00
12	Gate length/gate width	0.00	<=	0.13	<=	2.00
13	(Funnel width +gate width)/gate width	0.00	<=	1.00	<=	10.00
14	Capture (m)	10.00	<=	10.00		
15	Ave final concentration (g/m^3)	0.00	<=	10.00	<=	10.00
16						
17	**Design Dependent Parameters**					
18	Funnel depth (m)			6.50		
19	Side wall length (m)			1.28		
20	Gate depth (m)			6.00		
21	Gate length at centre (m)			1.28		
22	Reactive material volume (m^3)			70.199		
23	Non-reactive material volume (m^3)			0.000		
24						
25	**Objective: MIN PRB Cost =**	**$14,039.05**				Formula

Fig. 6.3. Screen shot of optimal solution for hypothetical example.

The next step in the design process is to run the chosen design through Visual MODFLOW to verify the accuracy of the functional approximations. As the chosen Visual MODFLOW grid size was only 0.25m by 0.25m in the vicinity of the PRB, gate width and length measurements of the chosen design were adjusted to the nearest 0.25m. Table 6.4.7 shows that the capture and residence of the adjusted GRG solution are almost identical to that produced by the equivalent Visual MODFLOW model.

The optimal (non-adjusted) design can now be presented to the decision-maker with a recommendation to proceed to pilot-scale installation. This involves installing a scaled down design in actual site conditions as a final check before full-scale installation (see Section 2.5). Pilot-scale installations are an excellent way to check the validity of a PRB design, as computer models are only an approximation of reality. Lessons learned from monitoring the performance of a pilot-scale installation may result in design amendments to the full-scale installation.

Table 6.4.7
Hypothetical Example Solution Verification

	Optimal PRB	Adjusted PRB	Visual MODFLOW	Units
Min PRB cost	14056.46	13768.13	13768.13	$
W_F	0.00	0.00	0.00	m
W_G	9.98	10.00	10.00	m
L_G	1.28	1.25	1.25	m
RM_{prop}	1.00	1.00	1.00	
CL_G	1.28	1.25	1.25	m
Capture	10.0	10.0	10.0	m
Res_{Centre}	15.0	14.7	14.7	d
Res_{Edge}	15.0	14.7	14.6	d

6.5 Summary

This chapter documents the development and testing of a new optimal design methodology for PRB systems. The proposed methodology includes simplified economic, hydraulic and geochemical aspects of the remediation situation and needs to be verified with site-specific computer modelling and pilot-scale testing before full-scale construction begins.

Section 6.2 presented the assumptions chosen to enable the development of a solvable form of this methodology. Relaxation of the assumptions is covered in Chapter 8. Section 6.2 also detailed PRB design definitions, the form of the objective function and model constraints. Section 6.3 covered the PRB design relationships and calculations, some of which were previously introduced in Chapter 5.

The performance of the GRG2, LGO and Evolver solvers were compared in Section 6.4.1 for a variety of example PRB design problems. Excel's standard GRG2 solver run from six carefully chosen starting points was chosen as the most practical option for the proposed PRB design methodology.

Application of this methodology was described in Section 6.4.2 via a hypothetical example situation. All necessary input information was detailed, and optimal designs from six starting points determined. The overall minimum cost design was adjusted to fit the chosen Visual MODFLOW grid spacing and then compared with the equivalent Visual MODFLOW model. This was to check the accuracy of the functional approximations between the design variables developed in Chapter 5. Accuracy of the functional approximations was very good for the chosen example. However, an accurate minimum cost solution is of little use if significant variability present in input data has not been considered in the design process. This situation will be discussed in the following chapter.

Chapter Seven

Optimisation Issues

7.1 Introduction

Chapter 5 presented functional approximations to relate PRB design variables with hydraulic performance. Chapter 6 set out an optimisation methodology for a defined subset of PRB designs and applied it to a hypothetical example. In this chapter, practical methods will be presented for dealing with uncertainty and variability in input data and examining the sensitivity of designs to small changes in design variables or constraint bounds.

7.2 Uncertainty and Variability in Input Data

Significant variation is expected in inputs to PRB design, particularly in aquifer characteristics (e.g. depth, porosity, hydraulic gradient and conductivity) and plume characteristics (width, depth and concentration distribution). Not all of this variation is quantifiable without significant expenditure. Uncertainty and variability are also expected in reactive material characteristics (e.g. bulk density, minimum required for contaminant degradation, regular proportion lost to flushing, substrate proportion in reactive material and available proportion after initial losses). Seasonal effects may also cause significant variation, particularly with respect to water table fluctuations and temperature effects on degradation rate.

The effects on optimal PRB designs of well characterised variability can be quantified by scenario analysis. Worst, average and best-case scenarios can be solved and analysed. The presence of multiple locally optimal designs in Section 6.4 suggests that different scenarios can produce significantly different optimal designs. The effects of less characterised variability (uncertainty) require more careful analysis. Factorial experimental designs are

proposed for uncertainty analysis as they allow a large number of factors (design inputs) to be examined in a statistically robust fashion without an excessive number of experimental runs.

7.2.1 Scenario Analysis

Scenario analysis involves finding the optimal PRB design for multiple sets of model inputs (scenarios). The first step in scenario analysis involves estimating the expected variability for each input variable of concern. Input scenarios for worst, average (base) and best cases (and more if desired) can then be determined with an estimate of probability of occurrence. A worst-case scenario could include a high estimate (say 2 standard deviations above the average) for expected flow rate combined with low estimate for expected degradation rate (e.g. high aquifer hydraulic conductivity and gradient, low aquifer porosity and contaminant degradation rate). The base-case scenario would then include average expected flow rate combined with average expected degradation rate, and the best-case scenario would include a low estimate for expected flow rate combined with a high estimate for expected degradation rate.

The optimal designs produced for each scenario would then be compared according to cost, design specifics and probability of occurrence. If the worst-case scenario was expected to have a reasonable probability of occurrence and the implications of not achieving the regulatory down-gradient contamination limit were serious enough, then adoption of the worst-case optimal design would be likely. However, if this design was significantly more expensive than the next best-case optimal design and its probability of occurrence and implications of incomplete remediation were not considered serious enough, then another design could be chosen or more scenarios run until the decision-maker was comfortable with the balance between cost and risk minimisation.

Table 7.2.1 presents a set of hypothetical user inputs employed for the scenario analysis. For this situation it was assumed that only three user inputs were likely to change significantly between scenarios. Probability of occurrence could also be estimated for each scenario.

Table 7.2.1 Scenario Analysis Inputs				
Name	**Worst**	**Base**	**Best**	**Units**
K_{Aq}	10.00	5.00	1.00	$m\ d^{-1}$
$Grad_{Aq}$	0.015	0.0125	0.010	$m\ m^{-1}$
$Initial_{Cont}$	105.00	87.50	70.00	$g\ m^{-3}$

7.2.1.1 NZ$40/m^3 reactive material scenario analysis example

The process described in Section 6.4.2 for the hypothetical example was followed for each scenario. Minimum cost solutions are presented in Table 7.2.2 and scenario analysis in Figure 7.1 (which also includes input information from Table 7.2.1). The initial feasible combinations of reactive material proportion and funnel width used in Section 6.4.2 were not always feasible for the chosen scenarios so different initial combinations were chosen. The same minimum cost solution was reached from all starting points for each scenario so we can be very confident that the solutions are globally optimal.

Table 7.2.2 $40/m^3 Reactive Material: Minimum Cost Solutions				
	Worst Case	**Base Case**	**Best Case**	**Units**
Min PRB cost	77,641	17,500	7,298	$
W_F	0.00	0.00	0.00	m
W_G	10.11	10.00	9.11	m
L_G	7.86	1.63	0.75	m
RM_{Prop}	0.54	0.90	0.54	
CL_G	7.73	1.64	0.55	m

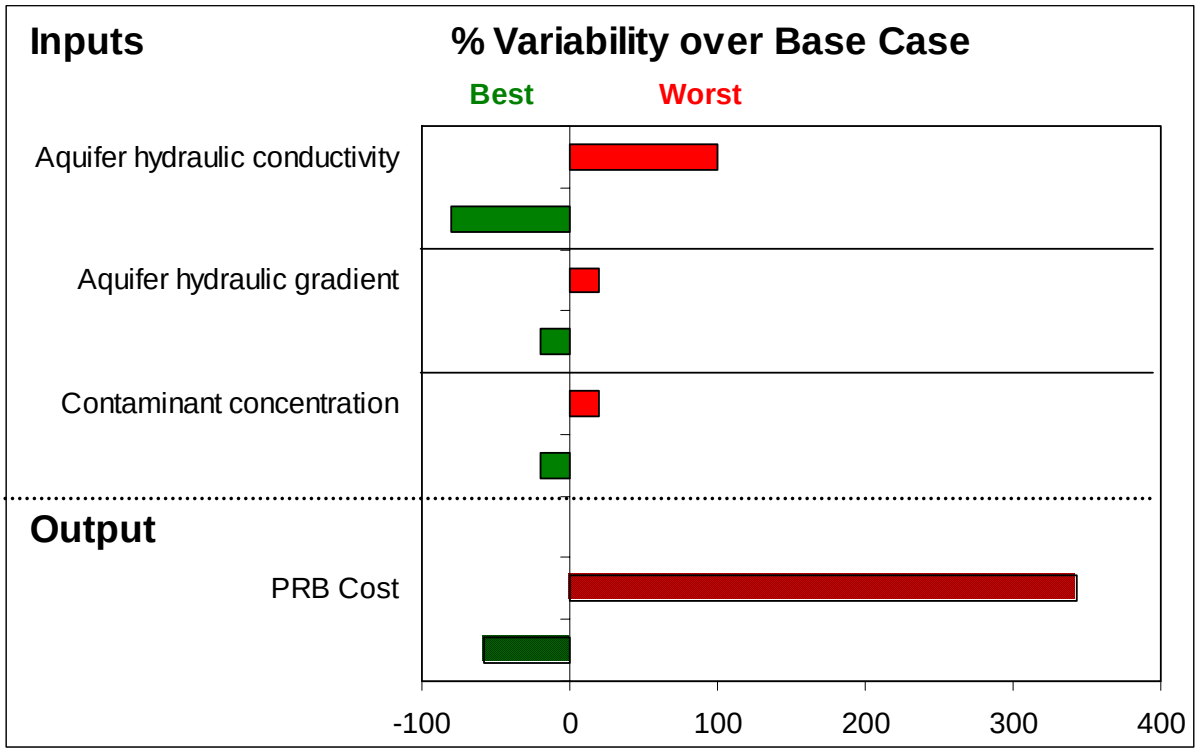

Fig. 7.1. $40/m^3 reactive material scenario analysis.

Table 7.2.2 shows a significant difference in optimal design cost between the three scenarios. This difference is quantified in Figure 7.1 with the best-case scenario showing ~60% reduction in PRB cost over the base-case and the worst-case scenario showing ~340% increase in PRB cost over the base-case. This difference is caused primarily by a difference in flow-through length, although the different reactive material proportions will also have some effect. Different flow-through lengths were expected, as the scenario inputs relate to contaminant velocity and concentration which affect required residence time and therefore gate length. Reactive material proportion affects degradation rate and gate/aquifer hydraulic conductivity ratio, which also affects residence time and therefore gate length. Gate width only reduces slightly from worst to best-case scenarios as required capture width has not changed. Up-gradient funnels are not a part of any globally optimal solutions. This is also expected, as the cost of reactive material relative to funnel material is low for this example.

Once each scenario solution has been verified by a Visual MODFLOW model, the task of the decision-maker is to determine whether to proceed with a pilot study of one (or more) designs or undertake further site characterisation to more accurately quantify variability in the chosen input parameters. Acceptance of the current worst-case scenario without further analysis

would require a high level of confidence in scenario accuracy and a high probability of occurrence of the worst-case conditions.

7.2.1.2 NZ$4000/m^3 reactive material scenario analysis example

The process described in Section 7.2.1.1 for the $40/m^3 reactive material was repeated for $4000/m^3 reactive material (and $5/m^3 non-reactive material). These costs were chosen to investigate the effect of high-cost reactive materials such as zero-valent iron on optimal PRB design. All other inputs were identical to the previous example. The initial feasible starting points used in Section 6.4.2 required adjustment to fit hydraulic conductivity ratio bounds as in the previous example. Minimum cost solutions are presented in Table 7.2.3 and scenario analysis in Figure 7.2 (which also includes input information from Table 7.2.1). This time a variety of minimum cost solutions were reached from the different starting points for each scenario. We must therefore be less confident than the previous example that the solutions are globally optimal. More starting points could be chosen to increase confidence but this is not considered necessary for the chosen example as the chosen starting points produced good coverage of the feasible region.

Table 7.2.3
$4000/m^3 Reactive Material: Minimum Cost Solutions

	Worst Case	Base Case	Best Case	Units
Min PRB cost	1,179,695	362,924	82,507	$
W_F	0.00	13.30	14.53	m
W_G	6.41	3.48	3.33	m
L_G	12.83	6.95	0.76	m
RM_{Prop}	0.19	0.19	0.73	
CL_G	12.12	6.54	0.35	m

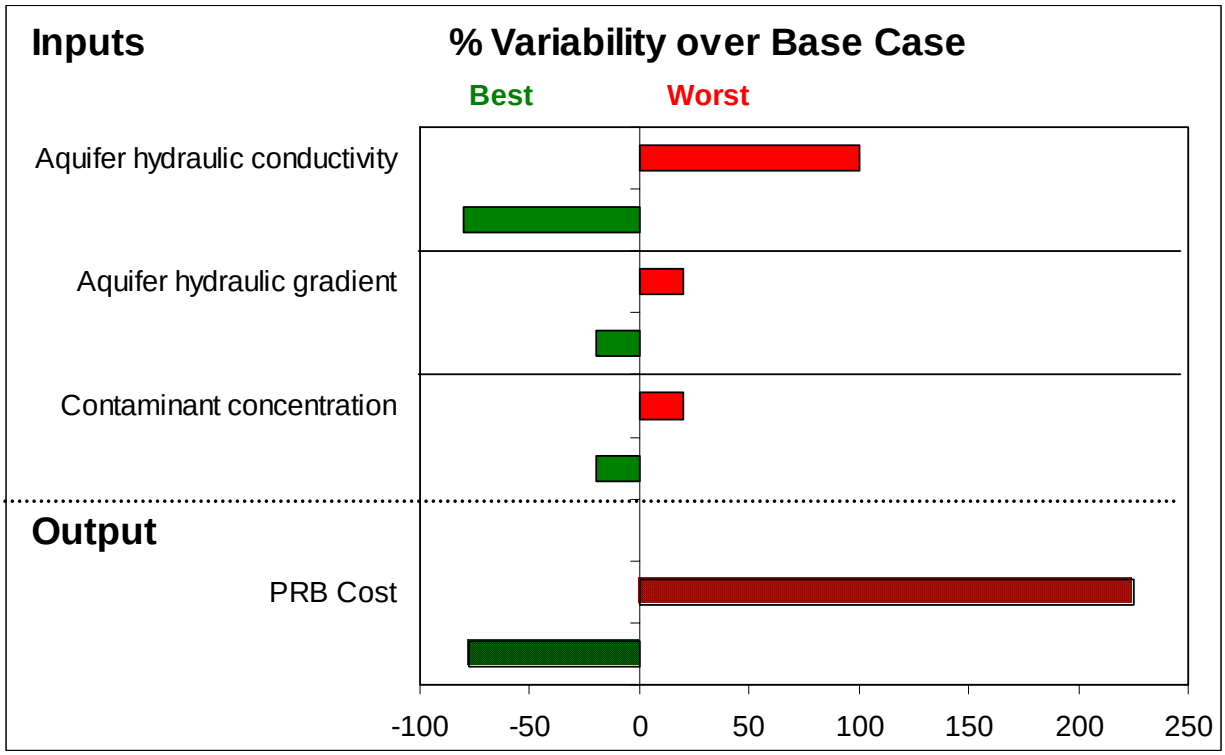

Fig. 7.2. $4000/m^3 reactive material scenario analysis.

Table 7.2.3 shows a significant difference in optimal design cost between the three scenarios. This difference is quantified in Figure 7.2 with the best-case scenario showing ~80% reduction in PRB cost over the base-case and the worst-case scenario showing ~225% increase in PRB cost over the base-case. Flow-through length has a significant effect on cost differences as in the previous example, although most other design variables also have an important effect this time.

Up-gradient funnels are a part of the base and best-case minimum cost solutions this time as the cost of reactive material relative to funnel material is much higher for this example. The worst-case design, however, utilises a much wider gate than the base-case but no funnels. Two other locally optimal solutions utilising 6m and 20m funnels were identified for the worst-case scenario, but they were 5% and 33% more expensive respectively than the minimum cost solution. The reactive material-to-funnel cost ratio is not high enough to make funnel inclusion more economic than a wider gate for all scenarios.

Table 7.2.3 also shows that reactive material proportion is the same for the base and worst-case scenarios, but significantly different for the best-case. A reactive material proportion less than 0.66 was not identified for any of the locally optimal best-case solutions.

Interpolation is not possible between scenarios for this example due to the different types of minimum cost designs. Further analysis would be recommended to the decision-maker for this situation due to the high cost of designs, significant difference between designs and the different types of minimum cost designs found. Design verification by Visual MODFLOW modelling would still be undertaken for the three minimum cost designs but pilot studies would not be recommended until further analysis was completed.

7.2.1.3 Discussion

Scenario analysis is considered a promising technique for including input variability into PRB design optimisation. It is not difficult or time-consuming but requires high quality information on input variability and scenario probabilities. One of the main advantages scenario analysis presents over standard one-way analysis of user inputs is that it can incorporate non-linear effects and interactions between chosen inputs.

If the decision-maker is confident about the inputs and outputs of the scenario analysis, then chosen scenario solutions are verified by Visual MODFLOW models and one (or more) designs chosen for a pilot study (taking into account the probability of occurrence of each scenario). Where there is a large difference in dollar terms between minimum cost solutions for each scenario, extra analysis could be considered if one of the modelled scenarios did not emerge as a clear preference. This could include careful checking of input data accuracy, scenario probability and the risk of under-design. It could also include detailed analysis of other locally optimal solutions close in cost to the minimum cost solution in case they have alternative benefits to offer the decision-maker. Development of new scenarios could also be undertaken, but interpolating between scenarios is not recommended without confirmation through the optimisation process.

The main weakness of scenario analysis is that the effects of all input variables under investigation are lumped together. It may be that only one or two of the variables are causing all the effect. Further allocation of time and money would be best directed toward improving characterisation and reducing uncertainty of these variables, identification of which requires a technique such as factorial analysis.

7.2.2 Factorial Experimental Designs

Factorial designs allow a large number of factors (independent variables) to be examined in a statistically robust fashion without an excessive number of experimental runs (*Box et al.*, 1978). Factors can be continuous or discrete. Experiments are performed to (1) screen a set of factors to learn which produce an effect, and (2) estimate the magnitude of the main effect of each factor and of the interactions between factors. All main effects and interactions can be estimated independently by choosing orthogonal experimental designs where the factor settings are completely uncorrelated with each other.

Factorial designs are identified by the number of factors and number of levels each factor is set to. A three-factor two-level design would involve low and high values for three PRB design input variables and require 2^3 ($level^{factor}$) = 8 experiments for a full factorial (saturated) design. The low and high values could be minimum and maximum expected values or a specified number of standard deviations either side of a (known) distribution mean.

As the number of experiments grows exponentially with the number of factors in two-level fully saturated designs, it may become uneconomic to investigate a large number of factors at once in this way. Fractional factorial designs may be more efficient in these circumstances. They involve adding extra factors to a fully saturated design without increasing the number of experiments. The effects of certain interactions between factors are combined in these designs, but any combined effect of interest can later be separated out by running further experiments.

Two-level fractional factorial designs are labelled 2^{k-p}, where k is the number of factors that could be evaluated in a full factorial design of size 2^k and p is the number of additional factors to be included. For example, when a fourth factor is incorporated into a 2^3 design of 8 runs, the resulting design is labelled a 2^{4-1} fractional factorial. Only half of the original 16 ($=2^4$) runs are required but the downside is that the main effect of each factor is combined with the three-factor interaction of the other factors. All two-factor interactions are also combined; for example the factor 1&2 interaction is combined with the factor 3&4 interaction. Higher-order fractional factorial designs (e.g. 2^{8-4}) result in more complex combinations of effects, which need to be considered when analysing the results.

The factor levels for each experiment are determined by the *design matrix*. The design matrix for a full three-factor two-level design is presented in Table 7.2.4. The low level for each factor is signified by a minus sign and the high level by a plus sign. It is important that the run order does not cause unknown or uncontrolled changes in experimental conditions that might bias the results. The optimal design methodology described in Section 6.4 negates any possible run order effects by using multiple starting positions for each design optimisation.

Table 7.2.4
Design Matrix for Full 2^3 Factorial Design

Run Number	Factor		
	X_1	X_2	X_3
1	-	-	-
2	+	-	-
3	-	+	-
4	+	+	-
5	-	-	+
6	+	-	+
7	-	+	+
8	+	+	+

All effects are estimated using a *model matrix*. The model matrix for a full three-factor two-level design is presented in Table 7.2.5. This model matrix consists of a column vector for the average (X_0), a column vector for each main effect (X_1, X_2, and X_3), a column vector for each interaction effect (X_1X_2,…,$X_1X_2X_3$), and a column vector of the minimum PRB cost (y). Interactions are represented in the matrix by cross-products, for example the elements in X_1X_2 are the products of X_1 and X_2. Statistically independent quantities are calculated by multiplying the y vector by each of the X vectors. The average response of the whole experiment is calculated from (X_0 . y)/8 as there are 8 runs. The main and interaction effects are calculated from the appropriate (X_i . y)/4 as they are the average of the four differences between the y's at their +1 level and the y's at their –1 level.

Table 7.2.5
Model Matrix for Full 2^3 Factorial Design

Run	X_0	X_1	X_2	X_3	X_1X_2	X_1X_3	X_2X_3	$X_1X_2X_3$	y
1	+1	-1	-1	-1	+1	+1	+1	-1	y_1
2	+1	+1	-1	-1	-1	-1	+1	+1	y_2
3	+1	-1	+1	-1	-1	+1	-1	+1	y_3
4	+1	+1	+1	-1	+1	-1	-1	-1	y_4
5	+1	-1	-1	+1	+1	-1	-1	+1	y_5
6	+1	+1	-1	+1	-1	+1	-1	-1	y_6
7	+1	-1	+1	+1	-1	-1	+1	-1	y_7
8	+1	+1	+1	+1	+1	+1	+1	+1	y_8

Factorial analysis on the minimum cost designs produced for each designated run consists of estimating the magnitude of the main effect of each factor and its interactions with other factors. Factorial analysis can also be used to estimate the statistical significance of all effects when random measurement or experimental errors are present (see *Berthouex and Brown*, 2002). The main effect of a factor measures the average change in PRB cost caused by changing the factor from a low to a high setting. An interaction between two or more factors measures the average change in PRB cost caused by changing the factors in combination. To gather the same information via scenario analysis would require one-way analysis of each user input and separate scenario analysis for each combination of user inputs.

The average change in minimum PRB cost over all experiments provides a general indication of how significant input variation is to the design problem at hand. Main effects and interactions are ordered for presentation to the decision-maker. The ranked order can be used to prioritise further analysis or characterisation and the magnitude of each effect provides the financial incentive to do this work. Further analysis could include field, laboratory or computer modelling experiments to determine the likelihood and regularity of the factor attaining specified levels.

7.2.2.1 NZ$40/m^3 reactive material full 2^3 factorial design example

The first step in a factorial design is to determine the factors and their bounds. For this example the same three factors analysed in the scenario analysis (Section 7.2.1) will be used. For the sake of comparison the lower and upper levels for each factor will be the best and worst-case scenario values respectively in Table 7.2.1. It is important that these levels cover

reasonable expected variation (e.g. two standard deviations either side of the mean) as opposed to extreme events. All design inputs are shown in Table 7.2.6.

Table 7.2.6
$40/m^3 Reactive Material: Full 2^3 Factorial Design Input

Identity	Factor	Lower	Upper	Units
X_1	$Grad_{Aq}$	0.010	0.015	m m^{-1}
X_2	$Initial_{Cont}$	70.0	105.0	g m^{-3}
X_3	K_{Aq}	1.000	10.000	m d^{-1}

The second step is to find the minimum cost solutions to the 2^3=8 runs detailed in Table 7.2.4. For example, the first run sets all input factors to their lower bound (equivalent to the best-case scenario in Section 7.2.1). The second run sets factor 1 to its upper bound and factors 2 and 3 to their lower bound. The eight runs cover every possible combination of the factors at their upper and lower bounds. Table 7.2.7 presents the minimum cost solutions reached for each run from six feasible starting points.

Table 7.2.7
$40/m^3 Reactive Material: Model Output for Full 2^3 Factorial Design

Run	MIN Cost	W_F	W_G	L_G	RM_{Prop}	CL_G
1	$7,298	0.00	9.11	0.75	0.54	0.55
2	$7,347	0.00	9.11	0.75	0.54	0.55
3	$7,347	0.00	9.11	0.75	0.54	0.55
4	$7,549	0.00	9.11	0.75	0.78	0.57
5	$32,963	0.00	10.05	3.29	0.54	3.23
6	$49,368	0.00	10.08	4.98	0.54	4.86
7	$52,076	0.00	10.08	5.26	0.54	5.14
8	$77,641	0.00	10.11	7.86	0.54	7.73

Table 7.2.7 shows that the same minimum cost solutions were found for the first three runs (when the design variables were rounded to 2 d.p.). This is because a flow-through length less than the modelled lower bound of 0.75m was required for each input combination. No minimum cost solution for this example employs funnels (due to the relatively cheap reactive

material) but variation occurs in all other design variables. Cost increases between experiments are primarily due to flow-through length increases (as in the scenario analysis). Minimum design cost for each run varies from $7,298 to $77,641 with an average design cost of $30,199.

The third step in a factorial design experiment involves calculating all main and interaction effects as described in Section 7.2.2 and Table 7.2.5. For example, the factor 1 ($Grad_{Aq}$) main effect is calculated by subtracting the average minimum cost of all solutions with factor 1 at its lower level (runs 1,3,5 and 7) from the average minimum cost of all solutions with factor 1 at its upper level (runs 2,4,6 and 8) as follows:

$$\mathbf{X_1 = \left(\frac{7347 + 7549 + 49368 + 77641}{4}\right) - \left(\frac{7298 + 7347 + 32963 + 52076}{4}\right)} \qquad \mathbf{7.2.1}$$

$$\mathbf{= 10555}$$

This process is repeated for factors 2 and 3. Two-factor interactions are calculated by subtracting the average minimum cost of all solutions where the two factors are different (i.e. one factor at its upper level and the other factor at its lower level) from the average minimum cost of all solutions where the two factors are the same. In the appropriate column of Table 7.2.5 this is shown by a –1 or +1 for each run, where this number is the product of the numbers in the individual columns. For example, the interactions between factors 1 and 2 can be found in the column labelled X_1X_2, where each entry for X_1X_2 is the product of the X_1 and X_2 entries for the same row. This column has +1 for runs 1, 4, 5 and 8 and -1 for the other runs. The effect is calculated as follows:

$$\mathbf{X_1X_2 = \left(\frac{7298 + 7549 + 32963 + 77641}{4}\right) - \left(\frac{7347 + 7347 + 49368 + 52076}{4}\right)} \qquad \mathbf{7.2.2}$$

$$\mathbf{= 2328}$$

This process is repeated for the two other two-factor interactions and the three-factor interaction. The only difference for the three-factor interaction is that its entries in Table 7.2.5 are the product of three individual entries. This means a +1 will occur when all factors are at their upper level or two are at their lower level (-1) and one is at its upper level (+1).

Ordered effects are presented in Table 7.2.8. Increasing factor 3 (aquifer hydraulic conductivity) from its low to high level causes minimum PRB cost to increase by $45,627. This is a much greater effect than any other factor or factor combination. The two factor interactions involving factor 3 are also significantly larger than the factor 1 and 2 interaction, most likely due to the effect of factor three. No further analysis is considered necessary as individual effects are always greater than the interactions they are likely to be a major contributor to.

Table 7.2.8
$40/m^3 Reactive Material: Ordered Effects

Order	Identity	Effect
1	$X_1X_2X_3$	$2,252
2	X_1X_2	$2,328
3	X_1X_3	$10,430
4	X_1	$10,555
5	X_2X_3	$11,783
6	X_2	$11,909
7	X_3	$45,627

Figure 7.3 presents the input variability for each factor (user input) and their proportional effects on PRB cost. The conclusion of this factorial analysis is that aquifer hydraulic conductivity is the primary contributor to PRB cost increases. Potential cost increases caused by variability in aquifer hydraulic conductivity are likely to be great enough to justify further characterisation and analysis. The aim of further characterisation and analysis is to quantify the most appropriate level of aquifer hydraulic conductivity as a design input given the costs and risks associated with under or over-design.

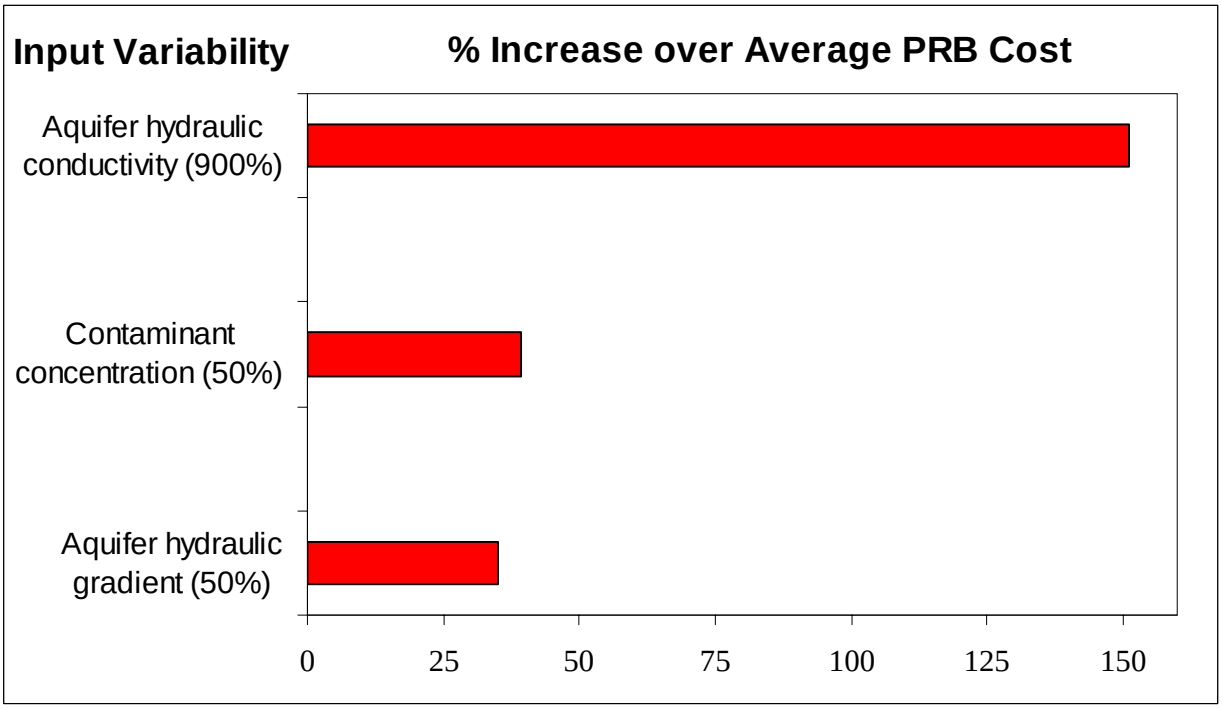

Fig. 7.3. \$40/m^3 reactive material factorial analysis.

7.2.2.2 NZ\$4000/m^3 reactive material fractional factorial analysis example

To illustrate fractional factorial analysis, the 2^3 design presented in Table 7.2.6 was expanded to a 2^{8-4} design by adding five new factors (plume width, regular proportion of substrate lost through flushing, available proportion of substrate after initial losses, substrate proportion in reactive material and substrate bulk density). All factors and their chosen bounds are presented in Table 7.2.9.

Table 7.2.9
\$4000/m^3 Reactive Material: 2^{8-4} Fractional Factorial Design Input

Identity	Factor	Lower	Upper	Units
X_1	K_{Aq}	1.000	10.000	m d^{-1}
X_2	$Grad_{Aq}$	0.010	0.015	m m^{-1}
X_3	$Initial_{Cont}$	70.00	105.00	g m^{-3}
X_4	W_{Pl}	8.00	12.00	m
X_5	$BulkDen_{Sub}$	1000000	1500000	g m^{-3}
X_6	$Lost_{Sub}$	0.08%	0.12%	d^{-1}
X_7	$Avail_{Sub}$	40.00%	60.00%	
X_8	$Prop_{Sub}$	40.00%	60.00%	

Factorial analysis with eight factors enables an in-depth analysis of uncertainty and variability in the chosen system but a full design would require 2^8 = 256 runs (with at least six optimisations from different starting points per run). By expanding a 2^4 full factorial design out to the 2^{8-4} design presented in Table 7.2.10 we are able to analyse the eight factors in only 2^4 = 16 runs. The first step in creating the chosen 2^{8-4} design matrix is to expand a 2^3 design out to a 2^4 design. This is achieved by copying the 2^3 design matrix presented in Table 7.2.4 to the first 3 columns and 8 rows of Table 7.2.10. A column of + signs is added (column 8) and then rows 9-16 are created by reversing the signs of rows 1-8 respectively.

Table 7.2.10
Design Matrix for 2^{8-4} Fractional Factorial Design

Run Number	Factor							
	X_1	X_2	X_3	X_4	X_5	X_6	X_7	X_8
1	-	-	-	+	+	+	-	+
2	+	-	-	-	-	+	+	+
3	-	+	-	-	+	-	+	+
4	+	+	-	+	-	-	-	+
5	-	-	+	+	-	-	+	+
6	+	-	+	-	+	-	-	+
7	-	+	+	-	-	+	-	+
8	+	+	+	+	+	+	+	+
9	+	+	+	-	-	-	+	-
10	-	+	+	+	+	-	-	-
11	+	-	+	+	-	+	-	-
12	-	-	+	-	+	+	+	-
13	+	+	-	-	+	+	-	-
14	-	+	-	+	-	+	+	-
15	+	-	-	+	+	-	+	-
16	-	-	-	-	-	-	-	-

The second step in creating the chosen 2^{8-4} design matrix involves creating columns X_4 to X_7 from the new 2^4 design matrix. Column X_4 in Table 7.2.10 is created by multiplying columns X_1, X_2 and X_8; column X_5 is created by multiplying columns X_1, X_3 and X_8; column X_6 is created by multiplying columns X_2, X_3 and X_8; and column X_7 is created by multiplying

columns X_1, X_2 and X_3. The resulting design matrix combines the main effects of each factor with three three-factor interactions and combines two-factor interactions in groups of four. The model matrix is too large to include here and analysis will only focus on main and two-factor effects. Main effects are still useful provided the three-factor effects are negligible. If any two-factor interaction combinations prove to be significant it may be necessary to conduct further runs to isolate out the individual effects.

The minimum cost design for each run was found from six feasible starting points as in Section 7.2.2.1. Minimum cost design details are presented in Table 7.2.11. The design cost range is \$80,231 to \$1,409,200 with an average of \$520,545. Significant variation is present in all design variables for this example. Comparison with the \$4000/m^3 reactive material scenario analysis in Section 7.2.1.2 is not appropriate due to the increase in factors being analysed.

Table 7.2.11
\$4000/m^3 Reactive Material: Model Output for 2^{8-4} Fractional Factorial Design

Run	MIN Cost	W_F	W_G	L_G	RM_{Prop}	CL_G
1	\$121,866	16.20	4.40	0.75	0.76	0.30
2	\$437,100	10.47	3.45	6.90	0.20	6.25
3	\$83,786	11.05	3.00	0.75	0.93	0.40
4	\$974,833	0.00	9.75	5.90	0.25	4.90
5	\$134,031	17.98	3.00	1.51	0.62	0.84
6	\$606,251	0.00	5.17	9.15	0.18	8.61
7	\$171,722	10.32	3.00	1.43	0.69	0.84
8	\$1,385,465	8.56	6.71	13.42	0.20	12.73
9	\$1,162,626	0.00	6.00	10.50	0.25	9.92
10	\$179,830	20.98	3.00	1.38	0.96	0.89
11	\$1,409,200	25.17	3.69	7.39	0.60	6.51
12	\$110,298	11.37	3.00	0.75	0.95	0.42
13	\$812,765	5.53	4.42	8.84	0.20	8.15
14	\$163,223	18.06	3.00	1.44	0.62	0.79
15	\$495,497	19.78	3.85	7.58	0.23	6.64
16	\$80,231	10.38	3.00	0.75	0.62	0.36

Ordered effects are presented in Table 7.2.12 with interactions greater than two factors assumed negligible. Increasing factor 1 (aquifer hydraulic conductivity) from its low to high level causes minimum PRB cost to increase by $779,844. As with the previous example this is a much greater effect than any other factor or factor combination. The two-factor interaction combination involving factors 1 and 3 (the largest individual effects) is also larger than most individual effects, but isn't expected to warrant further attention as it is smaller than the main effects of factors 1 and 3.

Table 7.2.12
$4000/m^3 Reactive Material: Ordered Effects

Order	Identity	Effect
1	X_5	-$92,151
2	$X_1X_5+X_2X_6+X_3X_8+X_4X_7$	-$78,795
3	X_8	-$62,327
4	$X_1X_8+X_2X_4+X_3X_5+X_6X_7$	-$56,783
5	X_7	-$48,084
6	$X_1X_7+X_2X_3+X_6X_8+X_4X_5$	-$32,506
7	$X_1X_6+X_2X_5+X_3X_4+X_7X_8$	$89,511
8	X_6	$111,819
9	$X_1X_4+X_2X_8+X_3X_6+X_5X_7$	$136,667
10	$X_1X_2+X_3X_7+X_4X_8+X_5X_6$	$154,438
11	X_4	$174,896
12	X_2	$192,472
13	$X_1X_3+X_2X_7+X_4X_6+X_5X_8$	$212,071
14	X_3	$248,765
15	X_1	$779,844

Figure 7.4 presents the input variability for each factor (user input) and their proportional effects on PRB cost. The conclusion of this factorial analysis is that aquifer hydraulic conductivity is the primary contributor to PRB cost increases. Potential cost increases caused by variability in aquifer hydraulic conductivity are expected to be great enough to justify further characterisation and analysis. At the other end of the scale, three of the substrate

inputs produce moderate decrease in PRB cost when moved from their low to high levels as this increases degradation rate for the chosen model.

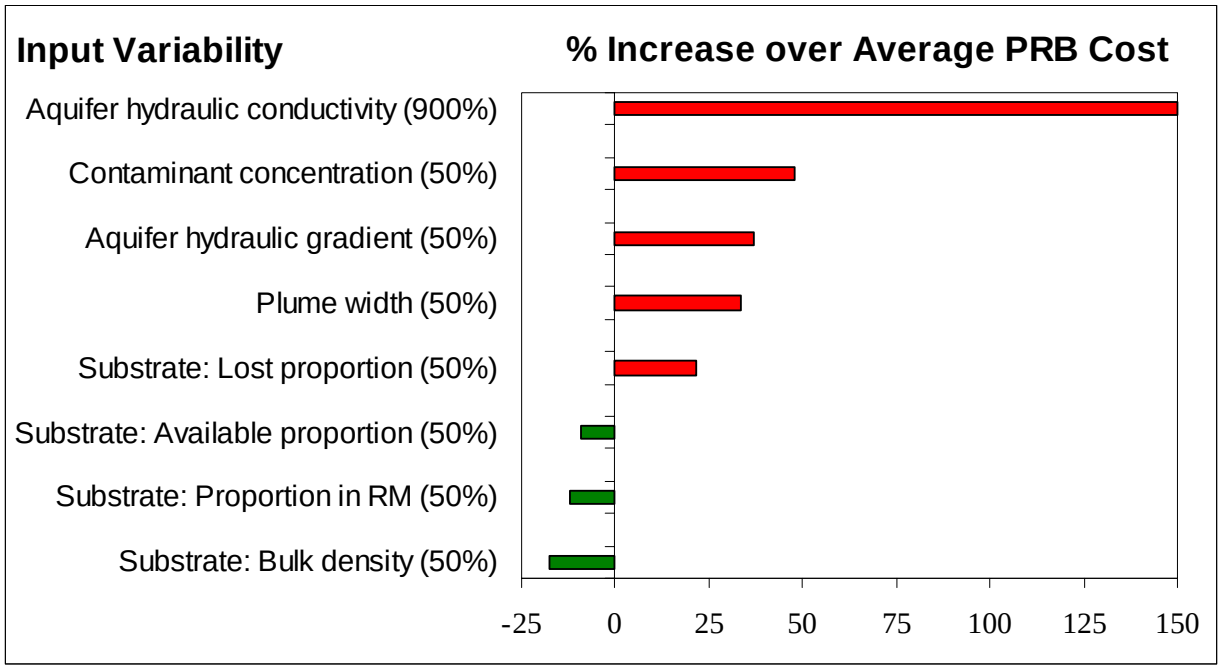

Fig 7.4. $4000/m^3 reactive material factorial analysis.

7.2.2.3 Discussion

Factorial analysis and fractional factorial analysis have been shown to produce the effect of each factor (user input) on minimum PRB cost when moved from a lower to upper level. These levels covered reasonable expected variation (e.g. two standard deviations either side of the mean) as opposed to extreme values. This information is proposed to be more useful to decision-makers than scenario analysis as it enables them to target their resources to the input factors most worthy of further analysis or characterisation. Modelling and analysis time to acquire this information is not great, especially when fractional factorial analysis is utilised.

Fractional factorial analysis was found to allow customised analysis of many user inputs in an efficient manner, provided higher order interactions can be assumed insignificant. Analysis of interaction effects involved checking that individual effects were greater than the interactions they were likely to be a major contributor to. Significant interaction effects larger than a contributing individual effect would suggest that future analysis should involve the factors in combination as well as independently.

7.3 Sensitivity of Optimal PRB Designs

Sensitivity analysis of optimal PRB designs is provided by the standard Excel solver for each decision variable and constraint. The reduced gradient value output for each decision variable shows the amount by which the total design cost would increase if an extra unit of the variable were added to the optimal design solution. This information is useful when the decision-maker wishes to adjust a chosen PRB design, for example by removing a small amount of up-gradient funnel. The Lagrange multiplier output produces the same information for the upper bound of constraints. This informs the decision-maker whether any constraint bounds are having a significant impact on the chosen PRB design. For example, if the chosen design is at the upper bound of a modelling constraint then a large negative Lagrange multiplier suggests it may be economic to conduct more computer modelling experiments so the constraint can be relaxed.

Of course any new design would need to meet all constraints, and speculation beyond a few units is not expected to be accurate as sensitivity values are linear approximations to non-linear functions. Manually adjusting a constraint bound or fixing a decision variable (through its bounds) and re-solving is recommended for accurate sensitivity analysis. Manual and automated sensitivity analysis will be compared in the following sections for the worst-case scenario examples presented in Sections 7.2.1.1 and 7.2.1.2.

7.3.1 NZ$40/m^3 Reactive Material Sensitivity Analysis Example

Tables 7.3.1 and 7.3.2 present the reduced gradient and Lagrange multiplier output for the decision variables and constraints respectively from the worst-case minimum cost design presented in Section 7.2.1.1. The objective function value (cost) of this design was $77,641.

The only non-zero reduced gradient value in Table 7.3.1 is for W_F (funnel width). This is because W_F is the only zero-valued decision variable in the chosen optimal design. If 1m of funnel width was forced into the optimal design (and current gradients can be extrapolated), the reduced gradient value suggests that the minimum PRB cost would increase by $1533.

Table 7.3.1
$40/m^3 Reactive Material
Sensivity Analysis: Decision Variables

Variable	Units	Optimal Value	Reduced Gradient
W_F	m	0.00	1533.24
W_G	m	10.11	0.00
L_G	m	7.86	0.00
RM_{Prop}		0.54	0.00

In order to test whether current gradients can be extrapolated, W_F is constrained to be equal to 1.0m and the problem re-solved using multiple starting points (manual sensitivity analysis). The optimal minimum cost solution was \$79,106 (W_F = 1.0, W_G = 9.9, L_G = 8.1, RM_{Prop} = 0.54). This is an increase of \$1465, which is acceptably close to the reduced gradient value. W_F was then constrained to be equal to 10.0m and the problem re-solved. The optimal minimum cost solution was \$87,797 (W_F = 10.0, W_G = 7.9, L_G = 9.6, RM_{Prop} = 0.54). This is an increase of \$10,156, significantly less than the expected increase of \$15,332 (10m * \$1533.24m^{-1}). Extrapolation of current gradients out to this extent is not realistic for funnel width in this example.

Table 7.3.2 shows the effect on minimum cost (the objective function value) when each constraint bound is relaxed. The lower bound on Capture and K_G/K_{Aq}, and the upper bound on $Final_{Cont}$ are binding constraints so have non-zero Lagrange multipliers.

For each extra metre of plume required to be captured, the Lagrange multiplier for Capture shows that \$6297 is expected to be added to the minimum cost design. The actual effect on minimum cost as a result of re-solving the model with increased capture of 1.0m was \$83,907 (W_F = 0.0, W_G = 11.1, L_G = 7.9, RM_{Prop} = 0.54), an increase of \$6266. The actual effect on minimum cost as a result of re-solving the model with increased capture of 7.0m (the maximum increase without exceeding maximum gate width bound) was \$120,082 (W_F = 0.0, W_G = 17.2, L_G = 7.8, RM_{Prop} = 0.54), an increase of \$42,441. This is only 3.7% less than the expected amount of 7m * \$6297m^{-1} = \$44,079. The Lagrange multiplier provides acceptable plume capture sensitivity accuracy for this example.

Table 7.3.2
$40/m^3 Reactive Material
Sensitivity Analysis: Constraints

Variable	Bound	Optimal Value	Lagrange Multiplier
L_G/W_G	>= 0.00	0.78	0.00
L_G/W_G	<= 2.00	0.78	0.00
$(W_F+W_G)/W_G$	>= 0.00	1.00	0.00
$(W_F+W_G)/W_G$	<= 2.00	1.00	0.00
Capture	>= 10.00	10.00	6297.23
$Final_{Cont}$	>= 0.00	10.00	0.00
$Final_{Cont}$	<= 10.00	10.00	-804.69
K_G/K_{Aq}	>= 1	1.00	31125.88
K_G/K_{Aq}	<= 10	1.00	0.00

Next, the upper bound on $Final_{Cont}$ was relaxed by 1.0g m^{-3} and then 10.0 g m^{-3}. The new minimum cost solutions were \$76,836 (W_F = 0.0, W_G = 10.1, L_G = 7.8, RM_{Prop} = 0.54) and \$69,588 (W_F = 0.0, W_G = 10.1, L_G = 7.0, RM_{Prop} = 0.54) respectively. The expected minimum cost solutions based on the Lagrange multiplier were very close at \$76,836 and \$69,594 respectively.

The high value (\$31,126 g/m^3) Lagrange multiplier for K_G/K_{Aq} raises some interesting questions. A lower bound of 1.0 for K_G/K_{Aq} was chosen after the computer modelling in Chapter 4 found that capture width dropped off significantly when $K_G/K_{Aq} < 1$. As the accuracy of extrapolating the functional approximations produced in Chapter 5 cannot be guaranteed, the accuracy of the Lagrange multiplier for $K_G/K_{Aq} < 1$ can also not be guaranteed. However, the magnitude of potential savings could provide the justification for further specific Visual MODFLOW modelling to test the performance of the chosen PRB with $K_G/K_{Aq} < 1$. The hypothetical laboratory tests presented in Table 6.4.3 showed that K_{mix} decreased from 24.0 to 3.5 m/d as reactive material proportion increased from 0 to 100%. With K_{Aq} = 10 for the chosen example, K_G/K_{Aq} will reduce from 1.0 to 0.35 as reactive material proportion is increased from its current optimal level of 54% to 100%. The combination of potential savings suggested by the Lagrange multiplier and leeway in reactive material proportion should provide sufficient justification for further analysis in this hypothetical case.

7.3.2 NZ$4000/m^3 Reactive Material Sensitivity Analysis Example

The same sensitivity analysis performed on the $40/m^3 reactive material worst-case scenario output was repeated for the equivalent $4000/m^3 reactive material example. Tables 7.3.3 and 7.3.4 present the reduced gradient and Lagrange multiplier output for the decision variables and constraints respectively from the worst-case minimum cost design presented in Section 7.2.1.2. The objective function value (cost) of this design was $1,179,695.

Table 7.3.3
$4000/m^3 Reactive Material
Sensivity Analysis: Decision Variables

Variable	Units	Optimal Value	Reduced Gradient
W_F	m	0.00	4406.46
W_G	m	6.41	0.00
L_G	m	12.83	0.00
RM_{Prop}		0.19	0.00

As with the previous example the only non-zero reduced gradient value in Table 7.3.2 is for W_F (funnel width). If 1m of funnel width was forced into the optimal design (and current gradients can be extrapolated), the reduced gradient value suggests that the minimum PRB cost would increase by $4406. W_F was constrained to be equal to 1.0m and the problem re-solved using multiple starting points. The optimal minimum cost solution was $1,183,653 ($W_F$ = 1.0, W_G = 6.3, L_G = 12.7, RM_{Prop} = 0.20). This is an increase of $3958, which is over 10% less than the reduced gradient value. W_F was then constrained to be equal to 10.0m and the problem re-solved. The optimal minimum cost solution was $1,352,478 ($W_F$ = 10.0, W_G = 6.0, L_G = 11.9, RM_{Prop} = 0.25). This is an increase of $172,783, significantly greater than the expected increase of $44,065 (10m * $4406.46m^{-1}). Extrapolation of current gradients even by 1.0m are not accurate for the chosen example.

Lagrange multiplier output in Table 7.3.4 shows three non-zero values, as the final values for L_G/W_G, Capture and $Final_{Cont}$ are all at their upper bounds.

Table 7.3.4
$4000/m^3 Reactive Material
Sensitivity Analysis: Constraints

Variable	Bound	Optimal Value	Lagrange Multiplier
L_G/W_G	>= 0.00	2.00	0.00
L_G/W_G	<= 2.00	2.00	-48333.46
$(W_F+W_G)/W_G$	>= 0.00	1.00	0.00
$(W_F+W_G)/W_G$	<= 2.00	1.00	0.00
Capture	>= 10.00	10.00	103953.28
$Final_{Cont}$	>= 0.00	10.00	0.00
$Final_{Cont}$	<= 10.00	10.00	-14061.80
K_G/K_{Aq}	>= 1	3.05	0.00
K_G/K_{Aq}	<= 10	3.05	0.00

The modelling constraint setting gate length to a maximum of twice the gate width was considered appropriate for most fully penetrating PRB designs. However, the optimal solution is at the upper bound of this constraint as the current hypothetical problem contains a high degradation requirement combined with a relatively narrow plume. The magnitude of the Lagrange multiplier (-$48,333 unit^{-1}) should provide the justification for site-specific Visual MODFLOW modelling to test the performance of increasing the gate length of the optimal PRB design. The spreadsheet optimisation model can then be used to calculate the cost of any new designs. If this issue arose regularly, further Visual MODFLOW modelling could also be undertaken to produce functional approximations that are accurate for L_G/W_G > 2.

The Lagrange multiplier for Capture shows that for each extra metre of plume required to be captured, $103,953 is expected to be added to the minimum cost design. The actual effect on minimum cost as a result of re-solving the model with increased capture of 1.0m was $1,292,206 ($W_F$ = 0.0, W_G = 7.0, L_G = 13.9, RM_{Prop} = 0.18), an increase of $112,511. The actual effect on minimum cost as a result of re-solving the model with increased capture of 10.0m was $1,971,016 ($W_F$ = 27.7, W_G = 7.9, L_G = 15.8, RM_{Prop} = 0.2), an increase of $791,321. This is nearly 25% less than the expected increase of 10*103,953 = $1,039,530 as the optimal solution has jumped to a different type of design containing a wide funnel and narrower gate.

Next, the upper bound on $Final_{Cont}$ was relaxed by 1.0g m^{-3} and then 10.0 g m^{-3}. The new minimum cost solutions were \$1,165,944 (W_F = 0.0, W_G = 6.4, L_G = 12.8, RM_{Prop} = 0.19) and \$1,048,655 (W_F = 0.0, W_G = 6.4, L_G = 12.7, RM_{Prop} = 0.17) respectively. The expected minimum cost solutions based on the Lagrange multiplier were \$1,165,633 and \$1,039,075. The Lagrange multiplier proved to be accurate for both situations in this case.

7.4 Summary

This chapter presented practical methods for dealing with uncertainty and variability in input data and examining the sensitivity of optimal designs to small changes in design variables or constraint bounds. In Section 7.2, scenario analysis was proposed for general analysis of input parameter variability and uncertainty while factorial analysis was proposed for more in-depth analysis. In Section 7.3, manual and automatic sensitivity analysis techniques were compared for their applicability to post-optimal PRB design analysis. Manual sensitivity analysis is recommended as it incorporates any non-linear effects that the model may have on the output.

Scenario analysis involves finding the minimum cost designs for multiple sets of input parameters (scenarios) rather than a single set. The probability of occurrence of each scenario is estimated and all information presented to the decision-maker. Their task is to decide whether to proceed with a pilot-study of an analysed scenario, request the processing of further scenarios or interpolate between scenarios if the design type remains the same. Two hypothetical examples containing NZ\$40/m^3 and NZ\$4000/m^3 reactive material were chosen to illustrate this concept.

Scenario analysis is considered a promising technique for including input variability into PRB design optimisation. It is not difficult or time-consuming but requires high quality information on input variability and scenario probabilities. One of the main advantages scenario analysis presents over standard one-way analysis of user inputs is that it can incorporate non-linear effects and interactions between chosen inputs.

Scenario analysis is especially recommended when high quality input information is available and variation is not expected in many input parameters. Factorial analysis is recommended for most other situations as it separates out the effects of multiple input factors at multiple levels without an excessive number of experimental runs. Computer processing and analysis time is likely to be greater than the equivalent scenario analysis, but the screening of important inputs allows future allocation of time and money to be targeted at improving characterisation and reducing uncertainty of input variation causing the greatest effect. A full factorial design example was presented in Section 7.2.2.1 for three input factors each at two levels (high and low). A fractional factorial design was then presented in Section 7.2.2.2 with a worked example involving eight input factors each at two levels, but only 1/16 of the optimisation runs required for a full 2^8 factorial design.

The sensitivity of optimal PRB designs to changes in decision-variable and constraint bounds was presented in Section 7.3. The most useful aspect of sensitivity analysis for this type of design tool is to identify areas for further investigation, be they the accuracy of input information, limitations of construction techniques, limitations of computer modelling and functional approximations, or model assumption issues. Manually changing decision variable or constraint bounds and re-solving using multiple starting points identifies the potential benefits of this investigation.

Excel generated sensitivity analysis is not recommended for the proposed PRB optimisation as it linearly extrapolates the chosen design. This may often be accurate enough for small changes in decision variable or constraint bounds but accuracy cannot be guaranteed for larger changes due to the non-linear objective function and the potential for the minimum cost solution to change to a different design type. However, the Lagrange multiplier example for K_G/K_{Aq} in Section 7.3.1 showed that Excel's built-in sensitivity analysis may be useful in helping to justify further hydrologic modelling or reactive material analysis. The built-in sensitivity analysis on an optimal design only requires a mouse click so there is no harm in using it as a quick check. Manual sensitivity analysis, however, only takes a few minutes and is proposed for general post-optimisation sensitivity analysis.

The final topic for discussion in this thesis is future research opportunities. The optimisation of the PRB technology is far from complete and some fresh input is required. Some ideas for further research are presented in the following chapter.

Chapter Eight

Future Research Opportunities

8.1 Introduction

The aim of this thesis was to create an optimal design methodology for PRB systems of practical use to decision-makers. This methodology is outlined in Figure 2.1 and described for the remediation of nitrate contamination. Subsequent chapters detailed this methodology as well as applying it to actual characterisation of reactive/non-reactive materials and hypothetical PRB design situations. Future research priorities will be primarily driven by how well the proposed methodology works in practical situations.

The relationship between reactive/non-reactive material characterisation carried out in the laboratory and how the materials behave in the field remains an important area of PRB research. Extension of the laboratory experiments presented in Chapter 3 to field sites is required in particular to determine input variability in optimisation model applications. The longevity of reactive materials and other replenishment issues are other important areas of continuing research, as the relative newness of PRB applications combined with the promising longevity of the materials has yielded little data to date.

A variety of PRB construction techniques are in use for different aquifer materials and construction depths. The relationship between modelled performance and actual performance under site conditions requires testing for all construction techniques. Site evaluation of proposed design enhancements such as the customised down-gradient gate face and deeper emplacement of impermeable walls than the gate is also required.

Cost minimisation of PRB systems is proposed through efficient designs that are targeted to a well characterised site. Further research is required to check if scenario analysis and factorial

analysis can provide an acceptable balance between cost minimisation and the consequences of under-design, or whether some form of safety factors will also be needed.

No computer model can accurately represent the complexities present in real remediation situations. Simplifying assumptions were proposed in Section 6.2 to enable development of a practically solvable model. Not all these assumptions will be acceptable for future PRB designs. The remainder of this chapter will discuss each simplifying assumption separately. Assumptions for the current formulation are:

1. Remediation of the whole plume down to the contaminant regulatory level.
2. Fully penetrating PRB systems.
3. Only one contaminant requiring remediation.
4. Only one reactive and one non-reactive material in the methodology at a time.
5. Gate and aquifer are homogeneous, isotropic and characterisation is not time-dependent over modelled area and time frame.
6. PRB system is centred on centre of plume and groundwater flow direction does not change with time.
7. Funnels are installed at right angles to the side walls.
8. Side wall length equals the gate length at its edge.
9. Contaminant concentration does not change over space (within plume) or time and natural attenuation is negligible.
10. All input parameters remain constant during PRB operating period.
11. All utilised functional relationships are continuous and differentiable.

8.2 Relaxation of Model Assumptions

8.2.1 Remediation of the Whole Plume down to the Contaminant Regulatory Level

Total plume capture and remediation down to the contaminant regulatory level are unlikely to be treated as hard constraints in practice. Incentives in the form of penalty costs are more likely to be used by regulatory agencies to encourage compliance. An alternative methodology for these situations could include the final contaminant concentration constraint

in the objective function as a penalty function (see *Daellenbach et al.*, 1983). In this way the severity of exceeding the regulatory limit can be included by adjusting the magnitude of the penalty. A very high penalty is essentially the same as treating compliance as a hard constraint.

Treating the penalty cost as a piecewise linear function enables a variety of realistic scenarios to be included. For example, no exceedence means no penalty cost but also no benefit. A small exceedence of the regulatory limit may incur a small fine and the cost of increased sampling until the regulatory limit is not exceeded. A larger exceedence may incur a larger fine and extra remediation measures. Provided all scenarios are approximately proportional to the level of exceedence then the penalty function can be defined as follows (where P_const(p) and P_linear(p) are the constant and linear portions of the penalty functions respectively):

If ($Final_{cont}$ <= $Limit_{cont}$) then

PenaltyCost = 0

Else If ($Limit_{cont}$ < $Final_{cont}$ <= Limit(2)) then

PenaltyCost = P_const(2) + P_linear(2)*($Final_{cont}$ - $Limit_{cont}$)

……

Else If (Limit(p-1) < $Final_{cont}$ <= Limit(p)) then

PenaltyCost = P_const(p) + P_linear(p)*($Final_{cont}$ – Limit(p-1))

End If

If the piecewise effects are not too extreme, it makes sense to approximate this piecewise linear function with a non-linear (and therefore differentiable), convex function. An exponential function is well suited to this type of approximation, effectively bounded and monotonically increasing. An appropriate exponential function could take the form:

$$\textbf{PenaltyCost} = \textbf{P\_const} * e^{(a0+a1*Limit_{cont})} \qquad \textbf{8.1}$$

This function would produce a lower bound of zero and no upper bound. The sign of P_const and a1 determine the direction of the curve. The magnitude of P_const and a1 determine the steepness of the curve. The mid-point of the curve is determined by (-a0/a1). Artificial Neural Networks can be used to optimally fit this curve but trial and error using a large value

for a1 and –a0/a1 slightly greater than $Limit_{cont}$ may be more efficient for simple problems. For example, if the contaminant regulatory limit was 12 g/m^3, setting P_const = $\$1*10^{10}$, a0 = -520 and a1 = 40 produces the following table of penalty costs:

Table 8.1
Penalty Cost Example

$Final_{cont}$ (g/m^3)	Penalty Cost ($)
0.0	$1.5*10^{-216}$
4.0	$4.5*10^{-147}$
8.0	$1.4*10^{-77}$
12.0	$4.2*10^{-8}$
12.2	$1.3*10^{-4}$
12.4	0.38
12.6	1125.35
12.8	$3.4*10^{6}$
13.0	$1*10^{10}$
14.0	$2.4*10^{27}$

8.2.2 Partially Penetrating PRB Systems

Fully penetrating PRB systems are unlikely to be practical or optimal for many real-world situations as many aquitards are too deep for current construction technologies. Sections 4.4.2 and 4.4.3 presented design enhancements to control vertical variation in capture width and residence time. Visual MODFLOW modelling of enhanced partially penetrating PRBs could be used to create functional relationships at multiple depths for PRB design variables. A significant amount of modelling would be required but multiple runs could occur simultaneously as runs are independent. An ideal outcome of the modelling would be to create functional relationships between capture width, residence time and gate depth for sets of PRB systems. This would enable gate depth to be included as a decision variable in the optimisation.

A second option for optimising partially penetrating PRBs is to use the current methodology to find the optimal PRB design for an equivalent fully penetrating system and then make the necessary adjustments for a partially penetrating design using post-optimisation Visual MODFLOW modelling. A necessary assumption for this option is that the optimal fully penetrating design type remains optimal for the equivalent partially penetrating situation. PRB design variables are then adjusted to counter the vertical flow effects within the partially penetrating PRB.

8.2.3 Multiple Contaminants

Table 8.2

Treatment Material and Treatable Contaminants (adapted from www.itrcweb.org)

Reactive Material	Target Contaminants	Status
Zero-Valent Iron	Halocarbons, Reducible metals	In Practice
Sawdust	Nitrate	In Practice
Limestone	Metals, Acid Water	In Practice
Sorptive Agents	Metals, Organics	In Practice, Field Demo
Reducing Agents	Reducible Metals, Organics	In Practice, Field Demo
Biological Electron Acceptors	Petroleum Hydrocarbons	In Practice, Field Demo
ZanF (Zeolite anchored Fe)	Lead and Cr(VI)	Lab Expts

Table 8.2 presents reactive materials that have been successfully used in laboratory, field or full-scale applications to remediate a variety of contaminants. Further information on these materials can be found in *Gavaskar et al.* [2000] and *Lee et al.* [2003]. For multiple contaminant situations, the PRB design is determined by the contaminant requiring maximum residence time and/or capture. Multiple reactive cells (gates) can be constructed in series if it

is not ideal or appropriate to mix the reactive materials. If the hydraulic conductivity of each reactive cell can be assumed (or constrained) to be identical, then the optimal design methodology presented in Section 6.2 would require adaptation so the gate length for each cell could be calculated separately.

8.2.4 Multiple Potential Reactive/Non-Reactive Materials

As the optimisation phase of the PRB design process is relatively quick, multiple potential reactive/non-reactive material combinations can be optimised and compared. However, laboratory testing of potential candidate materials can be time consuming and expensive so pre-screening of untested materials would be recommended. For each reactive/non-reactive material combination this would involve a separate optimisation using the appropriate reactive/non-reactive material characteristics and costs. The optimal design from each combination would be presented to the decision-maker for consideration. Further research to develop cost-effective pre-screening and column experiments more closely representative of actual site conditions would be very useful.

8.2.5 Heterogeneous and/or Anisotropic Sites

Aquifers that can be assumed homogeneous and isotropic are very rare. At a heterogeneous site, most of the groundwater and contaminant transport in the aquifer may be restricted to high hydraulic conductivity zones. The key to PRB optimisation in heterogeneous and/or anisotropic sites is adequate site characterisation. In many cases the current methodology should be adequate to find the minimum PRB type and shape. Careful site specific hydrologic (and possibly geochemical) modelling would then be undertaken to customise the chosen design to the site.

Another option is to construct an up-gradient (and possibly down-gradient) non-reactive homogeneous zone using a material or material combination of appropriate hydraulic conductivity (e.g. *Jefferis et al.*, 1997). Velocity equalisation walls, as discussed in Chapter 4, may also aid in creating more flow homogeneity in the gate. Hydrologic modelling and pilot scale site experiments would be required to test these design enhancements.

8.2.6 Plume Characterisation, Groundwater Flow Direction and Velocity

Sufficient attention to initial plume and aquifer characterisation should ensure the gate centreline matches the centre of the plume and gate length is sufficient for required residence time. Maintaining this match depends on seasonal effects and other time dependent issues affecting groundwater flow and velocity.

Groundwater flow direction and velocity is usually determined from a water table or potentiometric surface map constructed using water-level measurements taken at the site during a specific time. If there are likely to be significant changes in direction and/or velocity over the projected PRB operating horizon, then multiple scenarios of the optimisation procedure need to be run to understand the effects on optimal PRB design. Periodic checking of groundwater flow direction and velocity during PRB operation in addition to a contaminant concentration monitoring program will enable early identification of any groundwater flow direction and velocity changes.

Other approaches to groundwater flow direction and velocity estimation have been proposed. These include the three-point-problem approach of *Pinder and Abriola* [1982] and the *in situ* flow sensor approach of *Focht et al.* [1997]. An optimal PRB design should incorporate the effect of maximum variation in flow directions to avoid future situations where the plume may bypass the barrier. Design testing should also consider the maximum expected groundwater flow velocity otherwise contaminants may pass through the PRB before they are fully degraded. Maximum groundwater flow velocity usually occurs in the wintertime.

8.2.7 Angle between Funnel and Side Walls

Use of a right angle between all funnels and side walls was due to the conclusions of *Starr and Cherry* [1994]. They found this to be the most efficient configuration in isotropic aquifers when the ground water flow direction does not fluctuate significantly. Development of the functional relationships necessary to include fluctuating groundwater flow direction in the current methodology would be a huge task. Post optimisation computer modelling and in-situ pilot installations are expected to be a more efficient way of dealing with this situation.

8.2.8 Relationship between Side Wall and Gate Length

The Visual MODFLOW experiments presented in Chapter 4 found that flow deviated through a gate by means of an up-gradient funnel (or gate hydraulic conductivity significantly greater than the surrounding aquifer) always returned to its natural flow pattern. When no side walls were present, flow travelled through the sides of the gate, returning to natural flow patterns quicker than when side walls were present. This significantly increased the lateral variation in residence time, making efficient PRB design very difficult.

The only PRB designs not expected to require impermeable side walls are therefore designs without funnels and with gate hydraulic conductivity that is similar to the surrounding aquifer. For the \$40/m^3 chosen hypothetical examples this K_G/K_{Aq} ratio was achieved when reactive material proportion was close to 100%. Further research is recommended to test whether this is a realistic possibility in practice. No evidence was found in the Visual MODFLOW experiments to suggest that side wall lengths > 0 but less than the gate length would ever be beneficial.

8.2.9 Contaminant Concentration Variation

The concentrations of contaminant(s) and degradation by-product(s) are measured by taking and analysing groundwater samples at multiple depths from monitoring wells. These wells are situated up-gradient, inside, and down-gradient of the PRB system. *Warner et al.* [1998] presented the considerations that may be important in designing a monitoring program for a PRB system.

An important part of initial plume characterisation involves estimating spatial and temporal variation in contaminant concentration(s). Construction costs are generally the most expensive part of a PRB project so it is important that design changes due to unforeseen contaminant concentration variation are not necessary after PRB construction. A worst-case plume scenario would normally be considered unless there were particular reasons for considering other options. For example, a once-in-ten year rainfall event could significantly

increase contaminant concentration and dispersion, but this may be more efficiently countered with chemical injection as opposed to over-sizing the PRB just for this event.

Lateral variation in contaminant concentration could be included in the current design methodology via flow-through length calculations and/or gate mix distribution. Flow-through length of the customised down-gradient gate face is currently determined by a single residence time requirement and a lateral flow velocity distribution. Required residence time based on incoming contaminant concentration and/or degradation rate could instead be included as a lateral distribution.

The possibility of natural attenuation rates down-gradient from the PRB being affected by PRB installation and operation may also need to be considered. This is because the reactive material can be flushed out of the PRB by the groundwater flow. In this case a proportion of the PRB degradation rate could supplement the natural attenuation rate. Natural attenuation is not included in the current spreadsheet model.

8.2.10 Input Parameter Variation

Practical methods for dealing with uncertainty and variability in input data were presented in Chapter 7. Manual sensitivity analysis is proposed to cover uncertainty and variability in model bounds. Scenario analysis is especially recommended when high quality input information is available and variation is not expected in many input parameters. Factorial analysis is recommended for most other situations as it separates out the effects of multiple input factors at multiple levels without an excessive number of experimental runs. Fractional factorial designs may be more efficient than standard factorial analysis when a large number of factors need to be investigated at once. They involve adding extra factors to a fully saturated design without increasing the number of experiments. The effects of certain interactions between factors are combined in these designs, but any combined effect of interest can later be separated out by running further experiments. The proposed uncertainty analysis techniques can only provide quality output when they are fed quality input data. Research into more efficient and comprehensive characterisation techniques would be very beneficial.

8.2.11 Function Continuity

A method to approximate a piecewise linear penalty function with a continuous function was presented in Section 8.2.1. It may be realistic to treat other PRB cost inputs in a similar fashion. For example, installation and replenishment costs could be piece-wise functions as the type of construction equipment required depends on the type of aquifer material and the depth as well as shape of the PRB. Pre-construction and monitoring cost functions are also not expected to be continuous as they involve a number of discrete decisions (e.g. the number and brand of monitoring wells, the time between sampling events etc). The curve fitting software and Lagrange Method presented in Section 5.2 can be used to create continuous functions from these discrete sets of inputs.

8.3 Summary

This chapter presented some ideas for future related research and discussed the effects of relaxing the chosen model assumptions. The most important area for further research is considered to be improving the optimal PRB design model to cope with aquifers and contaminant plumes that are not homogeneous and may require partially penetrating PRBs. The assumptions of homogeneity and fully penetrating PRBs were considered necessary for creating a first-stage, solvable design model but these assumptions are expected to severely limit practical application. Post-optimisation site-specific computer modelling of optimal designs and pilot-scale emplacements are proposed as the best options in the meantime. Field testing of the accuracy of characterisation and construction techniques is also considered important to test the practicality of the proposed methodology.

Chapter Nine

Conclusions and Recommendations

9.1 Introduction

The aim of this thesis was to create an optimal PRB design methodology to aid decision-makers in finding minimum cost PRB designs to remediation problems in the presence of input uncertainty. During the course of this project PRBs have moved from a promising technology requiring further testing (*U.S. EPA*, 1998) to a mainstream technology with successful field and long-term full-scale applications for an increasing number of contaminants (e.g. *PEREBAR*, 2001; *U.S. EPA*, 2002a). The remediation industry has also become more focussed on the benefits of optimisation for accelerating site closeout, improving performance and reducing remediation costs (*U.S. EPA*, 2004b).

A variety of optimal design approaches for PRB systems have previously been proposed. All require limiting assumptions to make them solvable. The unique aspects of the proposed methodology are considered to be:

- design enhancements to improve the hydraulic performance of PRB systems;
- elimination of a time-consuming simulation model by determination of approximating functions relating design variables and performance measures for fully penetrating PRB systems;
- a versatile, spreadsheet-based optimisation model that locates minimum cost PRB designs using Excel's standard non-linear solver; and
- the incorporation of realistic input variability and uncertainty into the optimisation process via sensitivity analysis, scenario analysis and factorial analysis.

While none of the techniques used in this research are considered new in themselves, the chosen combination of techniques that enabled a simulation-optimisation problem involving input uncertainty to be set up in a computationally efficient spreadsheet model is considered

unique and generally applicable to other system optimisation problems. The practical application of this methodology to real situations has not been tested yet, but the huge computational and data burdens that have hindered practical application of other approaches incorporating uncertainty (see Section 1.3) do not exist in this approach. The main steps involved in applying this methodology to a different system include:

- system definition and computer model construction;
- computer modelling analysis of system performance;
- computer modelling experiments covering realistic system bounds to an acceptable degree of accuracy;
- development of functional relationships to replace the simulation model (where an analytical model does not already exist);
- development of an optimisation model and choice of appropriate solver;
- incorporation of input variability/uncertainty through robust analytical techniques such as factorial analysis; and
- post-optimisation, site-specific computer modelling and pilot studies.

Model verification and validation are very important at all stages of the methodology to trace and minimise errors or inaccuracies. The key step in terms of model accuracy and applicability of the proposed methodology is functional relationship development. The complexity of the relationships and the potential for error will increase with an increasing number of decision variables. Four decision variables were manageable for the chosen system but many more may not have been.

Conclusions reached during this project will be summarised in the following sections.

9.2 Characterisation of Reactive and Non-Reactive Material Combinations

Sawdust and pea gravel were chosen as the reactive and non-reactive materials respectively to test laboratory characterisation methods for determining their combined volume, effective porosity, hydraulic conductivity and degradation rate.

Sawdust proportion and slight compaction were both found to have an effect on the volumetric factor of the chosen particular sawdust and pea gravel combinations. Hydraulic conductivity was found to decrease with increasing sawdust proportion but levelled out when sawdust proportion was approximately 60%. Drainable porosity was found to increase with increasing sawdust proportion, but no significant change was noted between 0% and 40% sawdust proportion. Denitrification rate was also found to increase with increasing sawdust proportion although variation between replicates of approximately 30% was measured for most experiments.

Characterisation for six different ratios of sawdust to pea gravel (by volume) produced data points that could realistically be part of smooth polynomial interpolation functions, enabling the characterisation of any sawdust:pea gravel ratio. Translation of laboratory results to particular field sites and estimation of their variability under site conditions is important before the inclusion of characterisation functions in the optimisation model.

9.3 Hydraulic Performance Evaluation of PRB Design Enhancements.

Three-dimensional computer modelling identified capture width and residence time as the most useful performance measures for this type of optimisation and particle tracking as the most useful hydraulic performance evaluation method. Significant variation in capture and residence time was found to be caused by up-gradient funnels and/or a gate hydraulic conductivity that is significantly different from the surrounding aquifer.

The addition of velocity equalisation walls to a funnel-and-gate system was found to increase overall residence time while decreasing lateral variation in residence time. Customised down-gradient gate faces were found to enable maximum control over lateral variation in residence time. The emplacement of funnels and side walls deeper than the gate was found to minimise vertical variation in capture zone. Manipulation of a PRB's hydraulic conductivity within certain bounds was shown to be an effective means of minimising vertical variation in residence time while maximising hydraulic capture.

9.4 Determination of Relationships between Design Variables and Performance Measures for Fully Penetrating PRBs

Accurate functional relationships between PRB design variables and PRB performance measures were shown to be achievable for fully penetrating systems. Chosen design variables were gate length, gate width, funnel width and the reactive material proportion (represented by the gate hydraulic conductivity divided by the aquifer hydraulic conductivity). Chosen performance measures were edge residence, centreline residence and capture width.

A conclusion of *Teutsch et al.* [1997], where they stated that the gate hydraulic conductivity divided by the aquifer hydraulic conductivity did not have a significant effect on capture width, was found to be accurate only for a subset of PRB designs.

9.5 Optimal Design Development and Application

A spreadsheet based optimisation model coupled to Excel's standard non-linear GRG2 solver and run from carefully chosen multiple starting points was found to be an efficient and practical means of obtaining minimum cost PRB designs for specific situations. A comparison of the GRG2 solver with the LGO global solver and Evolver genetic-algorithm based solver determined that the GRG2 solver run from carefully chosen starting points spanning the feasible region was likely to find a global minimum solution faster than and at least as accurately as the LGO or Evolver solvers.

Verification of a chosen design by computer modelling and pilot-scale installation at the actual site are highly recommended so the design can be adjusted (where necessary) to actual site conditions before full-scale installation begins.

9.6 Optimisation Issues

Significant variation is expected in inputs to PRB design, particularly in aquifer and plume characteristics. Not all of this variation is quantifiable without significant expenditure. Uncertainty and variability is also expected in reactive material characteristics, particularly due to the effects of site conditions. Seasonal effects may also cause significant variation, particularly with respect to water table fluctuations and temperature effects on degradation rate.

The effects on optimal PRB designs of well characterised variability can be quantified by scenario analysis, which involves finding the optimal PRB design for multiple sets of model inputs (scenarios). Optimal designs are compared according to cost, design specifics and probability of occurrence to provide justification for a particular design choice, further characterisation or further analysis. Scenario analysis can incorporate non-linear effects and interactions between inputs which are not easily dealt with in standard one-way analysis of user inputs. However, the effects of all chosen inputs under investigation are lumped together which may result in unnecessary characterisation and analysis.

Scenario analysis is especially recommended when high quality input information is available and variation is not expected in many input parameters. Factorial analysis is recommended for most other situations as it separates out the effects of multiple input factors at multiple levels without an excessive number of experimental runs. Computer processing and analysis time is likely to be greater than the equivalent scenario analysis, but the screening of important inputs allows future allocation of time and money to be targeted at improving characterisation and reducing uncertainty of input variation causing the greatest effect.

Fractional factorial analysis may be more efficient than standard factorial analysis when uncertainty is present in many user inputs. Fractional factorial analysis selects a particular

fraction of the factorial experiments for the purpose of screening out the factors most worthy of further analysis.

Sensitivity analysis is recommended to identify areas for further investigation, be they the accuracy of input information, limitations of construction techniques, limitations of computer modelling and functional approximations, or model assumption issues. Excel generated sensitivity analysis is not recommended for the proposed PRB optimisation as it linearly extrapolates the chosen design. This may often be accurate enough for small changes in decision variable or constraint bounds, but accuracy cannot be guaranteed for larger changes due to the non-linear objective function and the potential for the minimum cost solution to change to a different design type. Manual sensitivity analysis, however, only takes a few minutes and is proposed for general post-optimisation sensitivity analysis.

9.7 Future Research Opportunities

The most important area for further research is considered to be improving the optimal PRB design model to cope with aquifers and contaminant plumes that are not homogeneous and may require partially penetrating PRBs. The assumptions of homogeneity and fully penetrating PRBs were considered necessary for creating a first-stage, solvable design model but these assumptions are expected to severely limit practical application. Further hydraulic modelling will be required to develop new functional relationships or extend the current ones. Post-optimisation site-specific computer modelling of optimal designs and pilot-scale emplacements are proposed as the best options in the meantime.

Factorial analysis is considered a promising and under-utilised technique for incorporating realistic input variability and uncertainty into the optimisation of environmental systems. Further research into environmental systems whose modelling or optimisation has been hindered by input uncertainty is recommended. Other recommendations when considering application of the proposed methodology include field testing of the accuracy of characterisation and construction techniques, and consideration of the chosen model assumptions and their potential for relaxation.

References

Aguando, E., Sitar, N., and Remson, I. (1977), "Sensitivity Analysis in Aquifer Studies", Water Resources Research, 13(4), pp. 733-737.

Ahlfeld, D.P., Mulvey, J.M., Pinder, G.F., and Wood, E.F. (1988a), "Contaminated Groundwater Remediation Design Using Simulation, Optimisation, and Sensitivity Theory. 1. Model Development", Water Resources Research, 24(3), pp. 431-441.

Ahlfeld, D.P., Mulvey, J.M., Pinder, G.F., and Wood, E.F. (1988b), "Contaminated Groundwater Remediation Design Using Simulation, Optimisation, and Sensitivity Theory. 2. Analysis of a Field Site", Water Resources Research, 24(3), pp. 443-452.

Ahlfeld, D.P. (1990), "Two-Stage Groundwater Remediation Design", Journal of Water Resources Planning and Management, 116(4), pp. 517-529.

Ahlfeld, D.P., Page, R.H., and Pinder, G.F. (1995), "Optimal Ground-Water Remediation Methods Applied to a Superfund Site: from Formulation to Implementation", Ground Water, 33(1), pp. 58-70.

Ahlfeld, D.P., and Heidari, M. (1994), "Applications of Optimal Hydraulic Control to Ground-Water Systems", Journal of Water Resources Planning and Management, 120(3), pp. 350-365.

Ahlfeld, D.P., and Mulligan, A.E. (2000), "Optimal Management of Flow in Groundwater Systems", Academic Press, San Diego, California.

Ahn, J.S., Chona, C-M., Moona, H-S., and Kim, K-W. (2003), "Arsenic Removal using Steel Manufacturing Byproducts as Permeable Reactive Materials in Mine Tailing Containment Systems", Water Research, 37, pp. 2478–2488.

Aly, A.H., and Peralta, R.C. (1999a), "Comparison of a Genetic Algorithm and Mathematical Programming to the Design of Groundwater Systems", Water Resources Research, 35(8), pp. 2415-2425.

Aly, A.H., and Peralta, R.C. (1999b), "Optimal Design of Aquifer Cleanup Systems under Uncertainty using a Neural Network and a Genetic Algorithm", Water Resources Research, 35(8), pp. 2523-2532.

Amos, P.W., and Younger, P.L. (2003), "Substrate Characterisation for a Subsurface Reactive Barrier to Treat Colliery Spoil Leachate", Water Research, 37, pp. 108–120.

Andricevic, R., and Kitanidis, P.K. (1990), "Optimisation of the Pumping Schedule in Aquifer Remediation under Uncertainty", Water Resources Research, 26(5), pp. 875-885.

ANZECC (1992), "Australian and New Zealand Guidelines for the Assessment and Management of Contaminated Sites", Australian and New Zealand Environment and Conservation Research Council, National Health and Research Council.

Aravena, R., Evans, M.L., and Cherry, J.A. (1993), "Stable Isotopes of Oxygen and Nitrogen in Source Identification of Nitrate from Septic Systems", Ground Water, 31(2), pp. 180-186.

Askew, C.C. (1985), "Nitrate in Groundwater – A Review of the Issue with Emphasis on the New Zealand Situation", M.Sc. Thesis, University of Canterbury and Lincoln College, New Zealand, 120p.

Atwood, D.V., and Gorelick, S.M. (1985), "Hydraulic Gradient Control for Groundwater Contaminant Removal", Journal of Hydrology, 76, pp. 85-106.

AWRC (Australian Water Resources Council), (1983), "Nitrate Rich Groundwaters of Australia", Technical Paper No. 79, Dept. of Resources and Energy, Canberra, *(in Askew, 1985).*

Baber, H.L. (1977), "A Study of Some Nitrate and Phosphate Problems in New Zealand Agriculture", Ph.D. Thesis, University of Waikato, Hamilton, New Zealand, 303p, (*in Askew, 1985*).

Bakr, A.A. (1976), "Effects of Spatial Variations of Hydraulic Conductivity on Groundwater Flow", Ph.D. Thesis, New Mexico Institute of Mining and Technology, Socorro, NM, *(in Gorelick et al., 1993).*

Barkle G.F., Schipper, L.A., Burgess, C.P. and Painter, B.D.M. (2005), "Why Shallow Groundwater Bypassed a Denitrification Wall", (*submitted to Contaminat Hydrology).*

Battelle (1996), "Evaluation of Funnel-and-Gate Pilot Study at Moffett Federal Airfield with Groundwater Modelling", prepared for the U.S. Department of Defense, Environmental Security Technology Certification Program and Naval Facilities Engineering Service Centre, Port Hueneme, California, *(in Gavaskar et al., 1998).*

Baveye, P., and Valocchi, A. (1989), "An Evaluation of Mathematical Models for the Transport of Biologically Reacting Solutes in Saturated Soils and Aquifers", Water Resources Research, 25(6), pp. 1413-1421.

Bear, J. (1979), "Groundwater Hydraulics", McGraw-Hill, New York.

Bear, J., and Verruijt, A. (1987, 1990, 1992), "Modeling Groundwater Flow and Pollution", D. Reidel Publishing Co., Dordrecht, Holland.

Bear, J., and Nitao, J.J. (1999), "Flow and Contaminant Transport in the Unsaturated Zone" – *draft copy*, Kluwer Academic Publishers, Dordrecht, Holland.

Benner, S.G., Blowes, D.W., and Ptacek, C.J. (1997), "A Full-Scale Porous Reactive Wall for Prevention of Acid Mine Drainage", Groundwater Monitoring and Remediation, 17(4), pp. 99-107.

Benner, S.G., Gould, W.D. and Blowes, D.W. (2000), "Microbial Populations Associated with the Generation and Treatment of Acid Mine Drainage", Chemical Geology, 169(3-4), pp. 435-448.

Benner, S.G., Blowes, D.W., and Molson, J.W.H. (2001), "Modeling Preferential Flow in Reactive Barriers: Implications for Performance and Design", Ground Water, 39(3), pp. 371-379.

Benner, S.G., Blowes, D.W., Ptacek, C.J., and Mayer, K.U. (2002), "Rates of Sulfate Reduction and Metal Sulfide Precipitation in a Permeable Reactive Barrier", Applied Geochemistry, 17, pp. 301–320.

Berthouex, P.M., and Brown, L.C. (2002), "Statistics for Environmental Engineers (2nd Edition)", Lewis Publishers, Boca Raton, U.S.A., pp. 239-279.

Bilbrey, L.C., and Shafer, J.M. (2001), "Funnel-and-Gate Performance in a Moderately Heterogeneous Flow Domain", Ground Water Monitoring and Remediation, 21(3), pp. 144-151.

Blowes, D.W. and Ptacek, C.J. (1992), "Geochemical Remediation of Groundwater by Permeable Reactive Walls, Removal of Chromate by Reduction with Iron Bearing Solids", in *Proceedings of the Subsurface Restoration Conference*, Third International Conference on Groundwater Quality Research, Dallas, Texas, pp. 214-216.

Blowes, D.W. and Ptacek, C.J. (1994), "System for Treating Contaminated Water", U.S. Patent 5,362,394 filed March 3, 1992, issued Nov. 8, 1994, Canada Patent 2,062,204, filed March 3, 1992, allowed, January 2000 (U.K., Germany, France, Italy, Spain, Sweden).

Blowes, D.W., Robertson, W.D., Ptacek, C.J., and Merkley, C. (1994), "Removal of Agricultural Nitrate from Tile-Drainage Effluent Water Using In-Line Bioreactors", Journal of Contaminant Hydrology, 15, pp. 207-221.

Blowes, D.W. and Ptacek, C.J. (1996), "System for Treating Contaminated Water. Continuation in Part", U.S. Patent 5,514,279, filed October 27, 1994, issued May 7, 1996.

Blowes, D.W., Ptacek, C.J. and Baker, M. (1996), "Treatment of Wastewater", G.B. Patent 962338-7, filed November 11, 1996 (issued 2000), Canada Patent 2,190,038, filed November 11, 1996, U.S. Patent 08,745,734, filed November 12, 1996 (issued 1999).

Blowes, D.W., Gillham, R.W., Ptacek, C.J., Puls, R.W., Bennet, T.A., O'Hannesin, S.F., Hanton-Fong, C.J., and Bain, J.G. (1999a), "An *In Situ* Permeable Reactive Barrier for the Treatment of Hexavalent Chromium and Trichloroethylene in Ground Water: Volume 1, Design and Installation", EPA/600/R-99/095a, 111 pp.

Blowes, D.W., Puls, R.W., Gillham, R.W., Ptacek, C.J., Bennet, T.A., Bain, J.G., Hanton-Fong, C.J., and Paul, C.J. (1999b), "An *In Situ* Permeable Reactive Barrier for the Treatment of Hexavalent Chromium and Trichloroethylene in Ground Water: Volume 2, Performance Monitoring", EPA/600/R-99/095b, 207 pp.

Blowes, D.W., Puls, R.W., Gillham, R.W., Ptacek, C.J., Mayer, K.U., Hanton-Fong, C.J., Paul, C.J., and Bain, J.G.(1999c), "An *In Situ* Permeable Reactive Barrier for the Treatment of Hexavalent Chromium and Trichloroethylene in Ground Water: Volume 3, Multicomponent Reactive Transport Modelling", EPA/600/R-99/095c, 39 pp.

Blowes, D.W., Ptacek, C.J., Benner, S.G., McRae, C.W.T., Bennet, T.A., Puls, R.W. (2000), "Treatment of Inorganic Contaminants using Permeable Reactive Barriers", Journal of Contaminant Hydrology, 45, pp. 123–137.

Bollag, J.M., Drzymala, S., and Kardos, L.T. (1973), "Biological Versus Chemical Nitrite Decomposition in Soil", Soil Science, 116, pp. 44-, *(in Golterman, 1985).*

Boussaid, F., Martin, G., and Morvan, J. (1988), "Denitrification *In-situ* of Groundwater with Solid Carbon Matter", Environmental Technology Letters, 9, pp. 803-816.

Bowles, M., Bentley, L., Barker, J., Thomas, D., Granger, D., Jacobs, H., Rimbey, S., and Hoyne, B. (1995), "The East Garrington Trench and Gate System: It Works", via internet: http//:www.geo.ucalgary.ca/hydro/thomas/thomas.html.

Bowman, R.A., and Focht, D.D. (1974), "The Influence of Glucose and Nitrate Concentrations upon Denitrification Rates in Sandy Soil", Soil Biol. Biochem., 6, pp. 297-, *(in Golterman, 1985).*

Box, G.E.P, Hunter, W.G., and Hunter, J.S. (1978), "Statistics for Experimenters: An Introduction to Design, Data Analysis and Model Building", John Wiley & Sons, New York, pp. 329-405.

Bragan, R.J., Starr, J.L., and Parkin, T.B. (1997a), "Acetylene Transport in Shallow Groundwater for Denitrification Rate Measurement", Journal of Environmental Quality, 26, pp. 1524-1530.

Bragan, R.J., Starr, J.L., and Parkin, T.B. (1997b), "Shallow Groundwater Denitrification Rate Measurement by Acetylene Block", Journal of Environmental Quality, 26, pp. 1531-1538.

Brooke, A., Kendrick, D., and Meeraus, A. (1988), "GAMS: A User's Guide", Scientific Press, Redwood City, Calif.

Bryda, L.K., and Morris, P.E. (1997), "Emerging Technologies for *In Situ* Groundwater Remediation", Remediation, Summer 1997, pp. 109-125.

Burden, R.J. (1982), "Nitrate Contamination of New Zealand Aquifers: A Review", New Zealand Journal of Science, 25, 210p, *(in Woudberg, 1991).*

Burris, D.R., and Cherry, J.A. (1992), "Emerging Plume Management Technologies: *In Situ* Treatment Zones", in Eighth Annual Air and Waste Management Meeting, Kansas City, MO, June 21-26.

Carmichael, P.A., (1994), "Using Wood Chips as a Source of Organic Carbon in Denitrification: A Column Experiment and Field Study Implementing the Funnel and Gate Design", M.Sc. Thesis, University of Waterloo, Ontario, Canada, 156p.

Carsel, R.F., and Parrish, R.S. (1988), "Developing Joint Probability Distributions of Soil Water Retention Characteristics", Water Resources Research, 24(5), pp. 755-769.

Centi, G., and Perathoner, S. (2003), "Remediation of Water Contamination using Catalytic Technologies", Applied Catalysis B: Environmental, 41, pp. 15–29.

Chang, L.-C., Shoemaker, C.A., and Liu, P.L.-F. (1992), "Optimal Time-Varying Pumping Rates for Groundwater Remediation: Application of a Constrained Optimal Control Algorithm", Water Resources Research, 28(12), pp. 3157-3173.

Chow, V.T., Maidment, D.R., Mays, L.W. (1988), "Applied Hydrology", McGraw-Hill, New York, 572p.

Christiansen, B.A., and Hatfield, K. (1994), "*In Situ* Restoration of Contaminated Surficial Aquifers. Part 1: The Flow Process", in *Future Groundwater Resources at Risk*, Proceedings of the Helsinki Conference, IAHS Publ. No. 222, pp. 313-321.

Christodoulatos, C., Korfiatis, G.P., Pal, N., and Koutsospyros, A. (1996), "*In Situ* Groundwater Treatment in a Trench Bio-Sparge System", Hazardous Waste and Hazardous Materials", 13(2), pp. 223-236.

Colarullo, S.J., Heidari, M., and Maddock III, T. (1984), "Identification of an Optimal Ground-Water Management Strategy in a Confined Aquifer", Water Resources Bulletin, 20(5), pp. 747-760.

Colarullo, S.J., Heidari, M., and Maddock III, T. (1985), "Demonstrative Model for Identifying Ground-Water-Management Options in a Contaminated Aquifer", Groundwater Ser. 8, Kansas Geological Survey, Lawrence, Kansas.

Coley, D.A. (1999), "An Introduction to Genetic Algorithms for Scientists and Engineers", World Scientific Publishing Co. Pte. Ltd., Singapore.

Culver, T.B., and Shoemaker, C.A. (1992), "Dynamic Optimal Control for Groundwater Remediation with Flexible Management Periods", Water Resources Research, 28(4), pp. 629-641.

Czurda, K.A., and Haus, R. (2002), "Reactive Barriers with Fly Ash Zeolites for In-Situ Groundwater Remediation", Applied Clay Science, 21, pp. 13– 20.

Daellenbach, H.G., George, J.A., and McNickle, D.C. (1983), "Introduction to Operations Research Techniques (2nd Edition)", Allyn and Bacon, Inc., Boston, pp. 606-612.

Davis, K. (1995), "Brief Explanation of Superfund", via Internet. http://www.bus.orst.edu/FACULTY/NIELSON/industry/env-law/superf.htm

Day, S.R., O'Hannesin, S.F, and Marsden, L. (1999), "Geotechnical Techniques for the Construction of Reactive Barriers", Journal of Hazardous Materials, 67, pp. 285–297.

Della Rocca, C., Belgiorno, V. and Meriç, S. (2005), "Cotton-Supported Heterotrophic Denitrification of Nitrate-Rich Drinking Water With A Sand Filtration Post-Treatment", Water SA, 31 (2), pp. 229-236.

Dougherty, D.E., and Marryott, R.A. (1991), "Optimal Groundwater Management: 1. Simulated Annealing", Water Resources Research, 27(10), pp. 2493-2508.

Erickson, M., Mayer, A. and Horn, J. (2002), "Multi-Objective Optimal Design of Groundwater Remediation Systems: Application of the Niched Pareto Genetic Algorithm (NPGA)", Advances in Water Resources, 25(1), pp. 51-65.

(ESTCP) Environmental Security Technology Certification Program (1999), "Permeable Reactive Wall Remediation of Chlorinated Hydrocarbons in Groundwater", U.S. Department of Defence, Arlington, Virginia, www.estcp.org, 65p.

Everhart, D. (1997), "Theoretical Foundations of GROWFLOW", ARA-TR-96-5286-3, Prepared by Allied Research Associates, Inc. for U.S. Air Force, Tyndall Air Force Base, Florida, 27p.

Eykholt, G.R., Elder, C.R. and Benson, C.H. (1999), "Effects of Aquifer Heterogeneity and Reaction Mechanism Uncertainty on a Reactive Barrier", Journal of Hazardous Materials 68, pp. 41-64.

Fan, A.M., and Steinberg, V.E. (1996), Regulatory Toxicology and Pharmacology, 23, pp. 35-43.

Fahrner, S. (2002), "Groundwater Nitrate Removal Using a Bioremediation Trench", Honours Thesis, Department of Environmental Engineering, University of Western Australia, 126p.

Firestone, M. (1982) "Biological Denitrification", in *Nitrogen in Agricultural Soils*, (ed.) Stevenson, F.J., Agronomy, Vol. 22, Madison, American Society of Agronomy, Inc., pp. 289-326.

Fiorenza, S., Oubre, C., and Ward, C. (Eds.) (2000), "Sequenced Reactive Barriers for Groundwater Remediation", Lewis Publishers, Boca Raton, Florida.

Focht, D.D., and Verstraete, W. (1977), "Biochemical Ecology of Nitrification and Denitrification", in *Advances in Microbial Ecology*, Vol. 1, M. Alexander (Ed.), Plenum Press, *(in Golterman, 1985).*

Focht, R.M., Vogan, J.L., and O'Hannesin, S.F. (1997), "Hydraulic Studies of *In Situ* Permeable Barriers", 1997 International Containment Technology Conference Proceedings, St. Petersburg, Florida, pp. 975-981.

Francis, A.J., Slater, M.J., and Dodge, C.J. (1989), "Denitrification in Deep Subsurface Sediments", Geomicrobiology Journal, 7(1), pp. 103-116, *(in Korom, 1992).*

Freeze, R.A., and Cherry, J.A. (1979), "Groundwater", Prentice-Hall, New Jersey, 604p.

Freeze, R.A., and Gorelick, S.M. (1999), "Convergence of Stochastic Optimization and Decision Analysis in the Engineering Design of Aquifer Remediation", Ground Water, 37(6), pp. 934-954.

Gailey, R.M., and Gorelick, S.M. (1993), "Design of Optimal, Reliable Plume Capture Schemes: Application to the Gloucester Landfill Ground-Water Contamination Problem", Ground Water, 31(1), pp. 107-114.

Gandhi, S., Oh, B-T., Schnoor, J.L., and Alvarez, P.J.J. (2002), "Degradation of TCE, Cr(VI), Sulfate, and Nitrate Mixtures by Granular Iron in Flow-Through Columns under Different Microbial Conditions", Water Research, 36, pp. 1973–1982.

Garrido, J.M., Moreno, J., Méndez-Pampín, R., and Lema, J.M. (1998), "Nitrous Oxide Production under Toxic Conditions in a Denitrifying Anoxic Filter", Water Research, 32 (8), pp. 2550-2552.

Gavaskar, A.R., Gupta, N., Sass, B.M., Janosy, R.J., and O'Sullivan, D. (1998), "Permeable Barriers for Groundwater Remediation: Design Construction and Monitoring", Battelle Press, Colombus, Ohio, 176p.

Gavaskar, A.R. (1999), "Design and Construction Techniques for Permeable Reactive Barriers", Journal of Hazardous Materials, 68, pp. 41–71.

Gavaskar, A.R., Gupta, N., Sass, B.M., Janosy, R.J., and Hicks, J. (2000), "Design Guidance for Application of Permeable Reactive Barriers for Groundwater Remediation", Battelle Press, Colombus, Ohio, 167p.

Gill, P.E., Murray, W., and Wright, M.H. (1981), "Practical Optimization", Academic Press, London, 401p.

Gill, P.E., Murray, W., Saunders, M.A., and Wright, M.H. (1986), "User's Guide for NPSOL: A FORTRAN Package for Non-linear Programming", Dept. of Operations Research, Stanford Univ., Technical Report SOL 86-2.

Gillham, R.W., and Burris, D.R. (1992), "*In Situ* Treatment Walls – Chemical Dehalogenation, Denitrification, and Bioaugmentation", in *Subsurface Restoration*

Conference, Third International Conference on Ground Water Quality Research, June 21-24, 1992, Dallas, Texas, pp. 66-68.

Glass, C. and Silverstein, J. (1998), "Denitrification Kinetics of High Nitrate Concentration Water: pH Effect on Inhibition and Nitrite Accumulation", Water Research, 32(3), pp. 831-839.

Goldberg, D.E., (1989), "Genetic Algorithms in Search, Optimisation and Machine Learning", Addison-Wesley, Reading, Mass.

Golterman, H.L. (Ed.) (1985), "Denitrification in the Nitrogen Cycle", Plenum Press, New York, 294 pages.

Gorelick, S.M. (1983), "A Review of Distributed Parameter Groundwater Management Modelling Methods", Water Resources Research, 19(2), pp. 305-319.

Gorelick, S.M., and Voss, C.I. (1984), "Aquifer Reclamation Design: The Use of Contaminant Transport Simulation Combined with Non-linear Programming", Water Resources Research, 20(4), pp. 415-427.

Gorelick, S.M. (1987), "Sensitivity Analysis of Optimal Groundwater Contaminant Capture Curves: Spatial Variability and Robust Solutions", in *Solving Groundwater Problems with Models*, NWWA Conference Proceedings, pp. 133-146, National Well Association, Dublin, Ohio.

Gorelick, S.M., and Wagner, B.J. (1987), "Optimal Groundwater Quality Management under Parameter Uncertainty", Water Resources Research, 23(7), pp. 1162-1174.

Gorelick, S.M. (1990), "Large Scale Non-linear Deterministic and Stochastic Optimisation: Formulations involving Simulation of Subsurface Contamination", Mathematical Programming, 48, pp. 19-39.

Gorelick, S.M., Freeze, R.A., Donohue, D., and Keely, J.F. (1993), "Groundwater Contamination: Optimal Capture and Containment", Lewis Publishers, Boca Raton, Florida.

Grady, C.P.L., and Lim, H.C. (1980), "Biological Wastewater Treatment: Theory and Applications", Marcel Dekker, New York, NY.

Grathwohl, P. (1997), "Permeable Sorptive (+ Reactive) Walls for Treatment of Hydrophobic Organic Contaminant Plumes in Groundwater", 1997 International Containment Technology Conference Proceedings, St. Petersburg, Florida.

Guerin, T.F., Horner, S., McGovern, T., and Davey, B. (2002), "An Application of Permeable Reactive Barrier Technology to Petroleum Hydrocarbon Contaminated Groundwater", Water Research, 36, pp. 15-24.

Guiguer, N., Molsen, J., Frind, E.O., and Franz, T. (1992), "FLONET-Equipotential and Streamlines Simulation Package", Waterloo Hydrogeologic Software and the Waterloo Centre for Groundwater Research, Waterloo, Ontario, *(in Gavaskar et al., 1998).*

Guiguer, N., and Franz, T. (1996), "Visual MODFLOW User's Manual", Waterloo Hydrogeologic Software, Ontario, Canada.

Gupta, N., and Fox, T.C. (1999), "Hydrogeologic Modeling For Permeable Reactive Barriers", Journal of Hazardous Materials, 68, pp. 19–39.

Haitjema, H., Kelson, V., and de Lange, W. (2001), "Selecting MODFLOW Cell Sizes for Accurate Flow Fields", Ground Water, 39 (6), pp. 931-938.

Hamed, M.M., and Bedient, P.B. (1999), "Reliability-Based Uncertainty Analysis of Groundwater Contaminant Transport and Remediation", United States Environmental Protection Agency, Report EPA/600/R-99/028, 82p.

Hamming, R.W. (1962), "Numerical Methods for Scientists and Engineers", McGraw-Hill Book Company Inc., New York, pp. 91-97.

Harbaugh, A.W. (1990), "A Computer Program for Calculating Subregional Water Budgets using Results from the U.S. Geological Survey Modular Three-Dimensional Finite Difference Ground-Water Flow Model", U.S. Geological Survey Open-File Report 90-392, *(in Gavaskar et al., 1998).*

Hatfield, K., and Christiansen, B.A. (1994), "*In Situ* Restoration of Contaminated Surficial Aquifers. Part 2: The Chemical Process", in *Future Groundwater Resources at Risk*, Proceedings of the Helsinki Conference, IAHS Publ. No. 222, pp. 323-332.

Hatfield, K. (1997), "Funnel-and-Gate Design Method", ARA-TR-96-5286-4, prepared by Applied Research Associates, Inc. for U.S. Air Force, Tyndall Air Force Base, Florida.

Hatfield, K., Burris, D.R., and Wolfe, N.L. (1996), "Analytical Model for Heterogeneous Reactions in Mixed Porous Media", Journal of Environmental Engineering, 122(8), pp. 676-684.

Haugen, K.S., Semmens, M.J., and Novak, P.J. (2002), "A Novel *in situ* Technology for the Treatment of Nitrate Contaminated Groundwater", Water Research, 36, pp. 3497–3506.

Heidari, M., Sadeghipour, J., and Drici, O. (1987), "Velocity Control as a Tool for Optimal Plume Management in the Equus Beds Aquifer, Kansas", Water Resources Bulletin, 23(2), pp. 325-336.

Holland, J.H. (1975), "Adaptation in Natural and Artificial Systems", University of Michigan Press, Ann Arbor, *(in Aly and Peralta, 1999).*

Hopfield, J.J., and Tank, D.W. (1985), "Neural Computation of Decisions in Optimisation Problems", Biological Cybernetics, 52, pp. 141-152.

Howard, L.V., Hatfield, K., and Christiansen, B.A. (1995), "Minimum Cost Design of a Funnel-and-Gate System", Groundwater Management, R.J.Charbeneau (ed), ASCE, New York, pp. 259-264.

Hseih, P.A., and Freckleton, J.R. (1993), "Documentation of a Computer Program to Simulate Horizontal-Flow Barriers Using the U.S. Geological Survey Modular Three-Dimensional Finite Difference Ground-Water Flow Model", U.S. Geological Survey Open-File Report 92-477, *(in Gavaskar et al., 1998).*

Huck, P.M. (1990), "Measurement of Biodegradable Organic Matter and Bacterial Growth Potential in Drinking Water", Journal of the American Water Works Association, 82(7), p88, *(in Khan et al., 1998).*

Hunter, W.J. (2001), "Use of Vegetable Oil in a Pilot-Scale Denitrifying Barrier", Journal of Contaminant Hydrology, 52(1-2), pp. 119-131.

Hyndman, D.W., Dybas, M.J., Forney, L., Heine, R., Mayotte, T., Phanikumar, M.S., Tatara, G., Tiedje, J., Voice, T., Wallace, R., Wiggert, D., Zhao, X., and Criddle, C.S. (2000), "Hydraulic Characterization and Design of a Full-Scale Biocurtain", Ground Water, 38(3), pp. 462-474.

IBM Corporation, (1991), Optimisation Subroutine Library, Guide and Reference, release 2, 3rd ed., IBM Corp., Kingston, N.Y.

Interstate Technology and Regulatory Cooperation Work Group (ITRC), (1999), "Regulatory Guidance for Permeable Reactive Barriers Designed to Remediate Chlorinated Solvents (2nd Edition)", http://www.itrcweb.org.

Interstate Technology and Regulatory Cooperation Work Group (ITRC), (1999b), "Regulatory Guidance for Permeable Reactive Barriers Designed to Remediate Inorganic and Radionuclide Contamination", http://www.itrcweb.org.

Interstate Technology and Regulatory Cooperation Work Group (ITRC), (2000), "Emerging Technologies for Enhanced *In Situ* Biodenitrification (EISBD) of Nitrate-Contaminated Ground Water", http://www.itrcweb.org.

Interstate Technology and Regulatory Cooperation Work Group (ITRC), (2001), "Design Guidance for Application of Permeable Barriers to Remediate Dissolved Chlorinated Solvents", http://www.itrcweb.org.

Interstate Technology and Regulatory Cooperation Work Group (ITRC), (2002), "Advanced Techniques on Installation of Iron Based Permeable Reactive Barriers and Non-Iron Based Barrier Treatment Material", http://www.itrcweb.org.

Interstate Technology and Regulatory Cooperation Work Group (ITRC), (2002b), "A Systematic Approach to In Situ Bioremediation in Groundwater Including Decision Trees for In Situ Bioremediation of Nitrates, Carbon Tetrachloride, and Perchlorate", http://www.itrcweb.org.

Interstate Technology and Regulatory Cooperation Work Group (ITRC), (2005), "Permeable Reactive Barriers: Lessons Learned/New Directions", http://www.itrcweb.org.

Istok, J.D., Humphrey, M.D., Schroth, M.H., Hyman, M.R., and O'Reilly, K.T. (1997), "Single-Well 'Push-Pull' Test for In Situ Determination of Microbial Activities", Ground Water, 35, pp. 619–631.

Jeffries, K. "Reinventing Superfund: The Clinton Reform Proposal and an Alternative", via Internet, http://www.cei.org/superfnd.html.

Jefferis, S.A., Norris, G.H, and Thomas, A.O. (1997), "Developments in Permeable and Low Permeability Barriers", Land Contamination and Reclamation, 5(3), pp. 225-231.

Johnson, V.M., and Rogers, L.L. (1995), "Location Analysis in Ground-Water Remediation using Neural Networks", Ground Water, 33(5), pp. 749-758.

Kamolpornwijit, W., Liang L., West, O.R., Moline, G.R., and Sullivan, A.B. (2003), "Preferential Flow Path Development and its Influence on Long-Term PRB Performance: Column Study", Journal of Contaminant Hydrology, 66, pp. 161– 178.

Karatzas, G.P., and Pinder, G.F. (1993), "Groundwater Management using Numerical Simulation and the Outer Approximation Method for Global Optimisation", Water Resources Research, 29(10), pp. 3371-3378.

Karatzas, G.P., and Pinder, G.F. (1996), "The Solution of Groundwater Quality Management Problems with a Nonconvex Feasible Region Using a Cutting Plane Technique", Water Resources Research, 32(4), pp. 1091-1100.

Khan, E., Babcock, R.W. Jnr., Suffet, I.H., and Stenstrom, M.K. (1998), "Method Development for Measuring Biodegradable Organic Carbon in Reclaimed and Treated Wastewaters", Water Environment Research, 70(5), pp. 1025-1032.

Kinzelbach, W., Schafer, W., and Herzer, J. (1991), "Numerical Modeling of Natural and Enhanced Denitrification Processes in Aquifers", Water Resources Research, 27(6), pp. 1123-1135.

Kirkpatrick, S., Gelatt, C.D. Jr, and Vecchi, M.P. (1983), "Optimisation by Simulated Annealing", Science, 220, pp. 671-680.

Klute, A. (1986), "Methods of Soil Analysis, Part 1 – Physical and Mineralogical Methods (2nd Edition)", Soil Science of America.

Knowles, R. (1982), "Denitrification", Microbiol. Rev., 46, pp. 43-, *(in Golterman, 1985).*

Korom, S.F. (1992), "Natural Denitrification in the Saturated Zone: A Review", Water Resources Research, 28(6), pp. 1657-1668.

Korom, S.F., Schlag, A.J., Schuh, W.M. and Kammer Schlag, A. (2005), "In Situ Mesocosms: Denitrification in the Elk Valley Aquifer", Ground Water Monitoring and Remediation 25 (1), pp. 79-89.

Kuo, C.H., Michel, A.N., and Gray, W.G. (1992), "Design of Optimal Pump-and-Treat Strategies for Contaminated Groundwater Remediation using the Simulated Annealing Algorithm", Advances in Water Resources, 15(2), pp. 95-105.

Lee, S.-I., and Kitanidis, P.K. (1991), "Optimal Estimation and Scheduling in Aquifer Remediation with Incomplete Information", Water Resources Research, 27(9), pp. 2203-2217.

Lee, S., Lee, K., Park, S., Kim, H., and Park, J. (2003), "Simultaneous Removal of Lead and CR(VI) using ZanF", 2003 NZWWA Conference Proceedings, Auckland, New Zealand.

Leeuw, E.J., Kramer, J.F., Bult, B.A., and Wijcherson, M.H. (1996), "Optimisation of Nutrient Removal with On-Line Monitoring and Dynamic Simulation", Water Science Technology, 33(1), pp. 203-209.

Lin, H.J., Richards, D.R., Yeh, G.T., Cheng, J.R., Cheng, H.P., and Jones, N.L. (1996), "FEMWATER: A Three-Dimensional Finite Element Computer Model for Simulating Density Dependent Flow and Transport", U.S. Environmental Protection Agency technical report HL-96.

Lincoln Environmental (1997), "Nitrogen Inputs at Land Surfaces and Groundwater Quality. Review of Science, Policy and Management: International and New Zealand", Report No. 2776/1 to Canterbury Regional Council and MAF Policy, Christchurch, New Zealand.

Lynsley, R.K., Kohler, M.A., and Paulhus, J.L. (1975), "Hydrology for Engineers (2nd Edition)", McGraw-Hill, New York, 482p.

Mackay, D.M. and Cherry, J.A. (1989), "Groundwater Contamination: Limits of Pump-and-Treat Remediation", Environmental Science and Technology, 23, pp. 630-636.

MacQuarrie, K.T.B, Sudicky, E.A., and Robertson, W.D. (2001), "Numerical Simulation of a Fine-Grained Denitrification Layer for Removing Septic System Nitrate from Shallow Groundwater", Journal of Contaminant Hydrology, 52, pp. 29-55.

Maddock III, T. (1973), "Management Model as a Tool for Studying the Worth of Data", Water Resources Research, 9(3), pp. 270-280.

Mansfield, C.M., and Shoemaker, C.A. (1999), "Optimal Remediation of Unconfined Aquifers: Numerical Applications and Derivative Calculations", Water Resources Research, 35(5), pp. 1455-1469.

Manz, C., and Quinn, K. (1997), "Permeable Treatment Wall Design and Cost Analysis", 1997 International Containment Technology Conference Proceedings, St. Petersburg, Florida, pp. 788-794.

Marryott, R.A. (1989), "Optimal Groundwater Management using the Method of Simulated Annealing", M.S. thesis, Dept. of Civil Eng., Univ. of Calif., Irvine.

Marryott, R.A., Dougherty, D.E., and Stollar, R.L. (1993), "Optimal Groundwater Management: 2. Application of Simulated Annealing to a Field-Scale Contamination Site", Water Resources Research, 29(4), pp. 847-860.

Marryott, R.A. (1996), "Optimal Groundwater Remediation Design using Multiple Control Technologies", Ground Water, 34(3), pp. 425-433.

Mateju, V., Cizinska, S., Krejci, J., and Janoch, T. (1992), "Biological Water Denitrification – a Review", Enzyme and Microbial Technology, 14(3), pp. 170-183.

McDonald, M.G., and Harbaugh, A.W. (1988), "A Modular Three-Dimensional Finite-Difference Ground-Water Flow Model", Techniques of Water Resources Investigations of the U.S. Geological Survey, book 6, U.S. Government Printing Office, Washington D.C.

McGovern, T., Guerin, T.F., Horner, S., and Davey, B. (2002), "Design, Construction and Operation of a Funnel and Gate In-Situ Permeable Reactive Barrier for Remediation of Petroleum Hydrocarbons in Groundwater", Water, Air, and Soil Pollution, 136, pp. 11–31.

McKinney, D.C., and Lin, M-D. (1994), "Genetic Algorithm Solution of Groundwater Management Models", Water Resources Research, 30(6), pp. 1897-1906.

McKinney, D.C., and Lin, M-D. (1996a), "Genetic Algorithms for the Design of Groundwater Remediation Systems", in Proc. North American Water and Environment Congress, ASCE, New York, N.Y.

McKinney, D.C., and Lin, M-D. (1996b), "Pump-and-Treat Ground-Water Remediation System Optimisation", Journal of Water Resources Planning and Management, 122(2), pp. 128-136.

McMahon, P.B., Dennehy, K.F., and Sandstrom, M.W. (1999), "Hydraulic and Geochemical Performance of a Permeable Reactive Barrier Containing Zero-Valent Iron, Denver Federal Centre", Ground Water, 37(3), pp. 396-404.

McMurty, D.C., and Elton, R.O. (1985), "New Approach to *In Situ* Treatment of Contaminated Groundwater", Environmental Progress, 4(3), pp. 168-170.

Meggyes, T., and Simon, F. (2000), "Removal of Organic and Inorganic Pollutants from Groundwater using Permeable Reactive Barriers. Part 2: Engineering of Permeable Reactive Barriers", Land Contamination & Reclamation, 8 (3), pp. 175-187.

MfE (1992), "Potentially Contaminated Sites in New Zealand: A Broad Scale Assessment", Ministry for the Environment, Wellington.

MfE (1995), "Discussion Document on Contaminated Sites Management", Ministry for the Environment, Wellington.

Ministry of Health (1995), "Drinking-Water Standards for New Zealand: 1995", Ministry of Health, Wellington.

Minsker, B.S., and Shoemaker, C.A. (1996), "Differentiating a Finite Element Biodegredation Simulation Model for Optimal Control", Water Resources Research, 32(1), pp. 187-192.

Minsker, B.S., and Shoemaker, C.A. (1998a), "Computational Issues for Optimal *In Situ* Bioremediation Design", ASCE Journal of Water Resources Planning and Management, 124(1), pp. 39-46.

Minsker, B.S., and Shoemaker, C.A. (1998b), "Dynamic Optimal Control of *In Situ* Bioremediation of Groundwater", ASCE Journal of Water Resources Planning and Management, 124(3), pp. 149-161.

Moon, H.S., Ahn, K.-H., Lee, S., Nam, K., and Kim, J.Y. (2004), "Use of Autotrophic Sulfur-Oxidizers to Remove Nitrate from Bank Filtrate in a Permeable Reactive Barrier System", Environmental Pollution, 129, pp. 499–507.

Morgan, D.R., Eheart, J.W., and Valocchi, A.J. (1993), "Aquifer Remediation Design under Uncertainty using a New Chance Constrained Programming Technique", Water Resources Research, 29(3), pp. 551-561.

Morrison, S. (1998), "Research and Application of Permeable Reactive Barriers", U.S. Department of Energy, Grand Junction Office, 56p.

Morrison, S.J., Metzler, D.R., and Dwyer, B.P. (2002), "Removal of As, Mn, Mo, Se, U, V and Zn from Groundwater by Zero-Valent Iron in a Passive Treatment Cell: Reaction Progress Modeling", Journal of Contaminant Hydrology, 56, pp. 99–116.

Murtagh, B.A., and Saunders, M.A. (1982), "A Projected Lagrangian Algorithm and its Implementation for Space Non-linear Constraints", Numerical Programming Study, 16, pp. 84-117.

Murtagh, B.A., and Saunders, M.A. (1987), "MINOS 5.1", Technical Report SOL 83-20R, Dept. of Operations Research, Stanford University, Stanford, California.

Mylopoulous, Y.A., Theodosiou, N., and Mylopoulous, N.A. (1999), "A Stochastic Optimization Approach in the Design of an Aquifer Remediation under Hydrogeologic Uncertainty", Water Resources Management, 13, pp. 335–351.

National Academy of Sciences (1978), "Nitrates: An Environmental Assessment", Washington D.C., *(in Starr and Gillham, 1993).*

National Academy of Sciences (1994), "Alternatives for Groundwater Cleanup", Report of the National Academy of Science Committee on Groundwater Cleanup Alternatives, National Academy Press, Washington D.C.

National Research Council (1993), "*In Situ* Bioremediation: When Does it Work?", National Academy Press, Washington D.C., *(in Minsker and Shoemaker, 1997b)*

Naymik, T.G., and Gantos, N.J. (1995), "Solute Transport Code Verification Report for RWLK3D, Internal Draft, Battelle Memorial Institute, Colombus, Ohio, *(in Gavaskar et al., 1998).*

NCCB (North Canterbury Catchment Board and Regional Water Board) (1986), "The Christchurch Artesian Aquifers, p100, *(in Woudberg, 1991).*

Nelson, L.B. (1972), "Agricultural Chemicals in Relation to Environmental Quality: Chemical Fertilisers, Present and Future", Journal of Environmental Quality, 1, pp. 2-6, *(in Askew, 1985).*

Neuman, S.P. (1973), "Calibration of Distributed Parameter Groundwater Flow Models Viewed as a Multiple Objective Decision Process Under Uncertainty", Water Resources Research, 9(4), pp. 1006-1021.

Nolan, B.T., Ruddy, B.C., Hitt, K.J., and Helsel, D.R. (1997), "Risk of Nitrate in Groundwaters of the United States – A National Perspective", Environmental Science and Technology, 31(8), pp. 2229-2236.

Nommik, H. (1956), "Investigations on Denitrification", Acta Agriculture Scandinavia, 6, pp. 195-228.

Novotny, V., and Chesters, G. (1981), "Handbook of Nonpoint Pollution; Sources and Management", Van Nostrand Reinhold Environmental Engineering Series, Litton Publishing Inc., New York.

NRC (National Research Council) (1978), "Nitrates: an Environmental Assessment. A Report Prepared by the Panel on Nitrates of the Coordinating Committee for Scientific and Technical Assessments of Environmental Pollutants", National Academy of Sciences, Washington D.C., *(in Askew, 1985).*

Nyer, E.K., and Duffin, M.E. (1997), "The State of the Art of Bioremediation", Ground Water Monitoring and Remediation, 17(2), pp. 64-69.

N.Z. Ministry of Health (2000), "Drinking Water Standards for New Zealand 2000", Ministry of Health, Wellington, New Zealand, ISBN 0-478-23964-5, 145p.

Oberlander, T.M., and Muller, R.A. (1978), "Physical Geography Today: A Portrait of a Planet (2nd Edition)", Random House Inc., *(in Askew, 1985).*

O'Brien, K., Keyes, G., and Sherman, N. (1997), "Implementation of a Funnel-and-Gate™ Remediation System", Proceedings 8th International Energy Week Conference and Exhibition, Houston, Texas, pp. 211-216.

Oh, B-T, and Alvarez, P.J.J. (2002), "Hexahydro-1,3,5-Trinitro-1,3,5-Triazine (RDX) Degradation in Biologically-Active Iron Columns", Water Air and Soil Pollution, 141, pp. 325–335.

Ott, N. (2000), "Permeable Reactive Barriers for Inorganics", U.S. Environmental Protection Agency, Office of Solid Waste and Emergency Response, Technology Innovation Office, Washington, DC, http://www.clu-in.org.

Painter, B.D.M. (2004), "Reactive Barriers: Hydraulic Performance and Design Enhancements", Ground Water, 42(4), pp. 609-619.

Papendick, R.I., and Runkles, J.R. (1965), "Transient-State Oxygen Diffusion in Soil: 1. The Case when Rate of Oxygen Consumption is Constant", Soil Science, 100(4), pp. 251-261.

Park, J-B., Lee, S-H., Lee, J-W., and Lee, C-Y. (2002), "Lab Scale Experiments for Permeable Reactive Barriers against Contaminated Groundwater with Ammonium and Heavy

Metals using Clinoptilolite (01-29B)", Journal of Hazardous Materials, B95, pp. 65–79.

Parkin, T.B. (1990), "Characterizing the Variability of Soil Denitrification", in *Denitrification in Soil and Sediment, Revbech, N.P. (Ed.)*, p213.

Pauwels, H., Kloppmann, W., Foucher, J-C., Martelat A. and Fritsche, V. (1998), "Field Tracer Test for Denitrification in a Pyrite-Bearing Schist Aquifer", Applied Geochemistry, 13 (6), pp. 767-778.

Pearlman, L. (1999), "Subsurface Containment and Monitoring Systems: Barriers and Beyond (Overview Report)", U.S. Environmental Protection Agency Office of Solid Waste and Emergency Response, Technology Innovation Office, Washington D.C., http://www.clu-in.org.

PEREBAR, (2001), "Long-term Performance of Permeable Reactive Barriers used for the Remediation of Contaminated Groundwater", 5th Framework Programme, Research and Technological Development Project, Contract Number: EVK1-CT-1999-00035, http://www.perebar.bam.de/.

Perrys (1999) *Personal communication with Perrys Consulting regarding per-unit construction costs for groundwater funnels and permeable reactive barriers in New Zealand.*

Phillips, R.E., Reddy, K.R., and Patrick, W.H. (1978), "The Role of Nitrate Diffusion in Determining the Order and Rate of Denitrification in Flooded Soils. Theoretical Analysis and Interpretation", Soil Sci. Soc. Amer. J., 42, pp. 272-, *(in Golterman, 1985).*

Pinder, G.F., and Abriola, L.M. (1982), "Calculation of Velocity in Three-Space Dimensions from Hydraulic Head Measurements", Ground Water, 20(2), pp. 205-209, *(in Gavaskar et al., 1998).*

Pollock, D.W. (1989), "Documentation of Computer Programs to Compute and Display the Pathlines using Results from the U.S. Geological Survey Modular Three-Dimensional Finite-Difference Groundwater Flow Model", Dept. of the Interior, U.S. Geological Survey, Open File Report 89-381, Reston, Virginia.

PRC Environment Management, Inc. (1996), "Naval Air Station Moffett Field, California, Iron Curtain Area Groundwater Flow Model", PRC, *(in Gavaskar et al., 1998).*

Ptacek, C.J. (1998), "Geochemistry of a Septic System Plume in a Coastal Barrier Bar, Point Pelee, Ontario, Canada", Journal of Contaminant Hydrology, 33, pp. 293-312.

Quinton, G.E., Buchanan, R.J. Jnr, Ellis, D.E., and Shoemaker, S.H. (1997), "A Method to Compare Groundwater Cleanup Technologies", Remediation, Autumn 1997, pp. 7-16.

Ranjithan, S., Eheart, J.W., and Garrett Jr, J.H. (1993). "Neural Network-Based Screening for Groundwater Reclamation under Uncertainty", Water Resources Research, 29(3), pp. 563-574.

Reed, P., Minsker, B., and Goldberg, D.E. (2000), "Designing a Competent Simple Genetic Algorithm for Search and Optimization", Water Resources Research, 36(12), pp. 3757-3761.

Reichard, E.G. (1995), "Groundwater-Surface Management with Stochastic Surface Water Supplies: A Simulation Optimisation Approach", Water Resources Research, 31(11), pp. 2845-2865.

Ritter, W.F., and Scarborough, R.W. (1995), "A Review of Bioremediation of Contaminated Soils and Groundwater", Journal of Environmental Science and Health, 30(2), pp. 333-357.

Ritzel, B.J., Eheart, J.W., and Ranjithan, S. (1994), "Using Genetic Algorithms to Solve a Multiple Objective Groundwater Pollution Containment Problem", Water Resources Research, 30(5), pp. 1589-1603.

Rizzo, D.M., and Dougherty, D.E. (1996), "Design Optimisation for Multiple Management Period Groundwater Remediation", Water Resources Research, 32(8), pp. 2549-2561.

Robertson, W.D., Blowes, D.W., and Ptacek, C.J. (1994), "Treatment of Agricultural Run-off", U.S. Patent 5,330,651 filed May 8, 1992, issued July 19, 1994, Canada Patent 2,068,283.

Robertson, W.D., and Cherry, J.A. (1995), "*In Situ* Denitrification of Septic-System Nitrate using Reactive Porous Media Barriers: Field Trials", Ground Water, 33, pp. 925-933.

Robertson, W.D., and Cherry, J.A. (1997), "Long-Term Performance of the Waterloo Denitrification Barrier", Land Contamination and Reclamation, 5(3), pp. 183-188.

Robertson, W.D., Blowes, D.W., Ptacek, C.J., and Cherry, J.A. (2000), "Long-Term Performance of In Situ Reactive Barriers for Nitrate Remediation", Ground Water, 38 (5), pp. 689-695.

Rockafellar, R.T., and Wets, R.J.-B. (1986a), "Linear-Quadratic Programming Problems with Stochastic Penalties: The Finite Generation Algorithm", in V.I. Arkin, A Shiraev and R.J.-B. Wets, (eds.), Stochastic Optimisation, Springer-Verlag, Berlin.

Rockafellar, R.T., and Wets, R.J.-B. (1986b), "A Lagrangian Finite Generation Technique for Solving Linear-Quadratic Problems in Stochastic Programming", Mathematical Programming Studies, 28, pp. 63-93.

Rogers, L.L. (1992). "Optimal Groundwater Remediation using Artificial Neural Networks and the Genetic Algorithm", Ph.D. thesis, Stanford University, Palo Alto, CA.

Rogers, L.L., and Dowla, F.U. (1994), "Optimisation of Groundwater Remediation using Artificial Neural Networks with Parallel Solute Transport Modelling", Water Resources Research, 30(2), pp. 457-481.

Rogers, L.L., Dowla, F.U., and Johnson, V.M. (1995), "Optimal Field-Scale Groundwater Remediation using Neural Networks and the Genetic Algorithm", Environmental Science and Technology, 29(5), pp. 1145-1155.

Rolston, D.E. (1981), "Nitrous Oxide and Nitrogen Gas Production in Fertilizer Loss", in *Denitrification, Nitrification and Atmospheric Nitrous Oxide*, Delwiche, C.C. (Ed.), John Wiley and Sons, New York, 286 pages.

Rorech, G.J., and Morello, B.S. (1995), "Groundwater Remediation Technology", Industrial Wastewater, November/December 1995, pp. 33-39.

Rosen, J.B. (1952), "Kinetics of a Fixed Bed System for Solid Diffussion into Spherical Particles", Journal of Chemical Physics, 20 (3), pp. 387-394, *(in Teutsch et al., 1997).*

Savoie, J.G., Kent, D.B., Smith, R.L., LeBlanc, D.R., and Hubble, D.W. (2004), "Changes in Ground-Water Quality near Two Granular-Iron Permeable Reactive Barriers in a Sand and Gravel Aquifer, Cape Cod, Massachusetts, 1997–2000", U.S. Geological Survey Water-Resources Investigations Report 03-4309 , 77 p.

Sawyer, C.S. (1992), "A Mixed-Integer Programming Model for Three Dimensional Groundwater Remediation Design", Ph.D. dissertation, University of Connecticut, Storrs.

Sawyer, C.S., Ahlfeld, D.P., and King, A.J. (1995), "Groundwater Remediation Design using a Three-Dimensional Simulation Model and Mixed-Integer Programming", Water Resources Research, 31(5), pp. 1373-1385.

Schipper, L.A., and Vojvodić-Vuković, M. (1998), "Nitrate Removal from Groundwater using a Denitrification Wall Amended with Sawdust: Field Trials", Journal of Environmental Quality, 27, pp. 664-668.

Schipper, L.A., and Vojvodić-Vuković, M. (1999a), "Denitrification Walls: A Practical Approach for Removing Nitrate from Shallow Groundwater", NZWWA 1999 Conference Papers, pp. 156-160.

Schipper, L.A. (1999b), "Groundwater Denitrification Wall: An Update", Water and Wastes in New Zealand, March 1999, pp. 46-47.

Schipper, L.A., and Vojvodić-Vuković, M. (2000), "Nitrate Removal from Groundwater and Denitrification Rates in a Porous Treatment Wall", Ecological Engineering, 14, pp. 269-278.

Schipper, L.A., and Vojvodić-Vuković, M. (2001), "Five Years of Nitrate Removal, Denitrification and Carbon Dynamics in a Denitrification Wall", Water Resources, 35, pp. 3473–3477.

Schipper, L.A., Barkle, G.F., Hadfield, J.C., Vojvodić-Vuković, M., and Burgess, C.P. (2004), "Hydraulic Constraints on the Performance of a Groundwater Denitrification Wall for Nitrate Removal from Shallow Groundwater", Journal of Contaminant Hydrology, 69, pp. 263– 279.

Schroth, M.H., Istok, J.D., Conner, G.T., Hyman, M.R., Haggerty, R., and O'Reilly, K.T. (1998), "Spatial Variability in In Situ Aerobic Respiration and Denitrification Rates in a Petroleum-Contaminated Aquifer", Ground Water, 36, pp. 925–937.

Sedivy, R.A., Schafer, J.M., and Bilbrey, L.C. (1999), "Design Screening Tools for Passive Funnel and Gate Systems", Groundwater Monitoring and Remediation, 19(1), pp. 125-133.

Shikaze, S., Austrins, C.D., Smyth, D.J.A., Cherry, J.A., Barker, J.F., and Sudicky, E.A. (1995), "The Hydraulics of a Funnel-and-Gate System: A Three-Dimensional Analysis", Solutions '95: International Association of Hydrogeologists Congress, June 5-7, Edmonton, Alberta, *(in Smyth et al., 1997)*.

Shikaze, S. (1997), "3D Numerical Modeling of Groundwater Flow in the Vicinity of Funnel-and-Gate Systems", Prepared by Allied Research Associates Inc. for U.S. Air Force, Tyndall Air Force Base, Florida, *(in Gavaskar et al., 1998).*

Shoemaker, S.H., Greiner, J.F., and Gillham, R.W. (1996), in *Assessment of Barrier Containment Technologies: A Comprehensive Treatment for Environmental Remediation Applications*. R.R. Rumer and J.K. Mitchell (Eds), Chapter 11: Permeable Reactive Barriers, report prepared for U.S. DOE, U.S. EPA, and DuPont Company.

Shouche, M., Petersen, J.N., and Skeen, R.S. (1993), "Use of a Mathematical Model for Prediction of Optimum Feeding Strategies for *In Situ* Bioremediation", Applied Biochemistry and Biotechnology, 39/40, pp. 763-779.

Simon, F., and Meggyes, T. (2000), "Removal of Organic and Inorganic Pollutants from Groundwater using Permeable Reactive Barriers. Part 1: Treatment Processes for Pollutants", Land Contamination & Reclamation, 8(2), pp. 103-116.

Simon, F., Meggyes, T., McDonald, C., and Tünnermeier, T. (2001), "In-Situ Reactive Barriers versus Pump-and-Treat Methods for Groundwater Remediation." Report on the Workshop held at the Federal Institute for Materials Research and Testing (BAM), Berlin, 18-19 October 2001.

Smalley, J.B., Minsker, B.S., and Goldberg, D.E. (2000), "Risk-Based in situ Bioremediation Design using a Noisy Genetic Algorithm", Water Resources Research, 36(10), pp. 3043-3052.

Smith, A., Hinton, E., and Lewis, R.W. (1983), "Civil Engineering System Analysis and Design", John Wiley & Sons Ltd., Chichester, *(in Howard et al., 1995).*

Smith, R.L. and Duff, J.H. (1988), "Denitrification in a Sand and Gravel Aquifer", Applied and Environmental Microbiology, 54(5), pp. 1071-1078.

Smith, R.L., Garabedian, S.P., and Brooks, M.H. (1996), "Comparison of Denitrification Activity Measurements in Groundwater using Cores and Natural-Gradient Tracer Tests", Environmental Science and Technology, 30, pp. 3448–3456.

Smith, D., and Lloyd-Jones, G. (1997), "Bioremediation: Harnessing Nature to Clean Up Pollution", Water and Wastes in New Zealand, 96, pp. 52-54.

Smith, C.C., Anderson, W.F., and Freewood, R.J. (2001), "Evaluation of Shredded Tyre Chips as Sorption Media for Passive Treatment Walls", Engineering Geology, 60, pp. 253-261.

Smith, R. L., J. K. Böhlke, S. P. Garabedian, K. M. Revesz, and T. Yoshinari (2004), "Assessing Denitrification in Groundwater using Natural Gradient Tracer Tests With ^{15}N: *In Situ* Measurement of a Sequential Multistep Reaction, Water Resources Research, 40, W07101, doi:10.1029/2003WR002919.

Smith, R.L., Buckwalter1, S.P., Repert D.A., and Miller, D.N. (2005), "Small-Scale, Hydrogen-Oxidizing-Denitrifying Bioreactor for Treatment of Nitrate-Contaminated Drinking Water", Water Research, 39 (10), pp. 2014-2023.

Smyth, D.J.A, Shikaze, S.G., and Cherry, J.A. (1997), "Hydraulic Performance of Permeable Barriers for *in situ* Treatment of Contaminated Groundwater", Land Contamination and Reclamation, 5(3), pp. 131-137.

Snape, I., Morris, C.E., and Cole, C.M., (2001), "The Use of Permeable Reactive Barriers to Control Contaminant Dispersal during Site Remediation in Antarctica", Cold Regions Science and Technology, 32, pp. 157-174.

Spector, M. (1998), "Production and Decomposition of Nitrous Oxide during Biological Denitrification", Water Environment Research, 70(5), pp. 1096-1098, and discussion with E. Stuart Savage, Water Environment Research, 71(1), p125.

Stanford, G., Van der Pol, R.A., and Dzienia, S. (1975), "Denitrification Rates in Relation to Total and Extractable Soil Carbon", Soil Science of America Proceedings, 39, pp. 284-289.

Starr, R.C., and Gillham, R.W. (1993), "Denitrification and Organic Carbon Availability in Two Aquifers", Ground Water, 31(6), pp. 934-947.

Starr, R.C., and Cherry, J.A. (1994), "In Situ Remediation of Contaminated Groundwater: The Funnel and Gate System", Ground Water, 32(3), pp. 465-476.

Steingruber, S.M., Friedrich, J., Gächter, R., and Wehrli, B. (2001), "Measurement of Denitrification in Sediments with the ^{15}N Isotope Pairing Technique", Applied and Environmental Microbiology, 67(9), pp. 3771-3778.

Stewart, L.W., Carlile, B.L., and Cassel, D.K. (1979), "An Evaluation of Alternative Simulated Treatments of Septic Tank Effluent", Journal of Environmental Quality, 8, pp. 397-403.

Suarez, M.P., and Rifai, H.S. (1999), "Biodegradation Rates for Fuel Hydrocarbons and Chlorinated Solvents in Groundwater", Bioremediation Journal, 3(4), pp. 337-362.

Sun, Y. (1995), "Optimisation of Pump-Treat-Inject Technology for Remediation of Contaminated Aquifers", Ph.D. thesis, Israel Institute of Technology, Haifa, Israel.

Teutsch, G., Tolksdorff, J., and Schad, H. (1997), "The Design of *in situ* Reactive Wall Systems – A Combined Hydraulical-Geochemical-Economical Simulation Study", Land Contamination and Reclamation, 5(3), pp. 125-130.

Therrien, R., and Sudicky, E. (1995), "Three-Dimensional Analysis of Variably-Saturated Flow and Solute Transport in Discreetly-Fractured Porous Media", Journal of Contaminant Hydrology, 23, pp. 1-44, ***(in Gavaskar et al., 1998).***

Tiedeman, C., and Gorelick, S.M. (1993), "Analysis of Uncertainty in Optimal Groundwater Contaminant Capture Design", Water Resources Research, 29(7), pp. 2139-2153.

Tiedje, J.M. (1988), "Ecology of Denitrification and Dissimilatory Nitrate Reduction to Ammonium", in *Biology of Anaerobic Microorganisms*, Zehnder, A.J.B. (ed.) John Wiley & Sons, Inc., pp. 179-244.

Todd, D.K. (1980), "Groundwater Hydrology (2nd Edition)", John Wiley & Son, New York.

Trudell, M.R., Gilham, R.W., and Cherry, J.A. (1986), "An In Situ Study of the Occurrence and Rate of Denitrification in a Shallow and Unconfined Aquifer", Journal of Hydrology, 83, pp. 251–268.

Tucciarelli, T., Karatzas, G.P., and Pinder, G.F. (1998), "A Primal Method for the Solution of the Groundwater Quality Management Problem", Operations Research, 46(4), pp. 463-473.

Tung, Y.-K. (1986), "Groundwater Management by Chance-Constrained Model", Journal of Water Resources Planning and Management, 112(1), pp. 1-19.

Tünnermeier, T., Simon, F.-G., and Meggyes, T. (2001), "Longevity of Permeable Reactive Barriers", Poster presentation at Permeable Reactive Barrier (PRB) Technology and its Current Status, 1st Workshop of the Permeable Reactive Barrier Network, April 26-27, 2001, Belfast, Northern Ireland, UK, http://www.perebar.bam.de.

U.S. Air Force (1997), "Design Guidance for Application of Permeable Barriers to Remediate Dissolved Chlorinated Solvents", U.S. Air Force, Environics Directorate, Tyndall AFB, Florida, Report DG1110-345-117, 192p.

U.S. Environmental Protection Agency (1973), "Nitrogenous Compounds in the Environment", U.S. Government Printing Office, Washington D.C., EPA-SAB-73-001, *(in Starr and Gillham, 1993).*

U.S. Environmental Protection Agency (1993), "Revisions to OMB Circular A-94 on Guidelines and Discount Rates for Benefit-Cost Analysis", Revised annually at http://www.whitehouse.gov/OMB/circulars/a094/a094.html#ap-c.

U.S. Environmental Protection Agency (1998), "Permeable Reactive Barrier Technologies for Contaminant Remediation", U.S. Government Printing Office, Washington D.C., EPA/600/R-98/125, 94p.

U.S. Environmental Protection Agency (1999), "Field Applications of *In Situ* Remediation Technologies: Permeable Reactive Barriers", U.S. Government Printing Office, Washington D.C., EPA-542-R-99-002, 122p.

U.S. Environmental Protection Agency (2001), "Cost Analyses for Selected Groundwater Cleanup Projects: Pump and Treat Systems and Permeable Reactive Barriers", U.S. Government Printing Office, Washington D.C., EPA 542-R-00-013, 23p.

U.S. Environmental Protection Agency (2002a), "Field Applications of *In Situ* Remediation Technologies: Permeable Reactive Barriers", U.S. Government Printing Office, Washington D.C., Contract 68-W-00-084, 30p.

U.S. Environmental Protection Agency (2002b), "Economic Analysis of the Implementation of Permeable Reactive Barriers for Remediation of Contaminated Ground Water", U.S. Government Printing Office, Washington D.C., Contract 68-C-99-256, 42p.

U.S. Environmental Protection Agency (2004a), "Biological PRB used for Perchlorate Degradation in Ground Water", Technology News and Trends, Issue 10, pp. 2-3.

U.S. Environmental Protection Agency (2004b), "Accelerating Site Closeout, Improving Performance, and Reducing Costs through Optimization", Conference Proceedings, June 15-17, 2004, Dallas, Texas.

Van der Hoek, J.P., Zwanikken, B., Griffioen, A.B., and Klapwijk, A. (1988), "Modelling and Optimisation of the Combined Ion Exchange/Biological Denitrification Process for Nitrate Removal from Ground Water", Journal for Water and Wastewater Research, 21(3), pp. 85-91.

Vidic, R.D., and Pohland, F.G. (1996), "Treatment Walls", Ground-Water Remediation Technologies Analysis Centre, TE-96-01, http://www.gwrtac.org.

Vidic, R.D. (2001), "Permeable Reactive Barriers: Case Study Review", Ground-Water Remediation Technologies Analysis Centre, http://www.gwrtac.org.

Vidumsky, J.E., and Landis, R.C. (2001), "Probabilistic Design of a Combined Permeable Barrier and Natural Biodegradation Remedy", in Volume 8, Bioaugmentation, Biobarriers, and Biogeochemistry, 2001 Bioremediation Symposium, Battelle Book 1-57477-118-3, San Diego, CA.

Viets, F.G., and Hageman, R.H. (1971), "Factors Affecting the Accumulation of Nitrate in Soil, Water, and Plants", Agricultural Handbook No. 413, U.S. Dept. of Agriculture, *(in Askew, 1985).*

Vogan, J.L. (1993), "The Use of Emplaced Denitrifying Layers to Promote Nitrate Removal from Septic Effluent", M.Sc. thesis, Dept. of Earth Sciences, Univ. of Waterloo, Waterloo Ontario.

Volokita M., Abeliovich A, and Soares, M.I.M. (1996), "Denitrification of Groundwater Using Cotton as Energy Source", Water Science and Technology, 34 (1-2), pp. 379-385.

Von Gunten, U., and Zobrist, J. (1992), "Redoxprozesse in Grundwasser-Infiltrations-Systemen: Experimentelle Simulation in Kolonnen, Vom Wasser, 78, pp. 259-271, *(in Zysset et al., 1994).*

Von Gunten, U., and Zobrist, J. (1993), "Biogeochemical Changes in Groundwater-Infiltration Systems: Column Studies", Geochim. Cosmochim. Acta, 57, pp. 3895-3906, *(in Zysset et al., 1994).*

Wagner, B.J., and Gorelick, S.M. (1989), "Reliable Aquifer Remediation in the Presence of Spatially Variable Hydraulic Conductivity: From Data to Design", Water Resources Research, 25(10), pp. 2211-2225.

Wagner, B.J. (1995), "Recent Advances in Simulation-Optimisation Groundwater Management Modelling", Reviews of Geophysics, Supplement, pp. 1021-1028.

Wagner, J.M. (1988), "Stochastic Programming with Recourse Applied to Groundwater Quality Management", Ph.D. thesis, Mass. Inst. of Technol., Cambridge.

Wagner, J.M., Shamir, U., and Nemati, H.R. (1992), "Groundwater Quality Management under Uncertainty: Stochastic Programming Approaches and the Value of Information", Water Resources Research, 28(5), pp. 1233-1246.

Wagner, J.M., Shamir, U., and Marks, D.H. (1994), "Containing Groundwater Contamination: Planning Models using Stochastic Programming with Recourse", European Journal of Operational Research, 77, pp. 1-26.

Wakatsuki, T., Esumi, H., and Omura, S. (1993), "High Performance and N & P-Removal On-Site Domestic Waste Water Treatment System by Multi-Soil-Layering Method", Water Science and Technology, 27(1), pp. 31-40, *(in Carmichael, 1994).*

Waller, G.R. (1994), "Development of a Design Basis for the Use of In-Situ Permeable Reactor Walls for Groundwater Remediation", M.Sc. Thesis, University of Austin, Texas.

Wang, F., Bright, J., and Hadfield, J. (2003), "Simulating Nitrate Transport in an Alluvial Aquifer: a Three-Dimensional N-Dynamics Model", Journal of Hydrology (N.Z.), 42(2), pp. 145-162.

Wang, M., and Zheng, C. (1997), "Optimal Remedial Policy Selection under General Conditions", Ground Water, 35(5), pp. 757-764.

Wang, M., and Zheng, C. (1998), "Ground Water Management Optimization using Genetic Algorithms and Simulated Annealing: Formulation and Comparison", Journal of the American Water Resources Association, 34(3), pp. 519-530.

Wang, W., and Ahlfeld, D.P. (1994), "Optimal Groundwater Remediation with Well Location as a Decision Variable: Model Development", Water Resources Research, 30(5), pp. 1605-1618.

Ward, S.G. (1995), "An Investigation of Nitrate in Groundwater Adjacent to Bardowie Farm, Hautapu, Cambridge, New Zealand", M.Sc. (Technology) in Earth Sciences thesis, University of Waikato, New Zealand.

Warner, S.D., Yamane, C.L., Gallinatti, J.D., and Hankins, D.A. (1998), "Considerations for Monitoring Permeable Ground-Water Treatment Walls", Journal of Environmental Engineering, 124(6), pp. 524-529.

Waterloo Hydrogeologic, Inc. (1996), "FLOWPATH Users Manual, Version 5.2.", Waterloo, Ontario, *(in Gavaskar et al., 1998).*

Well, R., Augustin, J., Meyer, K., and Myrold, D.D. (2003), "Comparison of Field and Laboratory Measurement of Denitrification and N_2O Production in the Saturated Zone of Hydromorphic Soils", Soil Biology and Biochemistry, 35, pp. 783-799.

Whiffen, G.J., and Shoemaker, C.A. (1993), "Non-linear Weighted Feedback Control of Groundwater Remediation under Uncertainty", Water Resources Research, 29(9), pp. 3277-3289.

Wilson, R.D., and Mackay, D.M. (1995), "A Method for Passive Release of Solutes from an Unpumped Well", Ground Water, 33(6), pp. 936-945.

Wijedasa, H.A., and Kemblowski, M.W. (1993), "Bayesian Decision Analysis for Plume Interception Wells", Ground Water, 31(6), pp. 948-952.

Woinarski, A.Z., Snape, I., Stevens, G.W., and Stark, S.C. (2003), "The Effects of Cold Temperature on Copper Ion Exchange by Natural Zeolite for use in a Permeable Reactive Barrier in Antarctica", Cold Regions Science and Technology, 37, pp. 159-168.

Woudberg, L.J. (1991), "Nitrate Contamination of Groundwater in New Zealand: Obstacles to the Decision Agenda", M.Sc. Thesis, Lincoln University, New Zealand.

WPCF (Water Pollution Control Federation), (1983), "Nutrient Control: Manual of Practice No. FD-7", Prepared by Task Force of Nutrient Control, Water Pollution Control Federation.

Xiang, Y., Sykes, J.F., and Thomson, N.R. (1995), "Alternative Formulations for Optimal Ground-Water Remediation Design", Journal of Water Resources Planning and Management, 121(2), pp. 171-181.

Xiang, Y., Sykes, J.F., and Thomson, N.R. (1996), "Optimisation of Remedial Pumping Schedules for a Ground-Water Site with Multiple Contaminants", Ground Water, 34(1), pp. 2-11.

Yang, X., Fan, L.T., and Erickson, L.E. (1995), "A Conceptual Study on the Bio-Wall Technology: Feasibility and Process Design", Remediation, Winter 1995/96, pp. 55-67.

Yeomans, J.C., Bremner, J.M., and McCarty, C.W. (1992), "Denitrification Capacity and Denitrification Potential of Subsurface Soils", Communications in Soil Science and Plant Analysis, 23, pp. 919–927.

Yoon, J., and Shoemaker, C.A. (1999), "Comparison of Optimization Methods for Ground-Water Bioremediation", Journal of Water Resources Planning and Management, 125(1), pp. 54-63.

Young, C.P. (1981), "The Distribution and Management of Solutes Derived from Agricultural Land in the Principal Aquifers of the United Kingdom with Special Reference to Nitrate", Water Science Technology, 13, pp. 1137-1152.

Zhen, C., and Uber, J.G. (1996), "Reliability of Remediation Designs in Presence of Modeling Error", Journal of Water Resources Planning and Management, 122(4), pp. 253-261.

Zheng, C. (1990), "MT3D Users Manual, Version 1.1", S.S. Papadopulos and Associates Inc., Rockville, Maryland.

Zheng, C., and Wang, P. (1999), "An Integrated Global and Local Optimisation Approach for Remediation System Design", Water Resources Research, 35(1), pp. 137-148.

Zysset, A., Stauffer, F., and Dracos, T. (1994), "Modeling of Reactive Groundwater Transport Governed by Biodegradation", Water Resources Research, 30(8), pp. 2423-2434.

Appendix A

Nitrate Contamination of Groundwater Systems

A.1 Introduction

The objective of the following appendix is to describe the general features of a groundwater system and the factors controlling the processes by which groundwater is contaminated with nitrate. The description is based on the assumption that regardless of its source, nitrate enters groundwater by moving through the soil-water zone overlying the water table. Groundwater contamination must therefore be a function of three factors:

1. the ability of nitrate to move within soil and water without losing its chemical identity,
2. the existence of a sufficient pool of nitrate within the soil-water zone, and
3. the existence of a mechanism whereby nitrate can be transported (leached) from the soil-water zone to the groundwater system.

A.2 Groundwater Systems

Subsurface water is a term used to denote all the water beneath the surface of the ground. The term *groundwater* is usually reserved for subsurface water that occurs beneath the water table in soils and geologic formations that are fully saturated. Water also occurs underground in unsaturated zones where interstices (gaps) are filled with both water and air. Groundwater is just one part of the earth's *hydrologic cycle,* which encompasses the endless circulation of water between ocean, atmosphere and land. Our interest centres on the land-based portion of the cycle as it might be operative on an individual watershed. Figure A.1 presents a schematic diagram of the hydrologic cycle on a watershed.

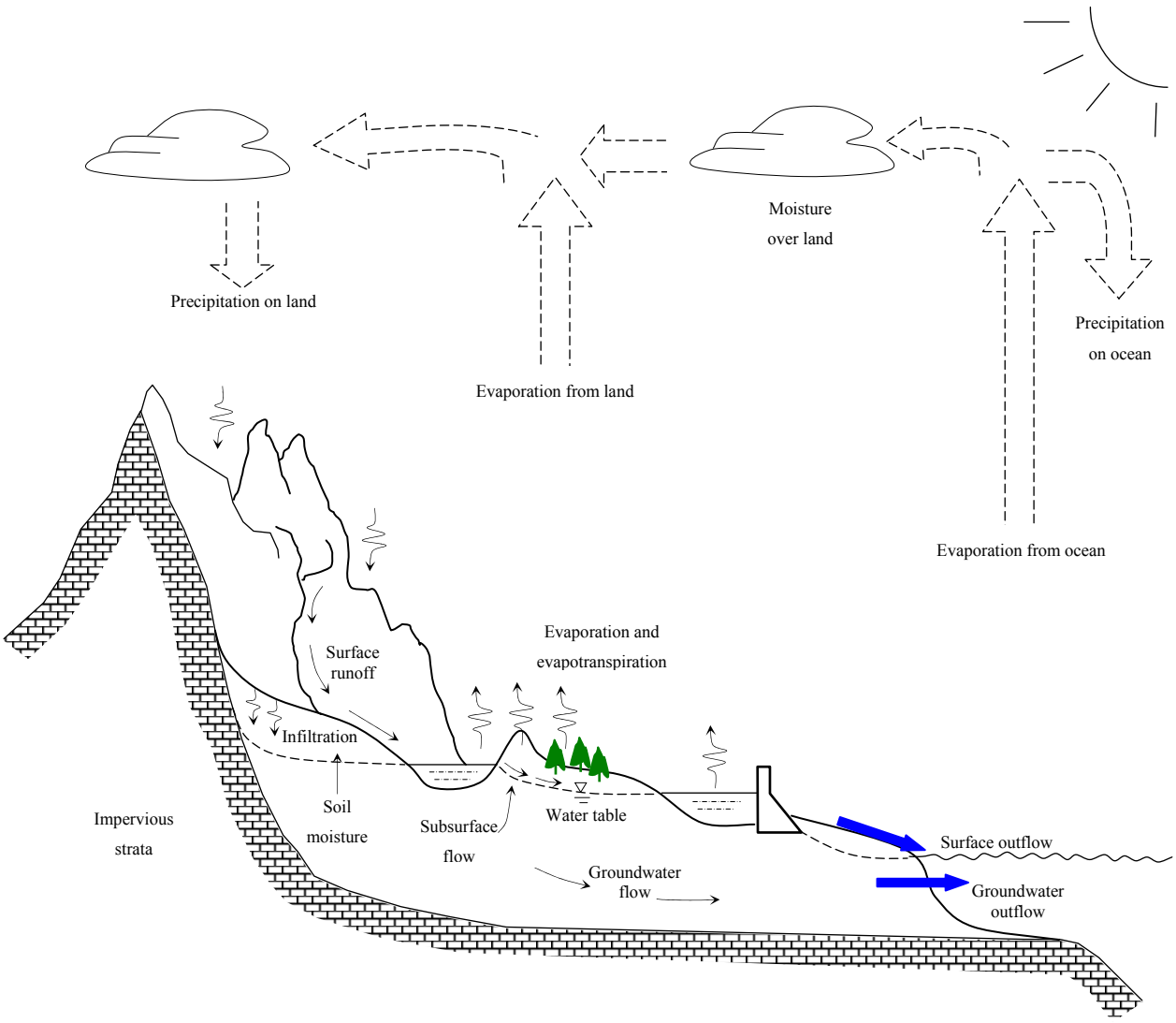

Fig. A.1. The hydrologic cycle (source: Chow et. al., 1988).

Inflow to the hydrologic system arrives as *precipitation*, in the form of rainfall or snowmelt. Outflow takes place as *streamflow* (or runoff) and as *evapotranspiration*, a combination of evaporation from open bodies of water, evaporation from soil surfaces, and transpiration from the soil by plants. Precipitation is delivered to streams on the land surface as *overland* flow to tributary channels. It is also delivered to streams by subsurface flow routes, as *interflow* and *baseflow* following *infiltration* into the soil.

A.2.1 Aquifers, Aquitards and Aquiludes

Groundwater is present in geological formations known as *aquifers*, *aquitards*, and *aquiludes*. *Freeze and Cherry* [1979] provide the following definitions. An *aquifer* is a "saturated permeable geologic unit that can transmit significant quantities of water under ordinary hydraulic gradients". *Aquitards* are layers that are much less pervious than the aquifer that underlies or overlies them, and often also much thinner. They "may be permeable enough to transmit water in quantities that are significant in the study of regional groundwater flow, but their permeability is not sufficient to allow the completion of production wells within them." An *aquilude* is "a saturated geologic unit that is incapable of transmitting significant quantities of water under ordinary hydraulic conditions."

Aquifers are usually classified according to their pressure system. A *confined* (or *pressure*) *aquifer* is an aquifer that is confined between two aquitards. An *unconfined* (*phreatic*, *water table*) *aquifer* is an aquifer in which the water table forms the upper boundary. Confined aquifers occur at depth, unconfined aquifers near the ground surface. There are special cases of both confined and unconfined aquifers, for example, artesian aquifers, perched aquifers, leaky phreatic aquifers, and leaky confined aquifers.

Water enters an aquifer through an area of recharge, an area where the water-bearing stratum is exposed to the atmosphere or is overlain by a permeable medium. It then moves from topographical highs to topographical lows under the influence of an effective potential gradient (gravity), and is discharged at a series of natural sites or abstracted at wells. For unconfined aquifers the whole surface area above the groundwater system can contribute to recharge. In areas with confined aquifers, the recharge area may be far removed from the points of discharge.

Without human interference, an aquifer fills and discharges excess water via several routes until quasi-equilibrium is reached. The principal sources of recharge are influent rivers and rainfall. The principal sources of discharge are effluent rivers and springs where the water table intersects the earth's surface. Where the water table is close to the surface, groundwater may also be discharged by direct evaporation or by plants that have deep roots (phreatophytes).

These various channels of groundwater discharge may be viewed as spillways of the groundwater reservoir. When groundwater levels are high, discharge through natural spillways tends to maintain a balance between inflow and outflow. During dry periods, natural discharge is reduced as the water table falls and may eventually cease. Confined aquifers do not undergo this natural adjustment as fast as unconfined aquifers.

From the preceding description, it is obvious to conclude that groundwater recharge provides the mechanism by which a compound can be leached from the soil zone into the groundwater system, while groundwater flow will move this compound down-gradient to some point of discharge. This process can be further clarified by more detailed descriptions of the various subsurface moisture zones.

A.2.2 Subsurface Moisture Zones

The saturated and unsaturated zones in a groundwater system are referred to as the *phreatic* and *aerated zones* respectively. Figure A.2 shows a schematic distribution of these zones for a homogeneous soil. The aerated zone usually consists of three sub-zones: the *soil-water zone*, the intermediate zone (or *vadose zone*), and the *capillary zone* (or *capillary fringe*). The boundary between the phreatic and aerated zones is known as the phreatic surface. This surface may be impervious under some circumstances (e.g., a confined aquifer).

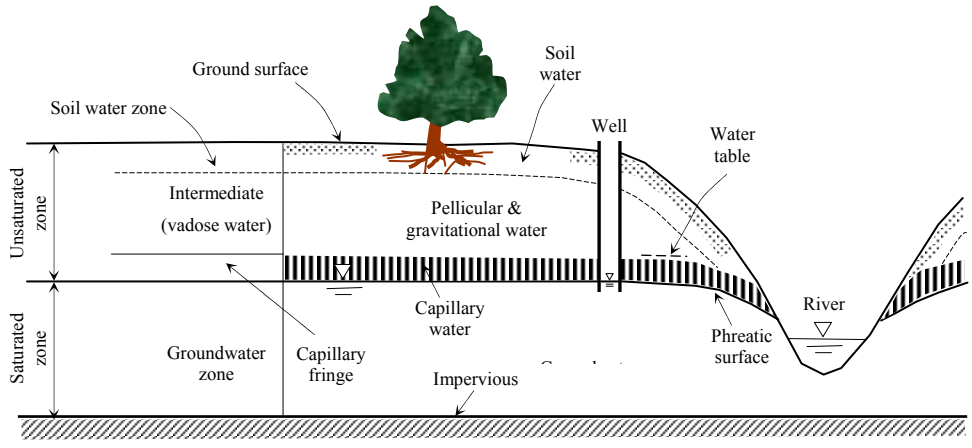

Fig. A.2. Subsurface moisture zones (source: Bear and Verruijt, 1987).

During the past few decades much research has been undertaken on improving our understanding of the process of water movement through a porous media. Once a solute such as nitrate enters a groundwater system, it is transported along with the mass flow of water. This movement is termed *advective* flow. The solute will also undergo *hydrodynamic dispersion*, which is a combination of mechanical mixing (velocity dependent) and molecular diffusion (time dependent). Over time these processes will result in an increasing contaminated zone with decreasing concentration (see Figure A.3). The rate and direction of flow are significantly affected by physical properties of the aquifer such as the heterogeneity and anisotropy within the aquifer. These processes are described in more detail in Section 1.2.1.

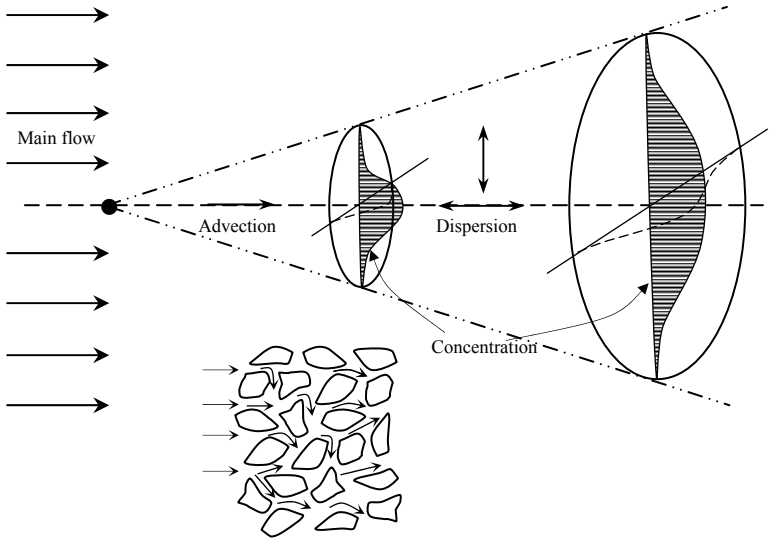

Fig. A.3. Pollutant spread in groundwater zones from a continuous source by advection and dispersion (source: Novotny and Chesters, 1981).

A.3 Biochemistry of Nitrogen

A.3.1 The Nitrogen Cycle

The major nitrogen species of the biosphere are all interrelated by a complicated series of biogeochemical processes known collectively as the *Nitrogen Cycle*. It is this cycle that determines the amount of nitrate available to be leached from the soil zone.

In its generalised form the cycle is divided into two sub-cycles. The first of these is characteristic of many of nature's mineral element cycles. Inorganic nitrogen, principally as nitrate and ammonium, is assimilated by plants and is either synthesised into structural material or is utilised as an active participant in the processes of the cytoplasmic membrane (surrounding the cellular contents of the plant, but excluding the nucleus). This organic material is then either consumed by animals or is returned directly to the soil. In either case, the eventual repository for this organic material is the soil, where microbial decomposition returns the nitrogen to its organic forms to begin a new repetition of the cycle.

Superimposed on this cycle is the denitrification reaction whereby nitrate ions in the subsurface serve as an electron acceptor in a series of oxidation reactions. As a result, nitrate is eventually reduced to nitrogen gas (or nitrous oxide) and is lost to the atmosphere. These forms of nitrogen are usable to most plants unless 'fixed' by specialist symbiotic and non-symbiotic microorganisms.

Obviously the Nitrogen Cycle is vastly more complex than is described above. A more accurate title might be the *Nitrogen Web*, as the idea of two simple loops superimposed on each other bears little relation to reality.

The literature contains numerous diagrams of the cycle with formats and scales reflecting the different perspectives and purposes of the authors. Figure A.4 illustrates the cycle with emphasis placed on those sources and transfers of nitrogen most relevant to the occurrence of nitrate in groundwater. Within this format, three distinct zones are recognised:

(1) *outside interchanges*, representing the sources and sinks of nitrate removed from the subsurface;
(2) *oxidising conditions*, representing the area of the soil profile above the water table; and
(3) *reducing conditions*, representing the area of the soil profile below the water table.

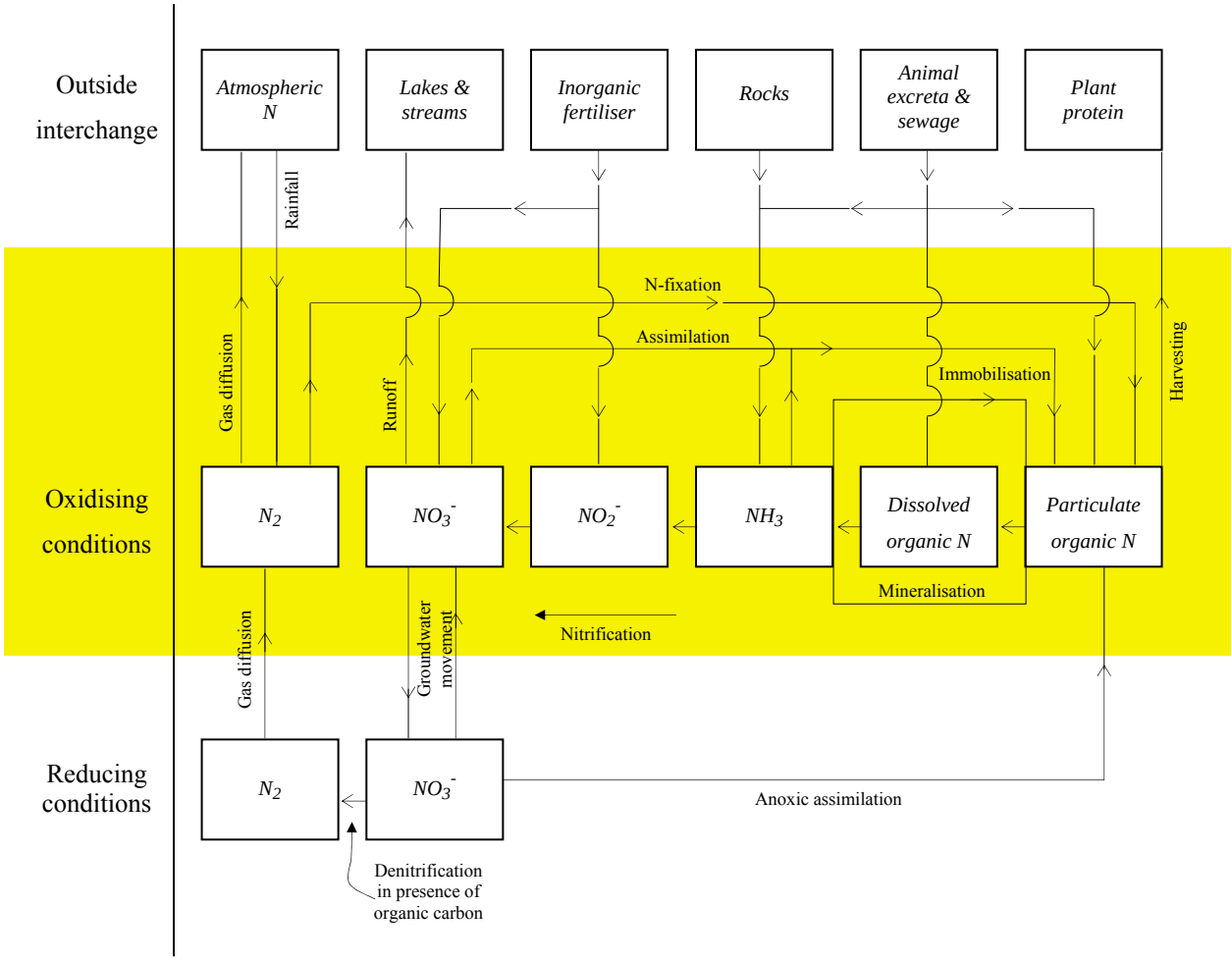

Fig. A.4. Simplified N-cycle with respect to the occurrence of nitrate in groundwater (source: AWRC, 1983).

The biospheric nitrogen cycle is driven primarily by biological transformations, although the atmospheric reactions in the cycle are chemical and photochemical. In terrestrial and aquatic systems, the major non-biological processes of the cycle involve phase transformations rather than chemical reactions. Despite the apparent complexity of Figure A.4, the presented biological transformations of nitrogen comprise only six major processes:

(1) *assimilation* of inorganic forms by plants and microorganisms to form organic nitrogen;

(2) *heterotrophic conversion* of organic nitrogen from one organism (food or prey) to another organism (consumer or predator);

(3) *ammonification*, the decomposition of organic nitrogen to ammonium;

(4) *nitrification*, the oxidation of ammonium to nitrite and nitrate;

(5) *denitrification*, the bacterial reduction of nitrate to nitrous oxide (N_2O) and molecular nitrogen (N_2) under anoxic (reducing) conditions; and

(6) *nitrogen fixation*, the reduction of nitrogen gas to ammonium and organic nitrogen by various microorganisms.

The detail of these processes will not be discussed here, but it is important to note that the cycle and its components are constrained by the principals of mass conservation. In the soil, for example, mass conservation requires that for some time period (Δt):

Net Change (NO_3) = Inputs – Outputs + Production – Consumption

where:
Net Change (NO_3) – Net change of NO_3 in soil volume during Δt;
Inputs – Inputs into the system via the boundaries during Δt;
Outputs – Outputs from the system via the boundaries during Δt;
Production - NO_3 production during Δt;
Consumption - NO_3 consumption during Δt;

and the boundaries are the ground surface and the base of the rooting or soil zones.

The preceding equation summarises all the processes that affect nitrate in the soil. Nitrate is transported in and out of the soil by various agencies, and, within the soil it may be produced and consumed in various transformations. Over time, mature undisturbed ecosystems tend toward quasi-equilibrium between inputs, outputs, production and consumption. For natural ecosystems the direct input of nitrate is minimal, while consumption tends to be limited by the rate of production. As a result, very little nitrate is ever made available for leaching except where there are circumstances that cause major changes to the rates of production and consumption.

Large, direct inputs of nitrate into the soil, or changes in the rate at which it is produced, can often exceed an ecosystem's capacity of assimilation. The result is that large quantities of nitrate are made available to be leached to groundwater. Such inputs and changes can be referred to as 'sources' of nitrate contaminated groundwater.

A.3.2 Sources of Nitrogen

The optimal method of treating groundwater contamination includes identifying the source of the problem so that further contamination can be minimised. However, if multiple sources of contamination exist, the differentiation between sources and identification of all possible sources can be very difficult to determine. Research into the use of stable isotopes to differentiate between multiple sources of contamination shows promise (e.g. *Aravena et al.*, 1993) but is not conclusive. Our knowledge of the complex processes and interrelationships between processes in terrestrial and aquatic ecosystems is also not complete yet. The key to approaching a particular nitrate contamination problem is therefore to thoroughly investigate the relevant ecosystem and the potential sources of nitrogen to that system.

There are seven basic sources of nitrogen: *soil nitrogen, animal wastes, commercial fertilisers, sewage outflows, municipal and industrial wastes, precipitation and the atmosphere, and natural sources*. Land use and waste disposal practices determine the impact of these nitrogen sources on the groundwater system. Table A.1 presents the relative impact of various practices on groundwater nitrate contamination in Canterbury, New Zealand. The remainder of this section is dedicated to describing the sources of nitrogen.

Table A.1
The Relative Impact of Various Practices on Groundwater Nitrate Contamination in Canterbury, New Zealand (sources: Burden, 1982 and NCCB, 1986).

Source	Type	Percentage
Dryland pasture	Non-point	36.0
Irrigated pasture	Non-point	29.0
Crop and horticultural land	Non-point	26.0
Piggeries, dairy farms, meat works	Point	5.9
Septic tanks	Point/Non-point	3.0
Land disposal of waste	Point	0.1

A.3.2.1 Soil nitrogen

The dominant storage of nitrogen in the soil is in the form of organic matter (~99%). From the Nitrogen Cycle we know that this pool is being added to by the breakdown of plant, animal and microbial material, and depleted by the process of mineralisation. However, soils vary greatly in their organic matter content, ranging from nearly 100 percent to less than 1 percent. Similarly, the nitrogen content of the soils organic matter can be highly variable, although 5 percent is considered a reasonable average.

One of the most widespread sources of nitrate in groundwater is from deep soil cultivation. Ploughing of old established grassland destroys naturally developed soil profiles, aerates lower soil zones and, in association with fallowing, increases the depth of moisture penetration. This leads to the decomposition of soil organic matter and the stimulation of the rates of nitrate mineralisation (*Young*, 1981).

Although the majority of soil nitrogen released in natural ecosystems is recycled within plants and animals, nitrogen can also be added to the soil's pool of organic matter through nitrogen fixation. This occurs when certain free-living bacteria convert molecular nitrogen (N_2) to ammonia (NH_3). Ammonia exists in solution as the ammonium ion (NH_4^+), a salt that higher organisms such as legumes can use. Figure A.5 shows the microbial relationships between nitrogen fixation, nitrification, and denitrification.

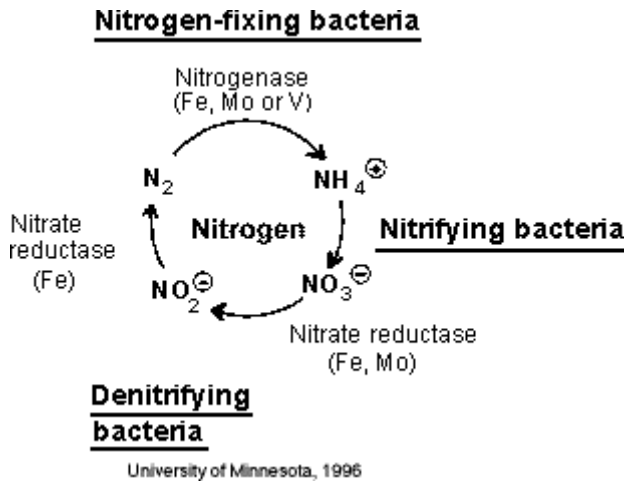

Fig. A.5. Microbial relationships between nitrogen fixation, nitrification, and denitrification (source: University of Minnesota website)

A.3.2.2 Animal wastes

Based on U.S. agricultural data, the NAS Committee on Nitrate Accumulation (AWRC, 1983) determined the approximate rate at which nitrogenous wastes are excreted by livestock. The greatest concentration of nitrogen is in urine and is a form readily available to plant growth. Only mature, healthy monogastric animals on good diets can excrete nitrogen as nitrate in urine (*Viets and Hageman*, 1971). However, urea and uric acid are rapidly hydrolysed to ammonium. This ammonium is either lost as ammonia by the process of volatilisation, or is reduced to nitrate via the process of nitrification (see Figure A.5 above).

Provided farmland is not over-stocked, animal wastes do not provide a significant nitrate contamination risk. However, high-density confinement of animals (for production efficiency or to escape harsh weather conditions) does pose a threat in terms of potential nitrate contamination.

A.3.2.3 Commercial fertilisers

Chemical nitrogenous fertilisers are generally made up of relatively simple inorganic compounds, the most common being urea, ammonia, ammonium nitrate, ammonium sulphate and ammonium polyphosphate (*Nelson*, 1972).

Even under ideal soil conditions, where no leaching occurs, it is rare for total nitrogen recoveries in crops to be greater than 95 percent of that applied. It is therefore not surprising that under average field conditions fertiliser recoveries in crops are often only between 50 and 60 percent (*AWRC*, 1983). Consequently, residual nitrate can accumulate rapidly in the soil if fertilisers are applied at rates that bring maximum crop yield. Large rainfall occurrences or over-irrigating practices will then flush this nitrate into the groundwater system, resulting in a potential contamination problem.

A.3.2.4 Sewage outflows

The average adult excretes essentially all the protein nitrogen consumed. It is estimated that the contribution of nitrogen from human wastes amounts to approximately 5 kg of nitrogen per person per year (*AWRC*, 1983). Therefore, sewage effluent percolation ponds and septic tanks in unsewered areas pose a potential nitrate contamination risk.

Most sewage treatment plants follow similar procedures. Raw sewage first undergoes primary sedimentation to remove the bulk of the solid organic matter. The supernatant fluid is then aerated to oxidise the organic and nitrogenous compounds. The resultant fluid, rich in ammonia, is rapidly nitrified by the appropriate bacteria to nitrite and nitrate. A period of induced anaerobiosis allows for the denitrification of this nitrogen and, following secondary sedimentation and chlorination, the treated effluent is discharged. The solid is then disposed of by burial, incineration or spreading on the land (*AWRC*, 1983).

These treatment procedures frequently remove less than half the nitrogen present in the waste. If disposal guidelines are not adhered to, this solid waste will pose a significant nitrate contamination risk.

A.3.2.5 Municipal and industrial wastes

Urbanisation has created other sources of nitrogenous wastes in addition to sewage. Waste water and industrial by-products, particularly from the fuel, food processing, dairy and meat industries are significant sources of nitrogenous waste. Refuse, much of which is dumped in high concentration on relatively small sites, also has the potential to leach nitrate into the groundwater system. In these situations the rate of loss is much slower than the rate of addition, suggesting that these sources are likely to continue releasing nitrates long after the site is filled and abandoned (*AWRC*, 1983).

A.3.2.6 Precipitation and the atmosphere

The nitrogen content of precipitation has been studied in many parts of the world. This nitrogen may be in the form of ammonia, nitrate and some organic components formed during the processes of volatilisation and combustion. Rainfall generally returns about twice as much ammonia as it does nitrate (*AWRC*, 1983). The amount of nitrogen in precipitation varies greatly around the world, but is only likely to pose a potential contamination risk near heavy industrial areas.

A.3.2.7 Natural sources

Natural deposits of nitrate occur in cave, caliche, guano and playa deposits. The most significant deposits are situated on the eastern slopes of the Coast Ranges of the Atacana Desert in Chile. There are also a number of locations in California and Nevada where nitrates

have naturally accumulated, and may, as shown by Headden (*Baber*, 1977) in Colorado, provide a source of nitrate in the groundwater.

A.4 Physical and Chemical Properties of Nitrate

The third factor controlling the contamination of groundwater by nitrate is the ability of the compound to move relatively freely within soil and water without losing its identity. This feature of nitrate depends on its physical and chemical properties.

Nitrate is the most oxidised form of nitrogen (+5) and as such exhibits a negative charge (anion). The nitrate salts of all common metals are quite soluble in water. However, when in dilute aqueous solutions, nitrate is chemically unreactive. Nearly all of its transformations are mediated biochemically. Nitrate also has very little tendency to form co-ordination complexes with metal ions in dilute aqueous solutions (*NRC,* 1978).

Ammonium on the other hand, is the most reduced form of nitrogen (-3) and exhibits a positive charge (cation). Although also readily soluble, ammonium is chemically volatile in dilute aqueous solutions that are basic in pH (*NRC,* 1978).

Within soils, fine clay particles become attached to small particles of soil humus, forming what is termed a clay-humus-complex. Because such particles are so small they behave very much like a large molecule, exhibiting an overall negative charge. As a consequence, these complexes attract free cations, such as ammonium, and hold them by adsorption. Because of its chemical structure, ammonium ions also have the ability to replace other cations held by clay-humus-complexes, principally sodium and potassium. Nitrate, however, generally does not react with such complexes and can be actively repelled by them (see Figure A.6). The major exception to this occurs when complexes are coated with iron. The complex then exhibits an overall positive charge and can thus become attractive to nitrate ions.

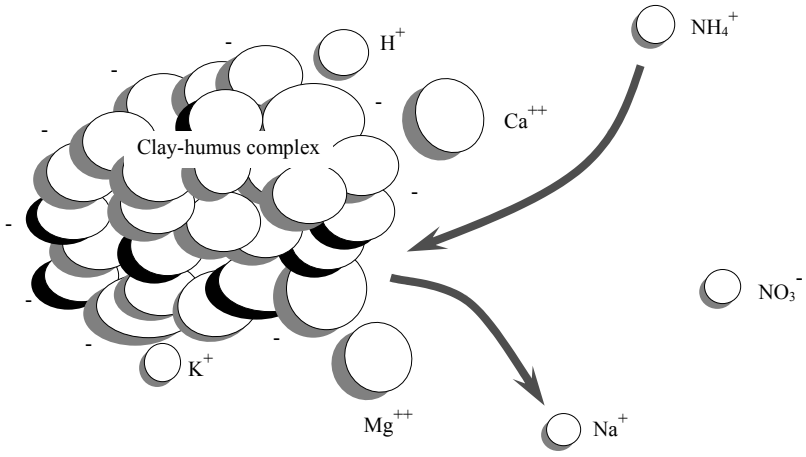

Fig. A.6. The interaction of free ions of nitrate and ammonium with a clay-humus-complex. (source: Askew, 1985).

A.5 Summary

The presence of nitrate in groundwater is a function of three factors:

- the physical and chemical nature of the compound,
- the nitrogen cycle, and
- the hydrologic cycle.

The hydrologic cycle controls the occurrence and movement of groundwater in a geologic formation. Water enters a groundwater system through a zone of recharge. It infiltrates the soil surface and percolates downward to the water table under the influence of gravity. This process provides the mechanism by which a compound can be leached from the soil zone.

The natural production and consumption of nitrate in the soil is controlled by a collection of biogeochemical processes known as the Nitrogen Cycle. In most natural undisturbed ecosystems little nitrate is ever available to be leached from the soil. Human land-use practices, principally effluent disposal and agriculture, upset this balance either through direct inputs of nitrate into the soil, or by altering the rate of nitrification.

Nitrate is a soluble, unreactive compound under aerobic conditions whose movement with water is not generally inhibited.

Appendix B

Computer Modelling Output and Analysis

This appendix contains tables of the modelled output and approximation parameters described in Chapter Five for the development of functional relationships between PRB design variables (PRB dimensions and $K_{prb/aq}$ ratio) and PRB performance measures (edge relative residence, centreline relative residence and relative capture).

Table B1

Gate Width = 3m

Edge Relative Residence Modelled Output

K_{prb}/K_{aq}	(Funnel+Gate) / Gate Width	Gate Length/Width 0.08	0.17	0.33	0.67	1.00	1.33	2.00
1	1	0.96	0.96	0.96	0.96	0.96	0.96	0.96
	2	0.49	0.55	0.64	0.74	0.79	0.82	0.86
	3	0.35	0.40	0.48	0.58	0.64	0.69	0.76
	4.33	0.27	0.31	0.37	0.45	0.51	0.56	0.64
	5	0.24	0.27	0.33	0.41	0.46	0.51	0.59
	7	0.19	0.22	0.25	0.32	0.36	0.40	0.48
	9.67	0.15	0.17	0.20	0.25	0.29	0.32	0.38
2	1	0.87	0.83	0.79	0.74	0.71	0.68	0.66
	2	0.46	0.49	0.54	0.59	0.60	0.60	0.61
	3	0.32	0.36	0.41	0.47	0.50	0.52	0.54
	4.33	0.24	0.27	0.31	0.37	0.40	0.43	0.46
	5	0.22	0.25	0.28	0.34	0.37	0.39	0.43
	7	0.17	0.19	0.22	0.27	0.29	0.31	0.36
	9.67	0.14	0.15	0.17	0.21	0.23	0.25	0.29
4	1	0.83	0.77	0.69	0.63	0.58	0.55	0.51
	2	0.42	0.45	0.49	0.51	0.51	0.50	0.48
	3	0.31	0.33	0.37	0.41	0.43	0.43	0.44
	4.33	0.24	0.25	0.28	0.33	0.35	0.36	0.38
	5	0.21	0.23	0.26	0.30	0.32	0.33	0.35
	7	0.16	0.18	0.20	0.24	0.26	0.27	0.29
	9.67	0.14	0.14	0.16	0.19	0.21	0.22	0.24
7	1	0.80	0.73	0.65	0.58	0.53	0.49	0.45
	2	0.42	0.43	0.46	0.48	0.47	0.45	0.43
	3	0.31	0.32	0.35	0.39	0.40	0.39	0.39
	4.33	0.23	0.25	0.27	0.31	0.32	0.33	0.34
	5	0.21	0.22	0.25	0.28	0.30	0.30	0.32
	7	0.16	0.17	0.19	0.22	0.24	0.25	0.27
	9.67	0.13	0.14	0.15	0.18	0.19	0.20	0.22
10	1	0.80	0.72	0.64	0.56	0.51	0.47	0.43
	2	0.41	0.42	0.45	0.46	0.45	0.43	0.41
	3	0.30	0.31	0.34	0.38	0.38	0.38	0.37
	4.33	0.23	0.24	0.27	0.30	0.31	0.32	0.32
	5	0.21	0.22	0.24	0.28	0.29	0.29	0.30
	7	0.17	0.17	0.19	0.22	0.23	0.24	0.26
	9.67	0.13	0.14	0.15	0.18	0.19	0.20	0.21

Table B2

Gate Width = 6m

Edge Relative Residence Modelled Output

K_{prb}/K_{aq}	(Funnel+Gate) / Gate Width	Gate Length/Width 0.08	0.17	0.33	0.67	1.00	1.33	2.00
1	1	0.96	0.96	0.96	0.96	0.96	0.95	0.95
	2	0.42	0.50	0.61	0.73	0.79	0.82	0.85
	3	0.30	0.36	0.45	0.56	0.64	0.69	0.75
	4	0.24	0.29	0.37	0.46	0.54	0.59	0.67
	5	0.20	0.25	0.31	0.40	0.47	0.52	0.59
	7	0.16	0.20	0.25	0.32	0.38	0.42	0.49
	10	0.13	0.15	0.19	0.25	0.29	0.33	0.39
2	1	0.84	0.80	0.76	0.72	0.70	0.68	0.65
	2	0.37	0.43	0.51	0.57	0.60	0.60	0.60
	3	0.27	0.31	0.37	0.45	0.50	0.51	0.53
	4	0.21	0.25	0.31	0.38	0.42	0.45	0.48
	5	0.18	0.21	0.26	0.32	0.37	0.39	0.43
	7	0.14	0.17	0.21	0.26	0.30	0.32	0.36
	10	0.11	0.13	0.16	0.20	0.24	0.26	0.29
4	1	0.77	0.71	0.65	0.60	0.57	0.54	0.50
	2	0.35	0.39	0.45	0.49	0.51	0.49	0.47
	3	0.24	0.28	0.33	0.39	0.43	0.43	0.43
	4	0.19	0.23	0.27	0.33	0.37	0.37	0.38
	5	0.17	0.19	0.23	0.28	0.32	0.33	0.35
	7	0.14	0.15	0.19	0.23	0.26	0.27	0.29
	10	0.10	0.12	0.15	0.18	0.21	0.22	0.24
7	1	0.74	0.67	0.60	0.54	0.52	0.48	0.44
	2	0.34	0.37	0.42	0.45	0.46	0.44	0.42
	3	0.24	0.27	0.31	0.36	0.39	0.39	0.38
	4	0.19	0.22	0.26	0.31	0.34	0.34	0.34
	5	0.17	0.19	0.22	0.27	0.30	0.31	0.31
	7	0.13	0.15	0.18	0.22	0.25	0.25	0.27
	10	0.10	0.11	0.14	0.17	0.20	0.20	0.22
10	1	0.73	0.65	0.58	0.52	0.50	0.46	0.41
	2	0.33	0.36	0.41	0.44	0.45	0.43	0.40
	3	0.23	0.26	0.31	0.35	0.38	0.37	0.36
	4	0.18	0.21	0.25	0.30	0.33	0.33	0.33
	5	0.16	0.18	0.22	0.26	0.29	0.29	0.30
	7	0.13	0.14	0.17	0.21	0.24	0.24	0.25
	10	0.10	0.11	0.14	0.17	0.19	0.20	0.21

Table B3

Gate Width = 9m

Edge Relative Residence Modelled Output

K_{prb}/K_{aq}	(Funnel+Gate) / Gate Width	Gate Length/Width 0.08	0.17	0.33	0.67	1.00	1.33	2.00
1	1	0.96	0.96	0.96	0.96	0.95	0.95	0.94
	1.89	0.41	0.50	0.63	0.75	0.80	0.83	0.86
	3	0.28	0.34	0.44	0.57	0.64	0.69	0.75
	3.89	0.23	0.28	0.37	0.48	0.55	0.61	0.68
	5	0.19	0.24	0.31	0.41	0.47	0.53	0.61
	7	0.15	0.19	0.24	0.32	0.38	0.43	0.50
2	1	0.82	0.78	0.74	0.72	0.69	0.67	0.64
	1.89	0.36	0.42	0.51	0.59	0.60	0.61	0.59
	3	0.24	0.29	0.36	0.46	0.49	0.52	0.53
	3.89	0.20	0.24	0.30	0.39	0.43	0.46	0.48
	5	0.17	0.20	0.26	0.34	0.37	0.40	0.43
	7	0.13	0.16	0.20	0.27	0.30	0.33	0.36
4	1	0.74	0.68	0.63	0.60	0.56	0.54	0.49
	1.89	0.33	0.38	0.45	0.51	0.50	0.49	0.46
	3	0.22	0.26	0.32	0.40	0.42	0.43	0.42
	3.89	0.18	0.22	0.27	0.34	0.36	0.38	0.38
	5	0.15	0.18	0.23	0.30	0.32	0.34	0.35
	7	0.12	0.14	0.18	0.24	0.26	0.28	0.29
7	1	0.70	0.63	0.58	0.55	0.50	0.48	0.42
	1.89	0.31	0.36	0.42	0.47	0.46	0.45	0.41
	3	0.21	0.25	0.30	0.37	0.38	0.39	0.37
	3.89	0.17	0.21	0.25	0.32	0.34	0.35	0.34
	5	0.14	0.17	0.22	0.28	0.30	0.31	0.31
	7	0.11	0.14	0.17	0.22	0.24	0.26	0.26
10	1	0.68	0.62	0.56	0.53	0.48	0.45	0.39
	1.89	0.30	0.35	0.40	0.45	0.44	0.43	0.38
	3	0.21	0.24	0.29	0.36	0.37	0.37	0.35
	3.89	0.17	0.20	0.25	0.31	0.33	0.34	0.32
	5	0.14	0.17	0.21	0.27	0.29	0.30	0.29
	7	0.11	0.13	0.17	0.22	0.23	0.25	0.25

Table B4

Gate Width = 18m

Edge Relative Residence Modelled Output

K_{prb}/K_{aq}	(Funnel+Gate) / Gate Width	Gate Length/Width 0.08	0.17	0.33	0.67	1.00
1	1	0.96	0.96	0.96	0.95	0.94
	2	0.36	0.46	0.60	0.73	0.78
	3	0.25	0.33	0.45	0.58	0.65
	4.22	0.20	0.26	0.36	0.47	0.55
2	1	0.78	0.75	0.74	0.70	0.67
	2	0.30	0.38	0.49	0.56	0.58
	3	0.22	0.27	0.37	0.45	0.49
	4.22	0.17	0.22	0.29	0.38	0.42
4	1	0.69	0.64	0.62	0.58	0.54
	2	0.27	0.34	0.43	0.48	0.48
	3	0.19	0.24	0.32	0.39	0.41
	4.22	0.15	0.19	0.26	0.32	0.35
7	1	0.64	0.59	0.57	0.52	0.48
	2	0.26	0.32	0.40	0.44	0.43
	3	0.18	0.23	0.30	0.36	0.37
	4.22	0.14	0.18	0.24	0.30	0.32
10	1	0.62	0.57	0.55	0.50	0.46
	2	0.25	0.31	0.39	0.43	0.42
	3	0.18	0.22	0.30	0.35	0.36
	4.22	0.14	0.18	0.24	0.29	0.31

Table B5

Edge Relative Residence Approximation (Stage 1)

Gate Width = 3m

Reciprocal Quadratic: y=1/(a+bx+cx^2)

K_{prb}/K_{aq}	Parameter	Gate Length/Width 0.08	0.17	0.33	0.67	1.00	1.33	2.00
1	a	0.0044	0.2334	0.5019	0.7014	0.7828	0.8420	0.9087
	b	1.0845	0.8389	0.5477	0.3336	0.2464	0.1859	0.1199
	c	-0.0450	-0.0289	-0.0081	0.0018	0.0046	0.0064	0.0066
	r^2	0.9996	0.9997	1.0000	1.0000	0.9990	0.9992	0.9994
2	a	0.0444	0.3411	0.6520	0.9632	1.1154	1.2468	1.3360
	b	1.1502	0.8921	0.6208	0.3782	0.2757	0.2016	0.1549
	c	-0.0446	-0.0266	-0.0082	0.0024	0.0075	0.0103	0.0072
	r^2	0.9999	0.9998	0.9999	0.9994	0.9992	0.9988	0.9984
4	a	0.0035	0.3409	0.8006	1.1605	1.4080	1.5494	1.7866
	b	1.2608	0.9931	0.6520	0.4157	0.2875	0.2349	0.1380
	c	-0.0562	-0.0330	-0.0078	0.0020	0.0080	0.0094	0.0127
	r^2	0.9993	0.9998	0.9997	0.9994	0.9980	0.9977	0.9973
7	a	0.0981	0.3926	0.8661	1.2968	1.5688	1.7664	2.0331
	b	1.2012	1.0148	0.6782	0.4059	0.2833	0.2354	0.1468
	c	-0.0462	-0.0343	-0.0078	0.0065	0.0121	0.0117	0.0126
	r^2	0.9996	0.9997	0.9999	0.9987	0.9979	0.9976	0.9977
10	a	0.0375	0.3591	0.8558	1.3426	1.6083	1.8416	2.1026
	b	1.2727	1.0736	0.7170	0.4289	0.3214	0.2468	0.1781
	c	-0.0562	-0.0407	-0.0120	0.0026	0.0081	0.0104	0.0107
	r^2	0.9991	0.9997	0.9999	0.9991	0.9980	0.9970	0.9968

Table B6
Edge Relative Residence Approximation (Stage 1)
Gate Width = 6m
Reciprocal Quadratic: y=1/(a+bx+cx^2)

		Gate Length/Width						
K_{prb}/K_{aq}	Parameter	0.08	0.17	0.33	0.67	1.00	1.33	2.00
1	a	-0.3435	0.0537	0.4104	0.6559	0.7786	0.8475	0.9107
	b	1.4572	1.0321	0.6492	0.3836	0.2542	0.1926	0.1315
	c	-0.0699	-0.0415	-0.0175	-0.0041	0.0018	0.0033	0.0038
	r^2	0.9994	0.9995	0.9999	0.9992	0.9993	0.9990	0.9993
2	a	-0.3426	0.1305	0.6029	0.9673	1.1188	1.2126	1.3590
	b	1.6090	1.1665	0.7275	0.4130	0.2914	0.2391	0.1589
	c	-0.0730	-0.0447	-0.0168	0.0001	0.0028	0.0037	0.0056
	r^2	0.9992	0.9997	0.9996	0.9993	0.9982	0.9984	0.9987
4	a	-0.3488	0.1988	0.7442	1.2028	1.4440	1.5786	1.8015
	b	1.7290	1.2585	0.8092	0.4488	0.2759	0.2410	0.1646
	c	-0.0793	-0.0467	-0.0211	0.0003	0.0079	0.0073	0.0084
	r^2	0.9992	0.9998	0.9994	0.9986	0.9969	0.9973	0.9971
7	a	-0.2925	0.2644	0.8567	1.3886	1.5783	1.8277	2.0429
	b	1.7241	1.2786	0.8249	0.4471	0.3204	0.2225	0.1868
	c	-0.0773	-0.0460	-0.0197	0.0011	0.0033	0.0109	0.0071
	r^2	0.9993	0.9993	0.9995	0.9988	0.9984	0.9983	0.9964
10	a	-0.3869	0.2470	0.9177	1.4380	1.6610	1.8667	2.2257
	b	1.8472	1.3433	0.8181	0.4610	0.3037	0.2588	0.1542
	c	-0.0882	-0.0492	-0.0177	0.0006	0.0072	0.0076	0.0116
	r^2	0.9995	0.9998	0.9996	0.9977	0.9975	0.9953	0.9945

Table B7
Edge Relative Residence Approximation (Stage 1)
Gate Width = 9m
Reciprocal Quadratic: y=1/(a+bx+cx^2)

		Gate Length/Width						
K_{prb}/K_{aq}	Parameter	0.08	0.17	0.33	0.67	1.00	1.33	2.00
1	a	-0.5338	-0.1346	0.3797	0.6880	0.8043	0.8650	0.9436
	b	1.6637	1.2498	0.6825	0.3501	0.2386	0.1785	0.1107
	c	-0.0850	-0.0721	-0.0209	0.0003	0.0042	0.0047	0.0058
	r^2	0.9993	0.9993	0.9999	0.9997	0.9993	0.9996	0.9996
2	a	-0.6015	-0.0476	0.5947	0.9972	1.1697	1.2933	1.4164
	b	1.9316	1.4081	0.7758	0.3830	0.2637	0.1766	0.1332
	c	-0.1074	-0.0764	-0.0213	0.0015	0.0075	0.0113	0.0091
	r^2	0.9992	0.9997	0.9997	0.9992	0.9992	0.9986	0.9997
4	a	-0.6026	0.0800	0.7908	1.2551	1.4932	1.6268	1.8960
	b	2.0637	1.4627	0.8103	0.3928	0.2671	0.2068	0.1256
	c	-0.1065	-0.0697	-0.0179	0.0049	0.0112	0.0107	0.0138
	r^2	0.9994	0.9997	0.9996	0.9981	0.9981	0.9993	0.9991
7	a	-0.6285	0.1448	0.8856	1.4028	1.7244	1.8549	2.2460
	b	2.1676	1.5209	0.8524	0.3937	0.2388	0.1930	0.0897
	c	-0.1068	-0.0764	-0.0195	0.0089	0.0167	0.0144	0.0206
	r^2	0.9993	0.9998	0.9993	0.9986	0.9974	0.9975	0.9970
10	a	-0.6091	0.1116	0.8941	1.4393	1.8248	2.0132	2.4255
	b	2.1958	1.5805	0.9179	0.4320	0.2226	0.1648	0.0928
	c	-0.1108	-0.0768	-0.0289	0.0033	0.0205	0.0182	0.0201
	r^2	0.9987	0.9997	0.9998	0.9989	0.9987	0.9964	0.9962

Table B8
Edge Relative Residence Approximation (Stage 1)
Gate Width = 18m
Reciprocal Quadratic: y=1/(a+bx+cx^2)

K_{prb}/K_{aq}	Parameter	Gate Length/Width 0.08	0.17	0.33	0.67	1.00
1	a	-0.8945	-0.1644	0.3364	0.7395	0.8449
	b	2.0773	1.2716	0.7443	0.3068	0.2132
	c	-0.1403	-0.0641	-0.0391	0.0057	0.0045
	r^2	0.9996	0.9996	1.0000	0.9999	0.9997
2	a	-0.9470	-0.0465	0.6238	1.0502	1.2694
	b	2.3946	1.4484	0.7453	0.3746	0.2062
	c	-0.1638	-0.0666	-0.0179	0.0012	0.0143
	r^2	0.9992	0.9994	1.0000	0.9991	0.9991
4	a	-0.9341	0.1110	0.8447	1.4028	1.6553
	b	2.5171	1.5071	0.7802	0.2898	0.1634
	c	-0.1320	-0.0540	-0.0139	0.0291	0.0296
	r^2	0.9992	0.9997	0.9995	0.9995	0.9990
7	a	-0.8104	0.1741	0.9807	1.6068	1.8673
	b	2.4770	1.5842	0.7747	0.2805	0.1835
	c	-0.1024	-0.0620	-0.0026	0.0319	0.0280
	r^2	0.9994	0.9998	0.9997	0.9990	0.9987
10	a	-0.9312	0.2203	1.0416	1.7292	2.0116
	b	2.7050	1.5938	0.7856	0.2194	0.1134
	c	-0.1585	-0.0570	-0.0098	0.0464	0.0425
	r^2	0.9992	0.9993	0.9999	0.9984	0.9976

Table B9
Edge Relative Residence Interpolation (Stage 2)
Gate Width = 3m

Interpolation Function	Parameter	K_{prb}/K_{aq} 1	2	4	7	10
$a=(a_1+a_2x)/(1+a_3x+a_4x^2)$	a_1	-0.418	-0.360	-0.554	-0.347	-0.431
	a_2	5.207	5.239	6.831	5.625	5.771
	a_3	5.091	3.388	3.800	2.524	2.415
	a_4	-0.036	-0.060	-0.315	-0.172	-0.138
	r^2	0.9995	0.9997	0.9995	0.9996	0.9996
$b=1/(b_1+b_2x+b_3x^2)$	b_1	0.650	0.634	0.575	0.640	0.595
	b_2	3.317	2.898	2.645	2.194	2.189
	b_3	0.221	0.120	0.233	0.581	0.328
	r^2	0.9995	0.9998	0.9992	0.9982	0.9980
$c=(c_1+c_2x)/(1+c_3x+c_4x^2)$	c_1	-0.0692	-0.0728	-0.1158	-0.0625	-0.0782
	c_2	0.1268	0.1416	0.2110	0.1336	0.1425
	c_3	3.2733	4.4028	9.1506	0.8633	1.7708
	c_4	6.0879	3.8437	1.6119	3.9852	4.3047
	r^2	0.9984	0.9985	0.9977	0.9968	0.9973

Table B10
Edge Relative Residence Interpolation (Stage 2)
Gate Width = 6m

Interpolation Function	Parameter	K_{prb}/K_{aq} 1	2	4	7	10
$a=(a_1+a_2x)/(1+a_3x+a_4x^2)$	a_1	-1.167	-1.273	-1.319	-1.254	-1.738
	a_2	7.691	9.331	10.146	10.450	13.928
	a_3	7.475	6.401	5.513	5.004	7.074
	a_4	-0.094	-0.236	-0.370	-0.352	-0.840
	r^2	0.9998	0.9998	0.9999	0.9995	0.9996
$b=1/(b_1+b_2x+b_3x^2)$	b_1	0.428	0.390	0.379	0.386	0.343
	b_2	3.196	2.848	2.426	2.350	2.414
	b_3	0.246	0.124	0.450	0.385	0.393
	r^2	0.9999	0.9996	0.9995	0.9994	0.9994
$c=(c_1+c_2x)/(1+c_3x+c_4x^2)$	c_1	-0.1279	-0.1090	-0.1312	-0.1293	-0.1832
	c_2	0.1495	0.1626	0.1994	0.1959	0.2855
	c_3	7.6595	3.0315	5.3417	5.4985	9.8414
	c_4	6.7944	11.0327	4.6951	4.8586	4.0387
	r^2	0.9997	0.9997	0.9996	0.9986	0.9996

Table B11
Edge Relative Residence Interpolation (Stage 2)
Gate Width = 9m

Interpolation Function	Parameter	K_{prb}/K_{aq} 1	2	4	7	10
$a=(a_1+a_2x)/(1+a_3x+a_4x^2)$	a_1	-1.336	-1.733	-2.140	-2.388	-2.036
	a_2	6.880	10.202	14.309	16.589	13.815
	a_3	5.363	6.107	7.753	8.359	6.318
	a_4	0.410	0.010	-0.613	-0.983	-0.766
	r^2	0.9986	0.9991	0.9994	0.9995	0.9995
$b=1/(b_1+b_2x+b_3x^2)$	b_1	0.398	0.335	0.298	0.300	0.323
	b_2	2.320	2.104	2.171	1.827	1.444
	b_3	1.706	1.629	1.401	2.093	2.437
	r^2	0.9978	0.9985	0.9989	0.9995	0.9998
$c=(c_1+c_2x)/(1+c_3x+c_4x^2)$	c_1	-0.0727	-0.1201	-0.1397	-0.1366	-0.1529
	c_2	0.1303	0.2282	0.2793	0.2812	0.2671
	c_3	-4.8045	-1.7910	0.3435	0.0902	1.9551
	c_4	18.0075	13.4726	10.5334	7.2018	3.6599
	r^2	0.9992	0.9984	0.9984	0.9969	0.9989

Table B12
Edge Relative Residence Interpolation (Stage 2)
Gate Width = 18m

Interpolation Function	Parameter	K_{prb}/K_{aq} 1	2	4	7	10
$a=(a_1+a_2x)/(1+a_3x+a_4x^2)$	a_1	-2.640	-3.554	-3.922	-2.866	-3.828
	a_2	12.722	20.268	25.167	19.297	26.072
	a_3	10.159	13.001	13.142	7.873	11.012
	a_4	0.690	-0.754	-1.305	-0.065	-0.977
	r^2	1.0000	0.9998	1.0000	1.0000	1.0000
$b=1/(b_1+b_2x+b_3x^2)$	b_1	0.244	0.193	0.218	0.269	0.236
	b_2	2.825	2.647	1.914	1.256	1.155
	b_3	1.926	1.983	4.096	5.303	6.562
	r^2	0.9997	0.9997	1.0000	0.9997	0.9997
$c=(c_1+c_2x)/(1+c_3x+c_4x^2)$	c_1	-0.4921	-3.0452	-0.3565	-0.1250	-0.4716
	c_2	0.6624	5.4263	0.9328	0.3697	1.4131
	c_3	27.3404	188.1459	14.0923	-1.5544	15.6537
	c_4	-5.9651	-19.0248	2.7008	8.9864	3.3426
	r^2	0.9927	0.9995	0.9976	0.9999	0.9962

Table B13

Gate Width = 3m

Centre Relative Residence Modelled Output

K_{prb}/K_{aq}	(Funnel+Gate) / Gate Width	Gate Length/Width 0.08	0.17	0.33	0.67	1.00	1.33	2.00
1	1	0.96	0.96	0.96	0.96	0.96	0.96	0.96
	2	0.81	0.81	0.81	0.82	0.84	0.86	0.88
	3	0.67	0.67	0.66	0.68	0.71	0.74	0.78
	4.33	0.55	0.54	0.53	0.55	0.58	0.61	0.67
	5	0.50	0.50	0.49	0.50	0.53	0.56	0.62
	7	0.41	0.39	0.39	0.40	0.42	0.45	0.51
	9.67	0.32	0.31	0.31	0.32	0.34	0.36	0.41
2	1	0.94	0.91	0.87	0.80	0.76	0.72	0.68
	2	0.81	0.79	0.75	0.71	0.68	0.66	0.64
	3	0.67	0.66	0.63	0.60	0.59	0.58	0.58
	4.33	0.56	0.54	0.51	0.49	0.48	0.49	0.50
	5	0.51	0.50	0.47	0.45	0.45	0.45	0.46
	7	0.41	0.40	0.38	0.36	0.36	0.37	0.38
	9.67	0.33	0.33	0.31	0.29	0.29	0.30	0.31
4	1	0.93	0.89	0.83	0.73	0.66	0.61	0.55
	2	0.80	0.78	0.73	0.65	0.60	0.56	0.52
	3	0.69	0.66	0.62	0.56	0.52	0.50	0.47
	4.33	0.55	0.54	0.51	0.46	0.44	0.42	0.41
	5	0.51	0.50	0.47	0.42	0.40	0.39	0.39
	7	0.41	0.41	0.38	0.34	0.33	0.32	0.32
	9.67	0.33	0.33	0.31	0.28	0.27	0.26	0.27
7	1	0.93	0.89	0.81	0.70	0.62	0.56	0.49
	2	0.81	0.78	0.72	0.63	0.57	0.52	0.46
	3	0.69	0.66	0.62	0.54	0.50	0.47	0.43
	4.33	0.56	0.55	0.51	0.45	0.42	0.40	0.37
	5	0.51	0.50	0.47	0.42	0.39	0.37	0.35
	7	0.41	0.41	0.38	0.34	0.32	0.31	0.30
	9.67	0.34	0.33	0.31	0.28	0.26	0.25	0.25
10	1	0.93	0.88	0.81	0.68	0.60	0.54	0.46
	2	0.81	0.78	0.72	0.62	0.55	0.51	0.44
	3	0.67	0.67	0.61	0.54	0.49	0.45	0.41
	4.33	0.56	0.55	0.51	0.45	0.41	0.39	0.36
	5	0.51	0.50	0.47	0.41	0.38	0.36	0.34
	7	0.41	0.41	0.38	0.34	0.31	0.30	0.29
	9.67	0.34	0.33	0.31	0.27	0.26	0.25	0.24

Table B14

Gate Width = 6m

Centre Relative Residence Modelled Output

K_{prb}/K_{aq}	(Funnel+Gate) / Gate Width	Gate Length/Width 0.08	0.17	0.33	0.67	1.00	1.33	2.00
1	1	0.96	0.96	0.96	0.96	0.96	0.95	0.95
	2	0.82	0.81	0.81	0.82	0.84	0.86	0.88
	3	0.69	0.67	0.67	0.68	0.71	0.74	0.78
	4	0.59	0.58	0.57	0.58	0.62	0.65	0.70
	5	0.52	0.51	0.50	0.51	0.54	0.57	0.63
	7	0.43	0.41	0.40	0.41	0.44	0.47	0.53
	10	0.34	0.33	0.32	0.33	0.35	0.37	0.42
2	1	0.94	0.91	0.87	0.80	0.75	0.72	0.68
	2	0.82	0.79	0.76	0.71	0.68	0.66	0.64
	3	0.69	0.67	0.63	0.60	0.59	0.58	0.57
	4	0.59	0.58	0.55	0.52	0.51	0.51	0.52
	5	0.53	0.51	0.48	0.45	0.45	0.46	0.47
	7	0.43	0.42	0.39	0.37	0.37	0.38	0.40
	10	0.34	0.34	0.31	0.30	0.30	0.30	0.32
4	1	0.92	0.89	0.83	0.72	0.65	0.60	0.54
	2	0.81	0.79	0.74	0.65	0.60	0.56	0.51
	3	0.69	0.67	0.63	0.56	0.52	0.50	0.47
	4	0.60	0.59	0.54	0.49	0.46	0.44	0.43
	5	0.53	0.52	0.48	0.43	0.41	0.40	0.39
	7	0.43	0.43	0.40	0.36	0.34	0.33	0.33
	10	0.35	0.34	0.32	0.28	0.27	0.27	0.27
7	1	0.92	0.89	0.81	0.69	0.61	0.55	0.48
	2	0.82	0.79	0.73	0.63	0.57	0.52	0.46
	3	0.69	0.67	0.63	0.54	0.50	0.47	0.42
	4	0.60	0.59	0.55	0.48	0.44	0.42	0.39
	5	0.54	0.52	0.48	0.42	0.39	0.38	0.35
	7	0.44	0.43	0.40	0.35	0.33	0.31	0.30
	10	0.35	0.35	0.32	0.28	0.26	0.26	0.25
10	1	0.91	0.88	0.81	0.68	0.59	0.53	0.46
	2	0.81	0.79	0.73	0.62	0.55	0.50	0.44
	3	0.69	0.68	0.63	0.54	0.49	0.45	0.41
	4	0.61	0.59	0.55	0.47	0.43	0.41	0.37
	5	0.53	0.52	0.49	0.42	0.38	0.37	0.34
	7	0.44	0.43	0.40	0.35	0.32	0.31	0.29
	10	0.35	0.35	0.32	0.28	0.26	0.25	0.24

Table B15

Gate Width = 9m

Centre Relative Residence Modelled Output

K_{prb}/K_{aq}	(Funnel+Gate) / Gate Width	Gate Length/Width 0.08	0.17	0.33	0.67	1.00	1.33	2.00
1	1	0.96	0.96	0.96	0.96	0.95	0.95	0.94
	1.89	0.84	0.83	0.83	0.84	0.86	0.87	0.88
	3	0.69	0.68	0.67	0.69	0.72	0.75	0.79
	3.89	0.61	0.59	0.58	0.60	0.63	0.67	0.72
	5	0.54	0.52	0.51	0.52	0.56	0.59	0.65
	7	0.43	0.42	0.41	0.42	0.45	0.48	0.54
2	1	0.94	0.91	0.87	0.80	0.75	0.72	0.67
	1.89	0.83	0.81	0.77	0.72	0.69	0.67	0.63
	3	0.70	0.68	0.64	0.60	0.59	0.58	0.57
	3.89	0.61	0.60	0.56	0.53	0.52	0.52	0.52
	5	0.54	0.52	0.49	0.46	0.46	0.47	0.48
	7	0.44	0.42	0.40	0.38	0.38	0.38	0.40
4	1	0.93	0.89	0.83	0.72	0.65	0.60	0.53
	1.89	0.83	0.81	0.75	0.66	0.61	0.57	0.51
	3	0.70	0.68	0.63	0.56	0.52	0.50	0.46
	3.89	0.62	0.60	0.56	0.50	0.47	0.45	0.43
	5	0.54	0.53	0.49	0.44	0.42	0.41	0.39
	7	0.45	0.43	0.40	0.36	0.34	0.34	0.33
7	1	0.92	0.88	0.81	0.69	0.61	0.55	0.47
	1.89	0.83	0.80	0.74	0.64	0.57	0.52	0.45
	3	0.70	0.68	0.63	0.54	0.50	0.47	0.42
	3.89	0.62	0.60	0.56	0.48	0.45	0.42	0.39
	5	0.55	0.54	0.50	0.43	0.40	0.38	0.35
	7	0.45	0.44	0.41	0.35	0.33	0.32	0.30
10	1	0.92	0.88	0.81	0.68	0.59	0.53	0.44
	1.89	0.83	0.80	0.74	0.63	0.56	0.51	0.43
	3	0.70	0.68	0.63	0.54	0.49	0.45	0.40
	3.89	0.62	0.61	0.56	0.48	0.44	0.41	0.37
	5	0.55	0.54	0.50	0.43	0.39	0.37	0.34
	7	0.45	0.44	0.41	0.35	0.32	0.31	0.29

Table B16

Gate Width = 18m

Centre Relative Residence Modelled Output

K_{prb}/K_{aq}	(Funnel+Gate) / Gate Width	Gate Length/Width 0.33	0.67	1.00	1.33	2.00
1	1	0.96	0.96	0.96	0.95	0.94
	2	0.83	0.82	0.82	0.83	0.85
	3	0.71	0.69	0.69	0.71	0.74
	4.22	0.61	0.59	0.58	0.60	0.64
2	1	0.94	0.91	0.86	0.79	0.74
	2	0.83	0.80	0.76	0.71	0.67
	3	0.71	0.69	0.65	0.61	0.59
	4.22	0.61	0.59	0.56	0.52	0.52
4	1	0.92	0.89	0.82	0.71	0.63
	2	0.82	0.80	0.74	0.65	0.59
	3	0.71	0.69	0.64	0.56	0.52
	4.22	0.62	0.60	0.55	0.49	0.46
7	1	0.92	0.88	0.81	0.68	0.58
	2	0.83	0.80	0.73	0.62	0.55
	3	0.71	0.69	0.64	0.55	0.49
	4.22	0.62	0.60	0.55	0.47	0.43
10	1	0.92	0.88	0.80	0.66	0.57
	2	0.82	0.80	0.73	0.61	0.53
	3	0.71	0.69	0.64	0.54	0.48
	4.22	0.62	0.60	0.55	0.47	0.42

Table B17

Centre Relative Residence Approximation (Stage 1)

Gate Width = 3m

Reciprocal Quadratic: y=1/(a+bx+cx^2)

K_{prb}/K_{aq}	Parameter	Gate Length/Width 0.08	0.17	0.33	0.67	1.00	1.33	2.00
1	a	0.8240	0.8270	0.8290	0.8350	0.8571	0.8850	0.9200
	b	0.2175	0.2080	0.2020	0.1900	0.1679	0.1382	0.1000
	c	0.0028	0.0033	0.0037	0.0049	0.0055	0.0063	0.0065
	r^2	0.9993	0.9993	0.9988	0.9988	0.9986	0.9984	0.9932
2	a	0.8532	0.8814	0.9250	1.0372	1.1172	1.2123	1.3353
	b	0.2100	0.2050	0.2040	0.1901	0.1763	0.1520	0.1069
	c	0.0025	0.0032	0.0045	0.0065	0.0080	0.0090	0.0103
	r^2	0.9990	0.9984	0.9985	0.9981	0.9982	0.9981	0.9977
4	a	0.8550	0.9167	0.9912	1.1500	1.2988	1.4454	1.6492
	b	0.2000	0.1995	0.1980	0.1950	0.1860	0.1662	0.1400
	c	0.0033	0.0036	0.0042	0.0062	0.0074	0.0085	0.0100
	r^2	0.9987	0.9985	0.9985	0.9978	0.9979	0.9982	0.9976
7	a	0.8740	0.9234	1.0346	1.2042	1.4052	1.5995	1.9000
	b	0.1940	0.1925	0.1870	0.1800	0.1710	0.1561	0.1300
	c	0.0025	0.0035	0.0060	0.0080	0.0089	0.0105	0.0115
	r^2	0.9981	0.9988	0.9983	0.9981	0.9979	0.9981	0.9912
10	a	0.8621	0.9234	1.0276	1.2696	1.4525	1.6431	2.0189
	b	0.1980	0.1930	0.1920	0.1870	0.1845	0.1703	0.1191
	c	0.0028	0.0035	0.0050	0.0070	0.0082	0.0090	0.0115
	r^2	0.9982	0.9982	0.9985	0.9978	0.9972	0.9967	0.9978

Table B18
Centre Relative Residence Approximation (Stage 1)
Gate Width = 6m
Reciprocal Quadratic: y=1/(a+bx+cx^2)

K_{prb}/K_{aq}	Parameter	Gate Length/Width 0.08	0.17	0.33	0.67	1.00	1.33	2.00
1	a	0.8241	0.8098	0.8067	0.8155	0.8530	0.8969	0.9333
	b	0.2084	0.2241	0.2246	0.2144	0.1756	0.1381	0.1042
	c	0.0005	0.0007	0.0009	0.0017	0.0033	0.0049	0.0055
	r^2	0.9991	0.9992	0.9990	0.9987	0.9988	0.9982	0.9987
2	a	0.8610	0.8865	0.9260	1.0226	1.1282	1.2119	1.3229
	b	0.1900	0.2010	0.2080	0.2069	0.1809	0.1556	0.1256
	c	0.0025	0.0028	0.0031	0.0038	0.0052	0.0063	0.0059
	r^2	0.9986	0.9988	0.9984	0.9975	0.9972	0.9985	0.9984
4	a	0.8935	0.9337	0.9904	1.1798	1.3328	1.4721	1.7033
	b	0.1797	0.1757	0.1959	0.1871	0.1778	0.1641	0.1231
	c	0.0026	0.0029	0.0034	0.0053	0.0069	0.0075	0.0084
	r^2	0.9985	0.9987	0.9976	0.9982	0.9977	0.9973	0.9985
7	a	0.8978	0.9270	1.0408	1.2348	1.4343	1.6326	1.9110
	b	0.1733	0.1750	0.1790	0.1820	0.1712	0.1490	0.1363
	c	0.0028	0.0035	0.0045	0.0063	0.0080	0.0088	0.0088
	r^2	0.9982	0.9983	0.9977	0.9976	0.9968	0.9962	0.9969
10	a	0.9168	0.9486	1.0472	1.2569	1.4846	1.7116	2.0044
	b	0.1672	0.1720	0.1790	0.1820	0.1720	0.1451	0.1324
	c	0.0033	0.0036	0.0045	0.0065	0.0080	0.0092	0.0093
	r^2	0.9984	0.9976	0.9983	0.9977	0.9963	0.9984	0.9971

Table B19
Centre Relative Residence Approximation (Stage 1)
Gate Width = 9m
Reciprocal Quadratic: y=1/(a+bx+cx^2)

K_{prb}/K_{aq}	Parameter	Gate Length/Width 0.08	0.17	0.33	0.67	1.00	1.33	2.00
1	a	0.8200	0.8303	0.8400	0.8490	0.8969	0.9293	0.9777
	b	0.2060	0.2024	0.1890	0.1796	0.1394	0.1088	0.0700
	c	0.0015	0.0032	0.0042	0.0064	0.0077	0.0084	0.0085
	r^2	0.9992	0.9992	0.9988	0.9991	0.9983	0.9992	0.9996
2	a	0.8590	0.9100	0.9504	1.0517	1.1608	1.2418	1.3778
	b	0.1880	0.1860	0.1854	0.1780	0.1509	0.1267	0.1011
	c	0.0015	0.0030	0.0050	0.0075	0.0094	0.0100	0.0100
	r^2	0.9992	0.9988	0.9989	0.9983	0.9980	0.9985	0.9992
4	a	0.9022	0.9530	1.0283	1.2082	1.3730	1.5106	1.7703
	b	0.1615	0.1600	0.1598	0.1596	0.1379	0.1278	0.0912
	c	0.0046	0.0050	0.0079	0.0100	0.0128	0.0130	0.0130
	r^2	0.9989	0.9983	0.9988	0.9985	0.9976	0.9972	0.9986
7	a	0.9370	0.9759	1.0673	1.2625	1.4807	1.6800	2.0335
	b	0.1420	0.1461	0.1508	0.1614	0.1338	0.1200	0.0704
	c	0.0055	0.0060	0.0070	0.0102	0.0130	0.0140	0.0171
	r^2	0.9988	0.9985	0.9986	0.9981	0.9988	0.9981	0.9988
10	a	0.9400	0.9800	1.0673	1.2964	1.5486	1.7400	2.1830
	b	0.1400	0.1430	0.1490	0.1480	0.1200	0.1100	0.0547
	c	0.0060	0.0063	0.0070	0.0109	0.0154	0.0175	0.0186
	r^2	0.9988	0.9991	0.9986	0.9982	0.9978	0.9967	0.9980

Table B20
Centre Relative Residence Approximation (Stage 1)
Gate Width = 18m
Reciprocal Quadratic: y=1/(a+bx+cx^2)

K_{prb}/K_{aq}	Parameter	Gate Length/Width 0.08	0.17	0.33	0.67	1.00
1	a	0.8420	0.8607	0.8630	0.9075	0.9592
	b	0.1780	0.1711	0.1659	0.1286	0.0863
	c	0.0057	0.0071	0.0092	0.0127	0.0142
	r^2	0.9997	0.9995	0.9995	0.9992	0.9996
2	a	0.9165	0.9535	1.0058	1.1051	1.2131
	b	0.1390	0.1380	0.1370	0.1350	0.1215
	c	0.0080	0.0090	0.0105	0.0130	0.0140
	r^2	0.9991	0.9990	0.9989	0.9982	0.9989
4	a	0.9499	0.9850	1.0777	1.2545	1.4653
	b	0.1270	0.1240	0.1221	0.1210	0.0951
	c	0.0080	0.0100	0.0125	0.0140	0.0170
	r^2	0.9983	0.9989	0.9988	0.9983	0.9987
7	a	0.9543	1.0074	1.0914	1.3254	1.5500
	b	0.1200	0.1190	0.1180	0.1165	0.1140
	c	0.0080	0.0095	0.0125	0.0160	0.0170
	r^2	0.9984	0.9987	0.9993	0.9992	0.9977
10	a	0.9525	1.0074	1.1168	1.3817	1.6239
	b	0.1217	0.1180	0.1136	0.1099	0.1077
	c	0.0090	0.0100	0.0115	0.0150	0.0157
	r^2	0.9992	0.9987	0.9988	0.9991	0.9994

Table B21
Centre Relative Residence Interpolation (Stage 2)
Gate Width = 3m

Interpolation Function	Parameter	K_{prb}/K_{aq} 1	2	4	7	10
$a=a_1+a_2x+a_3x^2+a_4x^3$	a_1	0.829	0.829	0.823	0.836	0.797
	a_2	-0.040	0.298	0.498	0.520	0.772
	a_3	0.096	0.017	0.007	0.099	-0.145
	a_4	-0.026	-0.020	-0.025	-0.046	0.032
	r^2	0.9978	0.9997	0.9998	0.9997	0.9999
$b=b_1+b_2x+b_3x^2+b_4x^3$	b_1	0.215	0.209	0.197	0.195	0.199
	b_2	-0.013	-0.006	0.027	-0.015	-0.028
	b_3	-0.051	-0.036	-0.053	-0.012	0.029
	b_4	0.014	0.006	0.013	0.002	-0.018
	r^2	0.9972	0.9991	0.9967	0.9988	0.9986
$c=c_1+c_2x+c_3x^2+c_4x^3$	c_1	0.0026	0.0018	0.0028	0.0014	0.0018
	c_2	0.0038	0.0093	0.0050	0.0152	0.0118
	c_3	-0.0005	-0.0037	-0.0001	-0.0093	-0.0074
	c_4	-0.0002	0.0006	-0.0003	0.0021	0.0020
	r^2	0.9980	1.0000	0.9987	0.9948	0.9998

Table B22
Centre Relative Residence Interpolation (Stage 2)
Gate Width = 6m

Interpolation Function	Parameter	K_{prb}/K_{aq} 1	2	4	7	10
$a=a_1+a_2x+a_3x^2+a_4x^3$	a_1	0.835	0.844	0.854	0.851	0.882
	a_2	-0.176	0.217	0.436	0.495	0.374
	a_3	0.276	0.115	0.085	0.168	0.370
	a_4	-0.081	-0.052	-0.045	-0.075	-0.138
	r^2	0.9994	0.9999	0.9997	0.9998	0.9999
$b=b_1+b_2x+b_3x^2+b_4x^3$	b_1	0.200	0.180	0.172	0.164	0.156
	b_2	0.155	0.145	0.077	0.089	0.123
	b_3	-0.254	-0.199	-0.089	-0.119	-0.156
	b_4	0.076	0.056	0.019	0.034	0.044
	r^2	0.9986	0.9989	0.9821	0.9900	0.9903
$c=c_1+c_2x+c_3x^2+c_4x^3$	c_1	0.0008	0.0027	0.0021	0.0023	0.0028
	c_2	-0.0021	-0.0007	0.0046	0.0069	0.0049
	c_3	0.0071	0.0052	0.0006	-0.0008	0.0014
	c_4	-0.0024	-0.0021	-0.0007	-0.0005	-0.0011
	r^2	0.9986	0.9970	0.9970	0.9996	0.9997

Table B23
Centre Relative Residence Interpolation (Stage 2)
Gate Width = 9m

Interpolation Function	Parameter	K_{prb}/K_{aq} 1	2	4	7	10
$a=a_1+a_2x+a_3x^2+a_4x^3$	a_1	0.825	0.841	0.859	0.898	0.888
	a_2	-0.011	0.339	0.540	0.445	0.529
	a_3	0.113	-0.013	-0.021	0.203	0.159
	a_4	-0.035	-0.011	-0.011	-0.071	-0.050
	r^2	0.9953	0.9993	0.9999	1.0000	0.9996
$b=b_1+b_2x+b_3x^2+b_4x^3$	b_1	0.204	0.182	0.159	0.133	0.136
	b_2	0.008	0.051	0.025	0.101	0.066
	b_3	-0.102	-0.117	-0.053	-0.122	-0.093
	b_4	0.033	0.036	0.012	0.028	0.020
	r^2	0.9966	0.9982	0.9939	0.9900	0.9920
$c=c_1+c_2x+c_3x^2+c_4x^3$	c_1	0.0009	0.0004	0.0032	0.0045	0.0055
	c_2	0.0123	0.0161	0.0149	0.0092	0.0027
	c_3	-0.0066	-0.0088	-0.0066	-0.0010	0.0112
	c_4	0.0012	0.0015	0.0008	-0.0002	-0.0046
	r^2	0.9967	0.9992	0.9933	0.9970	0.9975

Table B24
Centre Relative Residence Interpolation (Stage 2)
Gate Width = 18m

Interpolation Function	Parameter	K_{prb}/K_{aq} 1	2	4	7	10
$a=a_1+a_2x+a_3x^2+a_4x^3$	a_1	0.839	0.882	0.906	0.922	0.911
	a_2	0.083	0.463	0.515	0.402	0.486
	a_3	0.002	-0.322	-0.056	0.438	0.520
	a_4	0.035	0.190	0.101	-0.212	-0.292
	r^2	0.9948	1.0000	0.9998	0.9999	1.0000
$b=b_1+b_2x+b_3x^2+b_4x^3$	b_1	0.177	0.141	0.132	0.121	0.126
	b_2	0.003	-0.027	-0.076	-0.014	-0.057
	b_3	-0.147	0.067	0.190	0.020	0.072
	b_4	0.054	-0.059	-0.151	-0.012	-0.033
	r^2	0.9989	0.9999	1.0000	0.9998	1.0000
$c=c_1+c_2x+c_3x^2+c_4x^3$	c_1	0.0045	0.0071	0.0054	0.0062	0.0085
	c_2	0.0161	0.0114	0.0366	0.0229	0.0064
	c_3	-0.0043	-0.0027	-0.0564	-0.0124	0.0133
	c_4	-0.0021	-0.0018	0.0314	0.0003	-0.0125
	r^2	1.0000	1.0000	0.9998	0.9995	0.9996

Table B25

Gate Width = 3m

Relative Capture Modelled Output

K_{prb}/K_{aq}	(Funnel+Gate) / Gate Width	Gate Length/Width 0.08	0.17	0.33	0.67	1.00	1.33	2.00
1	1	1.00	1.00	1.00	1.00	1.00	1.00	1.00
	2	1.47	1.40	1.33	1.27	1.20	1.20	1.07
	3	1.87	1.80	1.73	1.60	1.47	1.40	1.27
	4.33	2.47	2.40	2.27	2.07	1.93	1.80	1.60
	5	2.73	2.67	2.53	2.33	2.13	2.00	1.80
	7	3.53	3.47	3.33	3.07	2.87	2.67	2.33
	9.67	4.73	4.60	4.47	4.20	3.93	3.67	3.27
2	1	1.00	1.06	1.13	1.27	1.26	1.33	1.40
	2	1.47	1.47	1.47	1.53	1.53	1.53	1.47
	3	1.93	1.93	1.87	1.87	1.80	1.80	1.73
	4.33	2.47	2.47	2.47	2.40	2.33	2.27	2.13
	5	2.80	2.73	2.73	2.67	2.53	2.47	2.33
	7	3.60	3.60	3.53	3.47	3.33	3.20	3.00
	9.67	4.80	4.73	4.67	4.53	4.40	4.27	4.00
4	1	1.06	1.13	1.20	1.40	1.46	1.60	1.73
	2	1.53	1.53	1.60	1.67	1.73	1.80	1.87
	3	1.93	1.93	2.00	2.00	2.07	2.07	2.07
	4.33	2.53	2.53	2.53	2.53	2.53	2.53	2.53
	5	2.80	2.80	2.80	2.80	2.80	2.80	2.73
	7	3.67	3.67	3.67	3.67	3.60	3.60	3.47
	9.67	4.80	4.80	4.80	4.80	4.73	4.73	4.53
7	1	1.06	1.13	1.26	1.53	1.60	1.73	1.93
	2	1.53	1.53	1.60	1.73	1.87	1.93	2.07
	3	1.93	2.00	2.00	2.07	2.13	2.27	2.33
	4.33	2.53	2.53	2.60	2.67	2.67	2.73	2.73
	5	2.80	2.87	2.87	2.93	2.93	3.00	2.93
	7	3.67	3.67	3.73	3.73	3.73	3.80	3.73
	9.67	4.80	4.87	4.87	4.93	4.93	4.93	4.80
10	1	1.06	1.13	1.26	1.53	1.66	1.80	2.06
	2	1.53	1.60	1.67	1.73	1.87	2.00	2.13
	3	1.93	2.00	2.00	2.13	2.20	2.33	2.40
	4.33	2.53	2.60	2.60	2.67	2.73	2.80	2.80
	5	2.80	2.87	2.87	2.93	3.00	3.07	3.07
	7	3.67	3.67	3.73	3.80	3.80	3.87	3.80
	9.67	4.87	4.87	4.87	4.93	5.00	5.00	4.93

Table B26

Gate Width = 6m
Relative Capture Modelled Output

K_{prb}/K_{aq}	(Funnel+Gate) / Gate Width	Gate Length/Width 0.08	0.17	0.33	0.67	1.00	1.33	2.00
1	1	1.00	1.00	1.00	1.00	1.00	1.00	1.00
	2	1.40	1.37	1.30	1.23	1.20	1.17	1.13
	3	1.90	1.83	1.77	1.63	1.50	1.47	1.37
	4	2.33	2.30	2.20	2.03	1.90	1.80	1.67
	5	2.80	2.77	2.63	2.47	2.30	2.17	2.00
	7	3.73	3.67	3.57	3.33	3.13	2.97	2.70
	10	5.23	5.13	5.00	4.73	4.47	4.27	3.93
2	1	1.03	1.03	1.13	1.20	1.26	1.30	1.36
	2	1.47	1.47	1.47	1.47	1.47	1.50	1.50
	3	1.93	1.93	1.90	1.87	1.83	1.80	1.80
	4	2.40	2.37	2.37	2.30	2.23	2.17	2.10
	5	2.87	2.83	2.80	2.73	2.63	2.60	2.47
	7	3.80	3.77	3.73	3.63	3.50	3.43	3.27
	10	5.27	5.27	5.20	5.10	4.93	4.83	4.60
4	1	1.07	1.13	1.20	1.36	1.46	1.56	1.70
	2	1.50	1.50	1.53	1.60	1.67	1.73	1.80
	3	1.97	1.97	2.00	2.00	2.03	2.07	2.10
	4	2.43	2.43	2.43	2.43	2.43	2.43	2.43
	5	2.90	2.90	2.90	2.90	2.87	2.87	2.83
	7	3.83	3.83	3.83	3.80	3.73	3.73	3.63
	10	5.30	5.33	5.30	5.30	5.20	5.17	5.03
7	1	1.07	1.13	1.26	1.43	1.56	1.70	1.86
	2	1.50	1.53	1.57	1.67	1.77	1.87	2.00
	3	1.97	2.00	2.03	2.10	2.13	2.20	2.27
	4	2.43	2.47	2.47	2.53	2.53	2.57	2.63
	5	2.90	2.93	2.93	2.97	2.97	3.00	3.03
	7	3.83	3.83	3.87	3.90	3.87	3.87	3.87
	10	5.33	5.33	5.37	5.40	5.33	5.33	5.27
10	1	1.07	1.16	1.26	1.50	1.63	1.76	1.96
	2	1.50	1.53	1.60	1.70	1.80	1.90	2.07
	3	1.97	2.00	2.03	2.13	2.17	2.27	2.37
	4	2.43	2.47	2.50	2.57	2.60	2.63	2.73
	5	2.90	2.93	2.97	3.00	3.03	3.07	3.10
	7	3.83	3.87	3.90	3.93	3.93	3.93	3.93
	10	5.33	5.37	5.40	5.43	5.40	5.43	5.40

Table B27

Gate Width = 9m

Relative Capture Modelled Output

K_{prb}/K_{aq}	(Funnel+Gate) / Gate Width	Gate Length/Width 0.08	0.17	0.33	0.67	1.00	1.33	2.00
1	1	1.00	1.00	1.00	0.98	1.00	1.00	1.00
	1.89	1.40	1.36	1.29	1.22	1.20	1.18	1.13
	3	1.91	1.87	1.80	1.67	1.58	1.53	1.44
	3.89	2.33	2.29	2.20	2.04	1.93	1.87	1.76
	5	2.87	2.82	2.73	2.56	2.42	2.31	2.16
	7	3.87	3.80	3.69	3.49	3.31	3.16	2.91
2	1	1.04	1.09	1.13	1.20	1.24	1.29	1.35
	1.89	1.42	1.42	1.42	1.42	1.44	1.47	1.49
	3	1.96	1.96	1.93	1.89	1.87	1.84	1.82
	3.89	2.38	2.38	2.33	2.27	2.22	2.18	2.16
	5	2.91	2.89	2.87	2.78	2.71	2.67	2.58
	7	3.91	3.89	3.84	3.76	3.67	3.58	3.44
4	1	1.07	1.13	1.22	1.33	1.44	1.53	1.66
	1.89	1.47	1.47	1.51	1.56	1.62	1.67	1.78
	3	1.98	2.00	2.00	2.02	2.04	2.04	2.11
	3.89	2.40	2.42	2.42	2.42	2.42	2.42	2.44
	5	2.93	2.93	2.96	2.93	2.91	2.89	2.91
	7	3.93	3.96	3.96	3.91	3.89	3.84	3.82
7	1	1.09	1.15	1.27	1.42	1.55	1.66	1.84
	1.89	1.47	1.49	1.53	1.62	1.71	1.78	1.93
	3	2.00	2.02	2.04	2.09	2.13	2.18	2.27
	3.89	2.42	2.42	2.47	2.49	2.51	2.53	2.60
	5	2.96	2.96	2.98	3.00	3.02	3.02	3.07
	7	3.96	3.98	4.00	4.00	4.00	3.98	4.00
10	1	1.09	1.15	1.29	1.44	1.60	1.71	1.92
	1.89	1.47	1.49	1.56	1.64	1.76	1.84	2.00
	3	2.00	2.02	2.07	2.11	2.18	2.22	2.36
	3.89	2.42	2.44	2.47	2.51	2.56	2.58	2.69
	5	2.96	2.98	3.00	3.02	3.07	3.07	3.16
	7	3.96	3.98	4.00	4.02	4.04	4.04	4.09

Table B28

Gate Width = 18m

Relative Capture Modelled Output

K_{prb}/K_{aq}	(Funnel+Gate) / Gate Width	Gate Length/Width 0.08	0.17	0.33	0.67	1.00
1	1	1.00	1.00	1.00	0.99	1.00
	2	1.46	1.42	1.38	1.31	1.28
	3	1.98	1.93	1.87	1.77	1.70
	4.22	2.59	2.54	2.47	2.33	2.23
2	1	1.04	1.07	1.11	1.17	1.21
	2	1.50	1.49	1.48	1.48	1.48
	3	2.01	2.00	1.98	1.93	1.91
	4.22	2.62	2.61	2.58	2.52	2.48
4	1	1.07	1.11	1.19	1.30	1.38
	2	1.51	1.52	1.54	1.58	1.62
	3	2.03	2.03	2.03	2.04	2.06
	4.22	2.64	2.64	2.64	2.63	2.63
7	1	1.08	1.13	1.23	1.37	1.47
	2	1.52	1.54	1.57	1.63	1.70
	3	2.03	2.04	2.07	2.10	2.13
	4.22	2.66	2.67	2.68	2.69	2.71
10	1	1.09	1.14	1.24	1.39	1.51
	2	1.52	1.54	1.58	1.66	1.72
	3	2.04	2.06	2.08	2.11	2.17
	4.22	2.66	2.68	2.69	2.71	2.74

Table B29
Relative Capture Approximation (Stage 1)
Gate Width = 3m
3rd degree Polynomial Fit: y=a+bx+cx^2+dx^3

		Gate Length/Width						
K_{prb}/K_{aq}	Parameter	0.08	0.17	0.33	0.67	1.00	1.33	2.00
1	a	0.5015	0.5800	0.6347	0.7140	0.8215	0.8600	0.9049
	b	0.5172	0.4200	0.3449	0.2600	0.1395	0.1105	0.0426
	c	-0.0201	-0.0039	0.0080	0.0170	0.0275	0.0280	0.0310
	d	0.0012	0.0004	-0.0003	-0.0007	-0.0009	-0.0010	-0.0011
	r^2	0.9999	0.9999	0.9999	0.9999	0.9999	0.9999	0.9994
2	a	0.4879	0.6271	0.7441	1.0323	1.0475	1.1411	1.3124
	b	0.5299	0.4334	0.3587	0.1925	0.1823	0.1492	0.0169
	c	-0.0209	-0.0028	0.0094	0.0359	0.0302	0.0288	0.0472
	d	0.0013	0.0002	-0.0005	-0.0019	-0.0014	-0.0011	-0.0021
	r^2	0.9999	0.9999	0.9998	0.9999	0.9998	0.9998	0.9996
4	a	0.6220	0.7468	0.8318	1.1250	1.2149	1.4687	1.6575
	b	0.4477	0.3800	0.3673	0.2460	0.2179	0.0840	0.0154
	c	-0.0001	0.0087	0.0090	0.0200	0.0243	0.0430	0.0509
	d	-0.0002	-0.0005	-0.0005	-0.0007	-0.0010	-0.0017	-0.0023
	r^2	1.0000	1.0000	1.0000	1.0000	1.0000	1.0000	0.9998
7	a	0.6229	0.7150	0.9147	1.2100	1.4293	1.5388	1.8193
	b	0.4477	0.4144	0.3136	0.2182	0.1460	0.1408	0.0545
	c	-0.0026	0.0023	0.0211	0.0330	0.0378	0.0383	0.0450
	d	0.0001	-0.0001	-0.0012	-0.0017	-0.0017	-0.0017	-0.0019
	r^2	1.0000	0.9998	0.9999	0.9994	0.9998	0.9999	0.9999
10	a	0.5913	0.6984	0.9207	1.2215	1.4399	1.6152	1.9984
	b	0.4983	0.4442	0.3328	0.2192	0.1644	0.1330	-0.0164
	c	-0.0188	-0.0052	0.0151	0.0377	0.0364	0.0401	0.0572
	d	0.0013	0.0004	-0.0008	-0.0019	-0.0016	-0.0018	-0.0025
	r^2	1.0000	0.9999	0.9999	0.9998	0.9998	0.9999	0.9996

Table B30
Relative Capture Approximation (Stage 1)
Gate Width = 6m
3rd degree Polynomial Fit: y=a+bx+cx^2+dx^3

		Gate Length/Width						
K_{prb}/K_{aq}	Parameter	0.08	0.17	0.33	0.67	1.00	1.33	2.00
1	a	0.5467	0.5801	0.6520	0.7367	0.8281	0.8537	0.8881
	b	0.4397	0.3917	0.3053	0.2064	0.1131	0.0929	0.0605
	c	0.0010	0.0104	0.0235	0.0348	0.0456	0.0424	0.0388
	d	0.0002	-0.0004	-0.0011	-0.0015	-0.0021	-0.0018	-0.0014
	r^2	0.9999	0.9999	0.9998	0.9998	0.9999	0.9999	0.9999
2	a	0.5748	0.5825	0.7625	0.9060	1.0356	1.1368	1.2405
	b	0.4484	0.4473	0.3347	0.2472	0.1682	0.1069	0.0622
	c	0.0014	-0.0012	0.0179	0.0287	0.0372	0.0454	0.0453
	d	0.0001	0.0003	-0.0007	-0.0011	-0.0015	-0.0019	-0.0018
	r^2	1.0000	1.0000	0.9999	0.9999	0.9999	0.9999	0.9999
4	a	0.6165	0.7152	0.8294	1.0945	1.2348	1.4001	1.5967
	b	0.4447	0.3876	0.3340	0.2043	0.1653	0.0927	0.0266
	c	0.0018	0.0111	0.0196	0.0383	0.0389	0.0496	0.0537
	d	0.0001	-0.0004	-0.0008	-0.0017	-0.0016	-0.0021	-0.0022
	r^2	1.0000	0.9999	0.9999	0.9998	0.9998	0.9998	0.9997
7	a	0.6114	0.6696	0.9073	1.1465	1.3597	1.5451	1.7674
	b	0.4509	0.4444	0.3103	0.2241	0.1379	0.0880	0.0229
	c	-0.0001	-0.0005	0.0231	0.0350	0.0460	0.0500	0.0571
	d	0.0002	0.0003	-0.0010	-0.0015	-0.0020	-0.0021	-0.0024
	r^2	1.0000	0.9999	0.9999	0.9998	0.9999	0.9998	0.9999
10	a	0.6114	0.7447	0.8992	1.2394	1.4354	1.5852	1.8361
	b	0.4509	0.3874	0.3235	0.1880	0.1160	0.0992	0.0508
	c	-0.0001	0.0116	0.0219	0.0413	0.0511	0.0478	0.0486
	d	0.0002	-0.0004	-0.0009	-0.0018	-0.0023	-0.0019	-0.0018
	r^2	1.0000	0.9999	0.9999	0.9997	0.9997	0.9997	0.9997

Table B31
Relative Capture Approximation (Stage 1)
Gate Width = 9m
3rd degree Polynomial Fit: y=a+bx+cx^2+dx^3

K_{prb}/K_{aq}	Parameter	Gate Length/Width 0.08	0.17	0.33	0.67	1.00	1.33	2.00
1	a	0.5656	0.6187	0.7117	0.7861	0.8831	0.8897	0.9669
	b	0.4279	0.3549	0.2309	0.1247	0.0426	0.0407	-0.0535
	c	0.0072	0.0249	0.0527	0.0681	0.0769	0.0702	0.0877
	d	-0.0001	-0.0015	-0.0036	-0.0044	-0.0048	-0.0042	-0.0058
	r^2	1.0000	1.0000	0.9999	0.9999	1.0000	1.0000	0.9999
2	a	0.6279	0.7000	0.8166	0.9934	1.1112	1.1896	1.2767
	b	0.4067	0.3497	0.2572	0.1348	0.0652	0.0255	-0.0098
	c	0.0148	0.0255	0.0427	0.0633	0.0708	0.0742	0.0802
	d	-0.0008	-0.0015	-0.0025	-0.0037	-0.0040	-0.0041	-0.0050
	r^2	1.0000	0.9998	0.9999	0.9998	0.9999	1.0000	0.9999
4	a	0.6258	0.7290	0.9568	1.1379	1.3159	1.4879	1.6553
	b	0.4405	0.3752	0.2100	0.1158	0.0379	-0.0592	-0.0915
	c	0.0045	0.0190	0.0528	0.0730	0.0840	0.0991	0.0975
	d	0.0000	-0.0010	-0.0030	-0.0047	-0.0053	-0.0061	-0.0057
	r^2	1.0000	0.9999	1.0000	0.9999	0.9998	0.9998	1.0000
7	a	0.6698	0.7685	1.0066	1.2578	1.4739	1.6228	1.8652
	b	0.4023	0.3528	0.1936	0.0726	-0.0260	-0.0700	-0.1347
	c	0.0154	0.0228	0.0604	0.0819	0.0985	0.1015	0.1076
	d	-0.0008	-0.0011	-0.0039	-0.0052	-0.0062	-0.0062	-0.0064
	r^2	1.0000	0.9999	0.9998	0.9998	0.9999	0.9998	0.9998
10	a	0.6698	0.7868	1.0188	1.2778	1.5268	1.6762	1.9451
	b	0.4023	0.3250	0.2088	0.0726	-0.0301	-0.0694	-0.1410
	c	0.0154	0.0338	0.0554	0.0819	0.1001	0.1002	0.1111
	d	-0.0008	-0.0022	-0.0035	-0.0052	-0.0064	-0.0060	-0.0068
	r^2	1.0000	0.9999	0.9999	0.9999	0.9999	0.9999	0.9997

Table B32
Relative Capture Approximation (Stage 1)
Gate Width = 18m
Quadratic Fit: y=a+bx+cx^2

K_{prb}/K_{aq}	Parameter	Gate Length/Width 0.08	0.17	0.33	0.67	1.00
1	a	0.5331	0.5853	0.6374	0.6899	0.7517
	b	0.4542	0.3916	0.3316	0.2613	0.2064
	c	0.0080	0.0171	0.0245	0.0305	0.0343
	r^2	0.9999	0.9998	0.9997	0.9994	0.9994
2	a	0.5793	0.6553	0.7528	0.9062	0.9921
	b	0.4489	0.3916	0.3226	0.2181	0.1659
	c	0.0083	0.0171	0.0264	0.0391	0.0445
	r^2	0.9999	0.9998	0.9995	0.9996	0.9995
4	a	0.6262	0.7069	0.8682	1.0647	1.1905
	b	0.4256	0.3773	0.2808	0.1804	0.1283
	c	0.0124	0.0193	0.0332	0.0455	0.0508
	r^2	0.9999	0.9997	0.9996	0.9993	0.9990
7	a	0.6548	0.7455	0.9136	1.1516	1.3044
	b	0.4045	0.3563	0.2718	0.1571	0.1008
	c	0.0168	0.0238	0.0351	0.0496	0.0554
	r^2	0.9999	0.9999	0.9994	0.9988	0.9992
10	a	0.6639	0.7485	0.9236	1.1786	1.3489
	b	0.4034	0.3604	0.2718	0.1529	0.0906
	c	0.0167	0.0233	0.0351	0.0500	0.0571
	r^2	0.9998	0.9998	0.9997	0.9994	0.9983

Table B33
Relative Capture Interpolation (Stage 2)
Gate Width = 3m

Interpolation Function	Parameter	K_{prb}/K_{aq} 1	2	4	7	10
$a=a_1(a_2-\exp(-a_3x))$	a_1	0.480	0.918	1.551	1.576	2.145
	a_2	1.981	1.453	1.364	1.329	1.239
	a_3	1.218	1.367	0.615	0.842	0.574
	r^2	0.9948	0.9887	0.9952	0.9989	0.9984
$b=b_1(b_2-\exp(-b_3x))$	b_1	-0.544	-0.548	-0.727	-0.457	-0.611
	b_2	-0.012	-0.033	0.364	-0.091	0.136
	b_3	1.305	1.398	0.488	1.405	0.947
	r^2	0.9939	0.9824	0.9884	0.9945	0.9891
$c=c_1+c_2x+c_3x^2+c_4x^3$	c_1	-0.0253	-0.0352	0.0020	-0.0135	-0.0335
	c_2	0.1186	0.2028	0.0143	0.1269	0.1966
	c_3	-0.0880	-0.1885	0.0210	-0.1014	-0.1705
	c_4	0.0214	0.0538	-0.0079	0.0263	0.0475
	r^2	0.9868	0.9923	0.9844	0.9961	0.9976
$d=d_1+d_2x+d_3x^2+d_4x^3$	d_1	0.0015	0.0021	-0.0003	0.0007	0.0021
	d_2	-0.0065	-0.0123	0.0001	-0.0070	-0.0116
	d_3	0.0054	0.0121	-0.0013	0.0061	0.0106
	d_4	-0.0014	-0.0035	0.0004	-0.0016	-0.0030
	r^2	0.9834	0.9902	0.9888	0.9878	0.9932

Table B34
Relative Capture Interpolation (Stage 2)
Gate Width = 6m

Interpolation Function	Parameter	K_{prb}/K_{aq} 1	2	4	7	10
$a=a_1(a_2-\exp(-a_3x))$	a_1	0.432	0.870	1.363	1.589	1.590
	a_2	2.138	1.558	1.399	1.317	1.322
	a_3	1.360	1.013	0.737	0.791	0.876
	r^2	1.0000	0.9968	0.9992	0.9989	0.9993
$b=b_1(b_2-\exp(-b_3x))$	b_1	-0.466	-0.501	-0.511	-0.535	-0.475
	b_2	-0.083	-0.015	0.060	0.040	-0.075
	b_3	1.624	1.148	1.058	1.212	1.652
	r^2	1.0000	0.9958	0.9971	0.9951	0.9957
$c=c_1+c_2x+c_3x^2+c_4x^3$	c_1	-0.0074	-0.0074	-0.0040	-0.0114	-0.0094
	c_2	0.1068	0.0759	0.0906	0.1125	0.1273
	c_3	-0.0694	-0.0346	-0.0555	-0.0716	-0.0890
	c_4	0.0136	0.0049	0.0124	0.0162	0.0200
	r^2	0.9999	0.9882	0.9922	0.9912	0.9969
$d=d_1+d_2x+d_3x^2+d_4x^3$	d_1	0.0006	0.0005	0.0004	0.0008	0.0007
	d_2	-0.0056	-0.0033	-0.0047	-0.0060	-0.0067
	d_3	0.0037	0.0013	0.0033	0.0042	0.0050
	d_4	-0.0007	-0.0001	-0.0008	-0.0010	-0.0012
	r^2	0.9994	0.9902	0.9864	0.9837	0.9946

Table B35
Relative Capture Interpolation (Stage 2)
Gate Width = 9m

Interpolation Function	Parameter	K_{prb}/K_{aq} 1	2	4	7	10
$a=a_1(a_2-\exp(-a_3x))$	a_1	0.463	0.794	1.296	1.541	1.673
	a_2	2.134	1.696	1.423	1.370	1.343
	a_3	1.361	1.216	0.950	0.892	0.837
	r^2	0.9947	1.0000	0.9972	0.9989	0.9991
$b=b_1(b_2-\exp(-b_3x))$	b_1	-0.537	-0.499	-0.625	-0.638	-0.635
	b_2	0.084	0.054	0.182	0.238	0.259
	b_3	1.765	1.691	1.614	1.629	1.519
	r^2	0.9936	1.0000	0.9936	0.9977	0.9992
$c=c_1+c_2x+c_3x^2+c_4x^3$	c_1	-0.0095	0.0034	-0.0092	-0.0040	0.0010
	c_2	0.2385	0.1493	0.2022	0.2214	0.2057
	c_3	-0.2127	-0.1067	-0.1322	-0.1557	-0.1431
	c_4	0.0589	0.0256	0.0289	0.0365	0.0339
	r^2	0.9959	0.9998	0.9916	0.9945	0.9986
$d=d_1+d_2x+d_3x^2+d_4x^3$	d_1	0.0011	-0.0001	0.0010	0.0006	0.0002
	d_2	-0.0182	-0.0097	-0.0137	-0.0156	-0.0145
	d_3	0.0173	0.0078	0.0090	0.0115	0.0110
	d_4	-0.0050	-0.0021	-0.0019	-0.0027	-0.0027
	r^2	0.9927	0.9999	0.9954	0.9900	0.9960

Table B36
Relative Capture Interpolation (Stage 2)
Gate Width = 18m

Interpolation Function	Parameter	K_{prb}/K_{aq} 1	2	4	7	10
$a=a_1(a_2-\exp(-a_3x))$	a_1	0.296	0.611	0.851	1.044	1.179
	a_2	2.699	1.830	1.612	1.523	1.470
	a_3	1.720	1.574	1.540	1.300	1.125
	r^2	0.9925	0.9997	0.9998	1.0000	0.9999
$b=b_1(b_2-\exp(-b_3x))$	b_1	-0.326	-0.401	-0.418	-0.445	-0.475
	b_2	-0.534	-0.257	-0.186	-0.048	0.019
	b_3	2.160	1.854	2.118	1.745	1.577
	r^2	0.9964	0.9996	0.9996	0.9998	0.9996
$c=c_1+c_2x+c_3x^2+c_4x^3$	c_1	-0.0010	0.0003	0.0022	0.0091	0.0089
	c_2	0.1305	0.1113	0.1270	0.0986	0.0979
	c_3	-0.1855	-0.1059	-0.1213	-0.0657	-0.0634
	c_4	0.0903	0.0389	0.0429	0.0134	0.0137
	r^2	0.9977	0.9991	0.9993	1.0000	1.0000

Appendix C

Approximation of Down-Gradient Gate Face for Residence Time Equalisation

The customised down-gradient gate face was proposed in Section 4.4.1 as a means of controlling the lateral variation in residence time presented in Section 4.3.2. A methodology for estimating edge and centreline residence time was then presented in Section 5.2. Figure C.1 shows a quadratic function that uses edge and centreline residence time to approximate the down-gradient face shape for the PRB presented in Figure 4.10. The aim of this particular PRB was lateral equalisation of residence time for a homogeneous plume. A similar approach can also be used for other types of plumes, for example where the contaminant concentration decreases around the plume fringes.

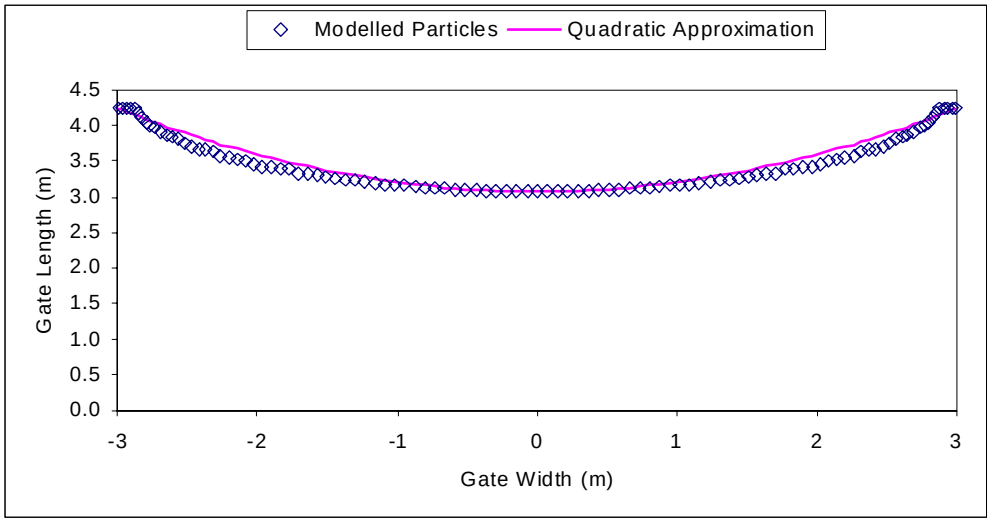

Fig. C.1. Plan view of quadratic approximation to modelled down-gradient face for the PRB described in Figure 4.10 (L_{SW}=4.25m, W_G=6m, D_G=6m, W_F=6m, K_G/K_{Aq}=10).

The following three–stage approach is proposed for down-gradient gate face approximation:

1) Find the centreline flow-through length to equalise centreline residence time with the residence time near the side wall (edge).
2) Fit an approximation curve through the chosen edge and centreline flow-through lengths.
3) Estimate the volume of the gate.

Using the PRB presented in Figure C.1 as an example, the first step involves plotting particle flow-through distance versus residence time down the centreline and also near the side wall (edge). Figure C.2 suggests that horizontal centreline speed can be assumed constant for the example PRB as a linear approximation matches the modelled particles. This means that the edge and centreline residence times at the modelled gate length can be used to estimate the centreline residence time at any other gate length within the modelled bounds. For example, the edge and centreline residence time at a flow-through length of 4.25m in Figure C.2 were 65.2 and 90.8 days respectively.

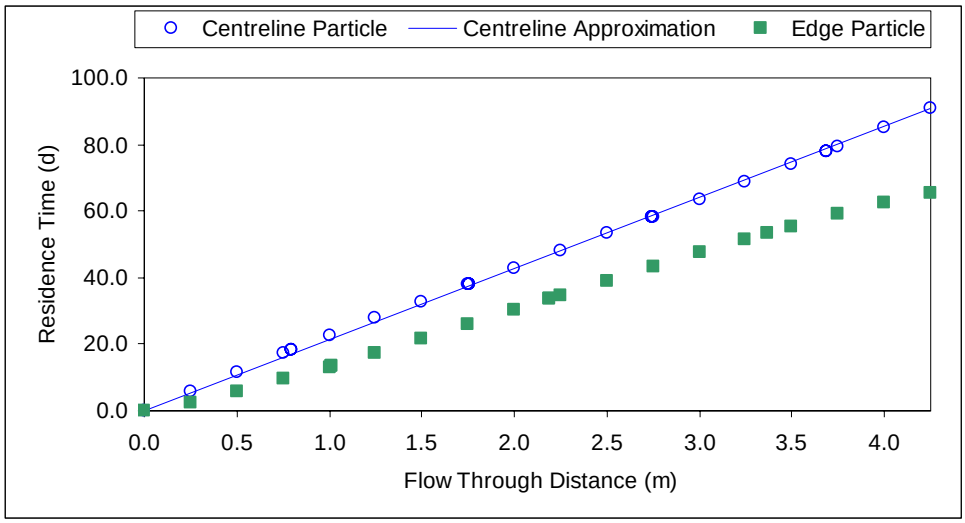

Fig. C.2. Comparison of centreline (with straight-line approximation) and edge particles for a fully penetrating PRB (L_{SW}=4.25m, W_G=6m, D_G=6m, W_F=6m, K_G/K_{Aq}=10).

The required centreline flow-through length can therefore be found from Equation C1 as follows:

$$\mathbf{CL_G = \frac{Res_{Edge}}{Res_{Centre}} * L_G = \frac{65.2}{90.8} * 4.25 = 3.05m} \qquad \mathbf{C1}$$

where CL_G is the required centreline length, Res_{Edge} and Res_{Centre} are the edge and centreline residence times, and L_G is the flow-through gate length next to the side wall.

As presented in Figure C.1, a simple quadratic approximation can now be used to estimate the flow-through gate length at any point *x* along the gate face for the example system as in Equation C2:

$$\mathbf{Len_G(x) = \frac{(L_G - CL_G)}{(W_G / 2)^2} * x^2 + CL_G} \qquad \mathbf{C2}$$

$$\mathbf{for \left(\frac{-W_G}{2} \le x \le \frac{W_G}{2} \right)}$$

Substituting the example values into Equation C2 yields:

$$\mathbf{Len_G(x) = \frac{(4.25 - 3.05)}{(6 / 2)^2} * x^2 + 3.05 = 0.133x^2 + 3.05} \qquad \mathbf{C3}$$

$$\mathbf{for \left(-3 \le x \le 3 \right)}$$

Standard calculus can then be used to estimate the gate reactive zone volume V_{GRZ} from gate width W_G, depth D_G, centreline length CL_G and edge length L_G as follows:

$$\mathbf{V_{GRZ}} = \mathbf{CL_G * W_G * D_G + 2 * D_G * \int_0^{W_G/2} \left(\frac{(L_G - CL_G)}{(W_G/2)^2} * x^2 + CL_G \right)}$$

$$= \mathbf{CL_G * W_G * D_G + 2 * D_G * \frac{(L_G - CL_G)}{(W_G/2)^2} * \frac{(W_G/2)^3}{3}} \qquad \mathbf{C4}$$

$$= \mathbf{W_G * D_G * \left(CL_G + \frac{(L_G - CL_G)}{3} \right)}$$

Substituting the example values into Equation C4 yields:

$$\mathbf{V_{GRZ}} = \mathbf{6 * 6 * \left(3.05 + \frac{(4.25 - 3.05)}{3} \right)} = \mathbf{124.2\ m^3} \qquad \mathbf{C5}$$